INFORMATION TO USERS

This manuscript has been reproduced from the microfilm master. UMI films the text directly from the original or copy submitted. Thus, some thesis and dissertation copies are in typewriter face, while others may be from any type of computer printer.

The quality of this reproduction is dependent upon the quality of the copy submitted. Broken or indistinct print, colored or poor quality illustrations and photographs, print bleedthrough, substandard margins, and improper alignment can adversely affect reproduction.

In the unlikely event that the author did not send UMI a complete manuscript and there are missing pages, these will be noted. Also, if unauthorized copyright material had to be removed, a note will indicate the deletion.

Oversize materials (e.g., maps, drawings, charts) are reproduced by sectioning the original, beginning at the upper left-hand corner and continuing from left to right in equal sections with small overlaps.

ProQuest Information and Learning
300 North Zeeb Road, Ann Arbor, MI 48106-1346 USA
800-521-0600

UMI®

SMART ENERGY DISSIPATION SYSTEMS FOR PROTECTION OF CIVIL INFRASTRUCTURES FROM NEAR-FIELD EARTHQUAKES

By

Wanlong He

A dissertation submitted to the Graduate Faculty in Engineering in partial fulfillment of the requirements for the degree of Doctor of Philosophy,

The City University of New York

2003

This manuscript has been read and accepted for the Graduate Faculty in Engineering in satisfaction of the dissertation requirement for the degree of Doctor of Philosophy.

08/1/2003
Date

Anil Kumar Agrawal
Professor Anil Agrawal

Chair of Examining Committee

August 4, 2003
Date

Mumtaz K. Kassir
Professor Mumtaz K. kassir

Executive Officer

Professor Michel Ghosn

Professor Feng-Bao Lin

Professor Subramaniam Kolluru

Dr. Mohammed Ettouney

Professor Andrew Smith

THE CITY UINVERSITY OF NEW YORK

Abstract

SMART ENERGY DISSIPATION SYSTEMS FOR PROTECTION OF CIVIL INFRASTRUCTURES FROM NEAR-FIELD EARTHQUAKES

By

Wanlong He

Advisor: Professor Anil Kumar Agrawal

The purpose of this research is to explore an effective control system for protection of structures from near-field ground motions. Based on the analysis of a large amount of recorded ground motions, an analytical model for the velocity pulse in near-field ground motions is developed. The closed-form solution for an elastic SDOF structures subject to such a pulse model is derived. The performance of various passive dampers for structures subject to near-field ground motions is also investigated using the proposed pulse model. Further, an innovative hybrid control system is proposed to protect structures from strong ground motions based on an optimal polynomial controller. The hybrid control system consists of passive dampers and active (or semi-active) actuators installed in parallel with the passive dampers. The control force of the hybrid control system is determined using the optimal controller. The linear part of the optimal polynomial controller is proportional to the response of the structure and it can be implemented by active (semi-active) actuators or passive linear viscous dampers. The nonlinear part is a high order function of the states of the structure and it can be implemented by active actuators or semi-active dampers. The performance of the hybrid control system is illustrated by applying this control system to protect a SDOF structure and a Benchmark cable-stayed bridge from seismic excitations. Numerical results

indicate that the hybrid control system is very effective in reducing the displacement of the structures for a broad spectrum of ground motions. Since the control force of the active or semi-active damper in the hybrid control system is naturally impulsive and is only required at a few instances during the entire seismic episode, this hybrid control system might be implemented easily and practically in the future. Furthermore, the proposed pulse model is also used to improve the performance of semi-active or active controllers by augmenting the structural system with the input shaping filter obtained from the pulse model. Numerical results demonstrate that a semi-active or active controller designed in such a manner is much more effective than passive viscous damper and active controller neglecting the ground motion information.

In memory of my father:

Mr. **HE MINLU**

ACKNOWLEDGEMENTS

I would like to express my sincere gratitude and appreciation to my advisor, Professor Anil K. Agrawal, for his expert guidance and mentorship, for his encouragement and support, during the period of my graduate study at The City College of New York. My sincere gratitude also goes to other faculty members in the Department of Civil Engineering for their helpful suggestions on this study. In particular, I would like to thank Professor John Fillos, Professor Mumtaz Kassir, Professor Michel Ghosn, Professor George Mylonakis, Professor Feng-Bao Lin, Professor Subramaniam Kolluru, and Professor Thomas Price for their encouragement and assistance during my graduate study. I am also grateful to Professor J.N. Yang at the University of California, Irvine, Professor Lawrence Bergman at the University of Illinois at Urbana-Champaign, and Professor Satish Nagarajaiah at the Rice University for their review of this manuscript and their valuable comments.

Finally, I would like to express my gratitude and love to my wife, Xiaoxia, and my brothers and sister, for their endless love and support, which made this mission possible.

The research presented in this dissertation is partially supported by grants from the National Science Foundation under grant number CMS-0099895 and Multidisciplinary Center for Earthquake Engineering Research (MCEER).

CONTENTS

LIST OF TABLES

LIST OF FIGURES

CHAPTER 1

INTRODUCTION

1.1 Statement of the Problem

Near-field (NF) ground motions have resulted in serious fatalities and heavy damage to critical infrastructures in the vicinity of seismic sources during recent earthquakes such as 1994 Northridge, 1995 Kobe and 1999 Chi-Chi earthquake. Evidence indicates that ground shaking near fault rupture may be characterized by a short-duration impulsive pulse with a high input energy imposed on the structure at the beginning of the earthquake. This pulse-type motion is particularly explicit in "forward direction" condition. Especially when the fault rupture propagates towards the site at a velocity close to the shear wave velocity, most of the seismic energy arrives at the site within a short time (Singh, 1985). The near-field phenomenon requires special consideration in the design of structures located in the near-field region, which is usually assumed to extend about 10 to 15 km from the seismic source (SEAOC blue book, 1996).

Besides forward directivity effects, near-field ground motions are more severe than "ordinary" ground motions recorded during the same event and under similar site conditions. Figure 1-1 shows velocity response spectra of near-field and ordinary ground motions. The curve in solid line (denoted as 15-D*) represents the mean velocity spectrum of a set of ordinary ground motions whose individual spectra resemble the UBC'97 soil type S_D spectrum. Other curves in Figure 1-1 correspond to the velocity spectra of individual near-field ground motions with forward directivity effects during various seismic events. The figure illustrates significant variations in the response of

SDOF systems subject to near-field ground motions. It also indicates that near-field ground motions impose seismic demands on structures that may be several times higher than those of the mean design level "ordinary" ground motions. Further, the severity of near-field ground motions leads to ductility demands that are significantly larger than those required by the UBC design ground motions.

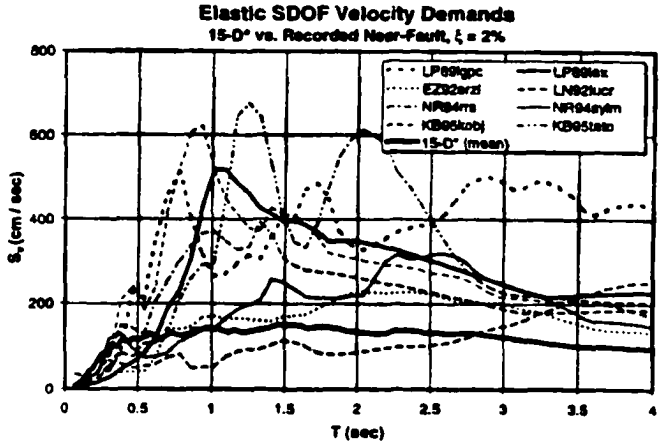

Figure 1-1: Velocity Response Spectra of Near-field and Ordinary Ground Motions [From Alavi and Krawinkler (2001)].

Recent seismic design codes, e.g. the 1997 UBC code, have incorporated near-field effects by introducing source type and distance dependent near-field factors to the customary design spectrum. Further, FEMA 273 (1997) and 368 (2000) allow the rehabilitation old buildings and the design of new buildings using passive energy dissipation devices. However, the design procedure for energy dissipation devices for structures subject to near-field ground motions is the same as that for "ordinary" ground motions, without considering the characteristics of near-field ground motions. It is well known that the same passive energy dissipation system performs differently under ground

motions with different characteristic. Likewise, while a particular passive energy dissipation system may be effective for a particular structure, it may not be effective at all for another type of structure. To-date, a systematic investigation of these aspects of passive energy dissipation systems has not been carried out because of the use of recorded ground motions with randomly different excitation characteristics and selected structural models. The development of design guidelines for applications of passive energy dissipation system for structures close to the seismic source requires a thorough understanding of near-field response phenomena. Consequently, FEMA 356 — *Prestandard and Commentary for the Seismic Rehabilitation of Buildings* (2000) has recommended the need for further basic research on near-field effects in the seismic design and rehabilitation of buildings using energy dissipation devices.

Significant progress has been made in the area of structural control technology for civil engineering structures during the last two decades (e.g., Housner et al. 1997). Semi-active control systems have been proposed to improve the performance of passive energy dissipation systems. Basically, semi-active control systems are obtained by parametric modifications of passive energy dissipation systems. For example, passive fluid viscous dampers modified by introducing an orifice control in the damper bypass to obtain active variable damping systems. Other examples of semi-active control systems are Magneto-Rheological (MR) dampers, Electro-Rheological (ER) dampers, Active Variable Stiffness dampers, Variable friction damper, etc. For structures equipped with semi-active control systems, while the response of the structure depends on the damper control force, the control force itself depends on the response and excitation characteristics. Unfortunately,

a majority of researchers either neglect the excitation characteristics in the controller design or assume simple white noise excitation models.

For active control systems, control forces are applied on structures using actuators or DC servo motors through control mechanisms, such as Active Tuned Mass Dampers (ATMD), Active Mass Drivers (AMD), etc. These systems usually require large external power supply to achieve desired vibration control objectives. The control force generated by active control system depends on the device characteristics and the characteristics of the external excitations. Hence, a control system designed by ignoring the characteristics of external excitations may not be effective in protecting structures during near-field earthquakes.

1.2 Need of Control Systems for Near-Field Earthquakes

Near-field ground motions are characterized by a short duration long period destructive impulsive pulses. These long period pulses are distinguishable in velocity and displacement records. The first strong seismological evidence for the near-field ground phenomenon was reported as early as 1955 (Benioff, 1955). Near-field effects received a wide recognition because of serious fatalities and heavy damages to structures during the 1994 Northridge earthquake, 1995 Kobe earthquake and 1999 Chi-Chi earthquake.

Conventional design and retrofit strategies, such as increasing or decreasing the stiffness of the structure by using the base isolation technology, are not efficient to protect structures during near-field ground motions. Increasing the stiffness shortens the period of system, resulting in a very large ductility demand for the structure. On the other hand, large displacement demands imposed by severe long period pulses in near-field

ground motions may be unacceptable for flexible structures such as base-isolated buildings.

The possible solution to this issue is to use passive energy dissipation devices or semi-active and active control systems. Recently, several researchers have proposed to mitigate the seismic hazard during near-field ground motions using passive viscous dampers or friction dampers. Hall et al. (1995), and Makris and Chang (1998) investigated the efficiency of base isolation system equipped with various energy dissipation mechanisms to protect the building during pulse-type near-field ground motions. They emphasized the use of energy dissipation devices, particularly viscous damper, as an effective technique to protect structures during near-field ground motions. However, Malhotra (1999) has shown that long period pulses contained in near-field records decrease the performance passive viscous dampers. In general, the performance of passive energy dissipation devices is dependent more on the ground motion than that of semi-active and active control systems, since the latter control systems adapt to the characteristics of ground motions through the real-time feedback. FEMA 273 (1997) and FEMA 368 (2000) allow the rehabilitation old buildings and the design of new buildings using passive energy dissipation devices, and semi-active or active control systems. However, it is imperative to develop of an effective structural control system for the protection of structures during near-field earthquakes.

1.3 Objective and Scope

In this research, a systematic investigation on the development of an effective structural control system to protect structures during near-field ground motions has been

conducted. The performance of a structural control system depends not only on the characteristic of the device, the control algorithm, and the controlled structure, but also on the properties of excitations. Traditionally, a structural control system is designed by neglecting the characteristics of ground motions and its effectiveness is investigated by considering available ground motion records. The main focus of this research is to investigate the properties of near-field ground motions and its effect on the performance of controlled structural system through an analytical model for near-field ground motion pulses. Based on an extensive investigation of the properties of near-field ground motions and their effect on passive damping systems, an innovative hybrid control system is proposed for the protection of structures from strong ground motions. Further, if the predominant period of the ground motions is known *a priori*, an effective and smart control system is also proposed by treating the ground motions as filtered white noise. The outline of the proposed research work is presented in the following:

Chapter 1 presents a brief introduction of issues related to near-field ground motions, the need of using structural control systems, and the objectives of the proposed research.

Chapter 2 presents a brief literature review on passive, active, semi-active and hybrid control systems.

Chapter 3 presents the mechanics and the development of large velocity pulses in near-field ground motions. A simple analytical model is presented to capture the long period pulses in the near-field ground motions. The properties of the analytical model are discussed. The closed form solution of SDOF system with passive viscous damper and subject to the analytical pulses is derived.

In Chapter 4, the performance of the supplemental energy dissipation devices installed in a SDOF elastic or elastic-perfectly-plastic structure subject to near-field velocity pulses is investigated. The energy transfer and energy dissipating property of the SDOF system with supplemental energy dissipation devices subject to velocity pulse are studied. Numerical simulations show that the performance of passive viscous dampers is highly dependent on long period pulses contained in ground motions. Similar conclusion is also obtained by a SDOF structure subject to 40 recorded and simulated near-field ground motions. This conclusion is further verified by applications to a complex model of the benchmark cable-stayed bridge.

In Chapter 5, the potential use of active control systems in protecting structures from near-field ground motions is investigated. Because of the impulsive pulses in near-field ground motions, a high-order nonlinear polynomial controller may be more effective than the linear controller such as LQR/LQG. The most attractive feature of nonlinear polynomial controllers is that they can respond quickly to high velocity impulsive excitations, since the control force is a nonlinear higher-order function of displacement and velocity of the structure. The performance of optimal polynomial controller to protect structures during near-field ground motions is illustrated. An active/active hybrid control system is implemented to achieve a multilevel control objective based on the optimal polynomial control algorithm, and it is investigated using 28 strong ground motions and 22 long duration ground motions. The control objective can also be achieved by using a passive/active hybrid control system, alternatively.

In Chapter 6, an innovative passive/semi-active hybrid control system is presented to protect structures during near-field ground motions. The hybrid control system consists

of a linear viscous damper installed in parallel with a semi-active friction damper. The semi-active friction damper is triggered only when the required control force exceeds certain lower threshold value and is saturated at an upper threshold value representing the device capacity. The design of the proposed hybrid control system is based on the optimal polynomial control algorithm investigated in Chapter 5. The application of the proposed hybrid control system is investigated for a SDOF structure and a benchmark cable-stayed bridge. Numerical simulations show that the hybrid control system is very effective in reducing the displacement of structures to a certain threshold value for a broad spectrum of ground motions.

In Chapter 7, a novel optimal controller is designed based on the augmented system including the structural system and the shape filter of near-field ground motions. The shape filter is obtained from the transfer function of the proposed velocity pulses in near-field ground motions presented in Chapter 3. The performance of the proposed control strategy is demonstrated through a base-isolated building subject to four typical near-field ground motions. The performance of the semi-active damper is compared with those of passive linear viscous damper and active controller when seismic excitations are treated as white noise.

Chapter 8 presents some major conclusions of this research and future research directions in the subject area.

CHAPTER 2

STATE-OF-THE-ART OVERVIEW

2.1 Introduction

Control of structures subject to seismic excitations represents a challenging task in civil engineering. The traditional approach for the seismic hazard mitigation is to design structures with sufficient strength capacity and the ability to deform in a ductile manner. Such a design philosophy is based on the assumption that the structures dissipate the input seismic energy in the form of the hysteretic energy through the damage in structural members. An alternative to the traditional aseismic design of structural systems is the use of structural control systems to dissipate the input seismic energy through hysteretic actions in these devices, thereby precluding inelastic deformations in structural members. These structural control devices can be classified as passive, active and semi-active control devices. Remarkable progress has been made over the last twenty years in finding innovative means of enhancing the performance of the structure under severe external excitations, especially after the recent destructive strong earthquakes, such as 1994 Northridge and 1995 Kobe earthquake. These innovations include the base isolation and passive energy dissipation devices operating in either passive or active mode, which enlarge the structural capacity to absorb the input energy and hence enhance its functionality and safety. The objective of this chapter is to provide an overview and assessment of various control systems with emphasis on recent advances.

2.2 Passive Control Systems

A passive control system is defined as a system, which does not require an external power source for operation and it utilizes the motion of the structure to develop the control forces. Control forces are developed as a function of the response of the structure at the location of the passive control devices. The operating principle of a typical passive control system is shown in Figure 2-1. A large number of passive energy dissipation devices have been developed and installed in structures for the performance enhancement during earthquake loads. In North America, passive energy dissipation systems have been implemented in approximately 103 buildings and many bridges, either for retrofit or for new constructions since the destructive Northridge Earthquake in 1994 (Soong and Spencer 2002). Similarly, large numbers of buildings have been designed with dampers or seismic isolation systems after the 1995 Kobe Earthquake in Japan (e.g., Wada et al. 2000).

A passive control system may be used to increase the energy dissipation capacity of a structure through discrete energy dissipation devices located either in combination with a seismic isolation system or over the height of the structure. Such systems may be referred to as supplemental energy dissipation systems. The objective of these systems is to absorb a significant amount of the seismic input energy, thus reducing the demand on the structural system. Depending on their construction, these systems may also increase the stiffness and strength of the structure in which they are installed. A passive control system does not require an external power source for operation. Rather, the motion of the structure is utilized to produce the relative motion within the passive control devices, which, in turn, dissipates energies. Supplemental energy dissipation devices may take many forms and may dissipate energies through a variety of mechanisms. Metallic energy

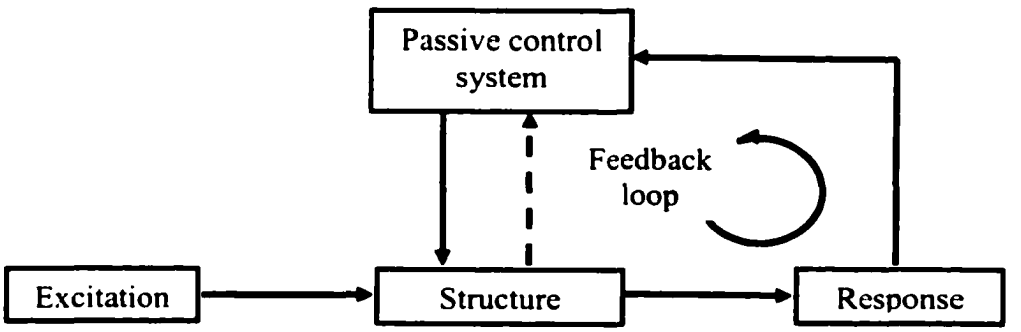

Figure 2-1: Schematic diagram of passive control system.

dissipation devices depend upon the plastic deformation of metallic materials, such as mild steel or lead (Skinner et al. 1975; Whittaker et al. 1991; Xia and Hanson 1992; Tsai and Tsai1995). Viscoelastic dampers use polymeric materials which dissipate energies when subject to shear deformations (Chang et al. 1992, 1995; Tsai and Lee 1993). Viscous fluid dampers dissipate energies when subject to the velocity input (Makris and Constantinou 1991; Makris et al. 1993a, 1993b). Friction dampers dissipate energies through the friction that develops between two solid bodies sliding against to one another (Pall and Marsh 1982; Filiatrault and Cherry 1990). Tuned mass dampers and tuned liquid dampers can also be treated as passive energy dissipation devices.

Seismic isolation systems represent another form of passive control systems. In these systems, a flexible isolation system is introduced between the foundation and the superstructure so as to increase the natural period of the entire system. The increase in the flexibility typically results in the rejection of a major portion of the earthquake energy; thereby reducing accelerations in the superstructure while increasing the displacement across the isolation level.

A major drawback of passive control systems is their inadaptability to external excitations. Since their control forces are developed as a function of the responses of structures, a passive control system designed for one ground motion may exhibit poor performance for other ground motion with different characteristics.

2.3 Active Control Systems

An active control system is defined as a system that typically requires a large power source for operation, such as electrohydraulic or electromechanical actuators. Control forces are developed based on the feedback information from the measured

response of the structure and/or the feed-forward information from the external excitation as shown in Figure 2-2. The measurements from the response and/or excitation are monitored by a controller (a computer) which, based on a pre-determined control algorithm, determines the appropriate control signal for operation of the actuators.

Literature reviews on active control systems can be found in Yang and Soong (1988), Soong and Reinhorn (1993), Soong and Constantinou (1994), Housner et al. (1997), Nishitani and Inoue (2001), etc. In contrast to passive control systems, active control systems require a large power source for operating electro-hydraulic actuators, which supply control forces to the structure. Control forces are developed based on the feedback from sensors that measure the excitation and/or the response of the structure. The feedback from the structural response may be measured at locations far from the location of the active control systems. Consequently, active control systems have wider ranges of adaptability for controlling the dynamic response of structures. However, the generation of control forces requires large power sources, which are on the order of tens of kilowatts for small structures and may reach several megawatts for large structures. As a result, it is difficult to practically implement a fully active control system to protect structures from strong earthquakes, since power supply required for the control system may be interrupted or shut down during strong earthquakes. However, active control algorithms are worthwhile to be further investigated because they form the basis of other promising control systems, such as semi-active control systems.

Advantages of active control systems include the ability to adapt to different loading conditions, such as pulse-type loadings, and to control different vibration modes of the structure. Advanced control theories have been investigated for applications of different

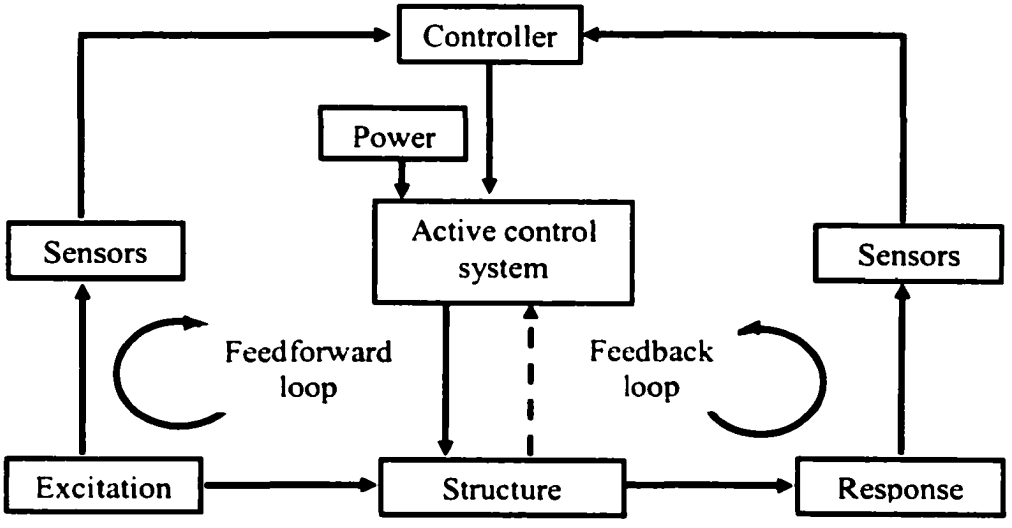

Figure 2-2: Schematic diagram of active control system

control systems to civil engineering structures. These techniques include μ-synthesis [e.g.. Hsu et al (1995)], neural network and fuzzy controllers [e.g., Wan et al (1995), Nagarajaiah (1994), Symans and Kelly (1999)], covariance control [e.g., Zhu and Skelton (1994); Lu and Skelton (1998)], LQG and H_2 methods [e.g., Spencer et al (1994; 1998a, b)], H_∞ techniques [e.g., Schmitendorf et al (1994), Jabbari et al (1995), Kose et al (1996, 1998), Alt et al (2000)], sliding mode control [e.g., Yang et al (1994e; 1995a, b; 1996a,b; 1997), Wu et al (1998), Matheu et al. (1998); Cai et al. (2000); Sarbjeet and Datta (2000); Zhao et al. (2000)], polynomial control [e.g., Agrawal and Yang (1995, 1996a, b, 1997, 1998), Yang et al (1996d), Spencer et al (1995), Tomasula et al (1996), etc.], and others [e.g., Spencer et al (1997a, b), Suhardjo et al (1992), Yang et al (1991; 1992a, b; 1994b, c, d; 2001), etc.].

2.4 Semi-Active Control Systems

A compromise between passive and active seismic response control systems has been developed recently in the form of semi-active control systems. A semi-active control system is defined as a system that typically requires a small external power source for operation (e.g. a battery) and utilizes the motion of the structure to develop the control forces, in which the magnitude of the control force can be adjusted by parametric control of the device using external power source. Control forces are developed based on the feedback from sensors that measure the excitation and/or the response of the structure. The feedback from the structural response may be measured at locations far from the location of the semi-active control system. A schematic diagram of a typical semi-active control system is shown in Figure 2-3.

Semi-active control systems maintain the reliability of passive control systems while taking advantage of the adaptability of an active control system. A semi-active control system can produce a large control force by dynamically changing the parameters such as the damping coefficient and/or the stiffness of the control device. The attention received in recent years can be attributed to the fact that semi-active control devices offer the same adaptability of active control devices without requiring a large power source. In fact, many can operate on the battery power, which is critical during seismic events when the main power source may fail. Furthermore, semi-active control devices do not have the potential to destabilize the structural system. Preliminary studies indicate that appropriately implemented semi-active systems perform significantly better than passive devices and have the potential to achieve the performance close to that of the fully active system, thus allowing for the possibility of the effective response reduction during a wide variety of dynamic loading conditions. An extensive review of semi-active systems investigated in the literature can be found in Housner et al. (1997), Symans and Constantinou (1999). A brief description of these devices is presented in the following.

The first application of semi-active control systems in the field of structural engineering was proposed by Hrovat et al. (1983). Since then, a large amount of research on the development and experimental tests of semi-active control systems has been conducted. Since most of these devices are in the preliminary stage of development rather than a mature product, the introduction of semi-active control system focuses on the description of semi-active control hardware and principles of their operation. Generally, energy dissipation semi-active dampers are classified as Variable Orifice Fluid Dampers, Controllable Friction Dampers, Variable Stiffness Dampers, and Controllable

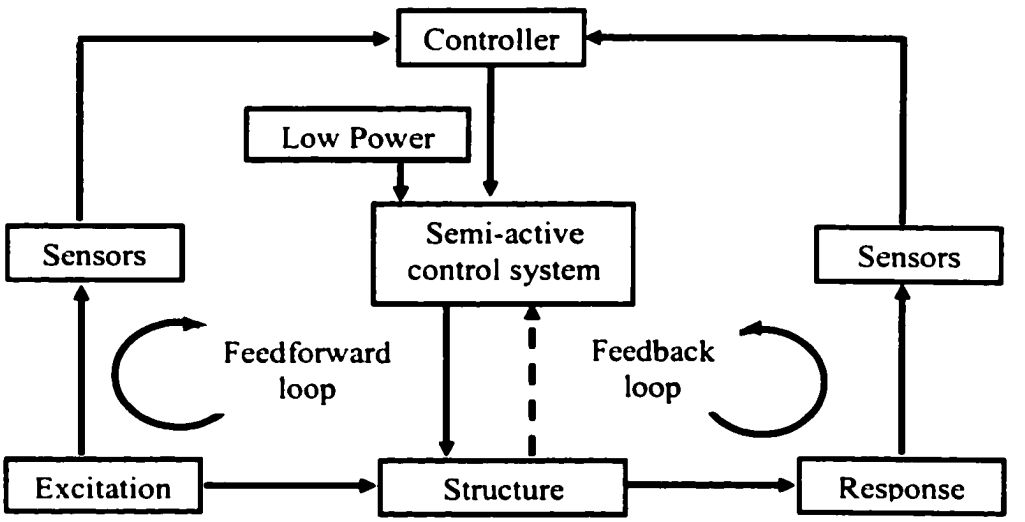

Figure 2-3: Schematic diagram of semi-active control system

Fluid Dampers, as described in the following.

2.4.1 Variable Orifice Viscous Dampers

Semi-active variable orifice viscous dampers typically consist of a hydraulic cylinder containing a piston head, which separates the two sides of the cylinder. As the piston is cycled, the fluid within the damper is forced to pass through small orifices at high speeds. The pressure differential across the piston head, and thus the output force, is modulated by an external control valve which connects the two sides of the cylinder. A servovalve is used to control the orifice. Variable viscous force of the damper is achieved by using a controllable, variable orifice valve to alter the resistance to flow of a conventional hydraulic fluid damper. The concept of applying variable-damping device to control the motion of bridges experiencing seismic motion was first discussed by Feng and Shinozuka (1990). Patten et al. (1994c) conducted experiments in which a hydraulic actuator with a controllable orifice was implemented in a single-lane model bridge to dissipate the energy induced by vehicle traffic. This experiment constitutes the first full-scale implementation of structural control in the United States.

Experimental studies have recently been completed by Symans and Constantinou (1997) on two different semi-active fluid damper systems. The semi-active fluid damper consists of a stainless steel piston rod, a bronze piston head and a piston rod make-up accumulator filled with thin silicone oil as shown in Figure 2-4. An external bypass loop containing a control valve is attached to the damper for modulating fluid flow. The variable damper servovalve is driven by an electric motor and contains a spool position feedback system. Physical characteristics of the tested dampers include a cylinder length of about 190 mm, a stroke of $\pm$ 76 mm, and a maximum output force of 8900 N. The

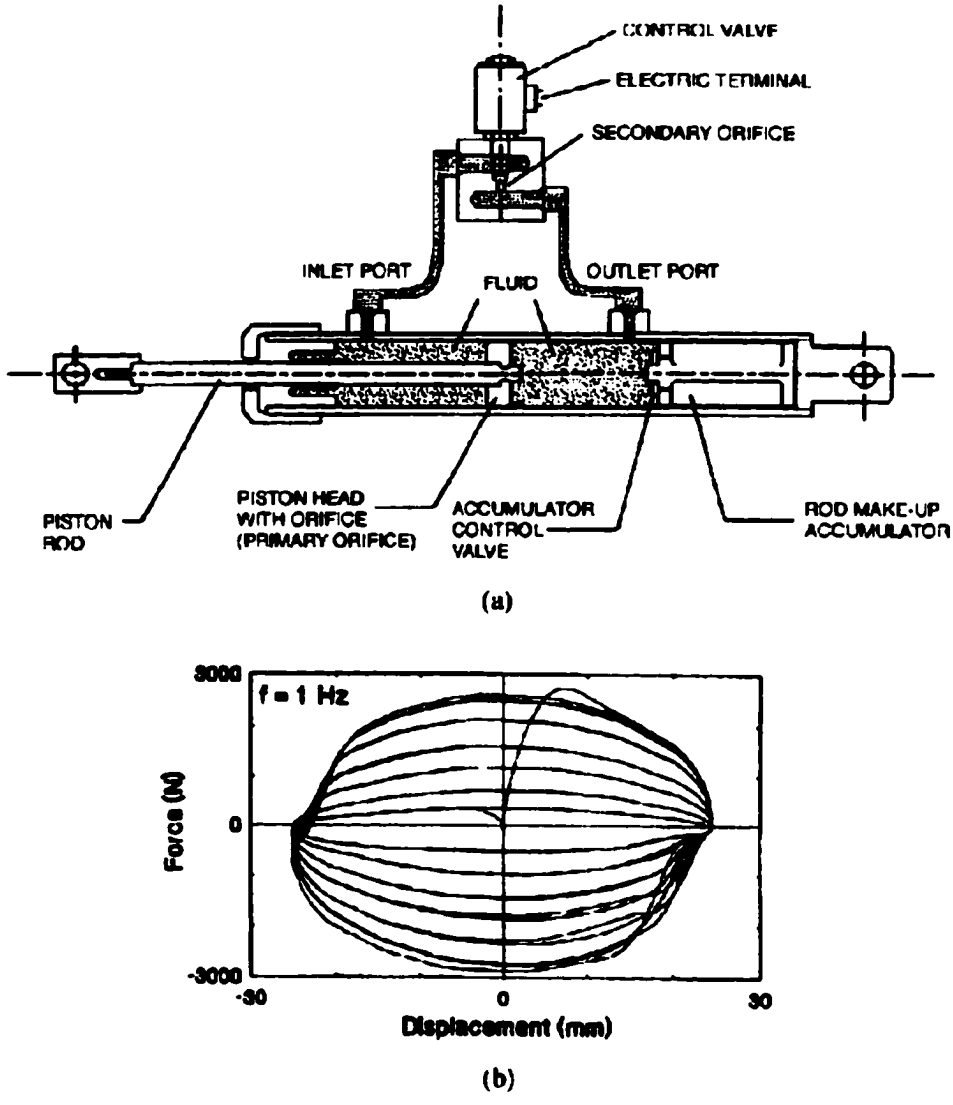

Figure 2-4: Semi-active variable orifice viscous damper tested by Symans (1997). (a) Schematic Diagram of the damper. (b) Hysteresis loops of the damper subjected to harmonic motion of 1Hz frequency and 25mm amplitude.

power required for operation of the two-stage damper and variable damper were approximately 55 W and 3.5 W, respectively.

Analytical models for describing the dynamic behavior of the fluid dampers were generated through extensive cyclic testing over a wide range of frequencies. It was shown that a simple phenomenological model consisting of a linear viscous dashpot with a voltage-dependent damping coefficient, $C(V)$, was sufficient for describing the damper behavior over the frequency range of interest for structural control applications. The output force F, is thus described by

$$F = C(V)\dot{x} \tag{2-1}$$

where $\dot{x}$ is the relative velocity of the piston head with respect to the damper housing and V is the servovalve command voltage.

Further investigations of semi-active variable orifice damper were conducted by some researchers in Japan. Kurata et al. (1999) and Niwa et al. (2000) implemented a full-scale variable-orifice damper and applied it on a real building to investigate its seismic response.

2.4.2 Controllable Fluid Dampers

The essential characteristic of controllable fluids is their ability to reversibly change from a free-flowing, linear viscous fluid to a semisolid with a controllable yield strength in milliseconds when exposed to an electric (for ER fluids) or magnetic (for MR fluids) field. Two fluids that are viable contenders for development of controllable dampers are: (1) electrorheological (ER) fluids; and (2) magnetorheological (MR) fluids. A number of ER fluid dampers have recently been developed, modeled, and tested for civil engineering applications. Recently developed MR fluids appear to provide an

attractive alternative to ER fluids for use in controllable fluid dampers. ER and MR dampers will be briefly introduced in the following.

2.4.2.1 Electro-Rheological dampers

Electrorheological (ER) dampers typically consist of a hydraulic cylinder containing micron-sized dielectric particles suspended within a fluid (usually oil). In the presence of a strong electric field, the particles polarize and become aligned, thus offering an increased resistance to flow. By varying the electric field, the dynamic behavior of an ER damper can be modulated. Electrorheological dampers have been investigated for seismic response control by Ehrgott and Masri (1992), Gavin et al. (1996a,b), Makris et al. (1996) and Burton et al. (1996).

As the applied electric field increases, the behavior of ER fluids changes from that of a viscous fluid to that of a yielding solid within milliseconds. More specifically, in the case of a steady, fully-developed flow, the shear resistance of ER fluids may be modeled as having a rigid component followed by a Newtonian component (Makris et al. 1996). A phenomenological model that defines such behavior consists of a Coulomb friction element in parallel with a linear viscous dashpot and is known as the Bingham model of viscoplasticity (Shames and Cozzarelli 1992). At the stress–strain level, the model is defined by

$$\tau = \tau_y \operatorname{sgn}(\dot{\gamma}) + \eta\dot{\gamma} \qquad (2\text{-}2)$$

where τ is the applied shear stress, τ_y is the yield stress, γ is the shear strain, η is the viscosity coefficient, $\operatorname{sgn}(\cdot)$ is the signum function and the overdot indicates differentiation with respect to time.

Experimental tests have been performed by Gavin et al. (1996b) on a large-scale ER control device. Makris (1997) have developed a large-scale 445kN (100 kips) capacity ER damper, which is shown in Figure 2-5(a). The ER fluid consisted of zeolite in a silicone oil and had a kinematic viscosity of 10 St. For the case of zero applied electric field, the damper behaves essentially as a linear viscous dashpot with a damping constant of about 3260 kN-s/m in a configuration with two bypasses and about 2170 kN-s/m in the case of three bypasses. Experimental test data is shown in Figure 2-5(b) for the damper with three bypasses and harmonic motion at a frequency of 0.2 Hz and amplitude of 2.54 cm (0.1 in.).

2.4.2.2 Magneto-Rheological dampers

Magnetorheological (MR) dampers are essentially magnetic analogs of ER dampers. Qualitatively, the behavior of the two types of dampers is very similar except that the control effect is governed by the application of an electric field in one case and by a magnetic field in the other. MR dampers typically consist of a hydraulic cylinder containing micron-sized, magnetically polarizable particles suspended within a fluid (usually oil). MR fluid behavior is controlled by subjecting the fluid to a magnetic field. In the absence of a magnetic field, the MR fluid flows freely while in the presence of a magnetic field, the fluid behaves as a semi-solid. MR dampers have been investigated for seismic response control by Dyke et al. (1996a) and Spencer et al. (1997a, b).

Figure 2-6(a) shows the schematic diagram of the prototype MR damper developed by Dyke et al. (1996a) and Spencer et al. (1997a,b). The damper has a stroke of 2.5 cm and a force capacity of 3 kN. An electromagnet located within the piston head is utilized to generate the magnetic field. The peak power required for operation of the

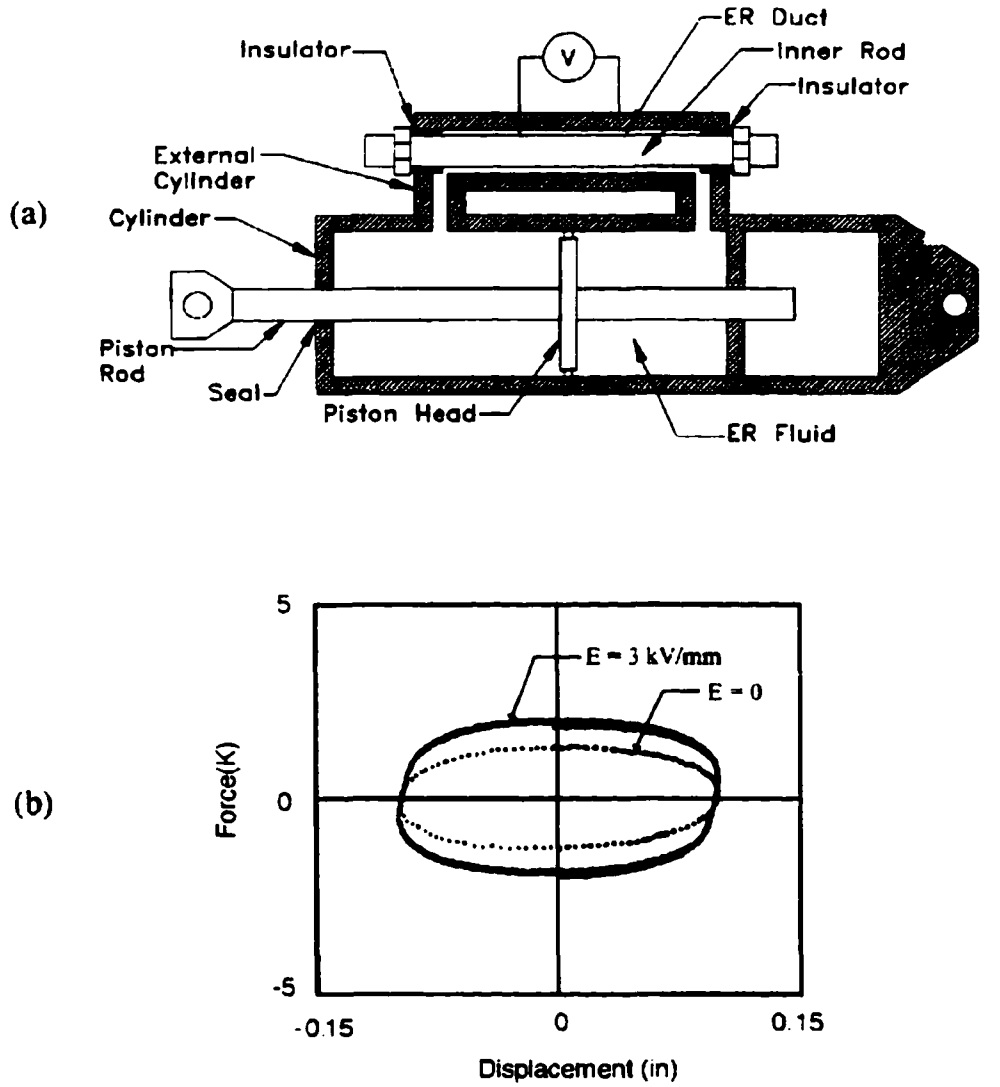

Figure 2-5: Semi-active Electrorheological damper tested by Makris (1997). (a) Schematic diagram of the damper. (b) Hysteresis loops of the damper subjected to harmonic motion at a frequency of 0.2 Hz and amplitude of 2.54 cm (0.1 in.)

damper is less than 10 W. For an imposed sinusoidal displacement of 2.5 Hz frequency and amplitude of 1.5 cm, the response of the MR damper is as shown in Figure 2-6(b) and Figure 2-6(c) for four different command voltage levels (0, 0.75, 1.5 and 2.25 V) with the force output increasing with increasing voltage level. At 0 V, the behavior of the MR damper is similar to that of a linear viscous damper. For voltage levels between 0 and 2.25 V, the damper exhibits behavior similar to that of a Coulomb friction element in parallel with a linear viscous dashpot.

A large-scale MR damper has recently been developed and is described by Spencer et al. (1997b) for seismic response control. The damper has a rated force output of 200 kN, a stroke of ± 8 cm, a maximum power requirement of about 22 W, a viscosity coefficient of 0.6 Pa-s, a maximum yield stress of 50 kPa, a length of about 1 m and weighs about 2.5 kN. In contrast to the small-scale damper, the large-scale damper contains a balanced piston rod and thus does not require an accumulator to accommodate piston rod volume fluid displacement. An accumulator is utilized, however, to accommodate thermal expansion of the fluid.

2.4.3 Variable Stiffness Dampers

Semi-active stiffness control devices are utilized to modify the stiffness and thus the natural vibration characteristics of the structure to which they are attached. Such systems have been investigated for seismic response control by Kobori et al. (1991,1993), Nemir et al. (1994), Yamada and Kobori (1995) and Yang et al. (1996d).

A semi-active stiffness system for seismic response control of structures has been described by Kobori et al. (1993). The system primarily controls the stiffness of a building to establish a non-resonant condition during earthquakes. The semi-active

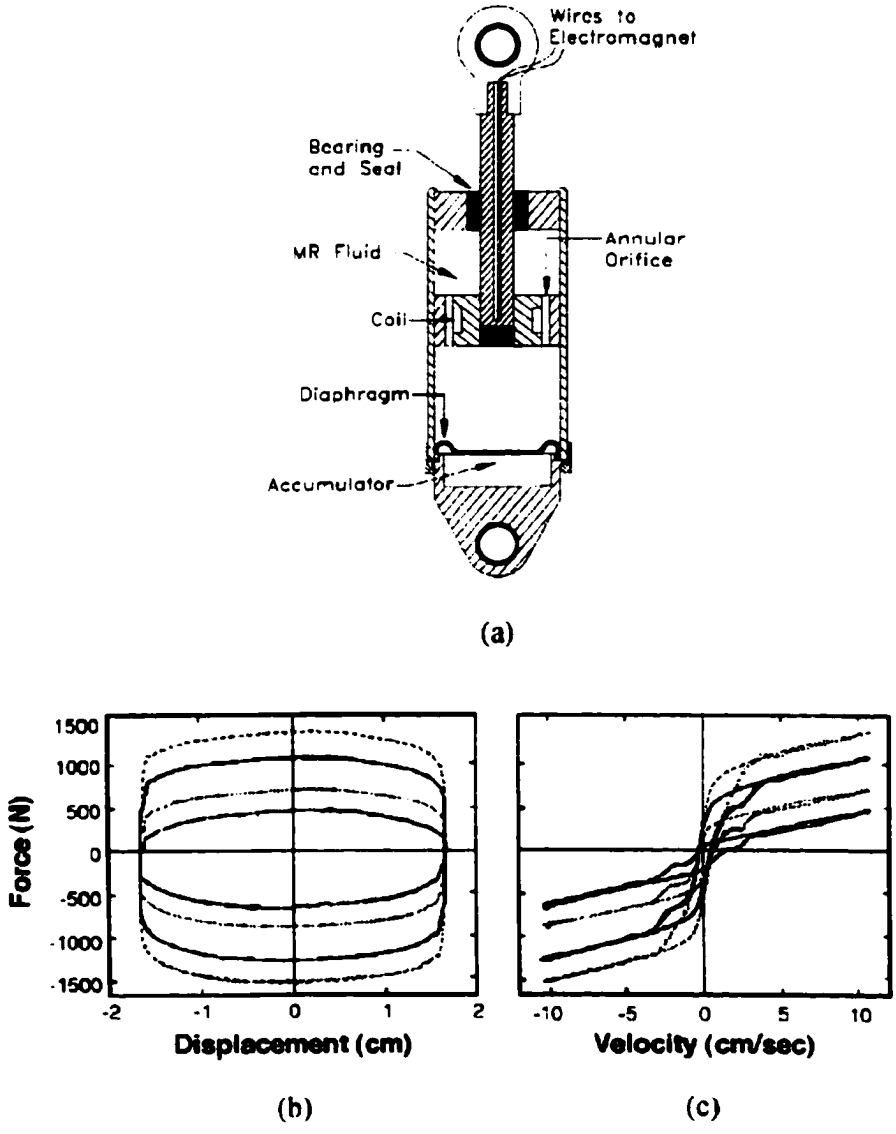

Figure 2-6: Semi-active Magnetorheological damper tested by Spencer (1997). (a): Schematic diagram of the damper. (b) & (c): Hysteresis loops of the damper for four different magnetic fields strengths and subjected to harmonic motion at a frequency of 2.5 Hz and an amplitude of 1.5cm.

stiffness devices are engaged or released so as to include or not include, respectively, the stiffness of the bracing system of the structure. A schematic diagram of the semi-active stiffness device in a chevron bracing arrangement is shown in Figure 2-7(a). The device is composed of a balanced (double-acting piston rod) hydraulic cylinder with a normally closed solenoid control valve inserted in the tube connecting the two cylinder chambers. The solenoid valve can either be on or off, thus opening or closing, respectively, the fluid flow path through the tube. When the valve is closed, the fluid can't flow and effectively locks the beam to the braces below. In contrast, when the valve is open the fluid flows freely and disengages the beam/brace connection. The operation of each device consumes approximately 20 W of power. The system may be regarded as fail-safe in the sense that the interruption of power causes the semi-active stiffness devices to automatically engage, thus increasing the stiffness of the structure.

Semi-active stiffness control devices have been installed within the chevron bracing [see Figure 2-7(b)] of a full-scale three-story steel structure in Tokyo, Japan (Kobori et al. 1993). Three different stiffness configurations are utilized: (1) braces unlocked, (2) braces locked in first story only, and (3) braces locked in all stories [see Figure 2-7(b)]. The first mode natural frequency with the braces unlocked and locked in all stories is about 1.0 Hz and 2.5 Hz, respectively. A control algorithm was developed which utilizes feed-forward information from the measured acceleration at the base of the structure. A motion analyzer uses the measured acceleration to estimate the response of the structure with the three different stiffness configurations. At each time step in the

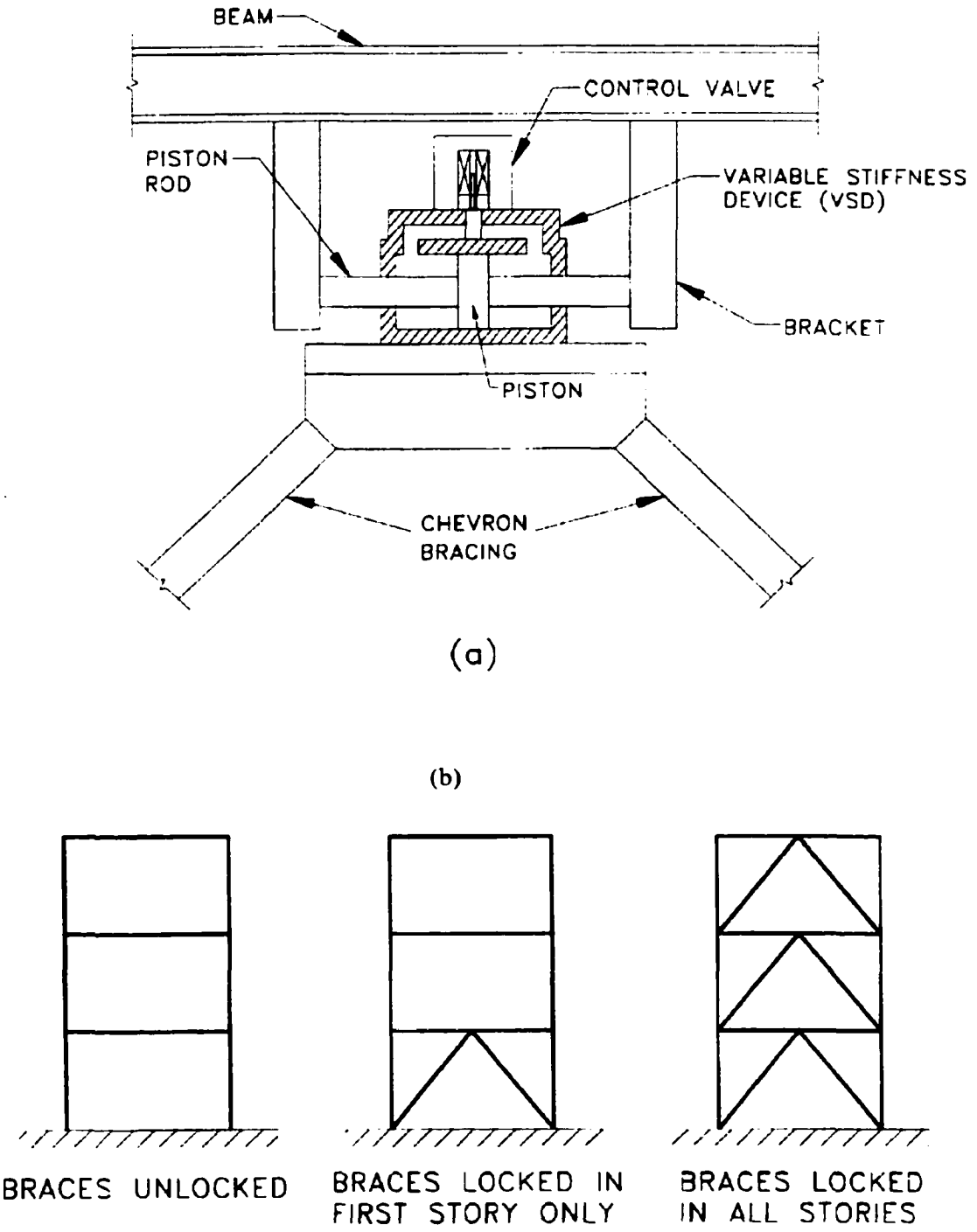

Figure 2-7: Semi-active Stiffness damper tested by Kabori (1993). (a) Installation detail. (b) Configurations within full-scale test structure.

analysis, the stiffness configuration which gives the least response is determined and appropriate command signals are sent to the stiffness control devices.

The stiffness damper proposed by Kobori et al. (1993) is usually termed as Active Variable Stiffness (AVS) damper. Further studies on active variable stiffness damper were conducted by Yamada and Kobori (1995) and Nasu et al. (2001). It is noted that variable stiffness is achieved by altering additional stiffness through an on/off switch. Discontinuous modifications of stiffness will increase acceleration and excite higher modes. In order to alleviate this problem, Yang et al (1999, 2000a,e), Agrawal and Yang (2000a,b) modified stiffness in a continuous fashion as shown in Figure 2-8. This semi-active stiffness damper consists of a cylinder-piston system with an on-off valve in the by-pass pipes connecting two sides of the cylinder as The stiffness damper can also be operated either in switching mode or resetting mode, termed as switching semi-active stiffness damper (SSASD) or resetting semi-active stiffness damper (RSASD), respectively.

The performance of the RSASD for models of fixed-base linear and nonlinear buildings has been investigated by Yang et al. (1999, 2000a). Agrawal and Yang (2000a,b) have investigated the performance of the RSASD for a base-isolated building subject to near-field earthquakes. Agrawal and He (2000) have investigated the application of the damper to a 20-story nonlinear benchmark building model developed by Ohtori et al. (2000). More recently, He et al. (2001) show the semi-active stiffness damper that is capable of control of the benchmark cable-stayed bridge developed by Dyke et al (2000). Numerical simulation results have demonstrated that the RSASD is effective in reducing peak dynamic response quantities of various structural systems

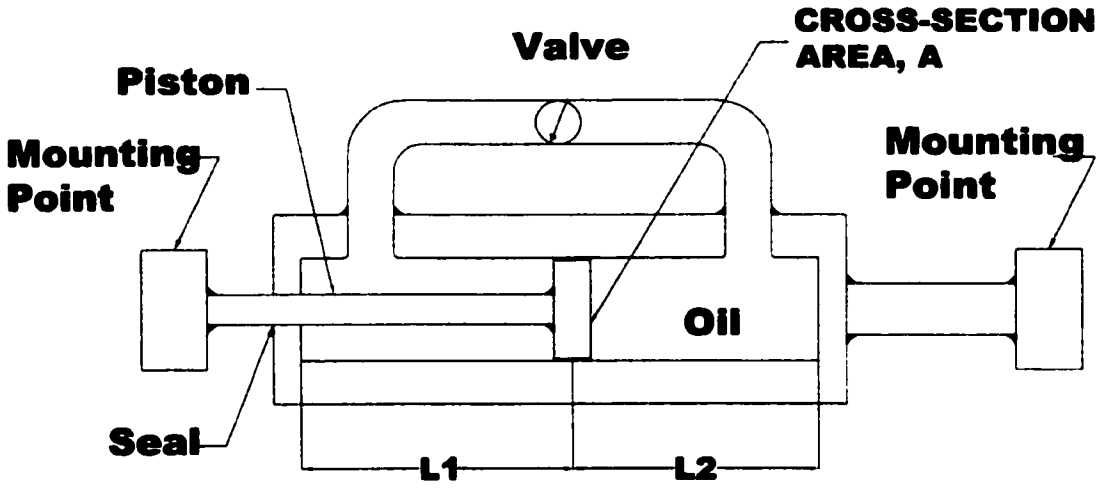

Figure 2-8: Schematic resetting semi- active stiffness damper (RSASD).

investigated in above-mentioned references.

2.4.4 Variable Friction Dampers

Various semi-active devices have been proposed that utilize forces generated by friction force to dissipate vibratory energy in a structural system. Akbay and Aktan (1991, 1995) proposed a variable-friction device that consists of a friction shaft that is rigidly connected to the structural bracing. The force at the frictional interface was adjusted by allowing slippage in controlled amounts. A similar device was considered at the University of British Columbia (Dowdell and Cherry 1994). Through analytical studies, the ability of these semi-active devices to reduce the inter-story drifts of a seismically excited structure was investigated (Dowdell and Cherry 1994).

An ideal friction damper may be considered to behave as a Coulomb element wherein the force output, F, is given by

$$F = \mu N \operatorname{sgn}(\dot{x}) \tag{2-3}$$

where μ is the coefficient of friction, N is the normal force at the friction interface and $\dot{x}$ is the velocity of motion. The hysteresis loop of the idealized friction damper subjected to harmonic motion is as shown in Figure 2-9. As the normal force of a semi-active friction damper is increased, the force–displacement hysteresis loop shown in Figure 2-9 expands in the vertical direction. Thus, the amount of energy dissipated per cycle of harmonic motion is controlled by the normal force of the semi-active friction damper.

Recently, a new type of semi-active friction damper, referred to as the semi active electromagnetic friction damper (SAEMFD), has been proposed by Agrawal and Yang (2000a,b) as shown in Figure 2-10. This device is based on regulation the friction force across the damper using an electromagnetic field. In this device, the normal force across the plates can be varied simply by regulating the electric current in solenoids across the

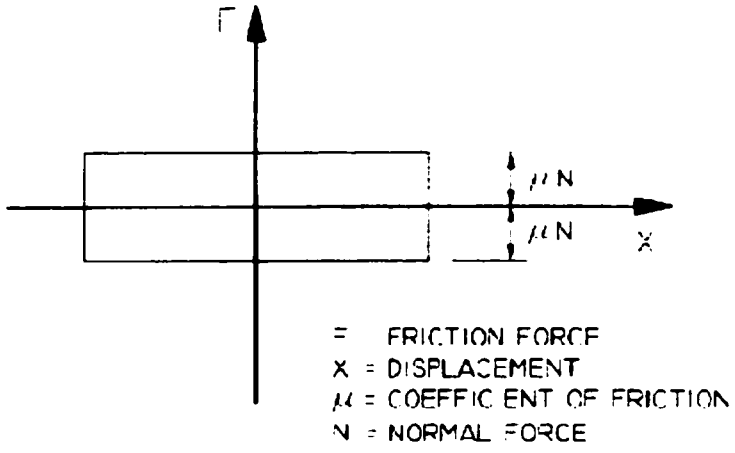

Figure 2-9: Hysteresis loop of idealized Coulomb friction damper

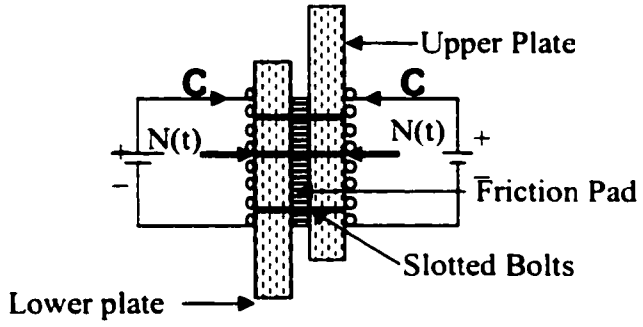

Figure 2-10: Schematic of the Semi-Active Electro-Magnetic Friction Damper proposed by Agrawal and Yang (2000a,b).

damper without any significant time-delay. The application of such devices to both base-isolated building and fix-based building is investigated by He et al. (2002).

2.5 Hybrid Control Systems

Hybrid control system consists of a combination of passive, active and semi-active control systems. One particular type of hybrid control systems, consisting of a passive base isolation system (either rubber-bearing isolators or sliding-bearing isolators) and active or passive control devices, has been found to be very effective for protecting structures subject to strong earthquakes. Early works in this subject can be found in [e.g., Reinhorn et al (1987), Yang et al (1991; 1992a, b; 1993; 1994a, c, d), Nagarajaiah et al (1993)]. Since the behavior of base isolation systems is either hysteretic or nonlinear, the hybrid control systems above involve control of nonlinear or hysteretic structures. Hence, different control theories have been used, for instance, dynamic linearization [Yang et al (1994d)], sliding mode control [e.g., Yang et al (1994e; 1995b, c; 1996b)], polynomial control [e.g., Yang et al (1996c)], fuzzy control [e.g., Nagarajaiah et al (1994), Symans and Kelly (1999)], and others [e.g., Nagarajaiah et al (1993)]. Semi-active control systems have also been used in the particular hybrid control systems mentioned above (i.e., along with base isolation systems), which are sometime referred to as smart (or intelligent) isolation systems [e.g., Johnson et al (1998), Yang et al (1994a, f; 1995c), Makris (1997), Symans and Kelly (1999), Yoshida et al (1999), Sahasrabudhe and Nagarajaiah (2000a, b; 2001), Nagarajaiah et al (2000a), Ramallo et al (2000a, b), Agrawal and Yang (2000a, b), Yang and Agrawal (2000c, e), Spencer et al (2000)]. This type of hybrid control systems has been shown to be effective for near-field earthquakes

[e.g., Nagarajaiah et al (2000a), Sahasrabudhe and Nagarajaiah (2000a, b), Yang and Agrawal (2000c, e; 2002b)].

2.6 Summary

In this chapter, recent development and application of various control systems have been evaluated. Passive energy dissipation devices have been successfully implemented in buildings around the world to protect structures from earthquake, wind or other dynamic loading. The main drawback of passive energy dissipation system is its inadaptability to external excitations. A passive control system designed for one ground motions may exhibit poor performance for other ground motions with different characteristic. On the other hand, active system has wider ranges of adaptability for controlling the dynamic response of structures. However, the required power source to generate of control forces is so large that it is hard to be implemented practically, since power supply required for the control system is usually interrupted or shut down during strong earthquakes. A compromise between passive and active seismic response control system is the semi-active control system, which is capable of achieving the same adaptability of active control devices while only requiring a very lower power source, which can be operated on battery power. These devices can be manufactured in large-scale to achieve full-scale structural control (Spencer et al. 1997b). The peak control force can be generated by ER damper is 445 KN (Makris 1997), and that of MR damper is 200 KN (Spencer et al. 1997). However, the major problem of ER damper and MR damper is the thermal expansion of the fluid due to thermal energy transferred from mechanical energy of the controlled structure, which prohibits the practical application of ER and MR damper. Thus, it is desired to develop new device or to explore new control

strategy using the existing control devices, which makes the mission of this research necessary and critical.

CHAPTER 3

ANALYTICAL MODEL FOR NEAR-FIELD GROUND MOTIONS

3.1 Introduction

Near-field (NF) ground motions are earthquake ground motions measured in the vicinity of an earthquake fault and they are responsible for causing extensive damages to structures during recent earthquakes, e.g., Northridge Earthquake in 1994, Kobe earthquake in 1995, Turkey earthquake in 1999 and Chi-Chi earthquake (Taiwan) in 1999. These ground motions are characterized by long-period pulses with high peak ground velocities and are being investigated intensively recently. The first seismological evidence of the near-field phenomenon was reported by Benioff (1955) in his explanation of the intensity patterns observed in 1952 Kern County, California earthquake. He showed that the propagation of fault rupture as a moving source could lead to different types of ground motions at opposite ends of the ruptured area, with larger intensities of higher frequency in the direction of propagation and smaller intensities and lower frequencies at the opposite end [Singh (1985)]. He also demonstrated the kinematics of moving radiation source along a straight line and its effect on the shapes. The peculiar structural response in the vicinity of seismic source, e.g., fling effect, was pointed out by Mahin et al. (1976) and Bertero et al. (1978) after the 1971 San Fernando earthquake. They found that the damage in the building of the Olive View Medical Center was the result of only a few large displacement excursions in the earthquake ground motion rather than a large number of oscillations, as in ordinary earthquake ground motions. They also concluded that short period structures designed according to code requirements could

experience large ductility demands when subject to near-field ground motions, and thus special design precautions should be taken for structures located near active faults.

After the 1979 Imperial Valley earthquake, Anderson and Bertero (1987) reported the sensitivity of inelastic near-field structural response and the fundamental period of structures with respect to the period of the velocity pulse contained in the near-field record. They emphasized the importance of directivity effects associated with the direction of rupture propagation.

Near-field effects received much recognition as a result of tremendous structural damages during the 1994 Northridge earthquake, 1995 Kobe earthquake and 1999 Chi-Chi earthquake. Malhotra (1999) studied the response characteristic of near-field pulse-like ground motions and showed that ground motions with high PGV/PGA ratio have wide acceleration-sensitive regions in their response spectra, which increase the base shear, inter-story drift and ductility demand of high-rise buildings. Liao et al. (2001) compared the dynamic behavior of reinforced concrete buildings subject to near-field and far-field ground motions. Their results indicate that the long-period responses in the response spectrum, PGV/PGA ratio and velocity pulse duration of near-field ground motions are higher than those of far-field ground motions. MacRae et al. (2001) investigated the near-field ground motion effects on simple structures. Their results showed that the inelastic demands of medium and longer period oscillators responding to the near-field strike-normal shaking increased for sites close to the fault as the distance along the fault from the epicenter increased. The inelastic response of short-period oscillators was not affected as much by the near-field shaking. Chopra and Chintanapakdee (2001) compared the response of single-degree-of-freedom (SDOF)

systems subject to near-field and far-field ground motions in the context of spectral regions. A systematic study was conducted by Alavi and Krawinkler (2001) to investigate the effect of near-field ground motions on frame structures. Several of these studies have shown that near-field ground motions, usually characterized by a long period pulse-like motion in the velocity time history, are particularly destructive for long period structures because of their large displacement demands. These indications challenge the concept of seismic base isolation, which is one of the most widely accepted and implemented seismic protective systems, since base-isolated structures are inherently flexible.

As a result, some researchers [e.g. Hall et al. (1995)] have raised concerns as to the efficacy of seismic isolation systems subject to near-field ground motions. Their results show that the displacement across the isolators due to the long period components of near-field ground motions may be much larger than that recommended by the 1997 Uniform Building Code. Hence, several researchers have investigated the use of smart protective systems for the protection of flexible structures from such ground motions. Kelly (1999) challenged the adequacy of sufficient damping in the seismic isolation buildings for protecting structures from near-field ground motions. Jangid and Kelly (2001), and Rao and Jangid (2001) investigated various types of dampers to reduce the peak drift of rubber-bearing isolators of base-isolated buildings subject to near-field ground motions, and suggested the use friction dampers as the most effective protective system. Yang and Agrawal (2002b) and He et al. (2002) proposed semi-active friction dampers to reduce peak drift of rubber-bearing isolators of base-isolated buildings subject to strong near-field ground motions. Recent studies [e.g., Makris (1997); Makris and Chang (1998, 2000a,b); Yang and Agrawal (2002b); Agrawal and Yang (2000a,b); He et

al. (2002); Chen and Chen (2000, 2001); Sahasrabudhe and Nagarajaiah (2000a, b; 2001); Nagarajaiah et al (2000a,b)] have shown that viscous dampers combined with friction dampers, or other semi-active control devices, are effective in suppressing undesirable large displacement of base isolated buildings.

In the research described above, effects of near-field ground motions on flexible structures have been investigated by using various earthquake ground motions recorded during Northridge, Kobe, Chi-Chi and other near-field earthquakes. Although this type of investigation confirms the destructive effects of near-field earthquakes on flexible structures and the effectiveness of smart (passive and semi-active) damping systems in reducing the dynamic response quantities of structures, a systematic study cannot be carried out using a few earthquake records. In this chapter, the mechanism of generating of the long period pulses in the near-field ground motion is briefly introduced. An analytical model for velocity pulses capable of capturing kinematics properties of near-field ground motions is proposed next. The verification of the proposed analytical model for near-field ground motions is presented in Chapter 3.5, 3.6 and 3.7. The properties of the proposed model are discussed in Chapter 3.8. In Chapter 3.9, the closed form solution of a SDOF structure subject to the proposed analytical model is obtained, and the properties of the closed form solutions for two special cases are also discussed. The issues associated with the near-field effect with respect to the current seismic design codes are discussed in Chapter 3.10.

3.2 Long-Period Pulses in Near-field Ground Motions

Long period pulses have been observed and identified in recent near-field earthquakes, i.e. Landers (1992), Northridge (1994), Kobe (1995) and Chi-Chi (1999). These long period pulses are produced either due to directivity or fling effects (Abrahamson, 2001). Long period pulses in near-field ground motions are strongly influenced by the orientation of the fault, the direction of the slip on the fault and the location of the recording station relative to the fault, which is referred to 'directivity effect' due to the propagation of the rupture towards the recording site. The effect of rupture directivity usually causes a large and long period pulse in the direction normal to the fault. The conditions required for the generation of this pulse are met when the direction of the SH radiation pattern is maximum in the slip direction and the direction of the rupture propagation coincide, which is automatically satisfied in strike-slip faults as illustrated in the left side of Figure 3-1 (Somerville and Graves, 1993). In contrast, the SV radiation has a minimum in the direction along the strike resulting in a smaller ground motion parallel to the fault. However, there may be a large static displacement in this direction as shown in the right of Figure 3-1. The development of long period pulses in the ground motion recorded at the Lucerne Valley Station during 1992 Landers earthquake due to the directivity effect is shown in Figure 3-2 as an example.

Fling effect, on the other hand, results from tectonic deformation at the site and is related to the slip on the fault near the site [Abrahamson (2001)]. Brodsky and Kanamori (2001) applied the theory of mechanical lubrication developed by Sommerfeld (1950) for journal bearings to earthquake faulting. If a fault zone is thin and slightly rough, and if the material in the fault zone behaves like a viscous fluid, then as the displacement and

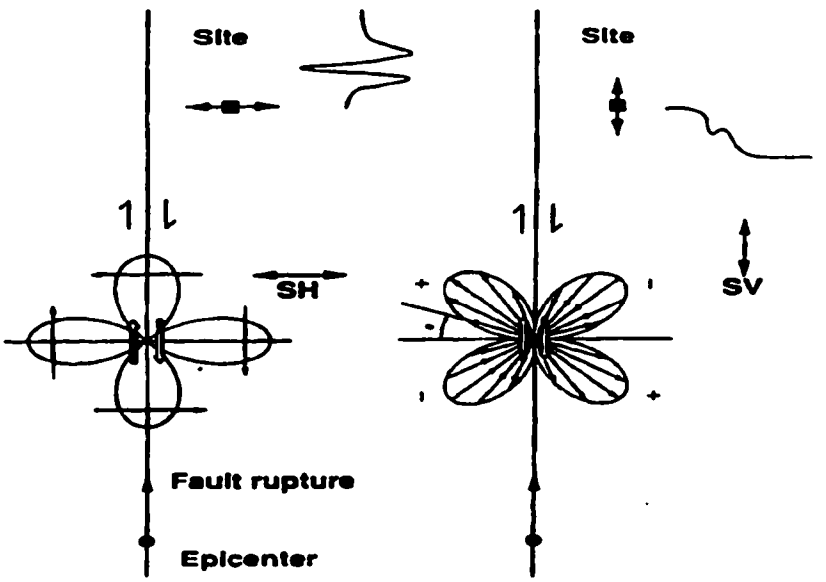

Figure 3-1: Schematic diagram of directivity effects for a vertical strike-slip fault (Somerville and Graves 1993).

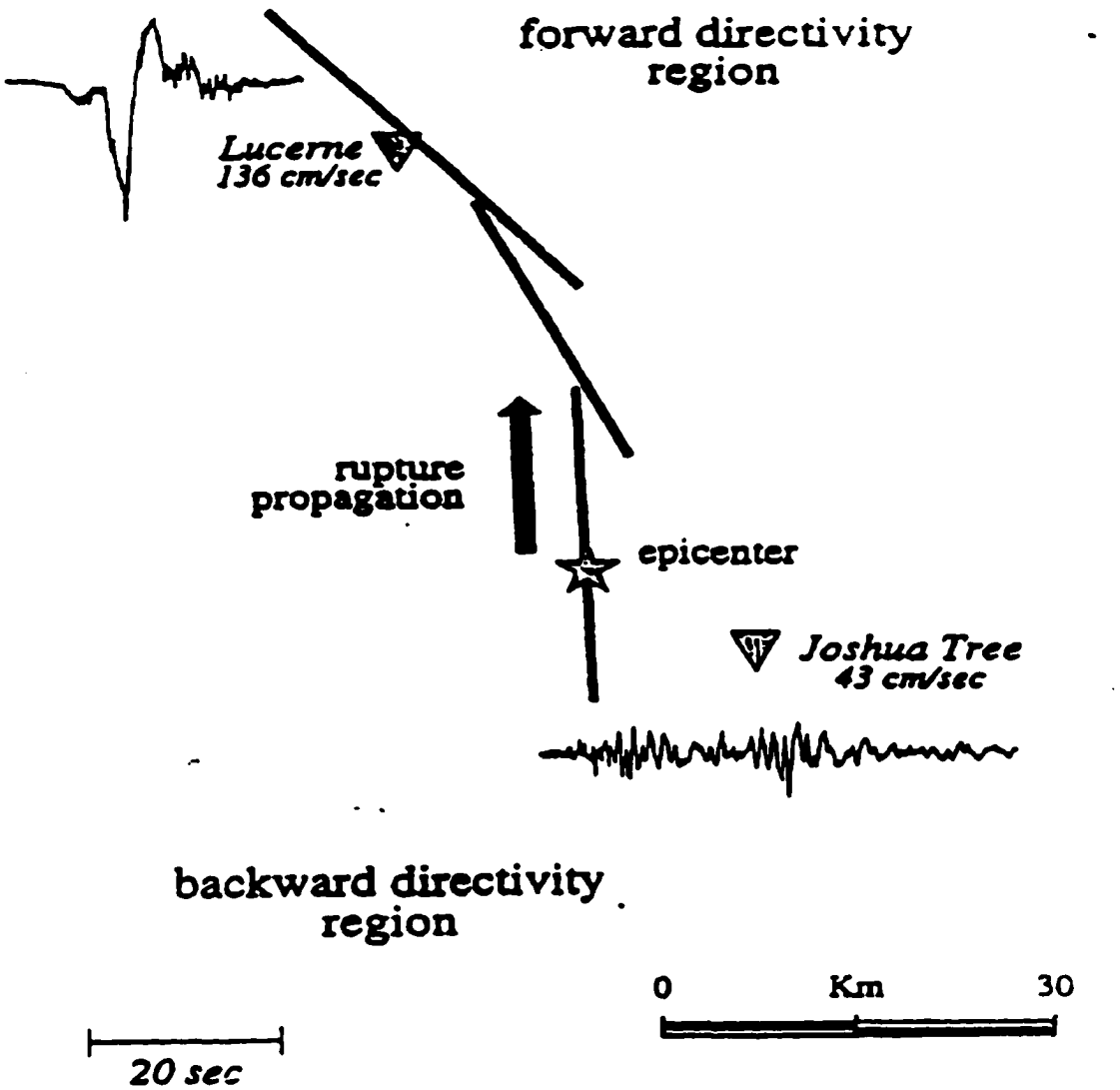

Figure 3-2: The development of long period pulse in Lucerne Valley record during 1992 Landers Earthquake due to directivity effect (Somerville and Graves 1993).

velocity of the fault motion increase, the fluid pressure within the fault zone rises. The increased pressure (i.e., lubrication pressure) reduces friction and increases the velocity of the fault motion. The lubrication pressure also elastically deforms the fault wall, widens the gap, and reduces the contact area between the asperities on the fault walls. This results in a reduction in high-frequency energy radiation produced by asperity collisions as shown in Figure 3-3. The long period pulses develop as the gap between the friction plate increases. The development of the long period pulses at TCU068NS station during 1999 Chi-Chi earthquake due to this mechanism is shown in Figure 3-4.

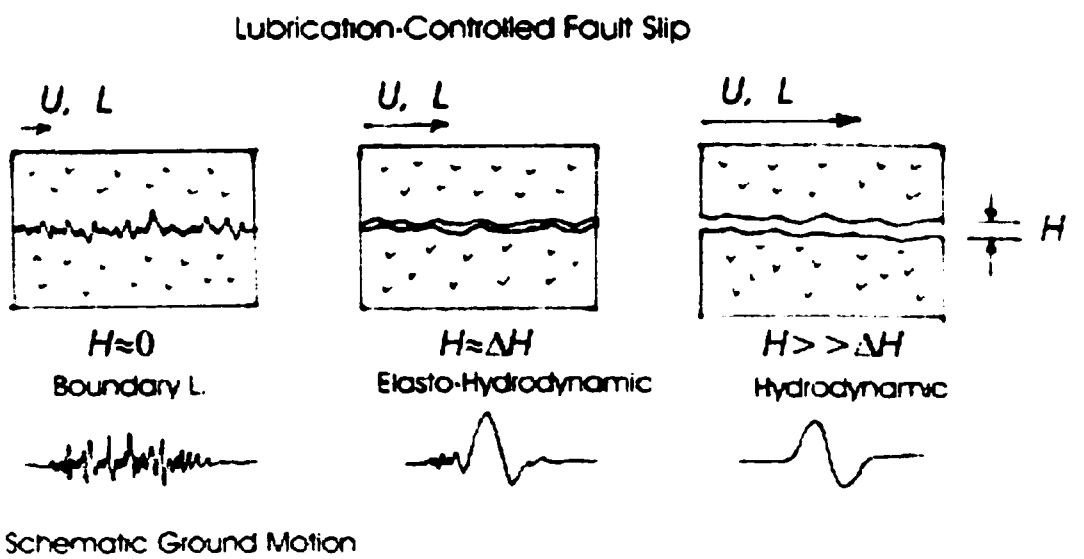

Figure 3-3: Mechanism of lubrication-controller fault slip theory (Brodsky and Kanamori, 2001).

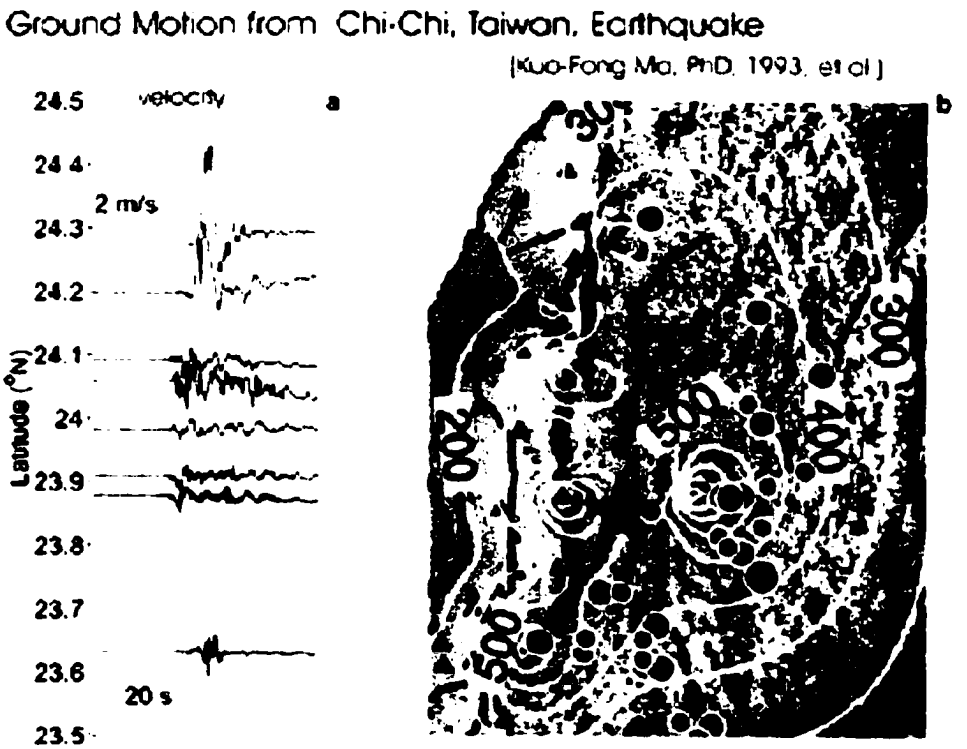

Figure 3-4: Development of long-period velocity pulses during 1999 Chi-Chi earthquake.

3.3 Existing Analytical Models for Near-field Ground Motions

Makris (1997) and Makris and Chang (1998) classified velocity pulses in near-field ground motions into three types of pulses; namely, type A pulse, type B pulse and type Cn pulses as represented by a unique set of closed-form tri-geometric functions as shown in Figure 3-5. Type A pulse is a forward ground motion; type-B is a cycloid pulse that approximates a forward-and-backward motion and a type Cn pulse approximates a ground motion pulse having n main pulses in its displacement time history. The formulations of these pulse types are presented in Makris and Chang (1998). The closed-form approximation of near-field ground motion pulses presented by Makris (1997), and Makris and Chang (1998, 2000a,b) is quite complicated since the three pulse types are modeled by three different sets of tri-geometric functions. To model a particular ground motion, only one set of tri-geometric function can be used. As a result, there are significant disagreements between recorded and modeled (closed-form) ground motion pulses, since recorded ground motion pulses don't fit well to any one type of A, B or Cn pulses exclusively. It has been observed that actual ground motion pulses are combinations of A, B or Cn pulses. Somerville (1998) developed a preliminary model that relates time domain parameters of the near-field ground motion pulses to the earthquake magnitude and distance. The pulse parameters used are the pulse period and the peak amplitude of the largest cycle of the velocity pulse. Alavi and Krawinkler (2001) analyzed a set of recorded pulses and classified these pulses as P1, P2 and P3 having 0.5, 1 and 2.5 cycles of motion, respectively. These pulses are similar to those proposed by Makris and Chang (1998). Abrahamson (2001) proposed to use a type A velocity to approximate the fling effect of near fault ground motions. However, these

models don't capture the kinematic characteristics of near-field ground velocity pulses realistically in order to conduct a systematic study on the effectiveness of various smart protective systems. In this study, an analytical model of the long period velocity pulse for the near-field ground motion is proposed. The efficiency of passive damping systems will be investigated using the proposed analytical model of near-field ground motions.

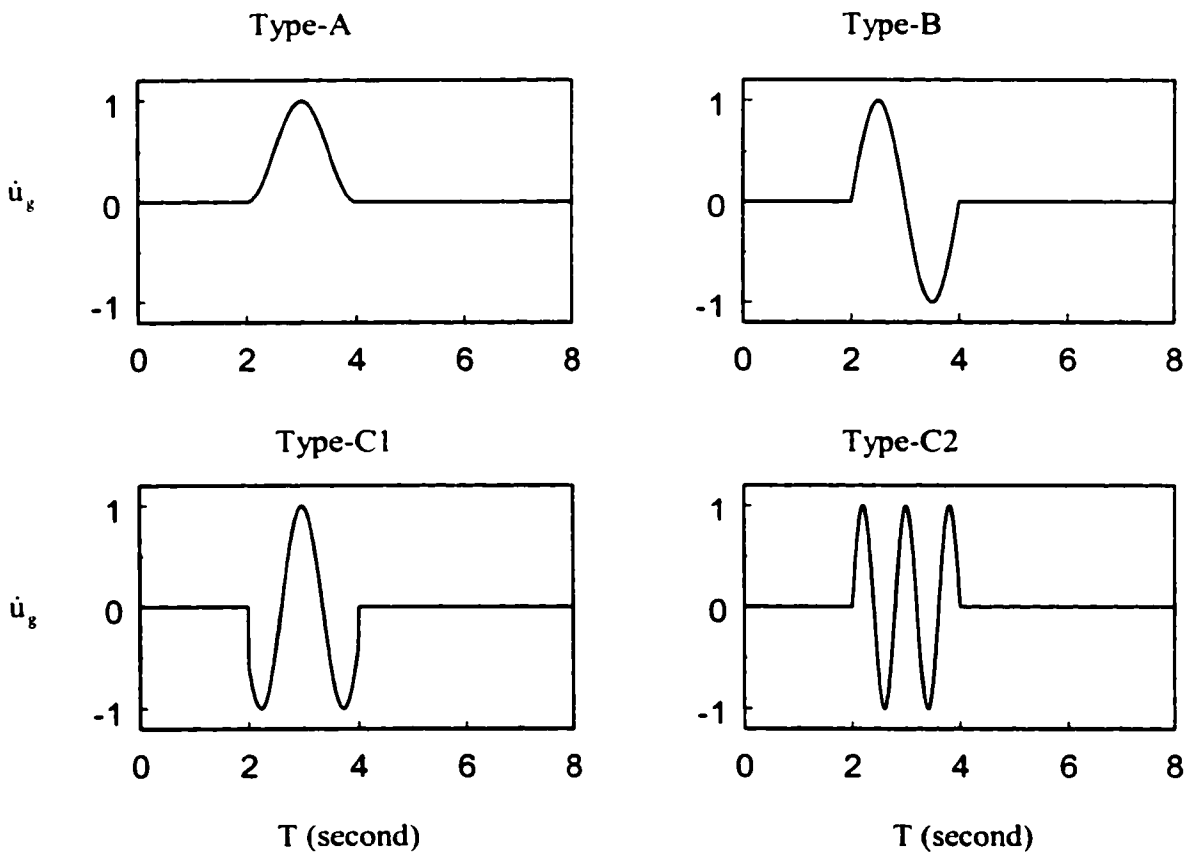

Figure 3-5: Near-field ground motion velocity pulse types A, B, C1 and C2 proposed by Makris (1997), Makris and Chang (1998, 2000).

3.4 Proposed Analytical Model for Near-field Ground Motions

Consider a near-field ground motions model in which the ground velocity pulse is modeled as:

$$\dot{u}_p(t) = C \cdot t^n e^{-at} \cdot \sin bt\,; \quad a = \zeta_p \omega_p;\ \ b = \omega_p \sqrt{1-\zeta_p^2} \tag{3-1}$$

In Equation (3-1), it is assumed that the velocity pulse is an enveloped sinusoidal function. The parameters a and n in Equation (3-1) determine the shape of the pulse envelop. The parameter ζ_p is the decaying factor, ω_p is the frequency and C is the amplitude constant of the pulse. Differentiating Equation (3-1), the acceleration $\ddot{u}_p$ of the pulse is obtained as

$$\ddot{u}_p(t) = C \cdot t^n e^{-at} \cdot \left[\left(\frac{n}{t} - a\right) \sin bt + b \cos bt \right] \tag{3-2}$$

The displacement u_p of the pulse can be obtained by integrating Equation (3-1). However, its explicit form is difficult to obtain if n is a real number. If n is an integer, the integration of Equation (3-1) is obtained as:

$$u_p(t) = C \cdot e^{-at} \sum_{r=0}^{n} \frac{(-1)^r n! t^{n-r}}{\rho^{r+1}(n-r)!} \sin[bt - (r+1)\alpha] + C \cdot \frac{(-1)^n n!}{\rho^{n+1}} \sin[(n+1)\alpha] \tag{3-3}$$

where ρ and α are given by

$$\rho = \sqrt{a^2 + b^2};\ \rho\cos\alpha = -a;\ \ \rho\sin\alpha = b \tag{3-4}$$

The displacement of ground motion u_p, Equation (3-3) can be rewritten as the following for the special case of n= 0 as,

$$u_p(t) = C \cdot \frac{-e^{-at}(a \sin bt + b \cos bt) + b}{a^2 + b^2} \tag{3-5a}$$

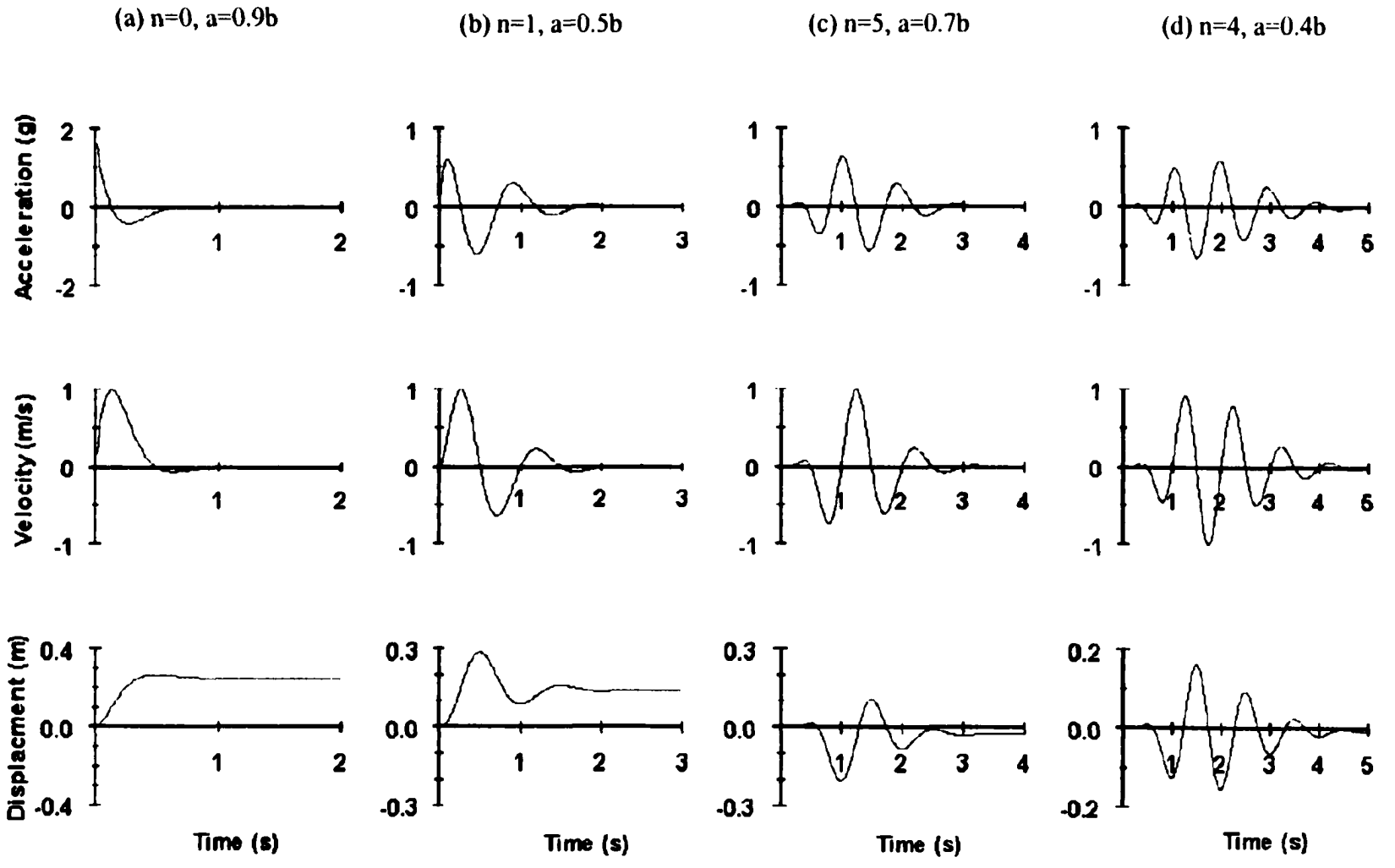

Figure 3-6: Acceleration, velocity and displacement time histories of proposed analytical pulse model for near-field ground motions with different shape parameters.

and for n = 1 as

$$u_p(t) = -\frac{C \cdot te^{-at}}{a^2 + b^2}(a\sin bt + b\cos bt) - \frac{C}{(a^2 + b^2)^2}\{e^{-at}[(a^2 - b^2)\sin bt + 2ab\cos bt] - 2ab\} \tag{3-5b}$$

The velocity pulse in Equation (3-1) can be defined in terms of the vector of parameters $\Theta = [C, n, a, b]$ as,

$$\dot{u}_p(t) = \dot{u}_p(t, \Theta) \tag{3-6}$$

In Equation (3-6), it is assumed that the starting time of velocity pulses is at t = 0. To obtain parameters for a particular ground motion, the starting time instant of the velocity pulse, t_0, should also be included in the vector of parameters, i.e., $\Theta = [C, n, a, b, t_0]$. To show the versatility of the proposed approach, ground velocity pulses generated by assuming different values of parameters n, a and b, and $t_0 = 0$, are shown in Figure 3-6. It is observed from Figure 3-6 that the proposed model is capable of generating various types of pulses observed in near-field ground motions. The parameter vector $\Theta = [C, n, a, b, t_0]$ for the proposed model can be obtained by a nonlinear regression to fit any specified ground motion as described in the following.

3.5 Recorded and Fitted Ground Motions

An estimated parameter vector Θ^* for the ground velocity model $\dot{u}_p(t, \Theta^*)$ that best fits a recorded ground velocity $\dot{u}_g(t)$ can be determined by a nonlinear regression. The estimated parameter vector Θ^* is the realization of Θ that minimizes the sum of squares of the difference between $\dot{u}_g(t_i)$ and $\dot{u}_p(t_i, \Theta)$ at discrete time instants t_i, i = 1, 2, 3, .., N,

$$S(\Theta) = \sum_{i=1}^{N}\left[\dot{u}_g(t_i) - \dot{u}_p(t_i;\Theta)\right]^2 \qquad (3\text{-}7)$$

where t_i, i=1,2,...,N are the times at which the recorded velocity time-history of the ground motion, $\dot{u}_g(t)$, is available. The minimization of $S(\Theta)$ in Equation (3-7) to obtain Θ^* can be accomplished by the Newton's method (Seber and Wild, 1989). Since the minimization of Equation (3-7) strongly depends on initial trial values of parameters, these initial values are determined as follows. The parameters b resembles the damped frequency of a single-degree-of-freedom system and it can be approximated as the predominant frequency, ω_g, of the recorded ground motion. An approximate value of parameter a can be assumed based on the number of cycles in the velocity pulse of the recorded ground motion. Other initial values for the parameters in Θ are set to be zero.

Using the minimization procedure described above, parameter vector Θ for the pulse velocity model in Equation (3-1) is have been obtained for 36 recorded ground motions around the world. The ground motions and the corresponding fitted model parameters are summarized in Table 3-1.

For the earthquakes presented in Table 3-1, it has been observed that the parameters a, b, n and C assume different values, depending on the pulse characteristics of the ground motion. In general, the pulse period, $T_p = 2\pi/\omega_p$, varies from 0.70 during 1989 Loma Prieta Earthquake to 8.90 seconds during the Chi-chi earthquake (TCU068W). The parameter b of the proposed pulse model is equivalent to the damped natural frequency of a SDOF system and the quantity $2\pi/b$ represents the damped natural period of the pulse model. Figure 3-7 shows the plot of $2\pi/b$ versus the

predominant period T_g of the recorded ground motion. The predominant period of the ground motion, T_g, is defined as the period at which the peak of the velocity response spectra for the recorded ground motion occurs. It is observed from Figure 3-7 that $2\pi/b$ is strongly correlated with T_g and general trend of the correlation suggests that $2\pi/b$ is almost equal to T_g. This strong correlation shows that the proposed velocity pulse model captures the period characteristics of recorded ground motions well.

Table 3-1: Recorded ground motions and fitted ground motion model parameters

Components	Events	C	n	a	b	t_0 (s)
TAB_LN	1978 Tabas, Mw=7.4, Tabas Station	-20.65	2.00	0.40	1.26	6.0
TAB_TR	1978 Tabas, Mw=7.4, Tabas Station	-36.65	1.97	0.40	1.26	6.0
KJM000	1995 Kobe, Mw=6.9, JMA Station	-190.00	2.00	1.10	6.00	6.5
KJM090	1995 Kobe, Mw=6.9, JMA Station	150.00	2.00	1.10	6.80	6.6
TAK000	1995 Kobe Earthquake, Mw=6.9, Takatori Station	-10.31	3.70	0.74	5.03	1.5
TAK090	1995 Kobe, Mw=6.9, Takatori Station	-90.70	1.00	0.54	5.25	2.0
RRS228	1994 Northridge, Mw=6.7, Rinaldi Receiving	-3200	2.8	3.5	6.00	1.6
RRS318	1994 Northridge, Mw=6.7, Rinaldi Receiving	-32.21	3.00	0.93	2.33	0.9
SYL090	1994 Northridge, Mw=6.7, Sylmar - Olive View	-18.29	4.00	1.09	2.73	1.0
SYL360	1994 Northridge, Mw=6.7, Sylmar - Olive View	432.06	3.20	2.02	3.03	2.3
LCN275	1992 Landers Earthquake, Mw=7.2, Lucerne Station	25.75	4.2	1.1	1.38	7.8
LCN000	1992 Landers Earthquake, Mw=7.2, Lucerne Station	17.44	4.20	1.34	1.59	6.3
ERZ_NS	1992 Erzincan, Turkey Mw=7.1, Duzce Station	70.57	5.00	1.80	2.75	0.6
ERZ_EW	1992 Erzincan, Turkey Mw=7.1, Duzce Station	-50.31	3.50	1.20	2.09	1.5

Table 3-1 (Continued)

PET000	1992 Cape Mendocino, Mw=7.0, Petrolia St.	-250.00	1.00	2.10	8.38	2.7
PET090	1992 Cape Mendocino, Mw=7.0, Petrolia Station	-112.88	4.90	2.00	2.71	0.5
LGP000	1989 Loma Prieta, Mw=6.9, LGPC station	-87.24	3.20	1.20	1.86	4.3
LGP090	1989 Loma Prieta, Mw=6.9, LGPC station	16.00	4.00	1.20	8.98	5.0
TCU68N	1999 Chi-Chi Earthquake, Mw=7.6, TCU068 Station	17.40	3.20	0.52	0.52	31.0
TCU68W	1999 Chi-Chi Earthquake, Mw=7.6, TCU068 Station	-66.65	1.97	0.40	0.58	32.0
TCU75N	1999 Chi-Chi Earthquake, Mw=7.6, TCU075 Station	9.20	1.00	0.10	1.00	23.0
TCU75W	1999 Chi-Chi Earthquake, Mw=7.6, TCU075 Station	96.95	3.20	1.18	1.14	26.0
TCU52N	1999 Chi-Chi Earthquake, Mw=7.6, TCU052 Station	13.21	3.00	0.49	0.63	30.0
TCU52W	1999 Chi-Chi Earthquake, Mw=7.6, TCU052 Station	-50.01	2.20	0.47	0.79	32.5
DZC180	1999 Duzce, Turkey Mw=7.1, Duzce Station	-40.25	1.20	0.33	1.09	2.9
DZC270	1999 Duzce, Turkey Mw=7.1, Duzce Station	58.50	1.20	0.34	1.14	3.3
CPM000	1992 Cape Mendocino, Mw=7.0, Cape Mendocino	80.64	4.50	1.50	1.53	0.3
CPM090	1992 Cape Mendocino, Mw=7.0, Cape Mendocino	-105.14	3.00	1.50	2.79	0.6
E06140	1979 Imperial valley, Mw=6.9, El Centro Array #6	90.17	3.00	1.20	2.24	4.0
E06230	1979 Imperial valley, Mw=6.9, El Centro Array #6	-80.40	3.50	1.20	1.86	3.0
E07140	1979 Imperial valley, Mw=6.9, El Centro Array #7	50.50	3.30	1.20	1.86	3.9
E07230	1979 Imperial valley, Mw=6.9, El Centro Array #7	-85.20	3.40	1.20	1.65	3.1
PTS225	1987 Superstitn Hills, Mw=6.7, Parachute Test Site	280.00	3.50	1.77	2.73	10.2
PTS315	1987 Superstitn Hills, Mw=6.7, Parachute Test Site	-88.00	2.50	1.20	2.06	10.8
SCS042	1994 Northridge, Mw=6.7, Sylmar – Converter	85.00	2.50	0.93	2.33	1.8
SCS142	1994 Northridge, Mw=6.7, Sylmar – Converter	-280	2.0	1.20	3.80	2.2

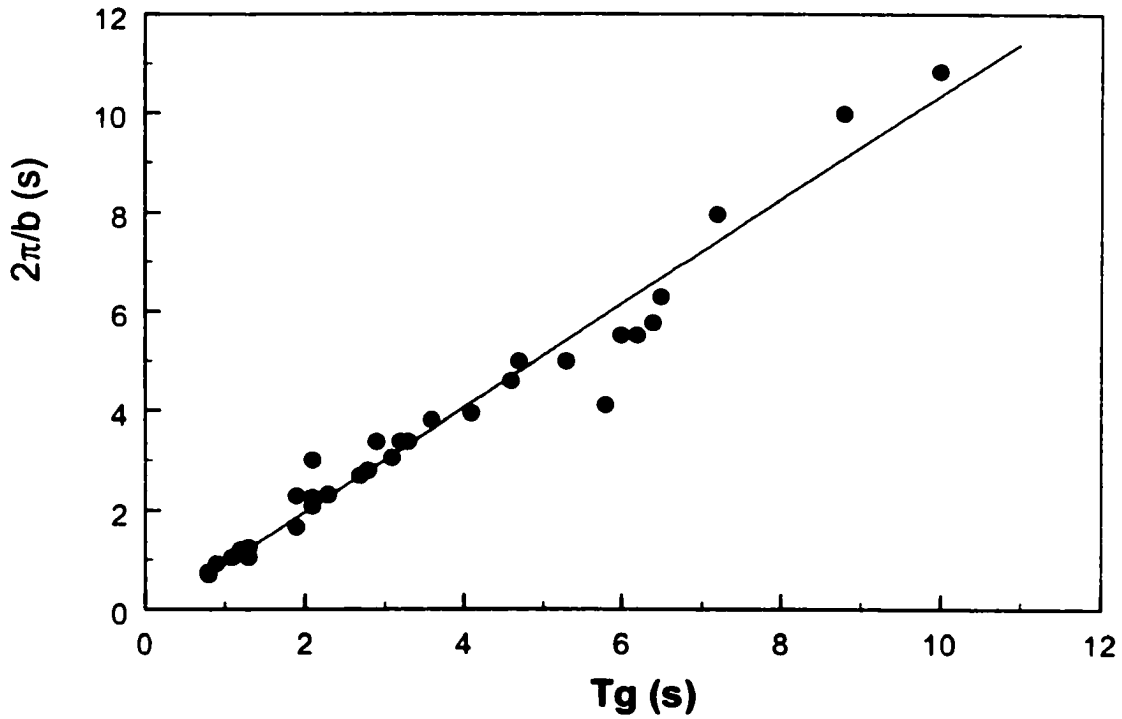

Figure 3-7: Parameter correlation of predominant period Tg and pulses approximation parameter b.

3.6 Examples of Recorded Ground Motions

Table 3-1 shows the parameters of the analytical pulse model for 36 recorded ground motions. To show the correlation of the analytical pulse model with those of recorded ground motions, displacement, velocity and acceleration time histories of ground motions at Rinaldi Receiving station (RRS228) during the Northridge (1994) earthquake, Lucerne Valley station during the 1992 Landers Earthquake (LCN275), El Centro Array # 6 during the 1979 Imperial Valley earthquake and TCU068N during the 1999 Chi-Chi earthquake are used in the following.

Example 1: Fault-normal components of 1994 Northridge earthquake at the Rinaldi station

Figure 3-8(a), (b) and (c) show plots of displacement, velocity and acceleration time-histories, respectively, of the fault-normal components of the Northridge earthquake recorded at the Rinaldi Receiving Station (RRS228) by thin solid curves. Because of a large positive and a smaller negative pulse in the velocity time-history, the ground motion resulted in a forward ground displacement that recovered partially and a permanent ground displacement after the earthquake. If the area under the negative velocity pulse were the same as the positive velocity pulse, the ground displacement would have recovered fully. It is obvious from the plot in Figure 3-8(b) that the velocity pulse in the fault normal component of the Rinaldi station record is neither a type A pulse nor a type B pulse of Makris and Chang (1998) as shown by dashed curves in Figure 3-8, since the recorded ground displacement has partially recovered at the end of the earthquake. Rather, the recorded ground motion is between type A (forward pulse) and type B pulses (forward-and-back pulse). It is also observed from Figure 3-8 that the recorded time

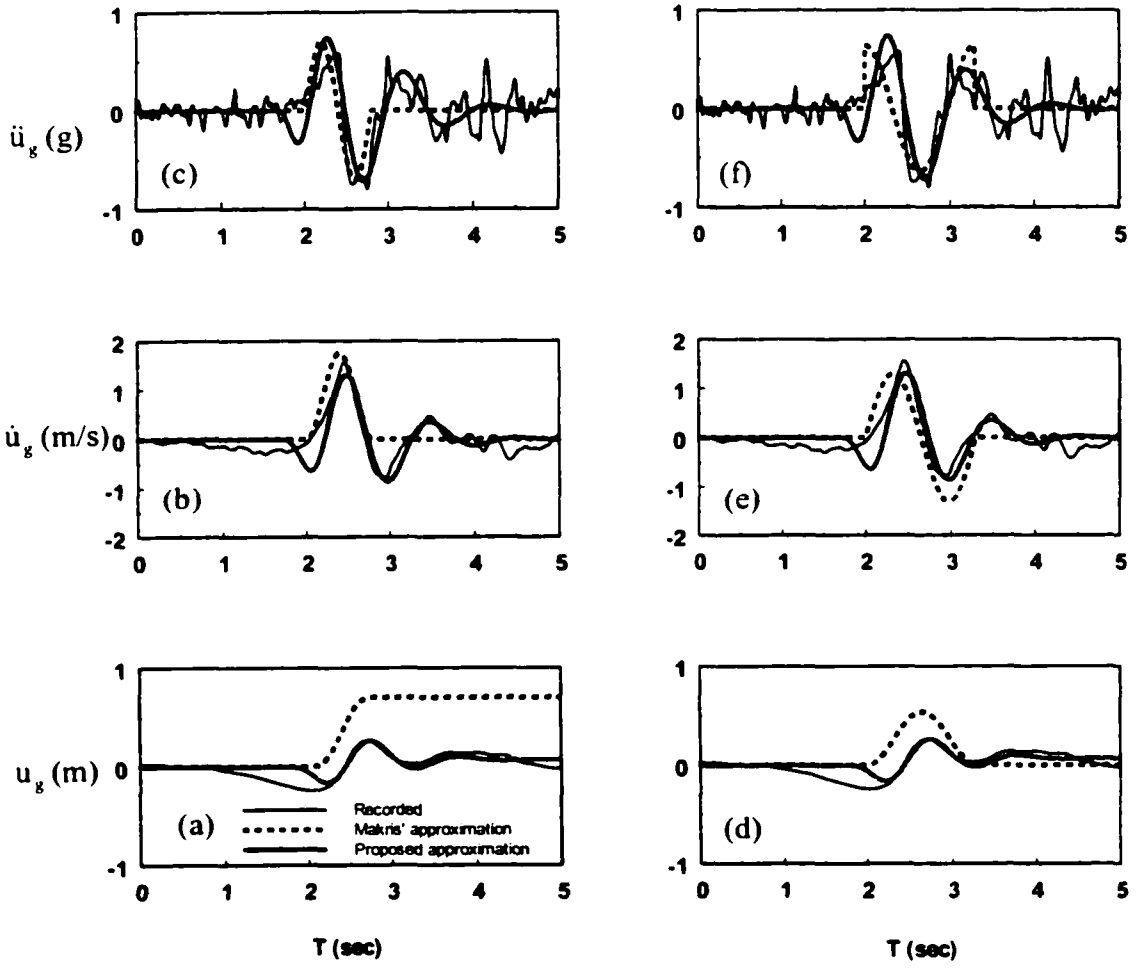

Figure 3-8: Fault normal components of the displacement, velocity and acceleration time histories at the Rinaldi station during the January 17th, 1994 Northridge Earthquake.

history of the ground velocity behaves like an enveloped decaying sinusoidal function. For this ground motion, parameters of the proposed analytical model in Equation (3-1) have been obtained through the least square minimization; with the results C=-3200, ω_p = 6.95 rad/sec (i.e., T_p= 0.90 sec.) n = 2.8 and ζ_p =50.4% (i.e., a=3.5 and b=6). Plots of displacement, velocity and acceleration of the analytical pulse model are shown by thick solid curves in Figure 3-8. A comparison of displacement, velocity and acceleration time-history plots in Figures 3-8(a)-(c) shows that the proposed analytical pulse model is a better representation of the kinematic characteristics of near-field pulses than Type A and Type B pulse models. Since the recorded velocity pulse is not exactly an enveloped decaying sinusoid, some disagreements with the recorded ground motion exist because of the random nature of earthquakes and the presence of high-frequency components. Since the proposed velocity pulse model has been developed primarily to optimize the parameters of energy dissipative systems for flexible structures, the response characteristics of these structures are not affected significantly by the high frequency components of recorded ground motions. This will be demonstrated later through the response spectra of recorded ground motions and the proposed pulse model.

Example 2: Fault normal components of the 1992 Landers, California earthquake

A situation similar to the Rinaldi component of the 1994 Northridge earthquake exists in the fault normal motion recorded at the Lucerne Valley station during the 1992 Landers Earthquake. Displacement, velocity and acceleration time-history plots of the recorded ground motion of this earthquake are shown in Figure 3-9(a)-(c), respectively, by a thin solid curve. It is observed from the velocity time-history in Figure 3-9(b) that a large positive pulse followed by a smaller negative pulse exists in the recorded ground

motion. The ground had a permanent displacement during this earthquake, as observed from Figure 3-9(a). If the area enclosed by the second positive pulse were the same as that enclosed by the negative pulse, the ground displacement would have fully recovered. Time history plots of pulses modeled as Type A and Type B are shown by dashed curves in Figure 3-9. The proposed analytical pulse model is applied to this earthquake with C=25.75 cm/s, ω_p = 1.76 rad/sec (T_p= 3.56 sec.), n = 4.2 and ζ_p =62.5% (i.e. a=1.1 and b=1.38) in Equations (3-1)~(3-3). Time-history plots of displacement, velocity and acceleration of the analytical pulse model for this earthquake are shown in Figure 3-9 by solid thick curves. It is observed from Figures 3-9 that neither type A pulse nor type B pulses are able to model the velocity and the displacement time-histories better then the proposed analytical pulse model. It is also observed that although the displacement and velocity histories using type-A pulse, type-B pulse and the proposed model represent the kinematics characteristic of the recorded motion, the peak ground acceleration using the these models is much smaller than the peak recorded value because of the presence of high frequency components.

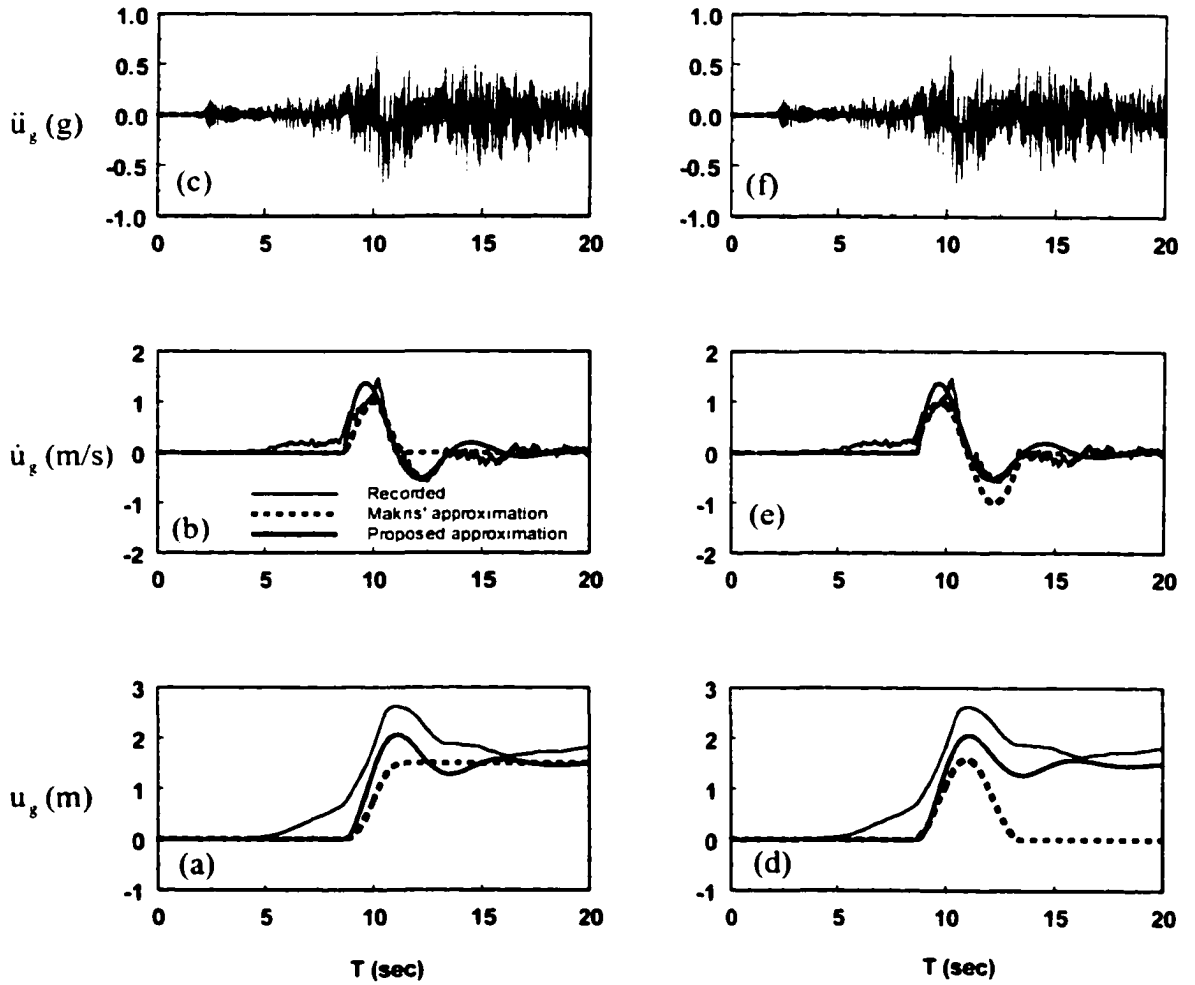

Figure 3-9: Fault normal components of the displacement, velocity and acceleration time histories recorded at the Lucerne Valley Station during the June 28th, 1992 Landers Earthquake.

Example 3: Fault-normal component of 1979 Imperial Valley earthquake at El Centro Station Array #6

Column (a) of the Figures 3-10 presents the time-history plots of acceleration, velocity and displacement of fault normal component of 1979 Imperial Valley earthquake measured at the El Centro Station Array # 6 as shown by the thin solid curves. It is observed that the ground displacement consists of one main long-period cycle, together with two small buildup and decaying half cycles. These long period pulses are even distinguishable in the ground acceleration time history where the high frequency components fluctuates around the long period pulses. Time-history plots of displacement, velocity and acceleration for the analytical pulse using the pulse parameters C=-80.4, n=3.5, a=1.2 and b=1.86 are shown by solid thick curves. It is observed that the plots for the analytical pulse match well with those of recorded ground motion for the main pulse, whereas the peak amplitude of other cycles is much smaller. For the situations where the peak amplitude of other minor cycles is significant compared to the main cycle, the analytical pulse model with a smaller value of ζ_p can model both the main and other significant cycles reasonably well.

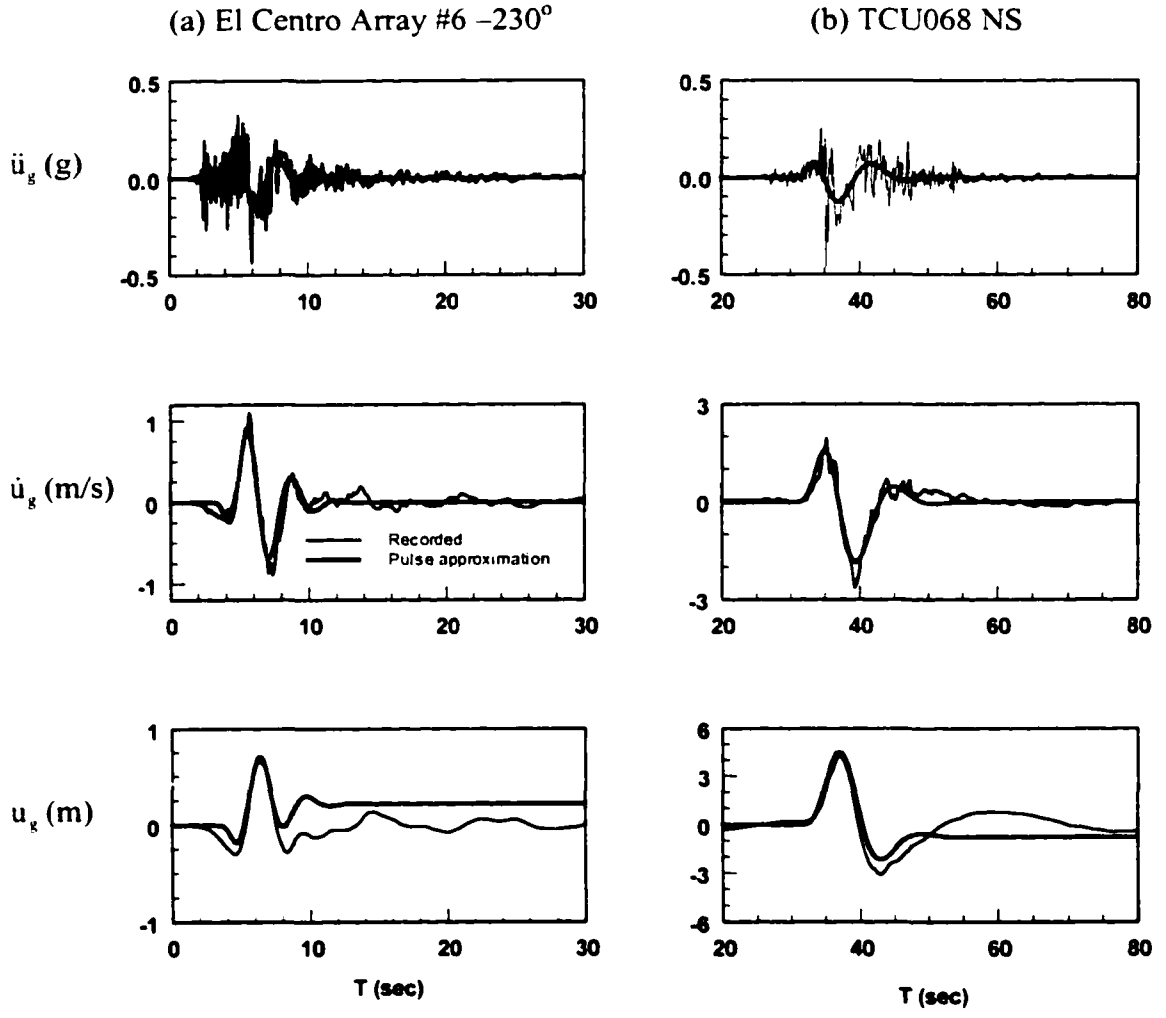

Figure 3-10: Acceleration, velocity and displacement time histories of recorded ground motions and pulse approximations: (a) E06230 recorded at El Centro Station Array #6 during the October 15, 1979 Imperial Valley earthquake; (b) NS component of TCU068 during September 20, 1999 Chi-Chi earthquake.

Example 4: North-South component of 1999 Chi-Chi earthquake at TCU068 station

Column (b) of Figure 3-10 shows the time-history plots of acceleration, velocity and displacement of north-south component of 1999 Chi-Chi earthquake measured at TCU068 station. Note that the PGV and PGD of this ground motion are the largest measured so far, which are 263.1 cm/s and 430 cm, respectively. The predominate period T_g of this record is 8.9 s. Similar to the previous examples, it is observed that long period pulses are even distinguishable in the ground acceleration time history, where the high frequency components fluctuates around the long period pulses. The pulse parameters C=22.0, n=3.2, a=0.52 and b=0.52 are capable of matching the long period pulse of this ground motion record to the analytical model, as shown in Column (b) of Figure 3-10.

Hence, the trajectory of the long period velocity pulses of ground motions can be captured well by the proposed analytical pulse model. The agreement between the proposed analytical model and the recorded ground motion is much better than those by Type A, B and Cn pulses. The shape of the long period pulses in the near-field ground motion depends on many factors, such as the topography of the earthquake area, the pattern of wave propagation, etc. A variety of the shapes of velocity pulses can be obtained by varying the parameters n and a. Since the proposed model only captures the dominant low frequency component and ignores the high frequency components, it underestimates the acceleration of the ground motion. Hence, the use of the proposed model for near-field ground motions may be reasonable only for long period structures, because high frequency components in the acceleration time history will have less effect on their response. This will be verified through the response spectra of the recorded ground motion and the pulse model in the following.

3.7 Response Verification

Numerical simulations are conducted to compare the dynamic responses of a SDOF oscillator subjected to the recorded ground motions and the proposed pulse model. Consider a single-degree-of-freedom (SDOF) structure subject to a horizontal ground motion $\ddot{u}_g$,

$$\ddot{x}(t) + 2\zeta\omega\dot{x}(t) + \omega^2 x = -\ddot{u}_g(t) \tag{3-8}$$

where ζ is the viscous damping ratio, ω is the natural frequency, $x(t)$ is the relative displacement of the oscillator, and $\ddot{u}_g(t)$ is ground motion acceleration. In order to justify the validity of the proposed pulse model for the near-field ground motion, the dynamic response of a SDOF oscillator subject to both the recorded ground motions and the analytical pulse model are investigated in the following.

The displacement, velocity, acceleration and input energy spectra for ground motions RRS228, LCU275, E06230 and TCU68N, as well as the corresponding analytical pulse model are plotted in Figure 3-11. In these figures, plots for recorded ground motions are indicated by thin solid curves and those for the proposed analytical model as denoted by the thick solid curves. It is observed that the spectra of the pulse model match well with that of the recorded ground motions, except for the acceleration spectra for short period structures. This is because the analytical model excludes the high frequency components of recorded ground motions. Further, the response of the long period structures depends mainly on the low frequency components in the ground motions, whereas the high frequency components affect the acceleration response of short period structures. For instance, the acceleration time history of LCU275 contains strong high frequency components as shown in Figure 3-9. These high-frequency components

are excluded in the analytical pulse model. As a result, the acceleration spectra of the recorded motions (thin solid curves) deviate from that of the pulse model (thick solid curves) for the short period structure. However, flexible structures will not be affected by the high frequency components as significantly as the short period structures. It is observed from the acceleration spectra that when the natural period of the structure T is greater than a certain value, the spectra of the proposed model agrees well with that of the recorded ground motions. Further, the value of T depends on the frequency of the velocity pulse. For example, the damper pulse period $2\pi/b$ for the 1994 Northridge earthquake recorded at the Rinaldi station is approximately 1.05 seconds. Hence, the acceleration spectra matches very well for $T > 1.5$ second for this earthquake. Also, the acceleration spectra for 1992 Landers Earthquake at the Lucerne Valley station matches well with that of for the proposed approximation for $T > 2.0$ sec because this ground motion contains distinct low frequency component with pulse period $2\pi/b = b=4.55$ seconds. Similarly, the acceleration spectra for E06230 and TCU68N using the analytical pulse model match very well with that of the recorded ground motions for $T > 4$ sec and $T > 10$ sec, respectively. The corresponding predominant damped pulse periods for these earthquakes are $2\pi/b = 3.38$ and 12.0 seconds, respectively. In addition to a good matching between the response spectra of recorded ground motions and that of the analytical pulse model, the displacement, velocity and input energy spectra of the pulse model have the same trend as the recorded ground motions. Consequently, the proposed pulse model can be used to investigate the response of structures and the performance of various damping systems for structures subject to near-field ground motions.

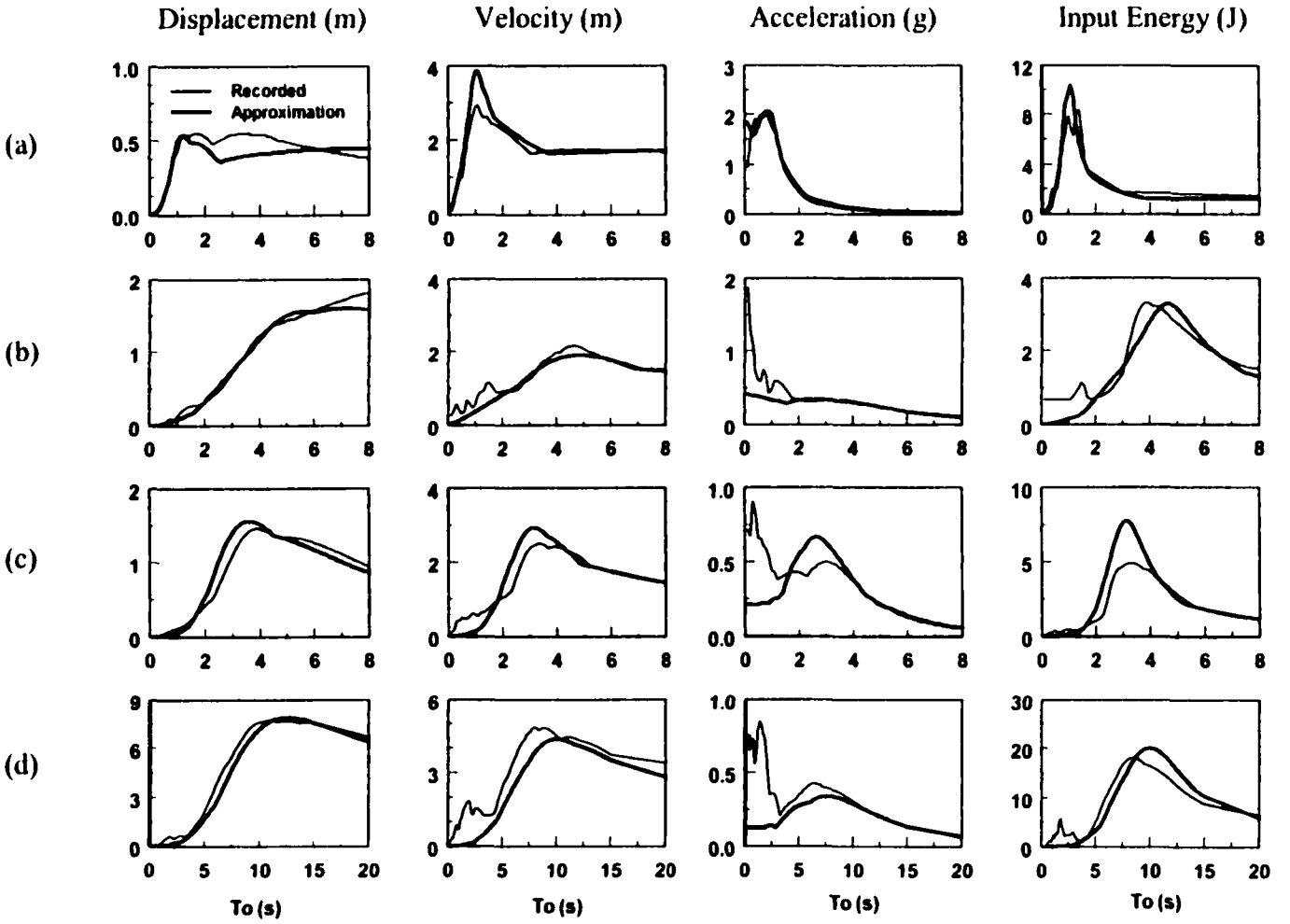

Figure 3-11: Response spectra of a SDOF structure subject to recorded ground motion and proposed approximation. Row (a): Fault normal component of Rinaldi Station record (1994 Northridge); Row (b): Fault normal component of Lucerne Valley Station record (1992 Landers earthquake); Row (c): Fault normal component of El Centro Station Array # 6 (1979 Imperial Valley earthquake); and (d): NS component of TCU68N (1999 Chi-Chi earthquake).

3.8 Properties of the Proposed Pulse Model

It is demonstrated in the previous sections that the proposed pulse model is capable of capturing the long period velocity pulses in the near-field ground motion. Before the response of structures subject to this velocity pulse is studied, it is worthwhile to investigate the properties of the pulse model. Different from the pulse models developed by other researchers, the proposed pulse model is a continuous function with a pulse buildup and decaying phases as shown in Figure 3-12. The shape of the pulse of the velocity time history is determined by the following envelop function

$$g(t) = t^n e^{-at} \tag{3-9}$$

where $a > 0$ and n are shape parameters which determine the shape of the envelop. For the special case in which n=0, Equation (3-9) represents an exponentially decaying function. Let's define

$$t_k = \frac{n}{a} = N \cdot T_p \; ; \; N = \frac{n}{2\pi\varsigma_p} \tag{3-10}$$

where t_k is the time instant when the function g(t) reaches its peak value and N is the number of cycles of the velocity pulse during the buildup phase. The parameter N determines the properties of the velocity pulse. Note that N = 0 represents the decaying sinusoidal velocity pulse of Equation (3-1) with n = 0.

It has been shown by various investigators [e.g., Manfredi (2001), Malhotra (1999), etc] that the peak ground acceleration (PGA), peak ground velocity (PGV), peak ground displacement (PGD) and their ratios, such as PGV/PGA and PGD/PGV, are important parameters for measuring the destructiveness of ground motions. PGV/PGA and PGD/PGV ratios are also used in the well-known Newmark-Hall spectra to define T_1

and T_2, which split the acceleration-sensitive, velocity sensitive and displacement sensitive regions. In this study, it is assumed that the proposed analytical pulse model approximates the low-frequency components in the near-field ground motion and it ignores the high frequency components. Hence, the PGA of the pulse model may be quite different than that of the recorded ground motions, since high frequency components fluctuate around long period pulses. However, these high-frequency components may have less effects on PGV and PGD. Nevertheless, it is worthwhile to discuss PGV/PGA and PGD/PGV ratios to understand some properties of near-field ground motions using the proposed analytical velocity pulse model. It is also pointed out that the peak velocities and displacements of recorded ground motions may be underestimated in some cases in the conventional processing of ground motion time histories, where additional corrections are applied to the displacement and velocity time histories to remove errors [e.g., Iwan and Chen (1994)].

For the proposed pulse model, PGV/PGA and PGD/PGV ratios are obtained through numerical calculations, since the explicit forms of PGA and PGD are difficult to derive, except for a special case, n=0 in Equation (3-5). Figure 3-13 shows the PGV/PGA and PGD/PGV ratios as a function of parameter N for various types of velocity pulses by selecting different values of parameters a and b in the pulse model in Equation (3-1). It is observed from Figure 3-13 that both PGV/PGA and PGD/PGV ratios depend on the number of cycles of velocity pulses in the buildup phase N and they are less sensitive to the decay parameter ζ_p (through parameters a and b). The ratio PGV/PGA converges to 1/b for N>0.5, which contains the important information about

the pulse period T_p, since $b = \omega_p\sqrt{1-\zeta_p^2} = \frac{2\pi}{T_p}\sqrt{1-\zeta_p^2}$. Hence, the relationship between the pulse period T_p and the PGV/PGA ratio can be expressed as

$$T_p = 2\pi\sqrt{1-\zeta_p^2}\cdot\frac{PGV}{PGA} \tag{3-11}$$

However, it is also observed from Figure 3-13 that the PGV/PGA ratio is less than 1/b if N<0.5, since the velocity pulse builds up abruptly and the corresponding PGA is relatively large. In such situations, the ground displacement is developed forward and recovered partially resulting in a permanent ground displacement after the earthquake. Consequently, the PGD/PGV ratio is greater than 1/b, as shown in Figure 3-13(b). Similarly, the PGV/PGA ratio converges to 1/b if the number of buildup cycles of velocity pulses, N, is greater than 1, since the forward displacement can be recovered fully only if the $N \geq 1$.

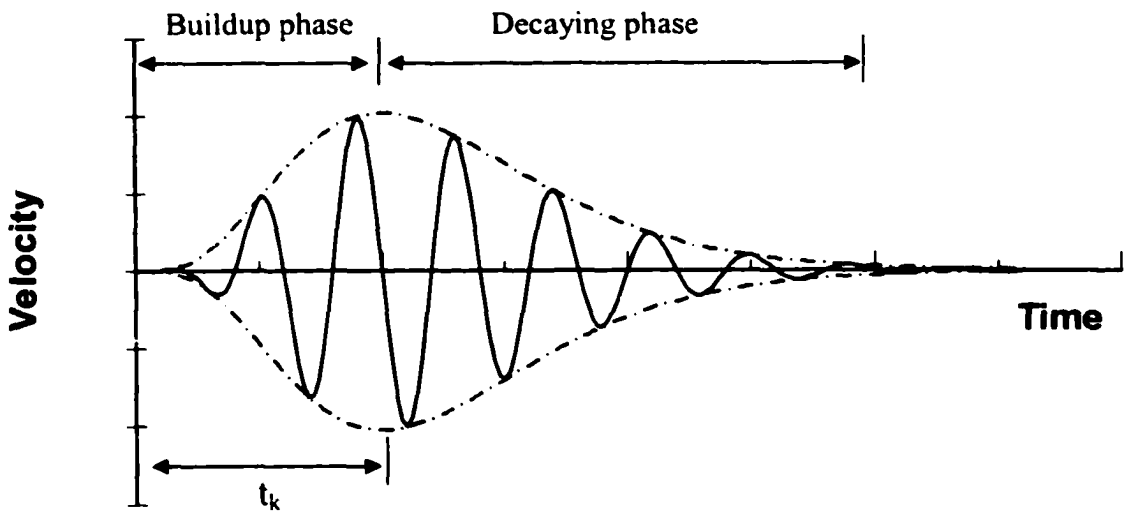

Figure 3-12: Velocity time history and envelop function

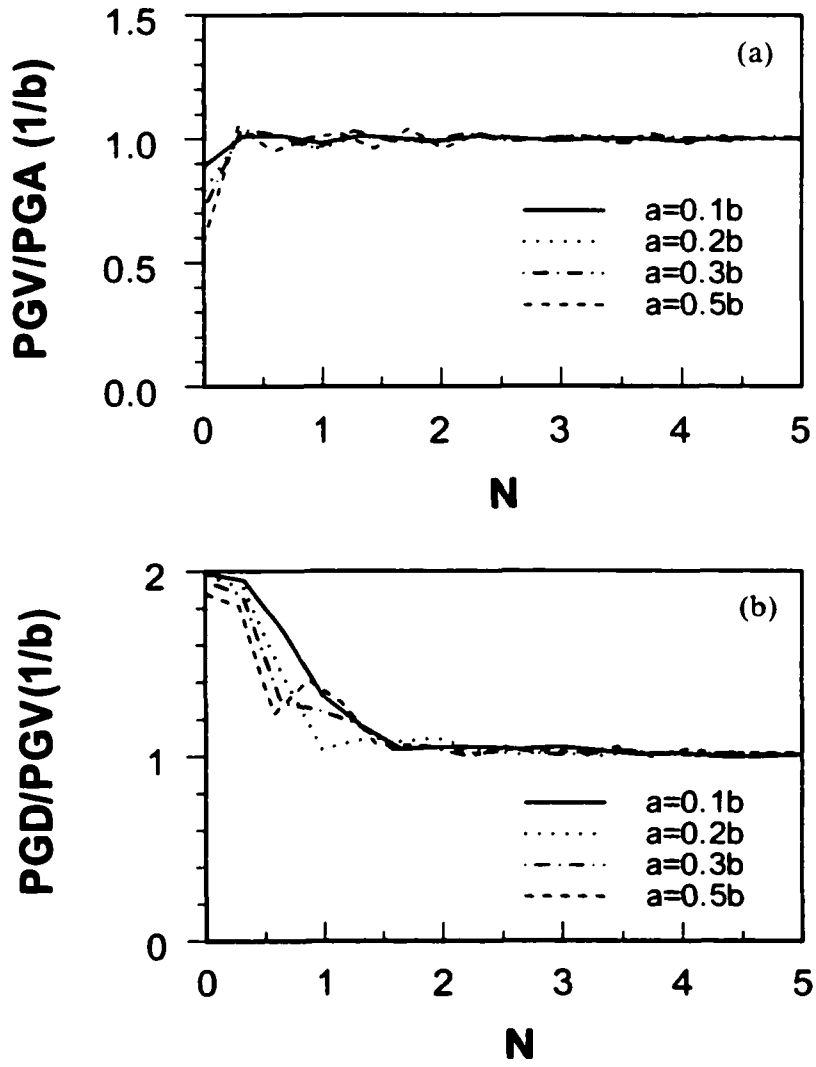

Figure 3-13: (a) PGV/PGA ratio vs. number of pulse cycle in building up phase; (b) PGD/PGV ratio vs. number of pulse cycle in building up phase.

Although it is difficult to derive analytical expressions for the peak values of the ground motion pulse, e.g., PGA, PGV and PGD, for a general value of n, expressions for these peak quantities can be easily obtained from Equations (3-1)-(3-3) for n=0 as follows:

$$PGA = \ddot{u}_p\Big|_{t=0} = Cb = C\sqrt{1-\zeta_p^2}\cdot\frac{2\pi}{T_p} \tag{3-12}$$

$$PGV = \dot{u}_p\Big|_{t=\frac{1}{b}\tan^{-1}(-\frac{b}{a})} = C\sqrt{1-\zeta_p^2}e^{-(a/b)\tan^{-1}(-b/a)} \tag{3-13}$$

$$PGD = u_p\Big|_{t=\frac{\pi}{b}} = \frac{Cb}{\omega_p^2}[1+e^{\frac{a\pi}{b}}] \tag{3-14}$$

For the case of n = 0, the velocity pulse in Equation (3-1) is reduced to a decaying sinusoidal pulse. It has been shown by He and Agrawal (2001) and Agrawal and He (2001) that the decaying sinusoidal pulse model is capable of modeling kinematic characteristics of ground velocity pulses. Hence, the study of PGA, PGV and PGD for the decaying sinusoidal pulse model (when n = 0) may lead to several important characteristics of recorded ground motions.

The PGA is a most commonly used measure of earthquake potential, but is not totally reliable especially for the near-field earthquake, since high frequency components usually fluctuate around the long duration pulse. It can be observed from Figure 3-7 that the PGA of Landers Earthquake at the Lucerne Valley station is 0.72g. The PGA of type A and type B pulses are 0.1g, 0.13g, respectively, and that of the proposed analytical model is 0.23g. However, it was demonstrated earlier that the proposed model as well as

the approximations proposed by Makris (1997) and Makris and Chang (1998, 2000a,b) are able to capture the major kinematic characteristics of the displacement and velocity responses for a flexible SDOF structure subject to near-field earthquakes, since the high frequency components in the recorded ground motion have insignificant effect on the response of flexible structures.

The PGV seems to be a more representative measure of the earthquake destructiveness as it is directly related to the energy demand. For near-field ground motions, the PGV represents the cumulative effect of the seismic energy radiating from the fault (Somerville and Graves 1993). Combining Equations (3-12) and (3-13), the equation for the PGV can be written as

$$\begin{aligned} PGV &= PGA\ \frac{T_p}{2\pi} e^{(a/b)\tan^{-1}(-b/a)} = \frac{T_p}{2\pi}.PGA.f(\zeta_p) \\ f(\zeta_p) &= e^{\frac{-\zeta_p}{\sqrt{1-\zeta_p^2}}\tan^{-1}\left(\frac{\sqrt{1-\zeta_p^2}}{\zeta_p}\right)} \end{aligned} \tag{3-15}$$

It can be observed from Equation (3-15) that the peak ground velocity (PGV) is proportional to the period of the ground motion, and it depends on the decay factor of the ground motion, ζ_p. For a given decay factor ζ_p and peak ground acceleration (PGA) ground motions with a higher frequency main pulse will have a smaller PGV, whereas with a lower frequency (longer period) main pulse will have a larger PGV. Hence, long period ground motion pulses have larger energy demands. The function $f(\zeta_p)$ in Equation (3-15) is a function of the decay factor ζ_p, and it decreases as the decay factor ζ_p increases as shown in Figure 3-14. It is observed from Figure 3-14 that the PGV decreases as the decay factor ζ_p increases. As a result, ground motion pulses with higher ζ_p, e.g., Type A pulse, will have a lesser energy demand, since it has a smaller PGV.

This implies that ground motions with a higher PGA but a smaller PGV will be less destructive as compared to ground motions with a smaller PGA but a higher PGV.

The PGD is another important parameter of ground motions. However, this value

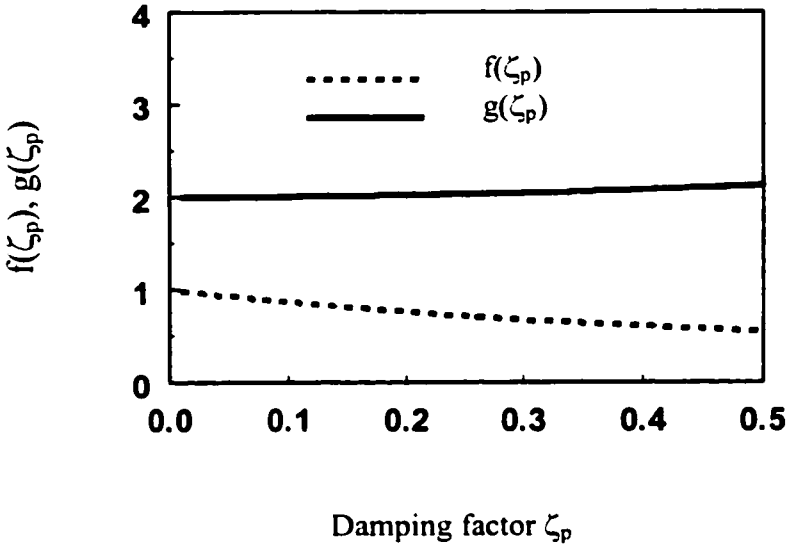

Figure 3-14: Damping factor ζ_p vs. function $f(\zeta_p)$ and $g(\zeta_p)$.

is not reliable since it is the second integration of the acceleration time history and the long period components may be filtered out.

The peak ratio PGV/PGA has been used as a measure of destructiveness by Zhu et al. (1988). Their study indicated that ground higher PGV/PGA values exhibit more damaging potential. Malhotra (1999) pointed out that near-field pulse-like ground motions with a high PGV/PGA ratio have wide acceleration-sensitive regions in their response spectra, which will increase the base shear, inter-storey drift and ductility demand of high-rise buildings. This conclusion was verified by Liao et al. (2001) and Chopra and Chintanapakdee (2001). If the proposed approximation of near field ground

motions contains reliable PGA and PGV value, the peak motion ratio PGV/PGA can be obtained from Equation (3-15) as:

$$\frac{PGV}{PGA} = \frac{T_p}{2\pi} e^{(a/b)\tan^{-1}(-b/a)} = \frac{T_p}{2\pi} \cdot f(\zeta_p) \tag{3-16}$$

Similarly, the PGD/PGV ratio can be obtained from Equations (3-13) and (3-14) as

$$\frac{PGD}{PGV} = \frac{T_p}{2\pi} \cdot \frac{(1+e^{\frac{a\pi}{b}})}{e^{(a/b)\tan^{-1}(-b/a)}} = \frac{T_p}{2\pi} \cdot g(\zeta_p); \quad g(\zeta_p) = \frac{(1+e^{\frac{a\pi}{b}})}{e^{(a/b)\tan^{-1}(-b/a)}} \tag{3-17}$$

It can be observed from Equations (3-16) and (3-17) that both PGV/PGA and PGD/PGV ratios contain the natural period T_p and decay factor ζ_p of the ground motion. Functions $f(\zeta_p)$ and $g(\zeta_p)$ are dependent on ζ_p as shown in Figure 3-14. It can be observed from Figure 3-14 that the function $g(\zeta_p)$ is almost a constant. When the damping ratio changes from 0 to 50%, $g(\zeta_p)$ changes from 2 to 2.13, indicating that if PGD and PGV are reliable, the natural period T_p can be estimated approximately as

$$T_p = \frac{PGD}{PGV} \cdot \frac{2\pi}{g(\zeta_p)} \tag{3-18}$$

For the recorded ground motion at Lucerne Valley Station during the 1992 Landers earthquake, it has been observed that PGD = 248cm, PGV = 152cm/m and ζ_p = 0.3 for the proposed analytical pulse model shown in Figure 3-7. For this case, it follows from Equation (3-17) that g(0.3) =2.05. Substituting these values in Equation (3-18), one obtains the natural period $T_p \approx 5.0$ sec, which is in agreement with the width of the velocity pulse T_g=4.62 sec as shown in Figure 3-7. It is noticed that when ζ_p = 0 and $g(\zeta_p)$=2, Equation (3-18) is the same as the formula proposed by Makris (1997) for Type

B pulse, i.e., $T_p = \frac{PGD}{PGV} \cdot \pi$, since the displacement due to the Type B pulse has fully recovered. Hence, the Type B pulse proposed by Makris is a full cycle pulse and it can be obtained from the proposed approximation by assuming ζ_p=0. For type A pulse, the formula presented by Makris is $T_p = \frac{PGD}{PGV} \cdot 2$, and the proposed formula in Equation (3-18) is $T_P = \frac{PGD}{PGV} \cdot Q$, where Q is less than π, since $g(\zeta_p)$ varies between 2 and 2.13 as the damping factor ζ_p varies between 0 and 50%.

Similar relationships can be investigated for PGA and PGV. It is observed that (i) when ζ_p =0 (i.e., the pulse resembles a Type B pulse), $f(\zeta_p)$ =1 and $PGA = PGV \cdot \frac{2\pi}{T_p}$, see Equation (3-16), and (ii) when ζ_p = 40% (for this case, the shape of the velocity pulse is similar to the type A pulse), f(0.4) $\approx$.061, and $PGA \approx \frac{1}{0.61} \cdot PGV \cdot \frac{2\pi}{T_p}$. Hence, for the ground motion pulse with the same PGV and natural period, the PGA of the ground motion increases as the damping ratio ζ_p increases. These results are in contrast to those presented by Makris (1997) and Makris and Chang (1998), where the PGA of the type A pulse is ½ of the PGA of type B pulse for a same value of PGV. Hence, the proposed near-field velocity pulse leads to a value of PGA that is closer to the recorded ground motions than that of Makris (1997) and Makris and Chang (1998).

From the discussions above, it is clear that the PGD/PGV and PGV/PGA ratios contain important information about the natural period of the ground motion T_p, which strongly affects the response of structures.

3.9 Closed-Form Solution of a SDOF Oscillator Subject to Analytical Velocity Pulses

It is demonstrated in the previous sections that the proposed analytical pulse model is capable of the capturing kinematic characteristics of long period pulses in near-field ground motions. Though the acceleration of the analytical pulse is smaller compared to that of the recorded ground motion, the energy contents of the analytical model are similar to those of the recorded ground motions. Further, the displacement spectrum of the analytical model matches well with that of the recorded ground motion, especially for long period structures, since the response of these structures is mainly affected by long period component in the ground motion represented in the analytical pulse model. The acceleration response spectrum of the analytical model matches well with that of the recorded ground motion only for long period structures, and the acceleration of stiff structures is affected by high frequency components of the recorded ground motion, which are excluded in the analytical model. Hence, the proposed analytical model can be used to investigate the response of flexible structures with various protective systems subject to near-field ground motions.

The closed-from solution of a SDOF system subject to the proposed analytical model is difficult to obtain except for two special cases where n is an integer in Equation (3-1). Consider a SDOF system subject to the proposed acceleration pulse in Equation (3-2), the general form of the equation of motion is given in Equation (3-8), where ζ is viscous damping ratio due to the inherent structural damping and the supplemental viscous damping if additional linear viscous dampers are added to the structure. Assuming the initial displacement and velocity of the structure are zero, i.e.,

$x(0) = \dot{x}(0) = 0$, the closed form solution of elastic the SDOF structure installed with linear viscous dampers can be obtained as follows.

3.9.1 Solution for n=0

The closed-form solution of Equation (3-8) subject to the acceleration pulse given by Equation (3-2) with n=0 is derived as:

$$x = C \cdot e^{a_0 t}(A_1 \cos b_0 t + A_2 \sin b_0 t) + C \cdot e^{at}(A_3 \cos bt + A_4 \sin bt) \qquad (3\text{-}19)$$

where a_0=-$\zeta\omega$ and $b_0 = \omega\sqrt{1-\zeta^2}$. Constants a and b are the same as that defined in Equation (3-1). Integration constants A_1, A_2, A_3 and A_4 can be obtained as

$$A_1 = \frac{\beta}{\omega} \cdot \frac{\sqrt{1-\zeta_p^2}[-1+\beta^2]}{1-4\zeta\zeta_p\beta+(4\zeta^2+4\zeta_p^2-2)\beta^2-4\zeta\zeta_p\beta^3+\beta^4} \qquad (3\text{-}20a)$$

$$A_2 = \frac{\beta}{\omega} \cdot \sqrt{\frac{1-\zeta_p^2}{1-\zeta^2}} \cdot \frac{[-\zeta+2\zeta_p\beta-\zeta\beta^2]}{1-4\zeta\zeta_p\beta+(4\zeta^2+4\zeta_p^2-2)\beta^2-4\zeta\zeta_p\beta^3+\beta^4} \qquad (3\text{-}20b)$$

$$A_3 = \frac{\beta}{\omega} \cdot \frac{\sqrt{1-\zeta_p^2}[1-\beta^2]}{1-4\zeta\zeta_p\beta+(4\zeta^2+4\zeta_p^2-2)\beta^2-4\zeta\zeta_p\beta^3+\beta^4} \qquad (3\text{-}20c)$$

$$A_4 = \frac{\beta}{\omega} \cdot \frac{[-\zeta_p+2\zeta\beta-\zeta_p\beta^2]}{1-4\zeta\zeta_p\beta+(4\zeta^2+4\zeta_p^2-2)\beta^2-4\zeta\zeta_p\beta^3+\beta^4} \qquad (3\text{-}20d)$$

where β is defined as the ratio of the pulse frequency to the natural free-vibration frequency of the structure, i.e.,

$$\beta = \omega_p/\omega \qquad (3\text{-}21)$$

The solution in Equation (3-19) consists of free and forced vibrations of the structure. The solution can be verified by letting the pulse decaying ratio $\zeta_p = 0$, which

correspond to a special case of sinusoidal pulse, that the excitation on the left hand side of Equation (3-8) is a harmonic cosine function. The general solution can be found in standard dynamic text books [e.g., Chopra (1995)]. Equation (3-19) can be further verified by numerical integration. Figure 3-15 shows the plots of the response of a SDOF structure obtained from the closed form solution in Equation (3-19) and that from numerical simulations. In this figure, a structure with natural period T=1 sec. and viscous damping ζ = 5% subject to a decaying Cycloidal pulse with T_p=1.5 s, decaying ratio ζ_p = 20% and peak acceleration of 0.5g. It can be observed from Figure 3-15, that the response obtained from the analytical solution in Equation (3-19) matches very well with that of the numerical simulation.

Figure 3-16 plots the coefficients A_1, A_2, A_3 and A_4 of the closed-form solution in Equation (3-19) by varying the period of the acceleration pulse with n=0 and ζ_p = 20%. The structure used herein is a SDOF base-isolated building with a natural period 2.5 sec and a viscous damping of 5%. It can be shown from Equation (3-20) that responses of both long period structures ($\beta \to \infty$) and short period structures ($\beta \to 0$) subject to a decaying velocity pulse will be very small, since the limits of coefficients A_i, i = 1, 2, 3 and 4, approach to zero for both cases,

$$\lim_{\beta \to 0} A_i = 0 \text{ and } \lim_{\beta \to \infty} A_i = 0, \text{ for i=1,...4} \qquad (3\text{-}22)$$

Similar to that of high frequency harmonic excitations, the displacement of structures is very small when subject to high frequency velocity pulses. Contrary to the static-like displacement of short-period structures when subject to low frequency (long-period) harmonic excitations, the displacement responses of short-period structures is zero when

subjected to decaying sinusoid velocity pulses. Noted that the limitation of the pulse acceleration $\ddot{u}_p(t)$ as $\beta \to 0$ is given by

$$\lim_{\beta \to 0} \ddot{u}_p = \lim_{\beta \to 0} e^{-\zeta_p \omega \beta t}\left[\sqrt{1-\zeta_p^2} \cdot \omega\beta \cdot \cos(bt) - \zeta_p \omega\beta \cdot \sin(bt)\right] = 0 \qquad (3\text{-}23)$$

For the special case with $\beta = 1$, the resonance does not occur if $\zeta_p \neq \zeta$. The coefficients in Equations (3-20) for this case can be obtained as

$$A_1 = A_3 = 0,\ A_2 = \frac{1}{2\omega(\zeta_p - \zeta)}\sqrt{\frac{1-\zeta_p^2}{1-\zeta^2}} \text{ and } A_4 = -\frac{1}{2\omega(\zeta_p - \zeta)} \qquad (3\text{-}24)$$

Thus, the general form of the analytical solution, Equation (3-19), can be rewritten for the special case with $\beta = 1$ as:

$$x = A_2 e^{-\zeta\omega t}\sin(\sqrt{1-\zeta^2}\,\omega t) + A_4 e^{-\zeta_p \omega t}\sin(\sqrt{1-\zeta_p^2}\,\omega t) \qquad (3\text{-}25)$$

It is observed from Equation (3-25) that the response of the structure depends on the structural damping ratio ζ and the pulse decaying ratio ζ_p. If $\zeta_p > \zeta$, then $|A_2| < |A_4|$, which indicates that the increase in the transient term (the first term) is smaller than the decrease in the steady state term (the second term) in Equation (3-25), and response of the structure will follow the motion of excitations. Likewise, the response will catch up with the motion of excitations if $\zeta_p < \zeta$. Typically, the peak response of the structure caused by the impulsive excitation usually occurs in the first cycle and decays very fast for $\zeta_p < \zeta$.

To study the relative decay of coefficients A_1, A_2, A_3 and A_4 in Eqs. (3-20) as a function of β, one defines the ratio of coefficients A_2 and A_1 in Equations (3-20) as

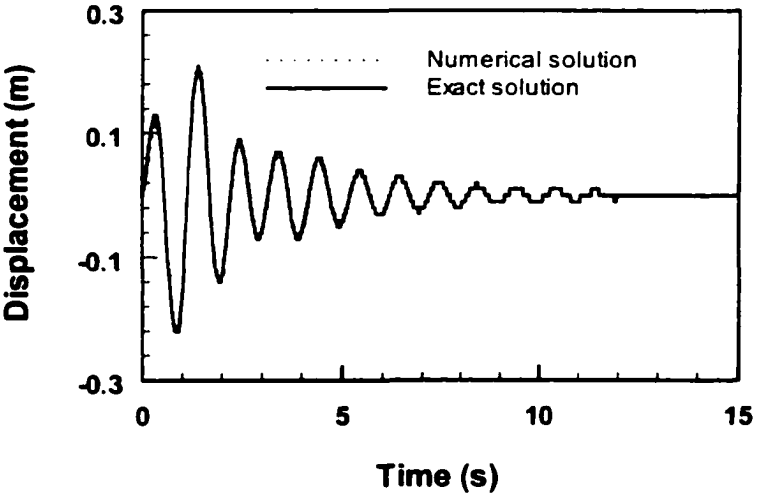

Figure 3-15: Comparison of exact solution and numerical solutions.

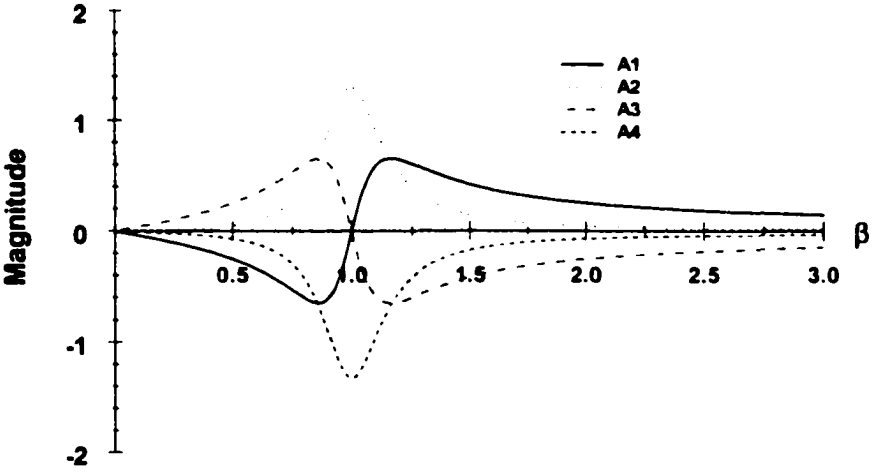

Figure 3-16: Coefficients of A_1, A_2, A_3, A_4 vs. β.

$$R_{21} = \left|\frac{A_2}{A_1}\right| = \left|\frac{\varsigma + \beta^2\varsigma - 2\beta\varsigma_p}{(\beta^2 - 1)\sqrt{1-\varsigma^2}}\right| \tag{3-26}$$

Similarly, the ratio of coefficients A_4 and A_1 in Equations (3-20) is defined as

$$R_{41} = \left|\frac{A_4}{A_1}\right| = \left|\frac{\varsigma_p + \beta^2\varsigma_p - 2\beta\varsigma}{(\beta^2 - 1)\sqrt{1-\varsigma_p^2}}\right| \tag{3-27}$$

The limits of R_{21} and R_{41} in Equations (3-26) and (3-27), respectively, for long period structures ($\beta \to \infty$) and short period structures ($\beta \to 0$) are obtained as

$$\lim_{\beta\to 0} R_{21} = \lim_{\beta\to\infty} R_{21} = \frac{\varsigma}{\sqrt{1-\varsigma^2}} \tag{3-28}$$

$$\lim_{\beta\to 0} R_{41} = \lim_{\beta\to\infty} R_{41} = \frac{\varsigma_p}{\sqrt{1-\varsigma_p^2}} \tag{3-29}$$

Though the coefficients A_1, A_2, A_3 and A_4 converge to 0 for the cases $\beta \to \infty$ and $\beta \to 0$, Equations (3-28) and (3-29) indicate that the convergence of ratios R_{21} (A_2 to A_1) and R_{41} (A_4 and A_1) is related to the damping of the structure ζ and the decay factor of ground motion ζ_p. It is observed from Equations (3-28) and (3-29) that the coefficients A_2 and A_4 converge to 0 slower than the coefficients A_1 and A_3 for small values of ζ and ζ_p, since $R_{21}<<1$ and $R_{41}<<1$ for small values of ζ and ζ_p. Thus, the displacement of the structure, Equation (3-19), is dominated by the terms related to cosine functions for large and small values of β, e.g., $\beta>1.5$ and $\beta<0.5$. It is obvious from Equations (3-20) and Figure (3-16) that $A_3=-A_1$. Hence, Equation (3-19) can be approximated for the structures with long (large β) and short periods (small β) as

$$x \approx A_1 e^{-\zeta\omega t}\cos(\sqrt{1-\zeta^2}\,\omega t) - A_1 e^{-\zeta_p\omega_p t}\cos(\sqrt{1-\zeta_p^2}\,\omega_p t) \qquad (3\text{-}30)$$

The analytical solution of a SDOF structure subject to an acceleration pulse with n=0 has been derived. The performance of supplemental linear viscous dampers for structures subject to pulse-type excitations will be discussed using the solutions derived above through numerical simulation results in the next chapter.

3.9.2 Solution for n=1

The closed-form solution of a SDOF structure subject to the acceleration pulse $\ddot{u}_p$ in Equation (3-2) with n=1 will be derived using Laplace Transform. The Laplace Transform of ground acceleration $\ddot{u}_p$ in Equation (3-2) can be obtained from that of Equation (3-1). Equation (3-1) can be rewritten for n=1 as

$$\dot{u}_p = C \cdot t \cdot e^{-at} \cdot \sin bt = t \cdot h(t)\,;\; h(t) = C \cdot e^{-at} \cdot \sin(bt) \qquad (3\text{-}31)$$

Then,

$$\mathscr{L}[h(t)] = H(s) = \frac{C \cdot b}{(s+a)^2 + b^2} \qquad (3\text{-}32)$$

$$\mathscr{L}[\dot{u}_p(t)] = \mathscr{L}[t \cdot h(t)] = -H'(s) = \frac{2Cb \cdot (s+a)}{[(s+a)^2 + b^2]^2} \qquad (3\text{-}33)$$

Since $\dot{u}_p(0) = 0$,

$$\mathscr{L}[\ddot{u}_p(t)] = s \cdot \mathscr{L}[\dot{u}_p(t)] = \frac{2Cb \cdot (s+a)s}{[(s+a)^2 + b^2]^2} \qquad (3\text{-}34)$$

Considering the Laplace Transform of the left hand side of Equation (3-8) by using $\ddot{u}_p(t)$ in place of $\ddot{u}_g(t)$, one obtains

$$X(s) = \frac{2Cb \cdot (s+a)s}{[(s+a)^2 + b^2]^2 \cdot (s^2 + 2\varsigma\omega s + \omega^2)} \tag{3-35}$$

For $a = \varsigma_p\omega_p$ and $b = \sqrt{1-\varsigma_p^2} \cdot \omega_p$, one obtains the solution x(t) from the inversed Laplace Transform of X(s) as

$$x(t) = C \cdot e^{-\varsigma\omega t} \cdot \left[B_1 \cos(\sqrt{1-\varsigma^2}\omega t) + B_2 \sin(\sqrt{1-\varsigma^2}\omega t) \right] + C \cdot e^{-\varsigma_p\omega_p t} \cdot \left[(B_3 + B_4 t) \cdot \cos(\sqrt{1-\varsigma_p^2}\omega_p t) + (B_5 + B_6 t) \cdot \sin(\sqrt{1-\varsigma_p^2}\omega_p t) \right] \tag{3-36}$$

where the coefficients B_1, B_2, B_3, B_4, B_5 and B_6 are obtained as

$$B_1 = \frac{2\sqrt{1-\varsigma_p^2}\beta \cdot [2\varsigma - \varsigma_p(3+4\varsigma^2)\beta + 8\varsigma\varsigma_p^2\beta^2 + \varsigma_p(2-4\varsigma_p^2)\beta^3 - 2\varsigma\beta^4 + \varsigma_p\beta^5]}{\omega^2[1 - 4\varsigma\varsigma_p\beta + (-2 + 4\varsigma^2 + 4\varsigma_p^2)\beta^2 - 4\varsigma\varsigma_p\beta^3 + \beta^4]^2} \tag{3-37a}$$

$$B_2 = \sqrt{\frac{1-\varsigma_p^2}{1-\varsigma^2}} \cdot \frac{2\beta \cdot [2\varsigma^2 - 1 - \varsigma\varsigma_p(1+4\varsigma^2)\beta + (2+8\varsigma^2\varsigma_p^2)\beta^2 - \varsigma\varsigma_p(6+4\varsigma_p^2)\beta^3 - (1-2\varsigma^2-4\varsigma_p^2)\beta^4 - \varsigma\varsigma_p\beta^5]}{\omega^2[1 - 4\varsigma\varsigma_p\beta + (-2 + 4\varsigma^2 + 4\varsigma_p^2)\beta^2 - 4\varsigma\varsigma_p\beta^3 + \beta^4]^2} \tag{3-37b}$$

$$B_3 = -B_1 = -\frac{2\sqrt{1-\varsigma_p^2}\beta \cdot [2\varsigma - \varsigma_p(3+4\varsigma^2)\beta + 8\varsigma\varsigma_p^2\beta^2 + \varsigma_p(2-4\varsigma_p^2)\beta^3 - 2\varsigma\beta^4 + \varsigma_p\beta^5]}{\omega^2[1 - 4\varsigma\varsigma_p\beta + (-2 + 4\varsigma^2 + 4\varsigma_p^2)\beta^2 - 4\varsigma\varsigma_p\beta^3 + \beta^4]^2} \tag{3-37c}$$

$$B_4 = \frac{\sqrt{1-\varsigma_p^2}\beta \cdot (1-\beta^2)}{\omega[1 - 4\varsigma\varsigma_p\beta + (-2 + 4\varsigma^2 + 4\varsigma_p^2)\beta^2 - 4\varsigma\varsigma_p\beta^3 + \beta^4]} \tag{3-37d}$$

$$B_5 = \frac{1 - 4\varsigma\varsigma_p\beta + (2\varsigma_p^2 - 1 - 4\varsigma^2 + 8\varsigma^2\varsigma_p^2)\beta^2 + 16\varsigma\varsigma_p(1-\varsigma_p^2)\beta^3 + (8\varsigma_p^4 - 8\varsigma_p^2 - 1 - 4\varsigma^2)\beta^4 + 4\varsigma\varsigma_p\beta^5 + (1-2\varsigma_p^2)\beta^6}{\omega^2[1 - 4\varsigma\varsigma_p\beta + (-2 + 4\varsigma^2 + 4\varsigma_p^2)\beta^2 - 4\varsigma\varsigma_p\beta^3 + \beta^4]^2} \tag{3-37e}$$

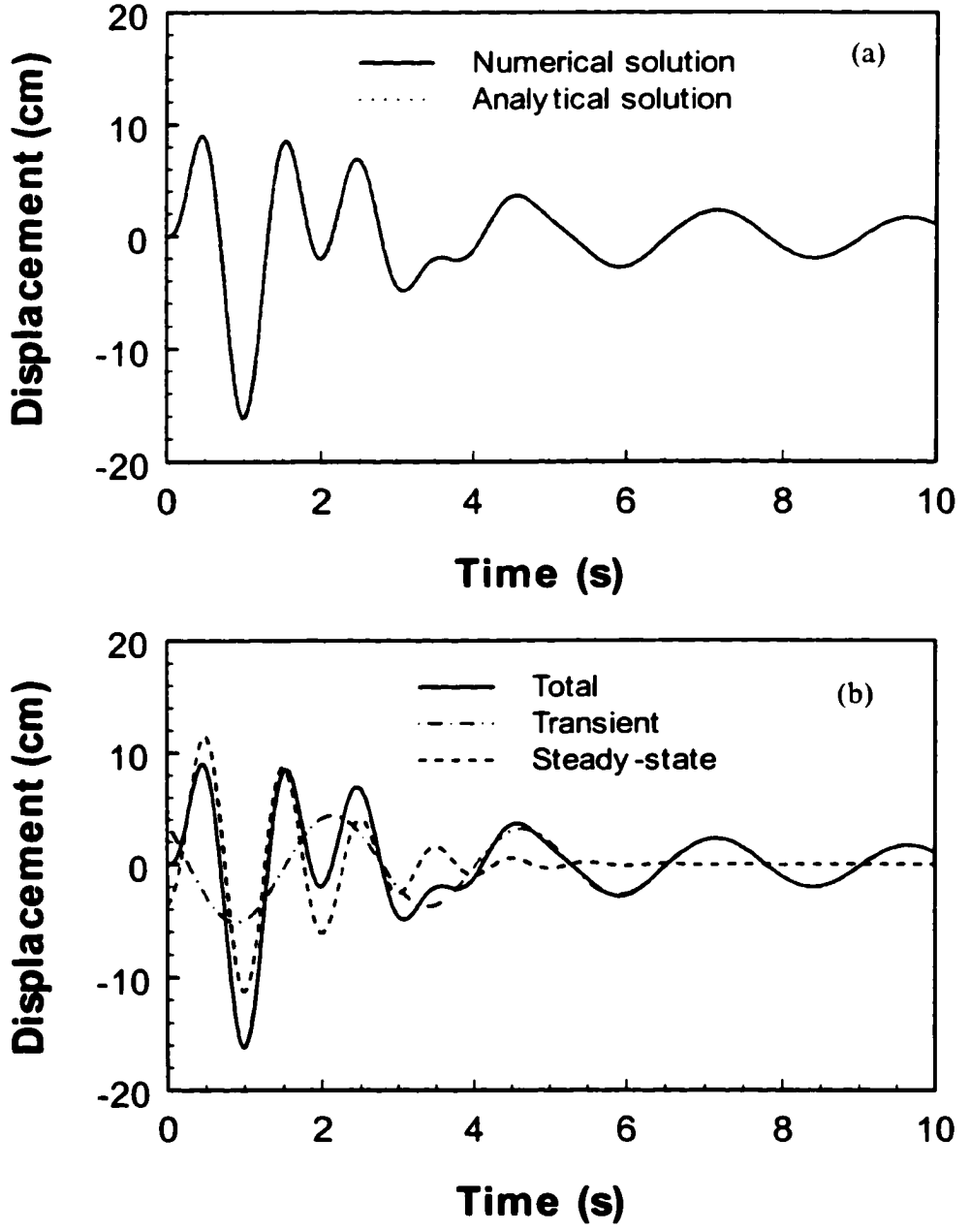

Figure 3-17: (a) Comparison of analytical solution with numerical solution; (b) Transient and steady-state response components of the total response.

$$B_6 = \frac{\beta \cdot (-\varsigma_p + 2\varsigma\beta - \varsigma_p\beta^2)}{\omega\left[1 - 4\varsigma\varsigma_p\beta + (-2 + 4\varsigma^2 + 4\varsigma_p^2)\beta^2 - 4\varsigma\varsigma_p\beta^3 + \beta^4\right]} \qquad (3\text{-}37f)$$

The general solution in Equation (3-36) for n = 1 can be verified by numerical integrations. Figure 3-17(a) plots the response of a SDOF structure obtained from the closed form solution and that from numerical simulations for a typical base- isolated building with a natural period T=2.5 sec and inherent structural damping ζ = 5% subject to pulse acceleration $\ddot{u}_p$ in Equation (3-2) with parameters C=2, n=1, ζ_p = 0.2 and ω_p = 1 sec. It is observed from Figure 3-17(a) that the response obtained from the analytical solution in Equation (3-36) matches very well with that of the numerical simulation.

The general solution in Equation (3-36) consists of the complementary solution and particular solution with six integration constants, B_1, B_2, B_3, B_4, B_5 and B_6. However, only four of these constants are independent since two of them are determined by the particular solution and the other two are obtained from two initial conditions, e.g., $x(0) = \dot{x}(0) = 0$. The general solution in Equation (3-36) consists of transient and steady-state responses. The first term in Equation (3-36) is the free vibration due to initial conditions, referred to the transient response, while the second term is the steady-state response due to the excitation. However, contrary to that of harmonic excitations, the steady-state response of the structure subject to pulse type excitations vanishes faster than that of the transient response, as shown in Figure 3-17(b).

It is observed from Equation (3-36) that the coefficients of sine and cosine terms of the steady-state response are functions of the first order of time t, similar to that of the excitation. It is further observed from Equations (3-20) and (3-36) that the constants B_4

and B_6 are identical to constants A_3 and A_4, which are the integration constants of the analytical solution for n=0 in Equation (3-20), i.e.,

$$B_4 = A_3 \text{ and } B_6 = A_4 \tag{3-38}$$

Figure 3-18 plots the coefficients B_1, B_2, B_3, B_4, B_5 and B_6 as a function of $\beta = \omega_p / \omega$ for n=1 and ζ_p=20% for a SDOF base-isolated building with a natural period

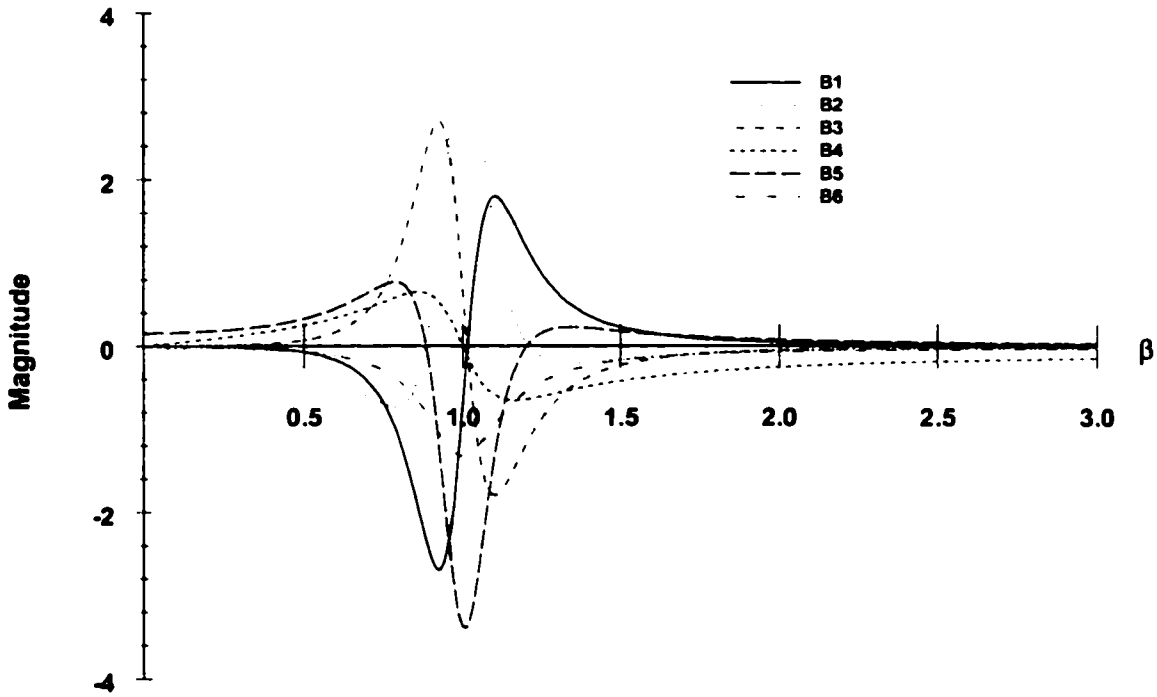

Figure 3-18: Integration constant B_1, B_2, B_3, B_4, B_5 and B_6 vs. β.

of 2.5 sec and a structural damping of 5%. Taking limits of the coefficients B_i, i = 1, 2,.., 6, it can be shown from Equation (3-36) that the displacement of the structure will be very small when subject to high frequency pulses (i.e., $\beta \rightarrow \infty$), since

$$\lim_{\beta \to \infty} B_i = 0, \text{ for } i = 1,\ldots 6 \tag{3-39}$$

On the other hand, limits of the coefficients B_i (i=1,..., 6) as $\beta \to 0$ are given by

$$\lim_{\beta \to 0} B_5 = \frac{1}{\omega^2}; \quad \lim_{\beta \to 0} B_i = 0 \text{ for i=1, 2, 3, 4, 6.} \tag{3-40}$$

Hence, low frequency velocity pulses cause static-like displacement to the structure, since the limit of $\ddot{u}_p(t)$ as $\beta \to 0$ is given by

$$\lim_{\beta \to 0} \ddot{u}_p = \lim_{\beta \to 0} e^{-\varsigma_p \omega_p t}\left[\sqrt{1-\varsigma_p^2} \cdot \omega\beta \cdot t\cos(bt) + (1-\varsigma_p \omega\beta) \cdot \sin(bt)\right] = \sin(\sqrt{1-\varsigma_p^2} \cdot \omega\beta \cdot t) \tag{3-41}$$

Since the peak magnitude of the excitation in Equation (3-41) is 1, the peak displacement of the structure is $x \approx 1/\omega^2 = B_5$.

To investigate the convergence of the integration constants B_1 to B_6 as $\beta \to \infty$ and $\beta \to 0$, the ratios of these constants to B_4 are defined as

$$R_{i4} = \frac{B_i}{B_4} \tag{3-42}$$

where

$$R_{14} = \frac{2 \cdot \left[2\varsigma - \varsigma_p(3+4\varsigma^2)\beta + 8\varsigma\varsigma_p^2\beta^2 + \varsigma_p(2-4\varsigma_p^2)\beta^3 - 2\varsigma\beta^4 + \varsigma_p\beta^5\right]}{\omega(1-\beta^2)\left[1-4\varsigma\varsigma_p\beta + (-2+4\varsigma^2+4\varsigma_p^2)\beta^2 - 4\varsigma\varsigma_p\beta^3 + \beta^4\right]} \tag{3-43}$$

$$R_{24} = \frac{2 \cdot \left[2\varsigma^2 - 1 - \varsigma\varsigma_p(1+4\varsigma^2)\beta + (2+8\varsigma^2\varsigma_p^2)\beta^2 - \varsigma\varsigma_p(6+4\varsigma_p^2)\beta^3 - (1-2\varsigma^2-4\varsigma_p^2)\beta^4 - \varsigma\varsigma_p\beta^5\right]}{\sqrt{1-\varsigma^2} \cdot (1-\beta^2) \cdot \omega \cdot \left[1-4\varsigma\varsigma_p\beta + (-2+4\varsigma^2+4\varsigma_p^2)\beta^2 - 4\varsigma\varsigma_p\beta^3 + \beta^4\right]} \tag{3-44}$$

$$R_{34} = -R_{14} \tag{3-45}$$

$$R_{54} = \frac{1-4\varsigma\varsigma_p\beta + (2\varsigma_p^2 - 1 - 4\varsigma^2 + 8\varsigma^2\varsigma_p^2)\beta^2 + 16\varsigma\varsigma_p(1-\varsigma_p^2)\beta^3 + (8\varsigma_p^4 - 8\varsigma_p^2 - 1 - 4\varsigma^2)\beta^4 + 4\varsigma\varsigma_p\beta^5 + (1-2\varsigma_p^2)\beta^6}{\sqrt{1-\varsigma_p^2} \cdot \beta(1-\beta^2) \cdot \omega \cdot \left[1-4\varsigma\varsigma_p\beta + (-2+4\varsigma^2+4\varsigma_p^2)\beta^2 - 4\varsigma\varsigma_p\beta^3 + \beta^4\right]} \tag{3-46}$$

$$R_{64} = \frac{-\varsigma_p + 2\varsigma\beta - \varsigma_p\beta^2}{(1-\beta^2)\cdot\sqrt{1-\varsigma_p^2}} \tag{3-47}$$

By using the ratios defined above, the properties of the displacement response in Equation (3-36) for structures subject to high frequency ($\beta \to \infty$), low frequency ($\beta \to 0$) and intermediate frequency ($\beta \to 1$) pulse excitations are discussed in the following.

3.9.2.1 High frequency pulse excitation $\beta \to \infty$

The limits of the ratios of coefficients B_i, i = 1, 2, .., 6 as $\beta \to \infty$ can be obtained as

$$\lim_{\beta\to\infty} R_{64} = \frac{\varsigma_p}{\sqrt{1-\varsigma_p^2}},\ \lim_{\beta\to\infty} R_{i4} = 0,\ \text{for i=1, 2, 3, 5} \tag{3-48}$$

Equation (3-48) indicates that the displacements of the structure, x(t), is dominated by the terms with coefficients B_4 and B_6 as the frequency of the pulse excitation increases beyond the natural frequency of the structure. In such a case, the displacement response in Equation (3-36) can be approximated by

$$x(t) \cong C\cdot e^{-\varsigma_p\omega_p t}\left[B_4 t\cos(\sqrt{1-\varsigma_p^2}\omega_p t) + B_6 t\sin(\sqrt{1-\varsigma_p^2}\omega_p t)\right] \tag{3-49}$$

Note that the displacement in Equation (3-49) strongly depends on the first term for small values of ζ_p, since the limit of R_{64} in Equation (3-48) will be very small, i.e., B_6 will be a very small number.

3.9.2.2 Low frequency pulse excitation $\beta \to 0$

The limits of coefficient ratios as $\beta \to 0$ are obtained as

$$\lim_{\beta\to 0} R_{i4} = \frac{4\varsigma}{\omega} \tag{3-50}$$

$$\lim_{\beta \to 0} R_{24} = \frac{-2 + 4\varsigma^2}{\sqrt{1-\varsigma^2} \cdot \omega} \tag{3-51}$$

$$\lim_{\beta \to 0} R_{34} = -\frac{4\varsigma}{\omega} \tag{3-52}$$

$$\lim_{\beta \to 0} R_{54} = \infty \tag{3-53}$$

$$\lim_{\beta \to 0} R_{64} = \frac{-\varsigma_p}{\sqrt{1-\varsigma_p^2}} \tag{3-54}$$

It is observed from Equations (3-50) to (3-54) that the limits of coefficient ratios for $\beta \to 0$ are dependent on the decay ratio of the velocity pulse, ζ_p, the natural frequency, ω, and damping ratio, ζ, of the structure. For small values of ζ and ζ_p, the ratios R_{14}, R_{34} and R_{64} will be very small. Thus, the displacement response in Equation (3-36) will be dominated by the terms related to integration constant B_2, B_4 and B_5 for the structure subject to pulse excitations whose frequency is rather smaller than that of the structures For such a case, the displacement in Equation (3-36) can be approximated by

$$x(t) \cong C \cdot e^{-\varsigma\omega t} \cdot B_2 \sin(\sqrt{1-\varsigma^2}\,\omega t) + C \cdot e^{-\varsigma_p \omega_p t} \cdot \left[B_4 t \cdot \cos(\sqrt{1-\varsigma_p^2}\,\omega_p t) + B_5 \cdot \sin(\sqrt{1-\varsigma_p^2}\,\omega_p t) \right] \tag{3-55}$$

3.9.2.3 Intermediate frequency pulse excitation $\beta \to 1$

To analyze the response quantities due to pulse excitations with the intermediate frequency range of $\beta = 1$, we normalize the integration constant B_1 to B_6 by B5 to obtain coefficient ratios

$$R_{i5} = \frac{B_i}{B_5}, \text{ for I=1,..., 4, 6} \tag{3-56}$$

where

$$\lim_{\beta \to 1} R_{15} = \lim_{\beta \to 1} \frac{B_1}{B_5} = \frac{\varsigma_p}{\sqrt{1-\varsigma_p^2}} \tag{3-57}$$

$$\lim_{\beta \to 1} R_{25} = \lim_{\beta \to 1} \frac{B_2}{B_5} = \frac{1-\varsigma\varsigma_p}{-1+\varsigma_p^2} \cdot \sqrt{\frac{1-\varsigma_p^2}{1-\varsigma^2}} \tag{3-58}$$

$$\lim_{\beta \to 1} R_{35} = \lim_{\beta \to 1} \frac{B_3}{B_5} = \frac{-\varsigma_p}{\sqrt{1-\varsigma_p^2}} \tag{3-59}$$

$$\lim_{\beta \to 1} R_{45} = \lim_{\beta \to 1} \frac{B_4}{B_5} = 0 \tag{3-60}$$

$$\lim_{\beta \to 1} R_{65} = \lim_{\beta \to 1} \frac{B_6}{B_5} = \frac{(\varsigma-\varsigma_p)\omega}{-1+\varsigma_p^2} \tag{3-61}$$

It is observed from Equations (3-57)-(3-61) that for small values of ζ and ζ_p, R_{15}, and R_{35} will be very small. Thus, for structures subject to pulse excitations with the same frequency as that of the structure and small values of ζ and ζ_p, the displacement response in Equation (3-36) is dominated by the terms associated with coefficients B_2, B_5 and B_6. For such structures, the response in Equation (3-36) can be approximated by

$$x(t) \cong C \cdot e^{-\varsigma\omega t} \cdot B_2 \sin(\sqrt{1-\varsigma^2}\,\omega t) + C \cdot e^{-\varsigma_p \omega t} \cdot (B_5 + B_6 t) \cdot \sin(\sqrt{1-\varsigma_p^2}\,\omega t) \tag{3-62}$$

The closed form solution will be shown in the next chapter to investigate the performance of various damping mechanics for structures subject to pulse-type excitations.

3.9.3 Solution for n ≥ 2

The closed form solutions of a SDOF structure subject to pulse excitations in Equation (3-2) for two special cases, n=0 and n=1, have been derived and discussed in the previous sections. The analytical solution of Equation (3-8) will be derived in the

following for the more general case where n in Equation (3-2) is an arbitrary positive integer. In such a case, the general solution is assumed to be

$$x(t) = x_h(t) + x_p(t) \tag{3-63}$$

where $x_h(t)$ and $x_p(t)$ are the homogenous and particular solutions, respectively, given by

$$x_h(t) = C \cdot e^{-\varsigma\omega t} \cdot \left[\overline{E}\cos(\sqrt{1-\varsigma^2}\,\omega t) + \overline{F}\sin(\sqrt{1-\varsigma^2}\,\omega t)\right] \tag{3-64}$$

$$x_p(t) = C \cdot e^{-at} \cdot \left[(\sum_{i=0}^{n} E_i t^i) \cdot \cos(bt) + (\sum_{i=0}^{n} F_i t^i) \cdot \sin(bt)\right] \tag{3-65}$$

In Equation (3-65), 2n+2 arbitrary constants E_i (i=0,1,...,n) and F_i (i=0,1,...,n) are determined by the particular solution, while constant $\overline{E}$ and $\overline{F}$ in Equation (3-64) are determined by initial conditions. The particular solution $x_p(t)$ will be derived in the following followed by the homogenous solution.

3.9.3.1 Particular solution $x_p(t)$

The first and the second derivatives of Equation (3-65) are given by

$$\dot{x}_p(t) = C \cdot e^{-at} \cdot \left\{\left[-a \cdot \sum_{i=0}^{n} E_i t^i + \sum_{i=0}^{n-1}(i+1)E_{i+1}t^i + b \cdot \sum_{i=0}^{n} F_i t^i\right]\cos(bt) + \left[-a \cdot \sum_{i=0}^{n} F_i t^i - b \cdot \sum_{i=0}^{n} E_i t^i + \sum_{i=0}^{n-1}(i+1)F_{i+1}t^i\right]\sin(bt)\right\} \tag{3-66}$$

$$\ddot{x}_p(t) = C \cdot e^{-at} \cdot \left\{\left[(a^2-b^2) \cdot \sum_{i=0}^{n} E_i t^i - 2a \cdot \sum_{i=0}^{n-1}(i+1)E_{i+1}t^i + \sum_{i=0}^{n-2}(i+1)(i+2)E_{i+2}t^i - 2ab \cdot \sum_{i=0}^{n} F_i t^i + 2b \cdot \sum_{i=0}^{n-1}(i+1)F_{i+1}t^i\right]\cos(bt) + \left[(a^2-b^2)\sum_{i=0}^{n-1} F_i t^i - 2a \cdot \sum_{i=0}^{n-1}(i+1)F_{i+1}t^i + \sum_{i=0}^{n-2}(i+1)(i+2)F_{i+2}t^i + 2ab \cdot \sum_{i=0}^{n} E_i t^i\right]$$

$$-2b\cdot\sum_{i=0}^{n-1}(i+1)E_{i+1}t^{i}\Big]\sin(bt)\Big\} \tag{3-67}$$

Substituting Equations (3-65) ~(3-67) and Equation (3-2) into Equation (3-8), one obtains

$$e^{-at}\cdot\cos(bt)\Big[(a^2-b^2-2a\varsigma\omega+\omega^2)\cdot\sum_{i=0}^{n}E_i t^{i}+2(\varsigma\omega-a)\cdot\sum_{i=0}^{n-1}(i+1)E_{i+1}t^{i}$$

$$+\sum_{0}^{n-2}(i+1)(i+2)E_{i+2}t^{i}+2b(\varsigma\omega-a)\cdot\sum_{i=0}^{n}F_i t^{i}+2b\cdot\sum_{i=0}^{n-1}(i+1)F_{i+1}t^{i}\Big]+$$

$$e^{-at}\cdot\sin(bt)\Big[(a^2-b^2-2a\varsigma\omega+\omega^2)\cdot\sum_{i=0}^{n}F_i t^{i}+2(\varsigma\omega-a)\cdot\sum_{i=0}^{n-1}(i+1)F_{i+1}t^{i}$$

$$+\sum_{0}^{n-2}(i+1)(i+2)F_{i+2}t^{i}-2b(\varsigma\omega-a)\cdot\sum_{i=0}^{n}E_i t^{i}-2b\cdot\sum_{i=0}^{n-1}(i+1)E_{i+1}t^{i}\Big]$$

$$\equiv b\cdot t^{n}e^{-at}\cos(bt)+n\cdot t^{n}e^{-at}\sin(bt)-a\cdot t^{n-1}e^{-at}\sin(bt) \tag{3-68}$$

Comparing the coefficients on the right and left hand sides of Equation (3-68), one obtains the following equations

$$(a^2-b^2-2\varsigma\omega a+\omega^2)E_n+2b(\varsigma\omega-a)F_n=b \tag{3-69a}$$

$$(a^2-b^2-2\varsigma\omega a+\omega^2)F_n-2b(\varsigma\omega-a)E_n=-a \tag{3-69b}$$

$$(a^2-b^2-2\varsigma\omega a+\omega^2)E_{n-1}+2(\varsigma\omega-a)n\cdot E_n+2b(\varsigma\omega-a)F_{n-1}+2bn\cdot F_n=0 \tag{3-70a}$$

$$(a^2-b^2-2\varsigma\omega a+\omega^2)F_{n-1}+2(\varsigma\omega-a)n\cdot F_n-2b(\varsigma\omega-a)E_{n-1}-2bn\cdot E_n=n \tag{3-70b}$$

$$(a^2-b^2-2\varsigma\omega a+\omega^2)E_i+2(\varsigma\omega-a)(i+1)\cdot E_{i+1}+(i+1)(i+2)\cdot E_{i+2}+$$

$$2b(\varsigma\omega-a)F_i+2b(i+1)\cdot F_{i+1}=0,\ \text{for } 0\le i\le n-2 \tag{3-71a}$$

$$(a^2-b^2-2\varsigma\omega a+\omega^2)F_i+2(\varsigma\omega-a)(i+1)\cdot F_{i+1}+(i+1)(i+2)\cdot E_{i+2}+$$

$$-2b(\varsigma\omega-a)\cdot E_i-2b(i+1)\cdot E_{i+1}=0,\ \text{for } 0\le i\le n-2 \tag{3-71b}$$

The constants E_i and F_i (i=0,1,...,n) in the particular solution can be obtained by solving Equation (3-69) to (3-71). These constants can be solved backward starting from Equation (3-69). E_n and F_n are independent of the rest of the other unknowns and can be obtained as

$$E_n = \frac{\sqrt{1-\varsigma_p^2}\beta\cdot(1-\beta^2)}{\omega\left[1-4\varsigma\varsigma_p\beta+(-2+4\varsigma^2+4\varsigma_p^2)\beta^2-4\varsigma\varsigma_p\beta^3+\beta^4\right]} \tag{3-72}$$

$$F_n = \frac{\beta\cdot(-\varsigma_p+2\varsigma\beta-\varsigma_p\beta^2)}{\omega\left[1-4\varsigma\varsigma_p\beta+(-2+4\varsigma^2+4\varsigma_p^2)\beta^2-4\varsigma\varsigma_p\beta^3+\beta^4\right]} \tag{3-73}$$

Note that E_n and F_n are coefficients of the same order of t in Equation (3-1) and they are independent of n. Hence, the solution in Equations (3-38) and (3-73) can be obtained as special cases of the present solutions for appropriate values of positive integer. Using Equations (3-72) and (3-73), one can solve En-1 and Fn-1 from Equation (3-70) as

$$E_{n-1} = \frac{-2n\sqrt{1-\varsigma_p^2}\beta\cdot\left[2\varsigma-\varsigma_p(3+4\varsigma^2)\beta+8\varsigma\varsigma_p^2\beta^2+\varsigma_p(2-4\varsigma_p^2)\beta^3-2\varsigma\beta^4+\varsigma_p\beta^5\right]}{\omega^2\left[1-4\varsigma\varsigma_p\beta+(-2+4\varsigma^2+4\varsigma_p^2)\beta^2-4\varsigma\varsigma_p\beta^3+\beta^4\right]^2} \tag{3-74}$$

$$F_{n-1} = n\cdot\frac{1-4\varsigma\varsigma_p\beta+(2\varsigma_p^2-1-4\varsigma^2+8\varsigma^2\varsigma_p^2)\beta^2+16\varsigma\varsigma_p(1-\varsigma_p^2)\beta^3+(8\varsigma_p^4-8\varsigma_p^2-1-4\varsigma^2)\beta^4+4\varsigma\varsigma_p\beta^5+(1-2\varsigma_p^2)\beta^6}{\omega^2\left[1-4\varsigma\varsigma_p\beta+(-2+4\varsigma^2+4\varsigma_p^2)\beta^2-4\varsigma\varsigma_p\beta^3+\beta^4\right]^2} \tag{3-75}$$

Comparing Equation (3-74) with Equation (3-36c), and Equation (3-75) with Equation (3-36e), one can show that $E_0=B_3$ and $F_0=B_5$ for a special case where n=1.

The unknowns E_i and F_i for i=0,1,...,n-2 in Equation (3-71) can be solved backward iteratively after solving E_n, F_n, E_{n-1} and F_{n-1} as shown in Equations (3-72)-(3-75). The iterative solutions of E_i and F_i are given by

$$E_i = \frac{C_1 \cdot E_{i+1} + C_2 \cdot E_{i+2} + C_3 \cdot F_{i+1} + C_4 \cdot F_{i+2}}{4b^2(a-\varsigma\omega)^2 + (a^2 - b^2 - 2a\varsigma\omega + \omega^2)^2} \tag{3-76}$$

$$F_i = \frac{C_1 \cdot F_{i+1} + C_2 \cdot F_{i+2} - C_3 \cdot E_{i+1} - C_4 \cdot E_{i+2}}{4b^2(a-\varsigma\omega)^2 + (a^2 - b^2 - 2a\varsigma\omega + \omega^2)^2} \tag{3-77}$$

where

$$C_1 = 2(1+i)\cdot(a-\varsigma\omega)\cdot(a^2+b^2-2a\varsigma\omega+\omega^2) \tag{3-78a}$$

$$C_2 = -(1+i)\cdot(2+i)\cdot(a^2+b^2-2a\varsigma\omega+\omega^2) \tag{3-78b}$$

$$C_3 = 2b(1+i)\cdot(a^2+b^2-2a\varsigma\omega-\omega^2+2\varsigma^2\omega^2) \tag{3-78c}$$

$$C_4 = -2b(1+i)\cdot(2+i)\cdot(a-\varsigma\omega) \tag{3-78d}$$

3.9.3.2 Homogenous solution $x_h(t)$

After the particular solution $x_p(t)$ is obtained, the homogenous solution $x_h(t)$ can be obtained using initial conditions. Assuming both the initial displacement and velocity are zeros, e.g., $x(0) = \dot{x}(0) = 0$, the integration constants $\overline{E}$ and $\overline{F}$ in Equation (3-64) can be derived as

$$\overline{E} = -E_0 \tag{3-79}$$

$$\overline{F} = \frac{(a-\varsigma\omega)E_0 - E_1 - bF_0}{\sqrt{1-\varsigma^2}\cdot\omega} \tag{3-80}$$

where E_0, E_1 and F_0 have been determined from the particular solution.

Thus, the general solution of a SDOF system subject to a pulse type excitation in Equation (3-2) where n is an arbitrary positive integer has been derived above. The explicit form of the integration constants is difficult to be obtained for any general positive value of n. However, these constants can be obtained iteratively as described above. The properties of the derived analytical solution in Equation (3-63) are not discussed here because of its complexity.

3.10 Design Consideration

Although the near-field phenomenon was reported as earlier as 1950's (Benioff, 1955), it is only recently that provisions for near-field effects appear in seismic design codes. For example, the 1997 Uniform Building Code incorporated near-field effects by introducing source type and distance dependent near-field factors in the customary design spectrum. However, these factors are not sufficient to solve the problem consistently. Hence, FEMA 356 — *Prestandard and Commentary for the Seismic Rehabilitation of Buildings* (2000) recommended basic research on near-field effects for the seismic design and rehabilitation of buildings. To take into account the near-field effect seismic design codes through the following factors should be considered:

1. Since near-field ground motions usually contain long period pulses which shift the velocity dependent region of the response spectra to the long period side, values of T_1 and T_2 used to separate the acceleration sensitive and displacement sensitive regions from velocity sensitive region must be redefined in the current seismic design codes to include near-field effect.
2. Displacement ductility demand for short period structures subject to near-field earthquakes increases significantly. Hence, the coefficient C_1 used in current

seismic design code may be underestimated for near-field effects. Moreover, the strength reduction factor curve for nonlinear structures, which is based on the linear response spectra, should be shifted to the long period side depending on the predominant period of near-field ground motions.

3. FEMA 356 (2000) and 368 (2000) allow the rehabilitation of old buildings and the design of new buildings using passive energy dissipation devices. The amount of supplemental damping as described by equivalent damping ratio may be inappropriate for near-field ground motions due to their impulsive characteristics.
4. The displacement reduction factor for supplemental passive dampers may overestimate the effect of damping for near-field ground motions.

Factors (1) and (2) above describing the effects of long period pulses in near-field ground motions on linear and nonlinear response spectra are beyond the scope of this research. It is well know that the response of a SDOF system subject to the ground motion is strongly dependent on the low frequency components in the ground motion, especially for long period structures, such as base-isolated buildings and high-rise buildings. However, for a given building site, the predominant period T_g is a relatively stable quantity. These parameters can be estimated by an attention model (Somerville 1998) to construct both linear and nonlinear response spectra of near-field ground motions. Again, research on these aspects is beyond the scope of this study and it will not be discussed further. The performances of various damping mechanics will be investigated and discussed in Chapter 4 using the proposed analytical velocity pulse.

3.11 Summary

In this chapter, an analytical model for velocity pulses in near-field ground motions is presented. It has been demonstrated that the proposed model is capable of capturing kinematic characteristics of long period velocity pulses in near-field ground motions. Although the acceleration of the proposed analytical model is poor in terms of PGA or acceleration time history, the energy contents of the analytical model are similar to that of the recorded ground motions. Further, the displacement spectrum of the analytical model matches well with that of recorded ground motion, especially for long period structures. This is because the responses of long period structures are mainly affected by the long period components in ground motions, which have already been represented by the analytical model. The acceleration response spectrum of the proposed analytical model matches well with that of the recorded ground motion only for long period structures, and the consolation for short period structures is less satisfactory, since the acceleration of stiff structures is affected by the high frequency components which are not included in the analytical model. It is believed that the proposed analytical model can be used to investigate the response of flexible structures subject to near-field ground motions. The closed from solution of a SDOF system subjected to the proposed analytical approximation is also derived in this chapter, and the properties of the analytical solutions for two special cases, of n=0 and n=1, are also discussed in detail. For near-field earthquakes, the impact factor to be considered in the current seismic design codes are also discussed.

CHAPTER 4

PERFORMANCE OF PASSIVE ENERGY DISSIPATION SYSTEMS

4.1 Introduction

It is well known that the performance of passive energy dissipation systems depends on ground motions. A passive energy dissipation system designed for one ground motion may perform poorly when subject to other ground motions with different characteristics. Being stochastic in nature, ground motions at one site may be different from others due to the mechanism of the seismic event, wave propagation, geological site condition, etc. If the characteristics of ground motions are ignored, it is impossible to explore the performance of various damping mechanisms affected by ground motions. Although several researchers have investigated the performance of passive energy dissipation systems through a rigorous statistical analysis using a large sample of ground motions, a systematic understanding of the effect of ground motions on the performance of passive energy dissipation system could hardly be achieved through such studies. In this chapter, the analytical pulse model proposed in Chapter 3 for near-field ground motions will be used to investigate the performance of passive energy dissipation systems installed in structures.

The mathematical formulation of a SDOF system subject to ground excitations will be presented in Section 4.2. The performance of supplemental linear viscous

dampers for elastic structures will be presented in Section 4.3, and that for inelastic structures in Section 4.4.

4.2 Mathematical Formulation

Consider a single-degree-of-freedom (SDOF) system with the governing equation of motion:

$$\ddot{x}(t) + 2\zeta\omega\dot{x}(t) + f_r(x) + u = -\ddot{x}_g(t) \tag{4-1}$$

where $x(t)$, $\dot{x}(t)$ and $\ddot{x}(t)$ are the relative displacement, velocity and acceleration of the structure, respectively, ζ is inherent structural damping ratio, ω is the natural frequency of the structure, $f_r(x)$ is the restoring force per unit mass (e.g., $f_r(x) = \omega^2 x$, if the structures is in the elastic range), u is control force per unit mass, and $\ddot{x}_g(t)$ is the earthquake ground motion.

Equipped with linear viscous damping system and a yielding damping system, both the elastic and elastic-perfect-plastic structures subject to near-field ground velocity pulses are considered for a systematic study in this chapter.

4.2.1 Linear viscous damper

The mechanisms and details about the linear damping devices were presented in Chapter 2. The forces provided by linear viscous dampers are proportional to the velocity across the damper and are given by,

$$u(t) = c\dot{x} \tag{4-2}$$

4.2.2 Passive Friction Damper

A yielding system, such as the hysteretic metallic damper, friction dampers, etc., is characterized by a displacement dependent hysteretic loop. Chapter 2 presents the description and mechanisms of some of the popular hysteretic damping systems. Without loss of generality, the nonlinear damper force of a general yielding system can be represented by the Bouc-Wen model as

$$u(t) = \alpha K_e x(t) + (1-\alpha) K_e u_y z(t) \tag{4-3}$$

where x(t) is the displacement across the damper, K_e is a reference stiffness, α is a parameter controlling post-yielding stiffness, u_y is the value of yield displacement and z(t) is a dimensionless hysteretic quantity given by

$$u_y \dot{z} + \gamma |\dot{x}(t)| z |z|^{n-1} + \beta \dot{x}(t) |z|^n - A\dot{x}(t) = 0 \tag{4-4}$$

where β, γ, n and A are dimensionless quantities that control the shape of the hysteretic loop. Equations (4-3) and (4-4) can be used to model various types of nonlinear energy dissipation systems. For example, appropriate values for parameters β, γ, n and A can be selected to model the elasto-plastic types of hysteretic loops for viscoelastic elements. The rigid plastic behavior for a pure Coulomb type friction damper can also be simulated by simply assuming A = 1, α = 0, $K_e u_y = \mu N$, and u_y with a sufficiently small quantity. Thus, the general form of the hysteretic force that represents a wide variety of elastic-plastic behavior can be written as

$$u(t) = \varepsilon \cdot (\ddot{x}_g)_{max} z(t) \tag{4-5}$$

where $\varepsilon = \left| u / \ddot{x}_{g\,max} \right|$ is the ratio of the magnitude of the damper force to the peak shaking force per unit mass due to the ground motion, and u is the damper force. As a special case, the damper force for a pure Coulomb friction damper is given by

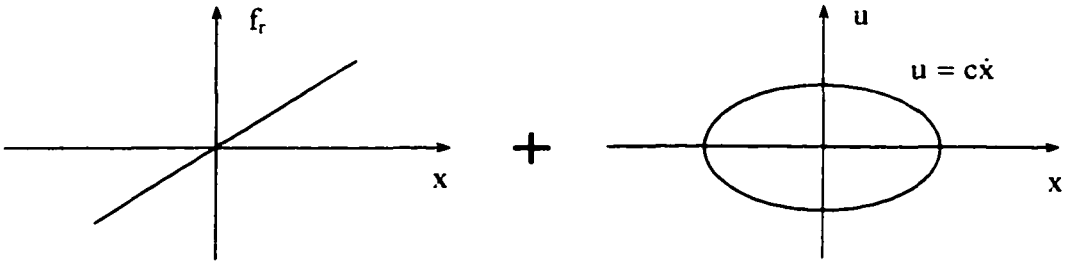

(a) Elastic system with linear viscous damper

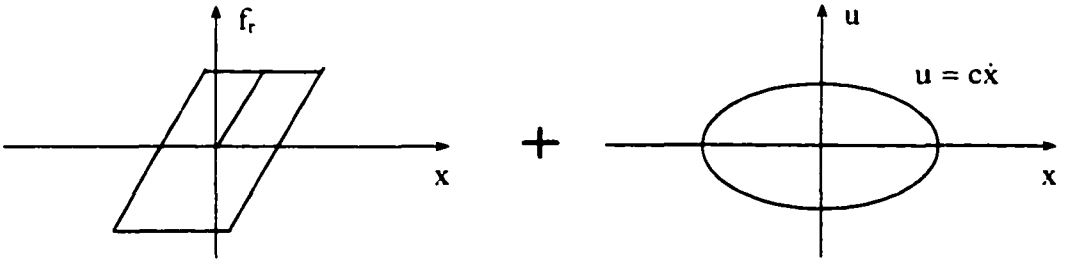

(b) Elastic-perfectly-plastic system with linear viscous damper

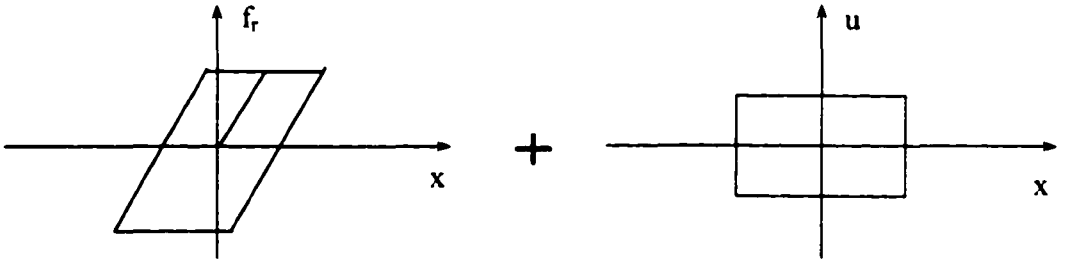

(c) Elastic-perfectly-plastic system with yielding damping system

Figure 4-1: Hysteretic loops of structures and passive dampers.

$$u = \mu N \, \mathrm{sgn}(\dot{x}) \tag{4-6}$$

where μ is the coefficient of friction and N is the normal force across the damper.

Figure 4-1 illustrates the force-displacement relations of a SDOF system with supplemental damping devices described above. Figure 4-1(a) shows an elastic structure with a linear viscous damper. Figures 4-1(b) and (c) show an elastic-perfectly plastic structure with a linear viscous damper and a passive friction damper, respectively. The performances of these systems subject to the analytical pulse model will be investigated in this chapter.

4.3 Elastic Structure with Linear Viscous Damper

Passive fluid viscous dampers are widely used to protect structures from strong ground motions. The *NEHRP Guidelines for the Seismic Rehabilitation of Buildings* (FEMA 368) presented the first comprehensive method for the analysis and design of structure equipped with passive energy dissipation devices. For base-isolated buildings, FEMA 368 presents a method for calculating the design displacement spectra $S_D(\zeta)$ for a given damping factor ζ from the 5% damped spectra $S_D(T,5\%)$ using the numerical damping coefficient B_D as

$$B_D = \frac{S_D(T,5\%)}{S_D(\zeta)} = \frac{1}{R} \tag{4-7}$$

where T is the elastic period of the structure and R is the displacement reduction factor. Table 4-1 below illustrates the displacement reduction factor R used in the codes. These values are based on the studies of Newmark and Hall (1982), Wu and Hanson (1989) and Sadek et al. (2000); however, without considering the near-field ground motion effects. Hence, a systematical investigation to the performance of supplemental damping for

structures subject to near-field ground motions is important. This objective can be achieved by using the analytical pulse model proposed in Chapter 3, which is capable of representing a wide range of pulses in near-field ground motions by varying the pulse parameters.

Table 4-1 Displacement reduction factors R used in codes

Damping ratio ζ	IBC (2000), UBC (1997), FEMA 273	FEMA 368
0.02	1.25	1.25
0.05	1.00	1.00
0.10	0.83	0.83
0.20	0.67	0.67
0.30	0.59	0.56
0.40	0.53	0.48
0.50	0.50	0.42

4.3.1 Pulse Excitations

Considering a linear base-isolated building with a natural period of T = 2.5 sec, and an inherent structural damping ratio of ζ = 5%, the displacement reduction factor R is defined as

$$R(\beta, \varsigma_g, n, \varsigma) = \frac{1}{B_D} = \frac{S_D(\varsigma)}{S_D(T,5\%)} \tag{4-8}$$

For a given structure with a natural period T and an inherent structural damping ratio of 5%, the displacement reduction factor R of supplemental linear viscous dampers depends on the supplemental damping ratio ζ and the characteristic of the ground excitation. The latter is described by three parameters ω_p, ζ_p and n in Equation (3-2). Note that ω_p is the pulse frequency, and ζ_p and n are the parameters describing the buildup and decaying envelop of the velocity pulses, as shown in Section 3.7. To illustrate how the ground

motion affects the performance of supplemental linear viscous dampers, the displacement reduction factor R will be calculated using the analytical pulse model presented in Chapter 3 by varying ζ_p from 0.05 to 0.95 and n from 0 to 5, for various pulse frequencies ω_p. Physically, the response reduction factor R represents the ratio of structural displacements with and without supplemental dampers. Hence, a smaller value of the displacement reduction factor R implies a better performance of a supplemental damping system.

4.3.1.1 Effects of Pulse Period T_p

A linear viscous damper with 25% supplemental linear viscous damping (i.e., a total of 30% linear viscous damping for the structure) is installed between the ground and the base of the base-isolated building. The displacement reduction factor R is plotted as a function of ζ_p for various values of β and n as shown in Figure 4-2, where β is the ratio of the frequency of the pulse excitation to that of the structure as defined in Equation (3-21), i.e; $\beta=\omega_p/\omega$. It is observed form Figure 4-2 that the displacement reduction factor R is highly dependent on the frequency ratio β. For given n and ζ_p, R is minimum (i.e., the performance of the damper is best) when $\beta \approx 1$, i.e., the structural frequency is close to that of the pulse excitation, ω_p. The performance of linear viscous damping degrades significantly as ω_p increases (i.e., $\beta > 1$) or decreases (i.e., $\beta < 1$) with respect to the structural frequency. Hence, linear viscous dampers will perform best for structures whose natural frequency is close to the frequency of the ground motion pulse, and it is less effective for structures subject to earthquake ground motions with $\beta > 4$ or $\beta < 0.2$. Further, the performance of linear viscous dampers degrades as the decay ratio ζ_p

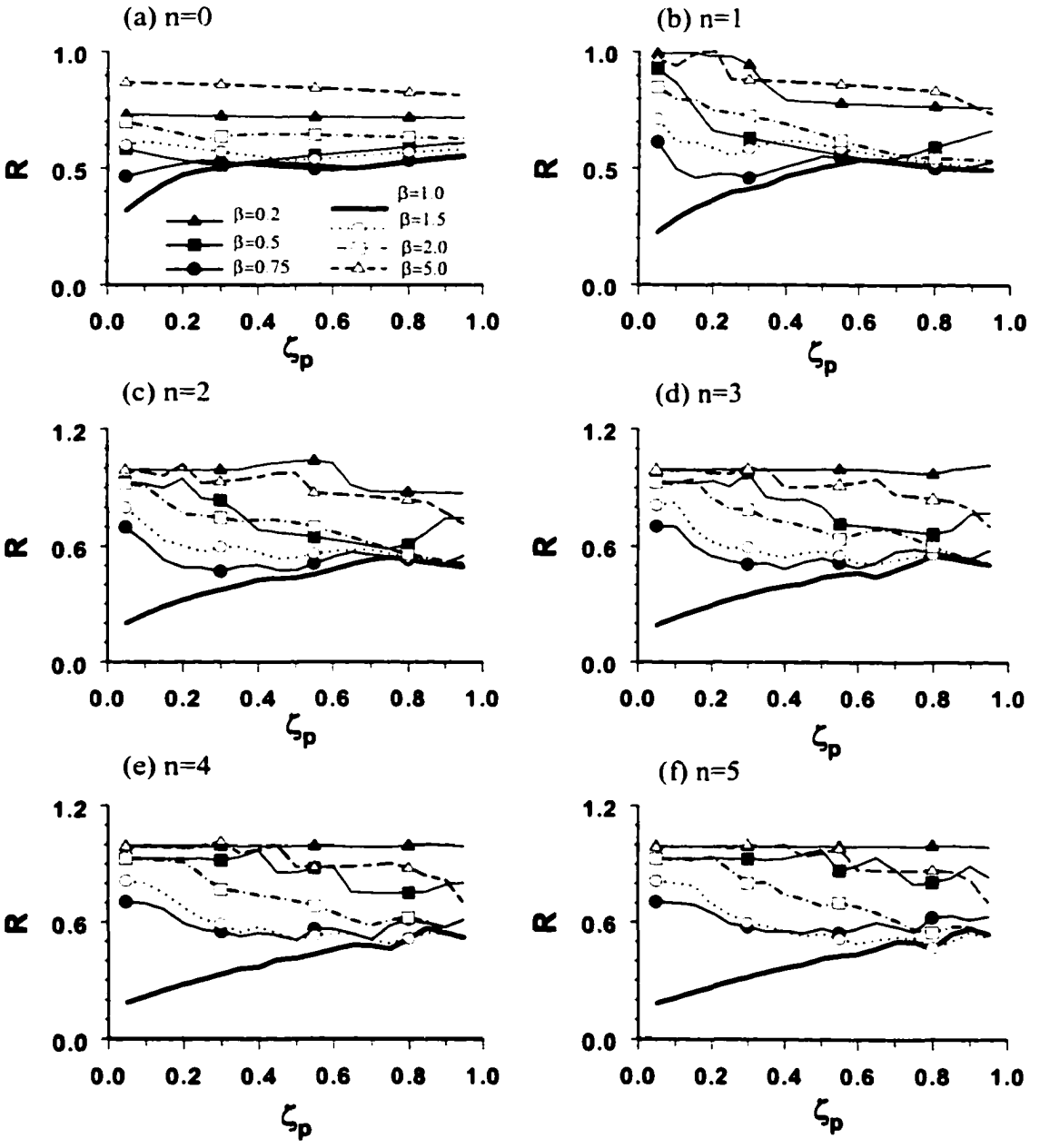

Figure 4-2: Displacement Reduction factor R for 30% linear viscous dampers installed in a SDOF structure subject to velocity pulses with n=0,1,2,3,4 and 5, and ζ_p varying from 0.05 to 0.95.

increases for all values of n when $\beta \cong 1$, and the performance improved as the decay ratio ζ_p increases for all other values of β.

Table 3-1 of Chapter 3 presents parameters of the pulse model for some typical near-field ground motions recorded around the world. For $\omega_p = \sqrt{a^2 + b^2}$ and $\zeta_p = a/\omega_p$, Table 4-2 below presents the approximate value of the response reduction factor, R, and the actual value of the response reduction factor, R^*, for some of the prominent near-field earthquakes.

Table 4-2 Response reduction factor R for Some Prominent Earthquakes

Earthquake	Component	ω_p (rad/sec)	ζ_p (%)	n	β	R	R*
1994 Northridge, M_w=6.7, Rinaldi Receiving	RSS228	6.1	0.18	2.8	2.76	0.74	0.82
1992 Landers Earthquake, M_w=7.2, Lucerne Station	LCN275	1.44	0.62	4.2	0.70	0.54	0.59
1999 Chi-Chi Earthquake, M_w=7.6, TCU068 Station	TCU68N	0.74	0.71	3.2	0.29	0.89	0.96
1979 Imperial valley, M_w=6.9, El Centro Array #6	E06140	2.54	0.47	3.0	1.01	0.52	0.47
1994 Northridge, M_w=6.7, Sylmar – Converter	SCS142	2.51	0.37	2.5	1.00	0.67	0.64
1992 Erzincan, Turkey M_w=7.1, Duzce Station	ERZ_NS	3.20	0.55	5.0	1.30	0.48	0.45
1999 Chi-Chi Earthquake, M_w=7.6, TCU075 Station	TCU75W	1.64	0.72	3.2	0.66	0.66	0.62
1978 Tabas Earthquake, M_w=7.4, Tabas Station	TAB_TR	1.32	0.31	1.97	0.52	0.69	0.74

It is obvious from Table 4-2 that the characteristics of ground motion pulses have a significant effect on the performance of a linear viscous damper installed in a linear structure, and the same linear viscous damper will have different performance earthquakes with different characteristics. It is also observed from Table 4-2 that the estimated values of the response reduction factors, R, obtained by the analytical pulse

models are quite close to that of the actual values R^* obtained by using the recorded ground motions if the predominant frequency components in ground motions are adequately modeled by the pulse model. This again shows that the proposed analytical pulse model is quite reasonable for the investigation of the performance of passive energy dissipation systems.

4.3.1.2 Effect of Pulse Shape Parameters n and ζ_p

Parameters ζ_p and n in Equation (3-1) are shape parameters which determine the envelop of the velocity pulse. To study the effects of these parameters on the displacement reduction factor, R, the abscissa ζ_p in Figure 4-1 is normalized to $N = n/2\pi\zeta_p$, where N is the number of cycles of velocity pulses during the buildup phase defined in Equation (3-10). Figure 4-3 shows the plots of R versus N for different values of β and n = 1 to 5. It is observed from Figure 4-3 that while R decreases with the increase of N for $\beta \cong 1$, it increases with N for other values of β.

4.3.2 Theoretical Analysis

Numerical results in the previous chapter demonstrate that the displacement reduction factor, R, of passive viscous dampers depends on the number of cycles of velocity pulses during the build-up phase, N, and the frequency ratio β of the excitation and the structure. A theoretical analysis is presented in the following to interpret this behavior. The base-isolated building with 30% damping (5% of inherent and 25% supplemental) is used as an example. The acceleration pulses in Equation (3-2) with n=1, ζ_p=0.15, and β= 0.4, 1.1 and 2.5, respectively, are used as excitations. Note that the

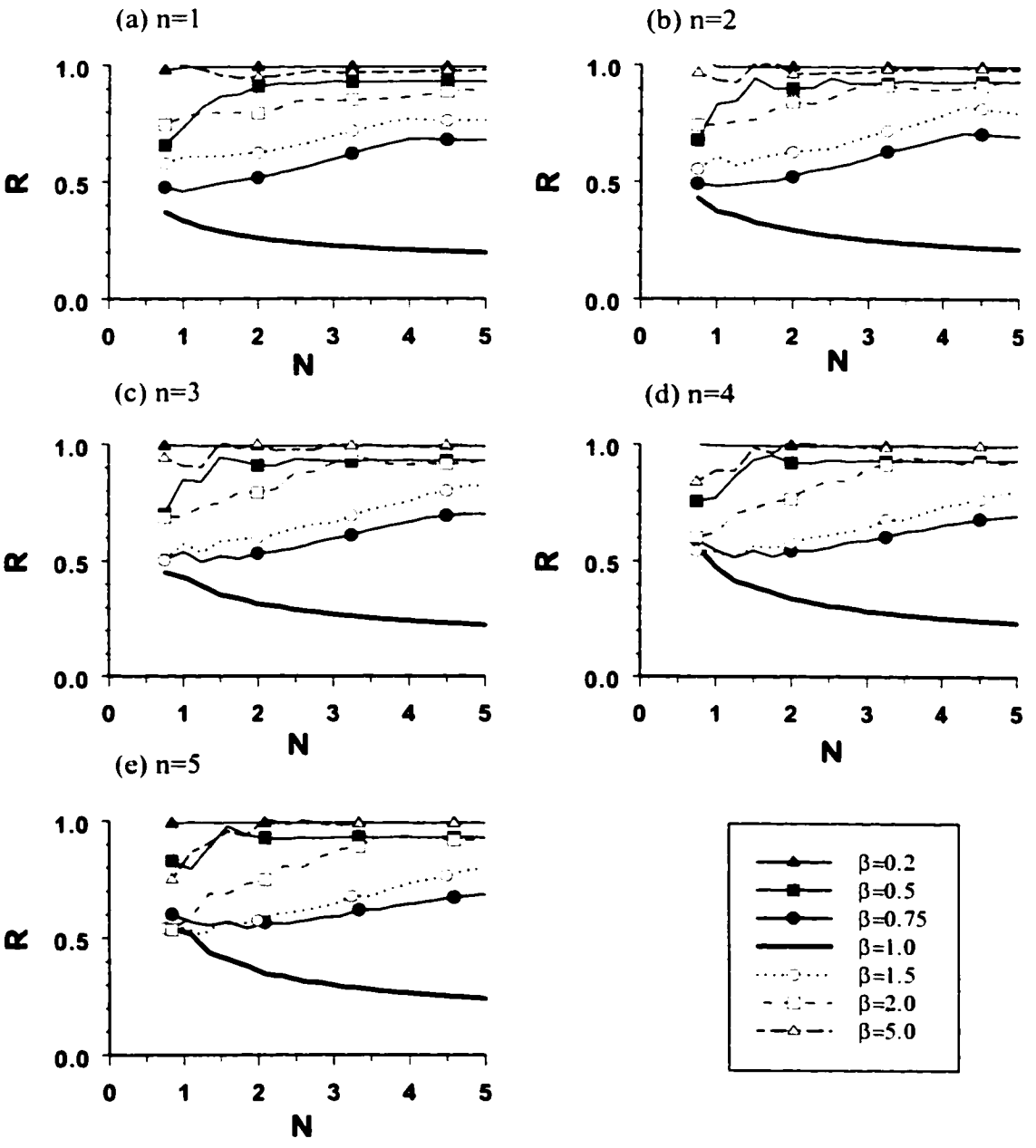

Figure 4-3: Displacement Reduction factor, R, vs. N for 30% linear viscous damper for a SDOF structure subject to velocity pulses with n=1, 2, 3, 4 and 5, and ς_p varying from 0.05 to 0.95.

analytical solution for the pulse excitation in Equation (3-2) for n=1 has been derived in the previous Chapter. The closed-form solution in Equation (3-36) can be rewritten as

$$x_t(t) = x_h(t) + x_p(t) \qquad (4\text{-}10)$$

where x_t, x_h and x_p are the general, homogenous and particular solutions, respectively. The homogenous solution is due to the free vibration of the structure and depends on the initial conditions, while the particular solution is due to the excitation. The analytical solutions x_h and x_p derived in Chapter 3 can be rewritten as

$$x_h(t) = x_1(t) + x_2(t) \qquad (4\text{-}11)$$

$$x_p(t) = x_3(t) + x_4(t) + x_5(t) + x_6(t) \qquad (4\text{-}12)$$

where

$$x_1(t) = e^{-\zeta\omega t} \cdot B_1 \cos(\sqrt{1-\zeta^2}\,\omega t) \qquad (4\text{-}13)$$

$$x_2(t) = e^{-\zeta\omega t} \cdot B_2 \sin(\sqrt{1-\zeta^2}\,\omega t) \qquad (4\text{-}14)$$

$$x_3(t) = e^{-\zeta_p\omega_p t} \cdot B_3 \cdot \cos(\sqrt{1-\zeta_p^2}\,\omega_p t) \qquad (4\text{-}15)$$

$$x_4(t) = e^{-\zeta_p\omega_p t} \cdot B_4 t \cdot \cos(\sqrt{1-\zeta_p^2}\,\omega_p t) \qquad (4\text{-}16)$$

$$x_5(t) = e^{-\zeta_p\omega_p t} \cdot B_5 \sin(\sqrt{1-\zeta_p^2} \cdot \omega_p t) \qquad (4\text{-}17)$$

$$x_6(t) = e^{-\zeta_p\omega_p t} \cdot B_6 t \cdot \sin(\sqrt{1-\zeta_p^2} \cdot \omega_p t) \qquad (4\text{-}18)$$

The displacement responses of both damped and undamped structure subject to the acceleration pulses described above are plotted in Figure 4-4. Displacements in this figure are normalized by letting C=1 in Equation (3-2). Figure 4-4(a) and 4-4(b) show the displacements of the SDOF base-isolated building for 5% and 30% damping ratios, respectively, where the frequency ratio is β=0.4. In this case, the structural period is

$T=0.4T_p$, i.e., the pulse has a longer period than the structure. It is observed from Figure 4-4 (a) that the total displacement x_t is dominated by the x_4 component of the particular solution x_p. The magnitudes of various components of the particular solution x_p depend on the coefficients B_1 to B_6. Figure 4-5 plots the coefficients B_1 to B_6 as functions of the structural damping ratio ζ. It has been shown in Chapter 3 that B_2, B_4 and B_5 are dominant terms in Equation (3-36) for structures with a low damping ratio ζ subject to long period pulses with a small decaying ratio ζ_p. For this case, the general solution in Equation (4-10) can be approximated by Equation (3-55) as

$$x_t(t) \cong x_2 + x_4 + x_5 \tag{4-19}$$

Among different terms in Equation (4-19), x_2 is the major contribution to the homogenous solution and x_5 only affects the phase of x_4 in Equation (4-19). The coefficients B_1 and B_3 shown in Figure 4-5(a) only affect the initial values of the homogenous solution and the particular solution at t=0. They have a less effect on the general solution, as shown in Figure 4-4 (b). Thus, x_4 is the dominant term in Equation (4-19). For $\beta = 0.4$, it is observed from Figure 4-5(a) that the damping ratio, ζ, has very little effect on the coefficient B_4, which determines the magnitude of the component x_4 of the particular solution x_p. Hence, the reduction in the total response of the structure, x_t, is very small because of the increase in the damping ratio from 5 to 30% is very small for the case of $\beta = 0.4$, as shown in Figure 4-4(b). Consequently, a structure subject to long-period excitations can hardly be benefited from the use of supplemental viscous dampers.

Figures 4-4(e) and (f) show the displacements of the structure with damping ratios 5 and 30%, respectively, where the frequency ratio, β, is 2.5. The solution in Equation (4-10) for this case can be approximated by Equation (3-49) for any structural damping

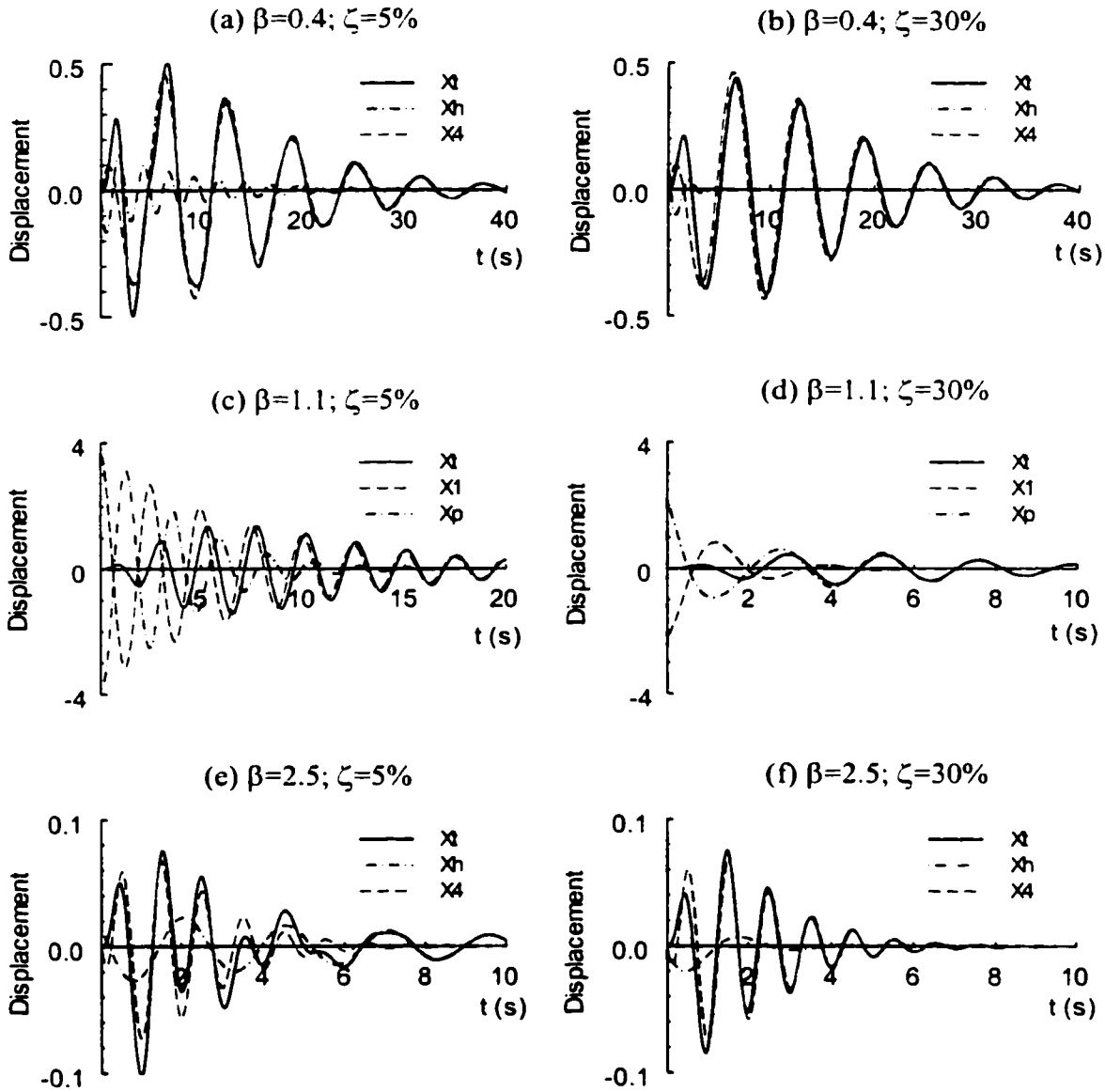

Figure 4-4: Displacement time histories of damped and undamped system subject to pulse accelerations with different frequency ratios, β.

(a) β=0.4

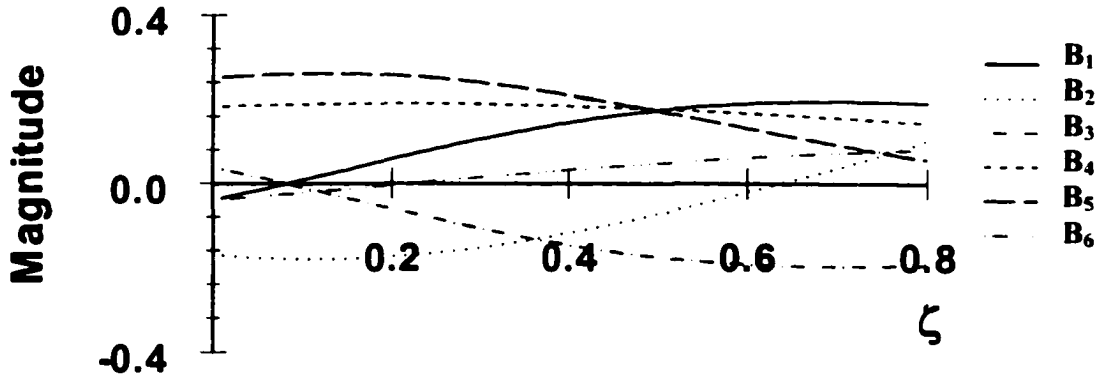

(b) β=1.1

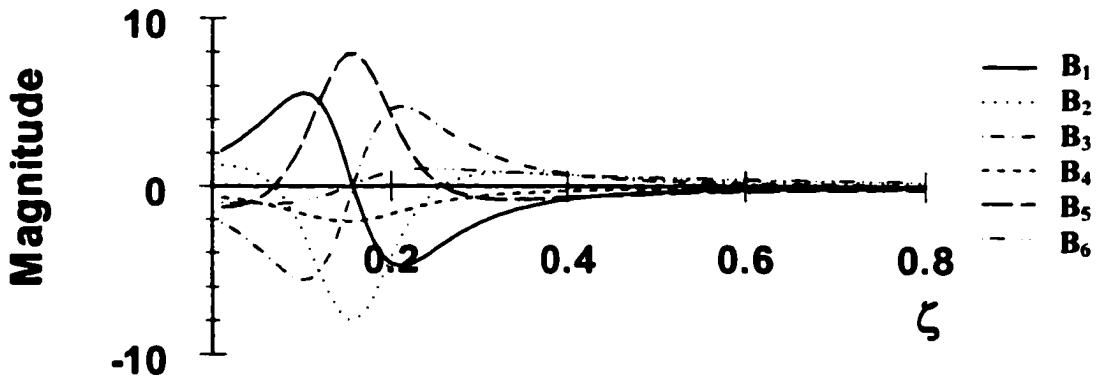

(c) β=2.5

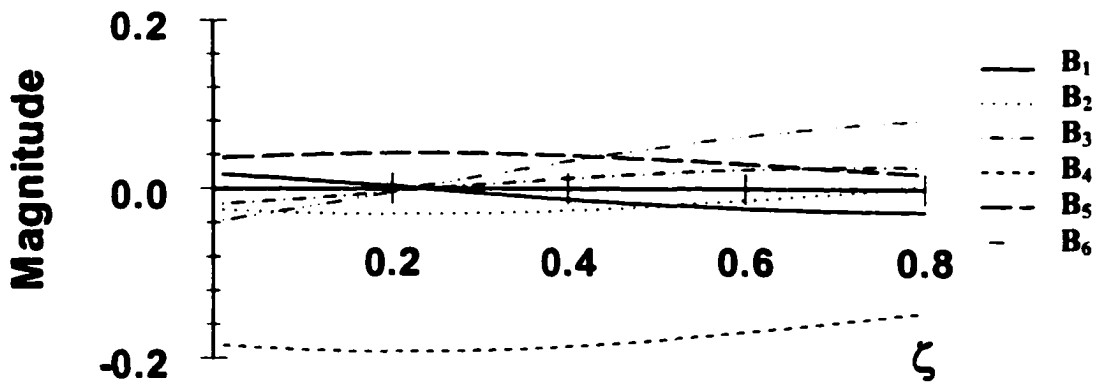

Figure 4-5: Coefficient B_1, B_2, B_3, B_4, B_5 and B_6 vs. viscous damping ratio ζ for a base-isolated building subject to acceleration pulses: (a) β=0.4; (b) β=1.1; (c) β=2.5.

ratio ζ. It is observed from Equation (3-49) that the x_4 and x_6 components mainly contribute to the response of the structure. However, it is observed from Figure 4-4(e) that the displacement response is dominated by the x_4 for structures subjected to short period pulses with a frequency ratio β=2.5. Figure 4-5(c) shows the plots of the coefficients B_1 to B_6 as functions of the structural damping ratio ζ for this case. From Figure 4-5(c), the coefficient B_4 is almost a constant with respect to the increase of the damping ratio ζ. This indicates that the displacement reduction can hardly be achieved by using passive linear viscous dampers in such a condition as shown in Figure 4-4 (f).

Figures 4-4(c) and (d) show the displacements of the building with 5 and 30% damping ratios, respectively, when subject to pulse excitations with β = 1.1. It is observed from these two figures that the passive viscous damper is very effective in reducing the displacement of the structure when subjected to excitations with $\beta \cong 1$. The contribution of from various components of homogeneous and particular solutions to the general solution is relatively complicated in such a condition. It has been shown by Equation (3-62) in Chapter 3 that the total solution is dominated by x_2, x_5 and x_6 for β=1. As β is increased to 1.1, the solution is mostly dominated by the x_1 component of the homogeneous solution and the particular solution x_p instead of x_2, x_5 and x_6 for β = 1. Plots of the coefficients B_1 to B_6 versus the damping ratio, ζ , are shows in Figure 4-5(b). It is observed that the coefficients B_1 to B_6 have high magnitudes for small damping ratio, ζ, and they decrease drastically with the increase of the damping ratio. Hence, for β = .1, the peak displacement is gradually built-up as shown in Figure 4-4 (c) and it decreases drastically with the increase of the damping ratio, ζ, as shown in figure 4-4(d).

4.3.3 Recorded Ground Motions

To verify the results obtained above using the pulse model, several impulsive ground motions recorded near the fault rupture are used herein. Two typical long period structures, the SDOF base-isolated building and the MDOF benchmark bridge model [Dyke et al (2000)], are used to investigate the efficiency of supplemental linear viscous dampers. The recorded near-field ground motions used are those used in system analyses for the SAC Steel Project as shown in Appendix I. The first set of ten 2-component acceleration time histories has been derived from historical ground motion records. The second set of ten 2-component acceleration time histories has been calculated from physical simulations of the fault rupture and seismic wave propagation through soil strata. The first ten recorded ground motions include several records for soil conditions different from S_D in UBC 1997 (soft soil). These records were adjusted to S_D.

The 20 time histories were selected to include near-field ground motions from earthquakes having a variety of faulting mechanisms (strike-slip, oblique, and thrust) in the magnitude range of 6.75 to 7.5. The closest distances for shallow crustal faults lie in the range of 0 to 10 km, and the closest distances for blind thrust faults lie in the distance range of 6 to 18 km. These magnitudes and distance ranges dominate the seismic hazard in Zone 4 for a return period of 10% in 50 years.

The time histories do not represent a statistical sample of such ground motion conditions, and were not scaled to represent a target spectrum. However, the variability among these 20 time histories is representative of the variability in recorded data for a given magnitude, distance and site conditions in empirical ground motion models. Although the 20 selected time histories are for a range of magnitudes and distances, they

form a set that provides a reasonable representation of the median and variability of the ground motions that a given site may experience from a nearby earthquake of magnitude in the vicinity of 7 and approximate distance of 5 km. This magnitude-distance pair is representative of earthquakes with exceedance probability 10% in 50 year in major urban regions of California.

4.3.3.1 Example 1: Base Isolated Building

The suite of 20 SAC ground motions described above is utilized for the SDOF base isolated building with a natural period of 2.5 sec and a damping ratio 5%. The displacement reduction factor R for 15% (10% supplemental damping) and 30% (25% supplemental damping) viscous damping for 20 sets of SAC near-field ground motions are plotted in Figure 4-6 as solid squares and circles for the fault normal and fault parallel components as a function of the predominant period T_g of each ground motion, respectively. Figure 4-6 also shows plots of R using the pulse model with n=0, ζ_p=20% and T_p varying from 0.05 s to 5 sec. A regression curve obtained from the results due to the recorded ground motions is also presented in Figure 4-6. It is observed from the curves in Figure 4-6 that the displacement reduction factor R obtained from velocity pulse model follows the trend of the regression curve from SAC near-field ground motions and it is mostly affected by the predominant period of the ground motion. It is interesting to note that the displacement reduction factors R recommended by FEMA 368 for 15% and 30% damping ratios are 0.740 and 0.588, respectively, independent of the ground motion. However, these values can only be achieved by some ground motions with a predominant period T_p around the natural period of the structure, T = 2.5 sec, and they may be overestimated for the base-isolated building subject to impulsive pulses with

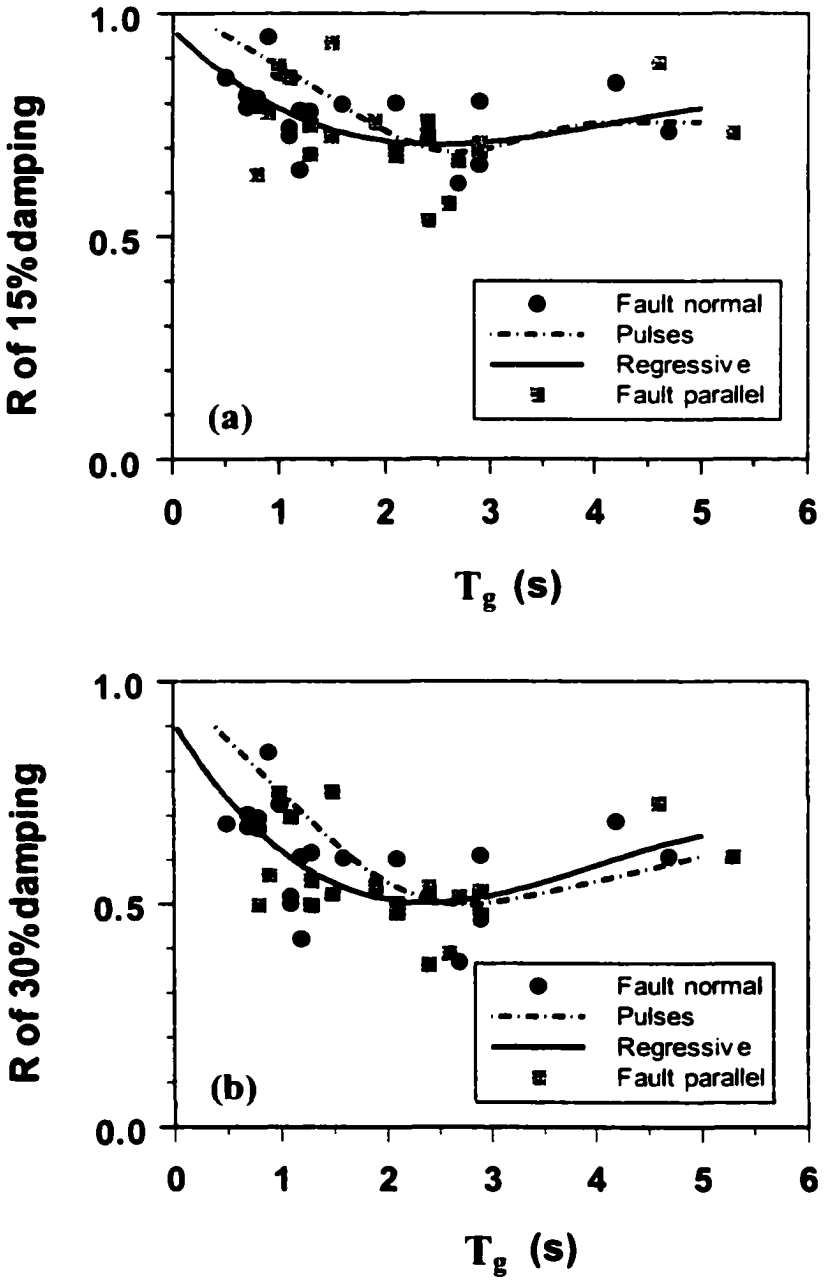

Figure 4-6: Displacement Reduction Factor R of: (a) 15% linear viscous damper; (b) 30% linear viscous damper.

$\beta>2$ or $\beta<0.5$.

4.3.3.2 Example 2: Benchmark Cable-Stayed Bridge

The second example used to illustrate the efficiency of passive linear viscous dampers affected by the ground motion is the benchmark cable-stayed bridge presented by Dyke et al. (2000). The model of the benchmark cable-stayed bridge is based on the Missouri 74-Illinois 146 cable-stayed bridge spanning the Mississippi River near Cape Girardeau, Missouri, and a schematic drawing of the bridge is shown in Figure 4-7. The proximity of the bridge site to the New Madrid seismic zone makes the protection of the bridge from seismic excitation of interest.

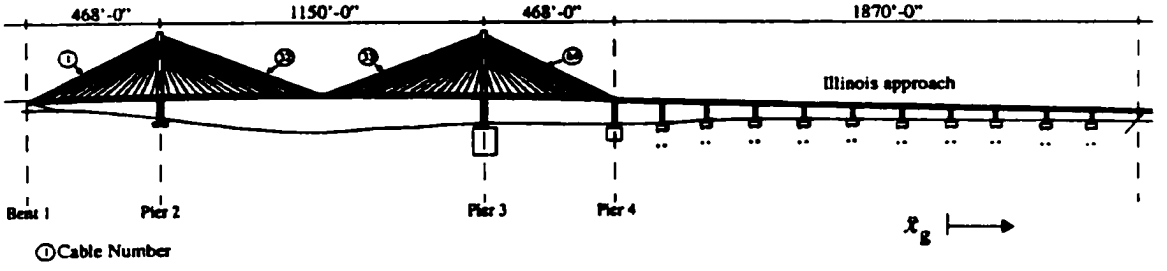

Figure 4-7: Drawing of the Cape Girardeau Bridge [Dyke et al (2002)].

The stiffness matrices of the linearized evaluation model of the benchmark cable-stayed bridge are determined through a nonlinear static analysis corresponding to the deformed state of the bridge with dead load. If lock-up devices are used between the deck and towers, the first ten frequencies of the evaluation model are 0.2899, 0.3699, 0.4683, 0.5158, 0.5812, 0.6490, 0.6687, 0.6970, 0.7102, and 0.7203 Hz, which is used as a basis of comparison for various controlled systems. If no connection or control devices

are employed between the deck and towers, the model is referred to as the uncontrolled case. The first ten frequencies for the uncontrolled case are 0.1618, 0.2666, 0.3723, 0.4545, 0.5015, 0.5650, 0.6187, 0.6486, 0.6965, and 0.7094 Hz, respectively. Detailed information about the cable-stayed bridge, including its modeling and the FEM package, can be found in Dyke et al (2000). Because the bridge is assumed to be attached to the bedrock, the effect of soil-structure interaction has been neglected. One-dimensional ground acceleration is assumed to be applied longitudinally, and acts simultaneously at all supports.

To evaluate the effectiveness of various control systems and algorithms, evaluation criteria J_1 to J_{18} have been presented [Dyke et al., (2000)]. The first six evaluation criteria J_1 to J_6 are related to the peak responses, where J_1 = the peak base shear of towers, J_2 = the peak shear force of towers at the deck level, J_3 = the peak overturning moment at the bases of towers, J_4 = the peak moment of towers at the deck level, J_5 = the peak deviation in cable tension, and J_6 = the peak displacement of the deck at the abutment. These criteria are normalized by the corresponding response quantities of the bridge with rigid links between the deck and towers. Since the bridge has two towers, all the peak response quantities related to the tower are normalized by the maximum of the peak response quantities of the two towers.

In this study, a total of 24 linear viscous dampers are installed and their distribution is shown in the parentheses of Figure 4-8, which is identical to that of the sample problem using actuators in Dyke et al. (2000). Two levels of linear viscous damping have been considered in this study. The first case of supplemental viscous damping coefficient, C=1750KN $(m/s)^{-1}$, referred to as high viscous damping case, has

the similar level of control force as the sample control force. The other case of supplemental viscous damping coefficient is C = 875KN $(m/s)^{-1}$, referred to as medium viscous damping case.

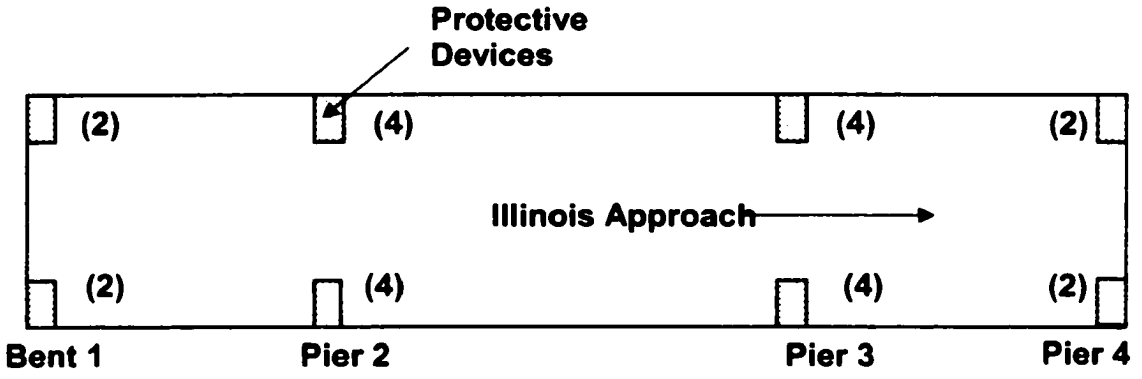

Figure 4-8: Locations of protective devices in Cable-Stayed Bridge.

In order to illustrate the performance of linear viscous dampers for the benchmark cable-stayed bridge, the suite of near-field ground motions developed for the SAC project is used. When neither control devices nor dynamically stiff shock transmission devices are used between the deck and towers, the fundamental natural period of the bridge is 6.18 s, which is larger than the predominant period of any of the near-field ground motions recorded before the 1999 Chi-Chi earthquake. To study the effects of ground motions with predominant periods around or larger than fundamental natural period of the cable-stayed bridge, ground motions recorded during 1999 Chi-Chi earthquake are also used for this example. These ground motions are: TCU065 N-S component (T_g = 6.4 s), TCU065 E-W component (T_g = 4.5 s), TCU068 N-S component (T_g = 8.0 s) and TCU068 E-W component (T_g = 8.8 s).

Similar to Equation (4-8), the criteria R_{Ji} is defined as

$$R_{Ji} = \frac{J_i(\varsigma)}{J_i(3\%)} \quad , i=1,2,....6 \tag{4-20}$$

where $J_i(\zeta)$ and $J_i(3\%)$ are evaluation criteria i of the bridge with passive dampers and the uncontrolled bridge (no control devices or dynamic shock transmissions between the towers and the deck). Note that the inherent damping ratio of the fundamental mode of the bridge is 3%.

Figures 4-9 to 4-14 show the plots of the criteria reduction factors for the cable-stayed bridge with the supplemental viscous damping as a function of the predominant period, T_g, of each ground motion for two levels of viscous damping ratios. It is observed from Figure 4-9 that the peak deck displacement reduction factor, R_{J6}, is highly correlated with the predominant period of the near-field ground motions. The supplemental viscous dampers achieve the best performance for ground motion whose predominant period, T_g, is in the vicinity of or longer than the fundamental natural period of the cable-stayed bridge. For example, For the TCU065 N-S component of the Chi-Chi earthquake, whose predominant period is T_g=6.4 sec, the deck displacement reduction factors for medium and high supplemental linear viscous dampers are 0.32 and 0.21, respectively. For earthquakes with fundamental periods around 2 sec., the performance of passive viscous dampers degrades significantly.

The criteria reduction factors for the bridge have also been investigated using the proposed pulse model with n = 0, decaying ratio ζ_p = 20% and T_p varying from 0.4 to 10 sec. The shape factor n=0 is used since the displacement reduction factor R for a SDOF structure is less affected by ζ_p for n=0 as shown in Figure 4-2. Also shown in Figure 4-9 to Figure 4-14 as dashed curves are the criteria reduction factors obtained using the analytical pulse model for the two levels of damping ratios. Results obtained by the

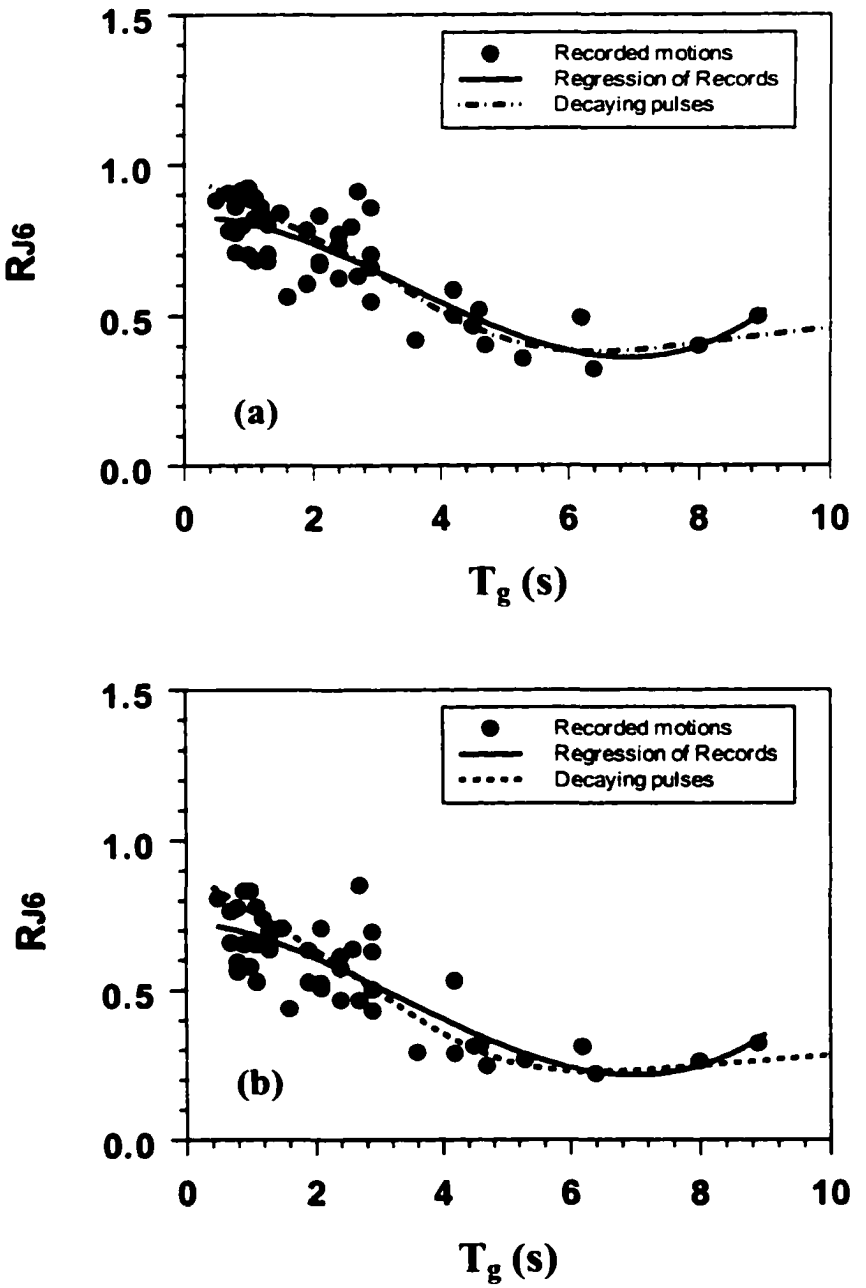

Figure 4-9: Criteria reduction factor of peak deck displacement, R_{J6}, of supplemental Viscous damper with damping coefficient: (a) C=875 KN.(m/s)$^{-1}$; (b) C=1750 KN.(m/s)$^{-1}$.

regression of the criteria reduction factors for the recorded ground motion are shown by the solid curves in these figures. It is observed from Figure 4-9 that the curves for the deck displacement reduction factor R_{J6} using the analytical pulse model match well with the regression curve of recorded ground motions. Hence, the proposed pulse model can be used to estimate the displacement reduction factor of passive viscous dampers for long period structures subject to near-field ground motions for a given site at which historical ground motions are not available. For such locations, approximate values of the pulse parameters T_p and ζ_p can be obtained by the attenuation relationship among the magnitude of earthquake, distance from the epicenter, soil types, etc.

It is also interesting to point out that the regression curve is available only up to $T_g = 6.4$ sec with the SAC suite of ground motions. To obtain regression curve for longer period ground motions, ground motions with longer pulse periods must be available. On the other hand, the analytical pulse model can be used to calculate R_{J6} for the entire range of ground motion periods, as shown in Figure 4-9.

The criteria reduction factors for the peak shear force at the tower base R_{J1} and the peak shear force of the tower at the deck level R_{J2} are plotted in Figure 4-10 and 4-11, respectively. It is observed that the correlation between the predominant period (T_g) of the ground motion and the criteria reduction factors R_{J1} and R_{J2}, corresponding to recorded ground motions for two levels of supplemental viscous damping ratios, is worse than that of R_{J6}. This may be due to the fact that both the shear forces at the tower base and the deck level depend directly on the absolute accelerations. The SAC suite of recorded ground motions contains several high-frequency (low period) components of different magnitudes in addition to the long-period pulse with a period T_p. As a result,

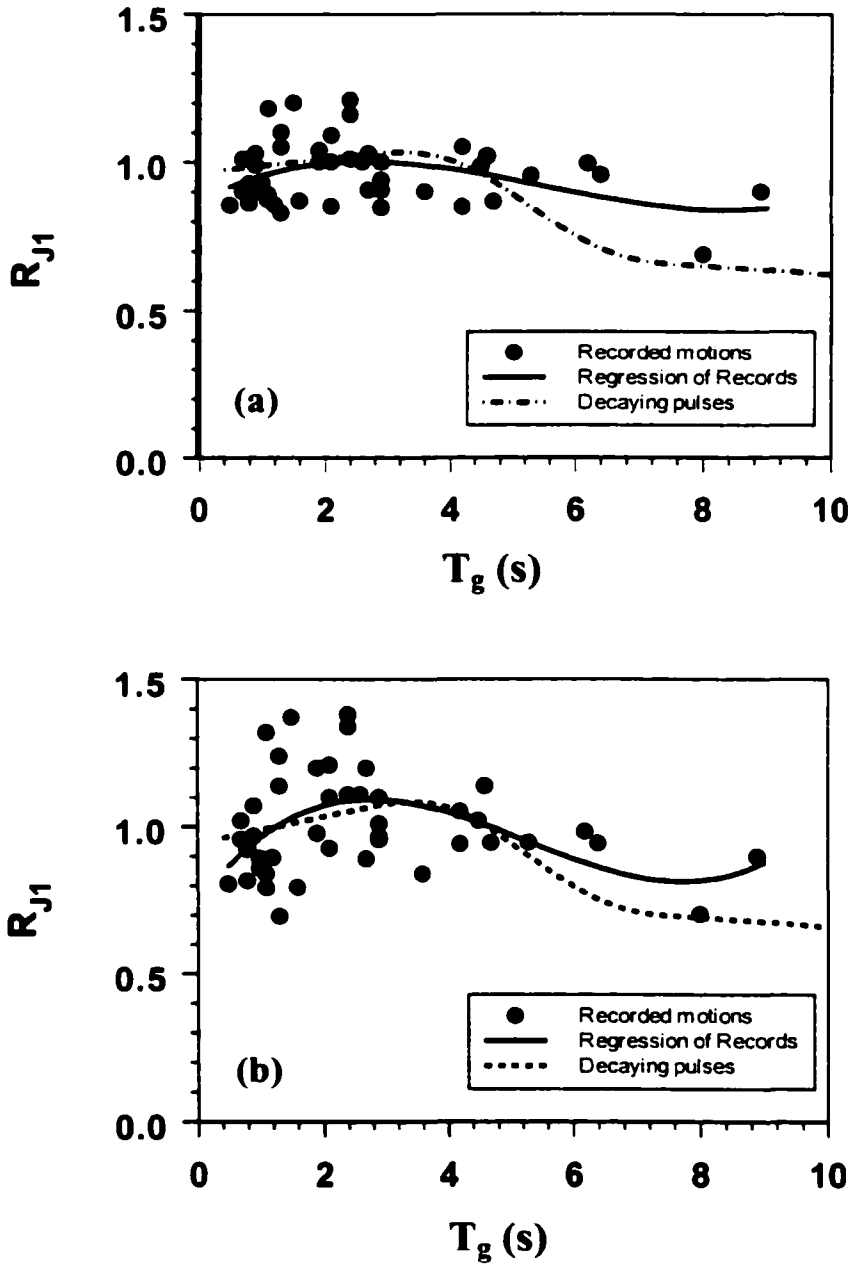

Figure 4-10: Criteria reduction factor of Peak shear force at the tower base, R_{J1}, for supplemental linear viscous damper: (a) damping coefficient C=875 KN.s/m; (b) damping coefficient C=1750 KN.s/m.

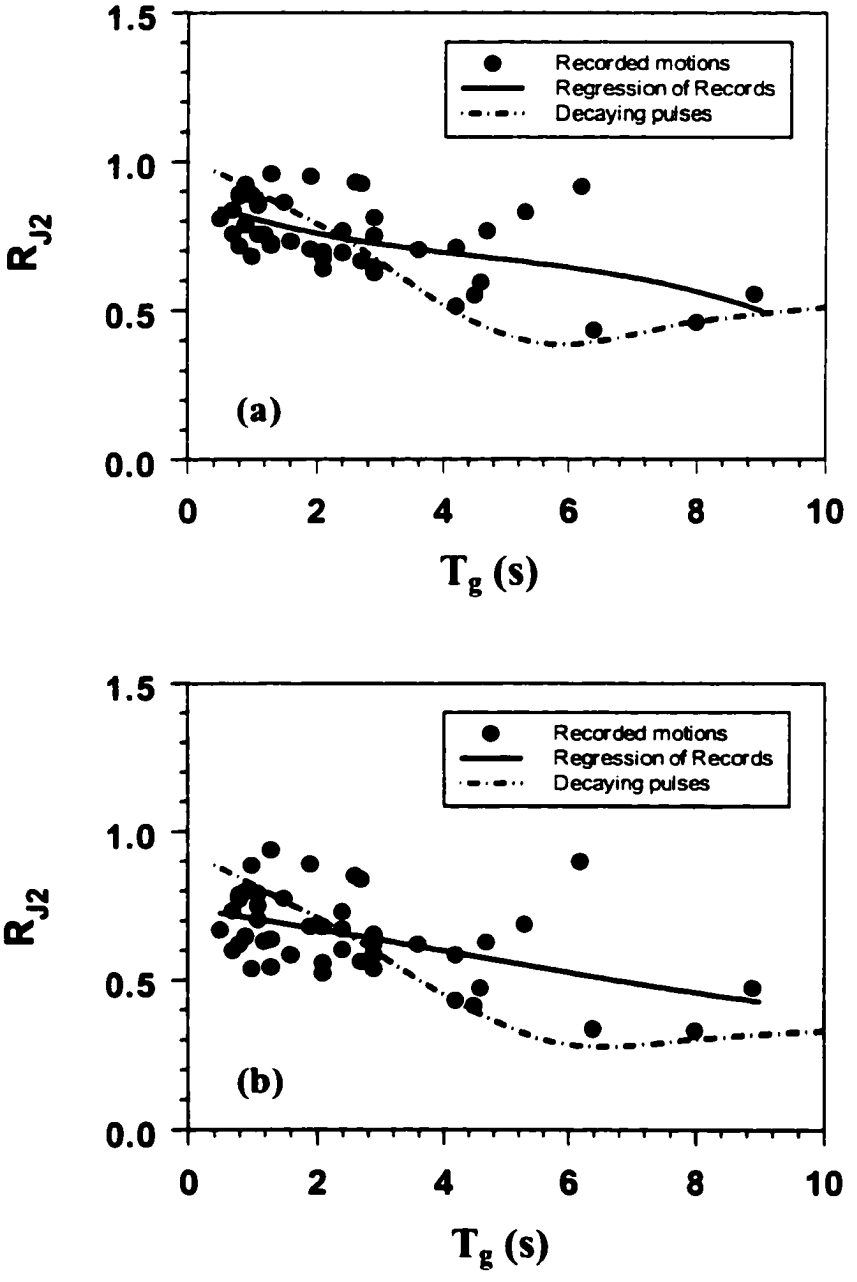

Figure 4-11: Criteria reduction factor of peak shear force at the tower base, R_{J2}, for supplemental linear viscous dampers with damping coefficient: (a) C=875; (b) C=1750 KN.s/m.

the criteria reduction factors R_{J1} and R_{J2} for a particular value of T_p vary widely for recorded ground motions. On the other hand, the pulse approximation only models the dominant long-period component of the ground motion. Figures 4-10 and 4-11 also show plots of the criteria reduction factors obtained using the regression of results obtained from recorded ground motion data. Because of a wide variation among the results for recorded ground motions, there is a poor agreement between the regression curve and the pulse model curve. However, it is observed from Figures 4-10 and 4-11 that the criteria reduction factors R_{J1} and R_{J2} tend to be closer to the results of the pulse model for long-period ground motions, since the destructiveness of these ground motions is more affected by the long-period components.

Figures 4-12 and 4-13 plot the criteria reduction factors for peak overturning moment at the tower base, R_{J3}, and peak moment of the tower at the deck level, R_{J4}, respectively. It is observed from these figures that these two criteria reduction factors are strongly correlated with the predominant period, T_g, of the ground motion, since both the moments of towers at the tower base and at the deck level depend on the peak deck displacement. The peak displacement of the bridge deck depends on the long-period component of recorded ground motions, as shown previously. The overturning bending moments at the tower base and at the deck level increase because of the increased level of the cable tension caused by larger deck displacements. In particular, R_{J4} is more directly dependent on the peak deck displacement than R_{J3}, since the former is caused by the cable tension forces while the later is caused not only by the cable tension forces, but also by the inertia force of the deck transmitted to the towers at the deck level. Figures 4-12 and 4-13 also show curves for the criteria reduction factors obtained using the pulse

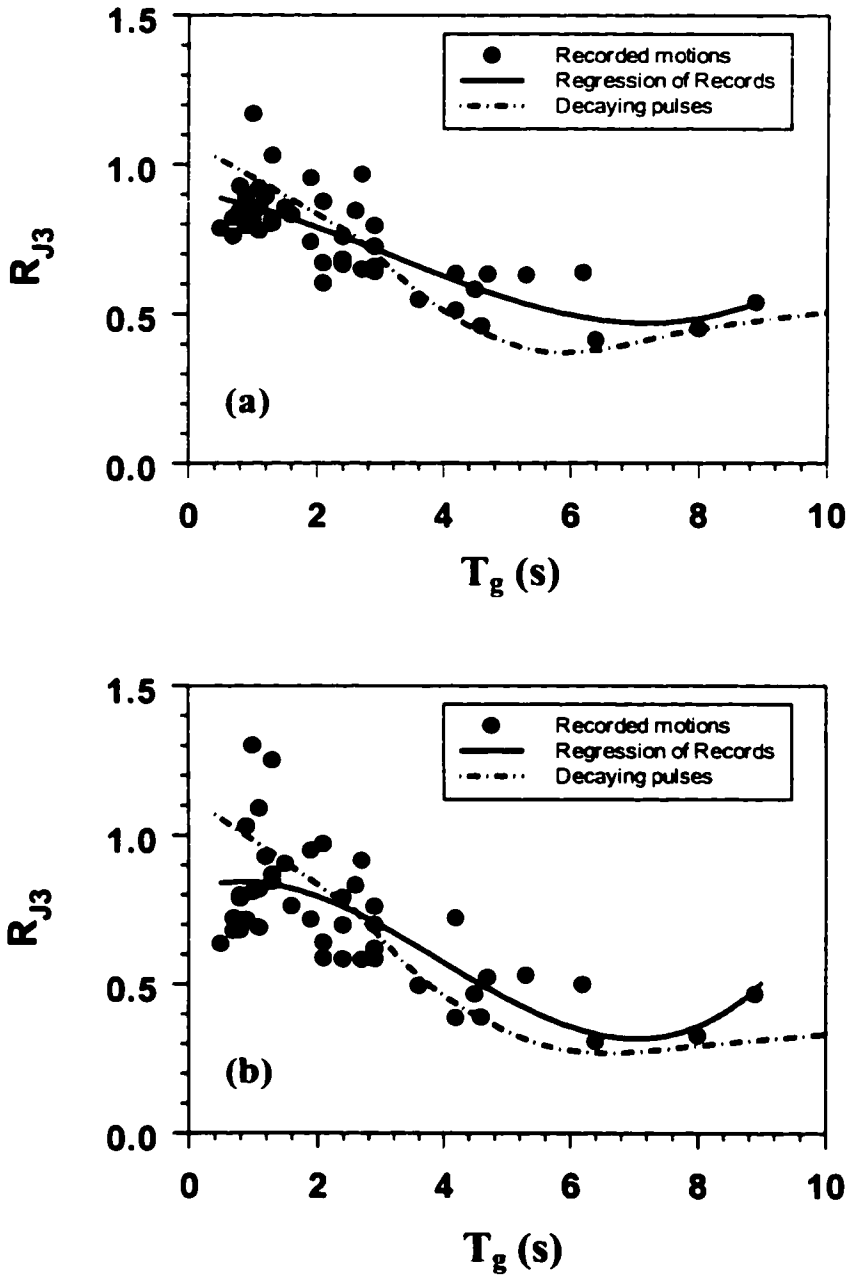

Figure 4-12: Criteria reduction factor of overturn bending moment at tower base, R_{J3}, of supplemental viscous dampers with damping coefficient: (a) C=875 KN.s/m; (b) C=1750 KN.s/m.

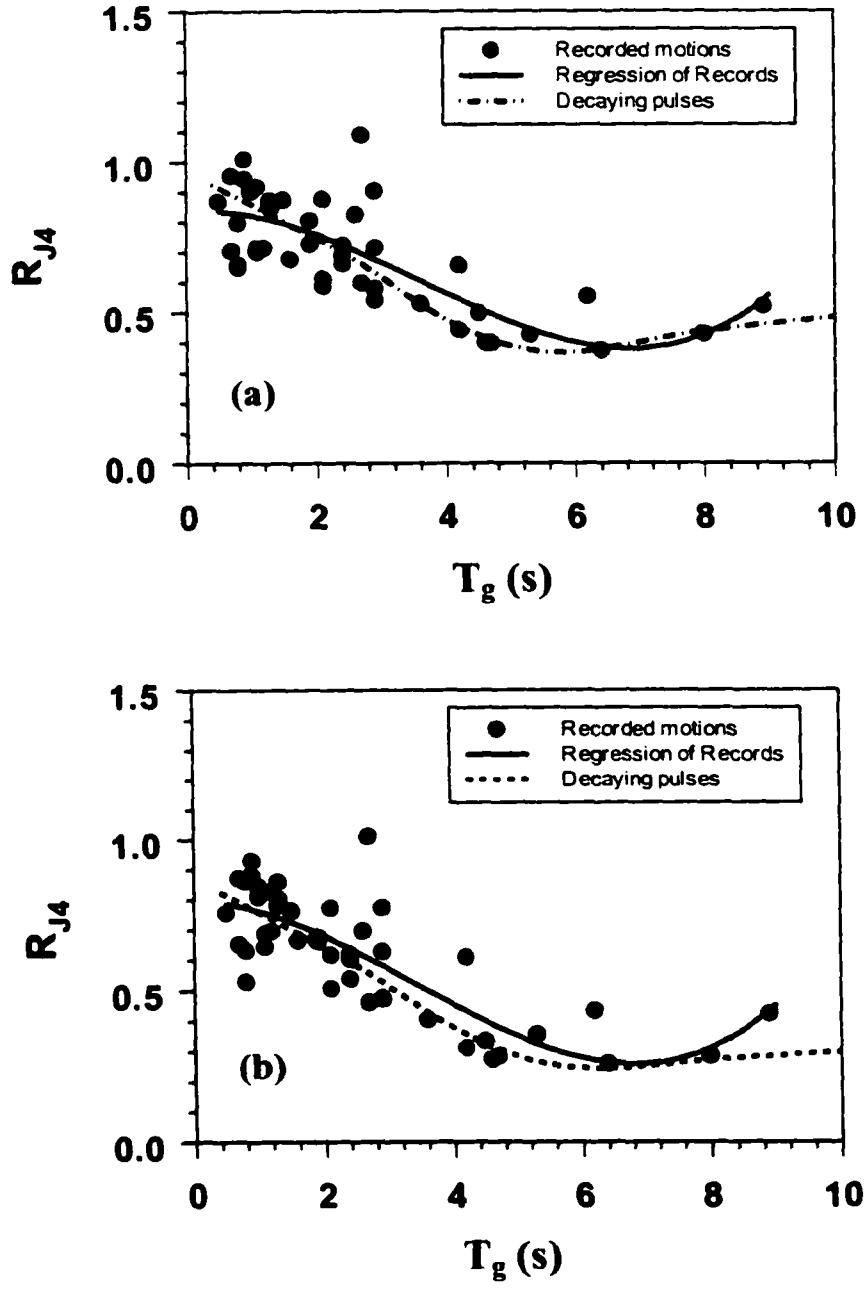

Figure 4-13: Criteria reduction factor of bending moment of tower at deck level, R_{J4}, of supplemental viscous dampers with damping coefficient: (a) C=875 KN.s/m; (b) C=1750 KN.s/m.

model. Although there is a wide variation between the criteria reduction factors R_{J3} and R_{J4} for recorded ground motions and for the pulse model at low-periods (high-frequencies) due to presence of high-frequency components in recorded ground motions. the general trend of curves for recorded ground motions is the same as that of the pulse model for long period components. This fact is also evident by a comparison between the regression curves based on the recorded ground motions and that using the pulse model.

Figure 4-14 shows the plots of the criteria reduction factor for the peak cable deviation, R_{J5}, for two levels of supplemental linear viscous dampers. As described earlier, since the peak cable tension depends on the peak deck displacement and the displacement of the tower at the anchorage point of the cable, the correlation between the peak cable tension and the predominant period, T_g, of the ground motion is strong. Again the general trend of the curves for recorded ground motions is similar to that for the pulse model. It is also observed that the peak cable tension has the largest reduction when the predominant period of the near-field ground motion is close to the fundamental period of the bridge.

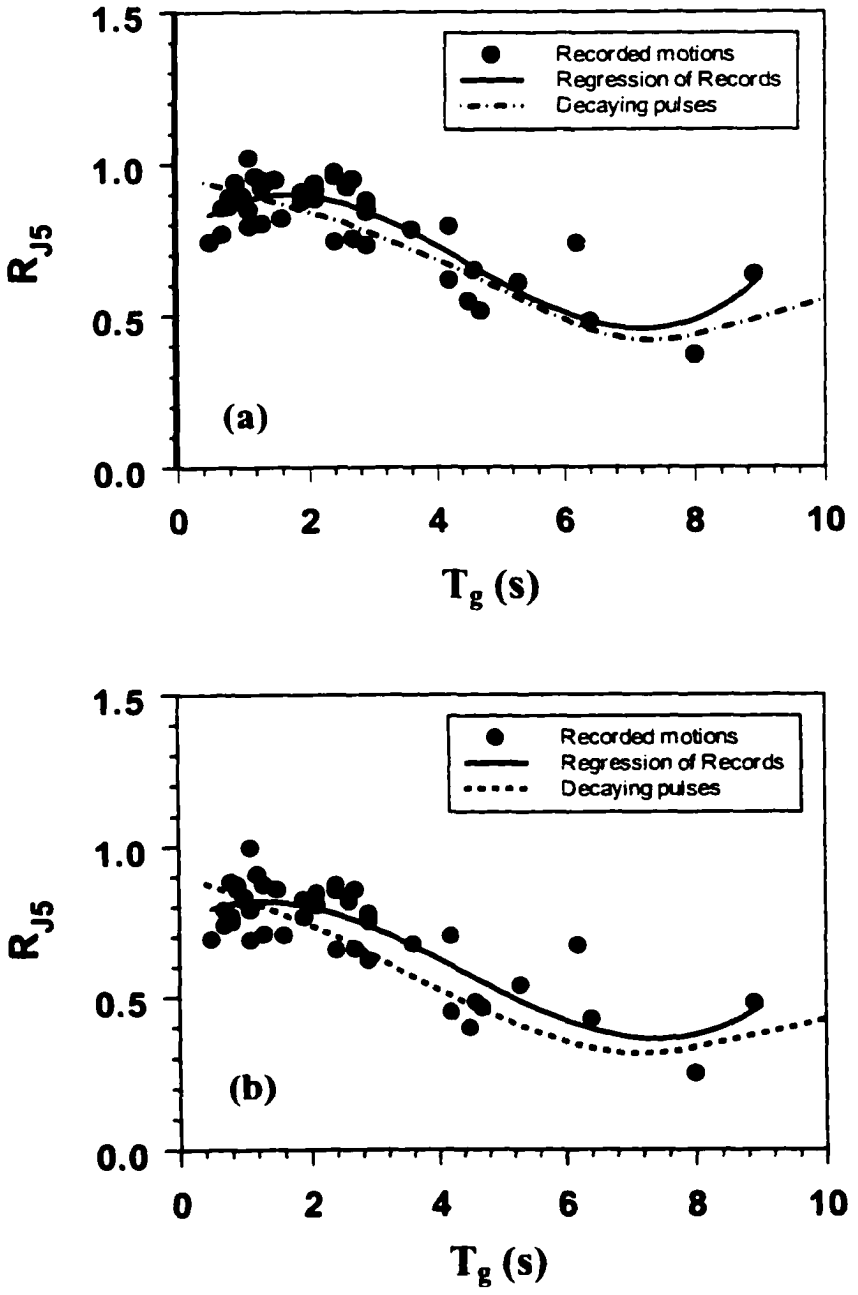

Figure 4-14: Criteria reduction factor of Peak cable deviations, R_{J5}, of supplemental linear viscous dampers with damping coefficient: (a) C=875 KN.s/m; (b) C=1750 KN.s/m.

4.3.3.3 Effect of ζ_p and n

It is clearly demonstrated above that the displacement reduction factors of supplemental linear viscous dampers depend on the predominant period of the near-field ground motion and the natural period of the structure. However, the effect of ζ_p and n on the performance of supplemental linear viscous dampers is relatively complicated. To show the effect of N, that is the number of cycles of velocity pulses during the buildup phase, two ground motions used above will be illustrated as examples herein. These recorded ground motions are the ERZ-NS and KJM090. The former was measured at Duzce Station during the 1992 Erzincan earthquake in Turkey, while the latter was recorded at JMA station during the 1995 Kobe earthquake. The time histories of these two ground motions and their corresponding pulse models are shown in Figure 4-15. The parameters of the pulse models are listed in Table 3-1. The number of cycles of velocity pulses during the buildup phase, N, for ERZ-NS is approximately 1, and that for KJM090 is approximately 2, as shown in Figure 4-15. The predominant period of ERZ-NS is approximately 2.3 sec and that of KJM090 is approximately 1.0 sec as shown in Appendix I. For the base-isolated building discussed above, the displacement reduction factor for a 30% viscous damping for ERZ-NS record is 0.48, and that for KJM090 is 0.68, where the predominant period of the former is around the natural period of the base isolated building, T=2.5 sec. However, by normalizing the predominant period of the KJM090 record to 2.3 sec, which is the same as that of ERZ-NS record, the displacement reduction factor for 30% viscous damping for the normalized KJM090 is obtained as 0.46, which is smaller than that of the ERZ-NS record.

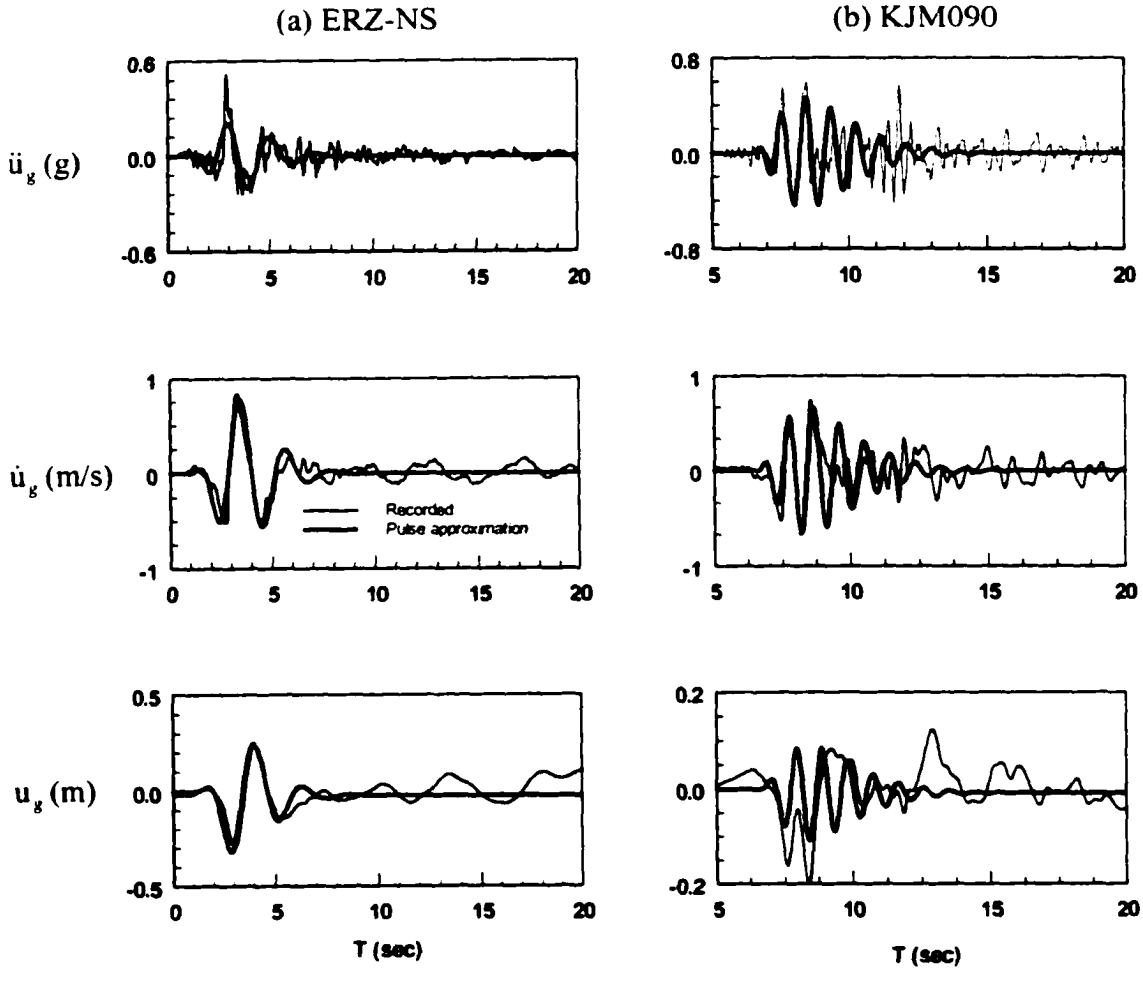

Figure 4-15: Acceleration, velocity and displacement time histories of recorded ground motions and pulse approximations: (a) E06230 recorded at El Centro Station Array #6 during the October 15, 1979 Imperial Valley earthquake; (b) NS component of TCU068 during September 20, 1999 Chi-Chi earthquake.

This is in agreement with the conclusion obtained for pulse excitations in Section 4.2.1.2, that the displacement reduction factor R decreases as N increases for pulses whose frequencies are in the vicinity of the frequency of the structure. The value of N for the normalized KJM090 is 2 while it is 1 for the EZR-NS record.

On the other hand, normalizing the predominant period of the ERZ-NS record to 1.0 sec, the displacement reduction factor for 30% viscous damping for the normalized ERZ-NS is 0.62, which is smaller than that of the KJM090 record. This agrees well with the results shown in Figure 4-3 (a)- (e). However, the dependence of the performance of supplement linear viscous dampers on n and ζ_p is straight forward compared to that of predominant period. It might be more affected by the approximation of these parameters.

4.3.3.4 Remark

The performances of supplemental linear viscous dampers for a base isolated building and a benchmark cable-stayed bridge subject to impulsive type near-field ground motions are investigated above. It has been demonstrated that:

1) Both the displacement reduction factor for the base isolated building and the peak deck displacement reduction factor for the cable-stayed bridge are highly dependent on the predominant period of the near-field ground motions. The displacement response of a typical long period structure is mostly affected by the long period component in ground motions. As a result, the performance of supplemental viscous dampers depends on the fundamental period of the structure and the predominant period of the ground motion.

2) The effect of ζ_p and n on the performance of supplemental linear viscous dampers is relatively complicated. However, it was demonstrated that the displacement

reduction factor also depends on the number of cycle of velocity pulses during the buildup phase if the ground motion is appropriately modeled by ζ_p and n.

3) The proposed pulse model is capable of capturing the predominant frequency in the near-field ground motion. Hence, the displacement response reduction factor for a long period structure can be estimated from the pulse model when the historical ground motions at a specified site are not available, since the predominant period T_g for such locations can be estimated from the attenuation relationship between the magnitude of the earthquake and the distance from the epicenter (Somerville 1998).

4) For the base-isolated building and the cable-stayed bridge, it has been shown that the displacement reduction factor obtained using the pulse model agrees well with that of the recorded ground motion. However, the response quantities such as the absolute acceleration, peak base shear, etc., may not be realistically obtained using the proposed pulse model, because the pulse model does not contain the high frequency components of the recorded ground motions.

4.3.4 Displacement Reduction Factor: Code requirement

The *NEHRP Guidelines for the Seismic Rehabilitation of Buildings* (FEMA 273) presented the first comprehensive method for the analysis and design of structures equipped with passive energy dissipation devices. The displacement reduction factors for high damping ratio described by FEMA are independent of ground motions, e.g., R is 0.59 for 30% equivalent damping ratio for base isolated building. However, this value can't be achieved for some near-field ground motions as shown in Table 4-2. Note that displacement reduction factors used in current codes are based on the studies of Newmark and Hall (1982), and Wu and Hanson (1989). The results of their studies are

based on the statistical analysis using ordinary ground motions without considering the near-field effect. These factors should be used with caution for structures subject to near-field ground motions as indicated in the previous sections, because they are strongly dependent on the predominant period of the ground motion.

4.4 Inelastic Structure with Linear Viscous or Yielding Damping System

The traditional approach for the seismic hazard mitigation is to design structures with a sufficient strength capacity and the ability to deform in a ductile manner. Such a design philosophy is based on the assumption that the structure dissipates the input seismic energy through the damage of structural members. Observations during recent destructive seismic events show that the displacement ductility ratio higher than 4 is an unacceptable level of damage to the structure. An alternative to the traditional seismic design is the use of supplemental energy dissipation devices.

The performance of passive linear viscous damper for elastic structures has been investigated in the previous chapter. It has been demonstrated that supplemental linear viscous dampers are very effective for structure subject to the near-field ground motion with a pulse period in the vicinity of the natural period of the structure. Since the structure may be subject to unexpectedly strong earthquakes, it is necessary to explore the post-yielding behaviors of the structure equipped with supplemental passive dampers, such as passive linear viscous dampers or yielding damping systems.

The objective of using energy dissipation devices is to dissipate or reduce the input seismic energy of the structure. The primary members of a structure are expected to be protected during strong earthquakes if equipped with energy dissipation devices. In

this case, part of the energy input from the ground motion will be dissipated by the supplementary energy dissipation elements.

4.4.1 Energy Balance Equation

As earlier as 1980, Iwan (1980) investigated the input energy dissipated due to the inelastic deformation during earthquakes by approximating the inelastic energy spectrum with an elastic structure using an equivalent viscous damping and an equivalent natural period. Later, Uang and Bertero (1990) systematically investigated the input energy and the energy dissipation in the structure in the form of the viscous and hysteretic energies. Fajar and Vidic (1994) constructed the E_H/E_I spectra, where E_H is the hysteretic energy and E_I is the input energy, for inelastic structures as a function of the damping, the ductility factor and the hysteretic behavior of the structures. Recently, Goel (1997), Fu and Kasai (1998) and Wong and Yang (2001) discussed the idea of the energy balance for designing supplementary energy dissipation devices. In the following, the energy transfer between supplemental energy dissipation devices and hysteresis actions in structural members, and the performance of supplemental energy dissipation devices in preventing the damage to the structural members will be investigated.

Assuming the initial displacement and velocity of the structure to be zero, multiplying Equation (4-1) by dx, and integrating it from time t_0 to t_1, one obtains the energy balance from time t_0 to t_1 as

$$\left[\frac{1}{2}\dot{x}^2\Big|_{t=t_1}\right]+\left[\int_0^{t_1} f_r\dot{x}dt\right]+\left[\int_0^{t_1} 2\zeta\omega\dot{x}^2dt\right]+\left[\int_0^{t_1} u\dot{x}dt\right]=\left[-\int_0^{t_1}\ddot{x}_g\dot{x}dt\right] \qquad (4\text{-}21)$$

The terms in brackets on the left side of the equation are the kinetic energy, strain energy, damping energy, and the control force energy, respectively. The term on the right hand

side is the input seismic energy. The right hand side of Equation (4-21) is a relative input energy rather than the absolute input energy. However, it can be used for structures in the realistic range [Uang and Bertero (1990)]. In Equation (4-21), various energy terms are expressed in terms of per unit mass of the structure. For any supplemental velocity dependent damper, e.g., passive viscous dampers in Equation (4-2), the fourth term in Equation (4-21) is always positive definite for any positive value of c. A similar argument applies to the friction damper in Equation (4-6) since $N > 0$. Hence, such supplemental damping systems are always dissipative in nature and they continuously dissipate energies.

In the following, the decaying velocity pulse [n=1 in Equation (3-1)] with a peak acceleration of 0.5g, a decay ratio of $\zeta_p = 0.2$ and $\omega_p = 2\pi$ (i.e., $T_p = 1.0$ sec) will be used to investigate the energy balance and energy dissipation of a SDOF structure equipped with supplemental passive dampers. The parameters for the Bouc-Wen model are: A=1, n=3, $\alpha=0$, $\beta=0.5$, $\gamma=0.5$ and u_y=1e-4.

4.4.2 Structure Without Dampers

A SDOF elastic-perfectly-plastic structure with an inherent viscous damping ratio of 5% and a natural period of the elastic structure varying from 0.05 to 5 s and subject to the velocity pulse in Equation (3-1) will be investigated. The plots for the seismic input energy of the structure with displacement ductilities μ=1, 2, 3, 4, 6 and 8 are shown in Figure 4-16(a), where μ=1 indicates that the structure is in the elastic range. It is observed that the input energy of the SDOF inelastic system is approximately independent to the strength of the structure in the short (i.e., $T/T_p < 0.25$ sec.) and long ($T/T_p > 2.5$ sec.) period ranges. The peak of the input energy spectrum corresponds to the predominant

period T_p of the ground motion and it shifts slightly towards the smaller period as the ductility increases. The input energy increases slightly as the ductility for the short and medium period SDOF systems ($T/T_p<0.5$) increases, and it decreases slightly as the ductility ratio for the long period SDOF systems ($T/T_p>1.0$) decreases.

In an elastic SDOF system, the input energy is completely dissipated by the viscous damping mechanism. If the inelastic deformation occurs, then the total input energy is partly dissipated by the viscous damping mechanism and partly dissipated

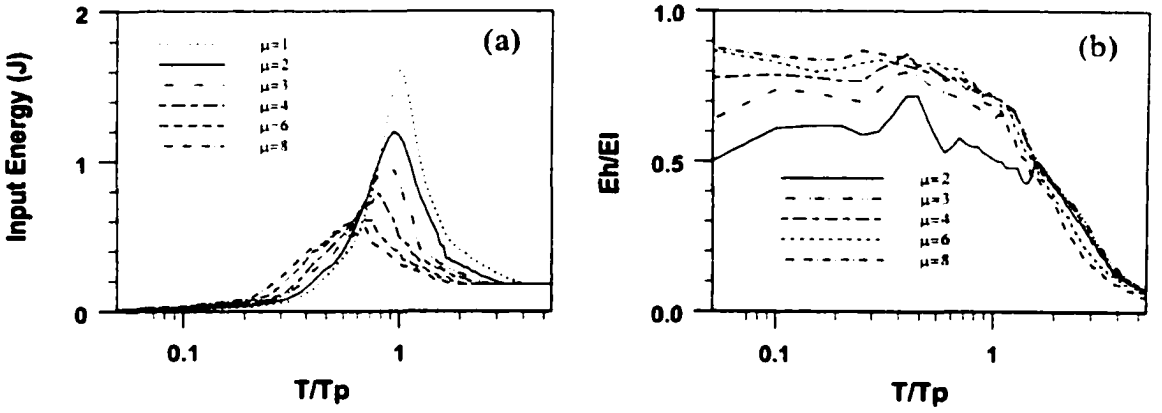

Figure 4-16: (a) Input Energy of uncontrolled SDOF structure; (b) Eh/EI ratio of uncontrolled structures.

through the hysteretic damage of the structure. Figure 4-16(b) shows the plots of the E_H/E_I ratio for the inelastic structure with different ductilities, where E_H is the hysteretic energy and E_I is the input energy. It is observed that the energy dissipated through the hysteretic actions increases for ductilities between 2 and 4, and the increase in the hysteretic energy (i.e., damage to the structure) is smaller for $\mu > 4$ for the structure in the period range $T/T_p <1$. The E_H/E_I ratio is close to the predominant ground motion period T_p for a given ductility demand μ. This characteristics of the E_H/E_I spectra is similar to that presented by Fajar and Vidic (1994). For structures with $T/T_p>1$, the E_H/E_I ratio

decreases gradually to zero for all displacement ductilities, since the present study uses the relative input energy approach.

4.4.3 Passive Viscous Damper

The SDOF structure with displacement ductilities of μ=1 and 4 are assumed to be equipped with supplemental passive viscous dampers. The damping coefficient of the supplemental damper is designed such that the total damping ratio (i.e., supplemental +inherent) of the structure increases to 15% and 30%, respectively. To increase the damping ratio of the structure to such levels is practical using commercially available passive dampers. Figure 4-17 shows the input energy spectra of the structure with displacement ductilities μ=1 and 4. It is observed from Figure 4-17(a) that the input energy decreases tremendously as the viscous damping is increased for the elastic

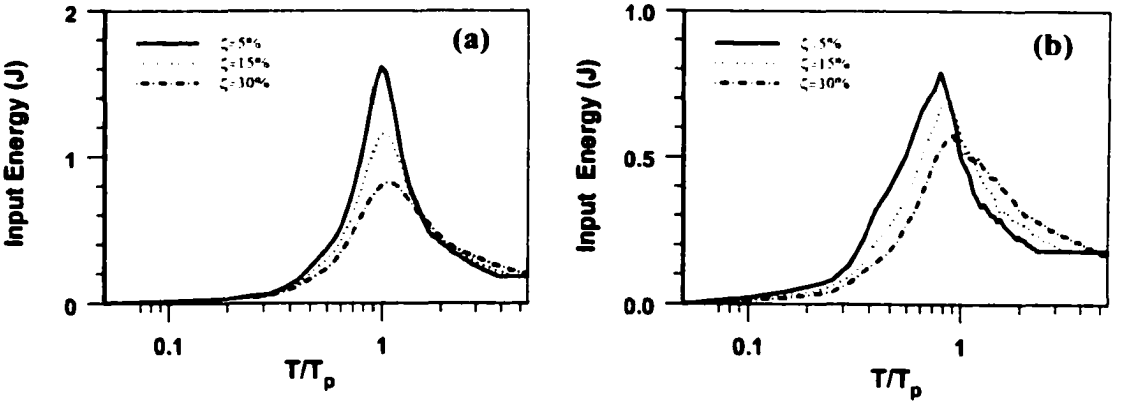

Figure 4-17: Input energy spectra of the structure with supplemental viscous dampers: (a) μ=1; (b) μ=4.

structure with a natural period around T_p, i.e., $T/T_p \approx 1$. For the inelastic structure with μ=4, it is observed from Figure 4-17(b) that the peak input energy without any supplemental dampers is 0.8 J as compared to 1.3 J for the elastic structure. The reduction in the input seismic energy for the inelastic structure is achieved at the expense of

damage to the structure. A further increase in the damping ratio of the structure through supplemental dampers has a lesser effect in reduction of the peak input energy as compared to the elastic structure. In fact, increasing the damping ratio of the inelastic structure with μ=4 reduces the input energy for structures with $T/T_p < 1$ and it increases the input energy for long period structures with $T/T_p > 1.0$.

Figure 4-18 shows plots for the hysteretic and viscous energies dissipated for the inelastic structure with μ=4 equipped with supplemental passive dampers. It is observed from Figure 4-18(a) that the supplemental dampers are effective in reducing the hysteretic damage for structures with a natural period $T/T_p < 2$. For long period structures with a period $T/T_p > 2$, supplemental passive dampers are ineffective in reducing the hysteretic damage to the structure. On the other hand, the energy dissipated

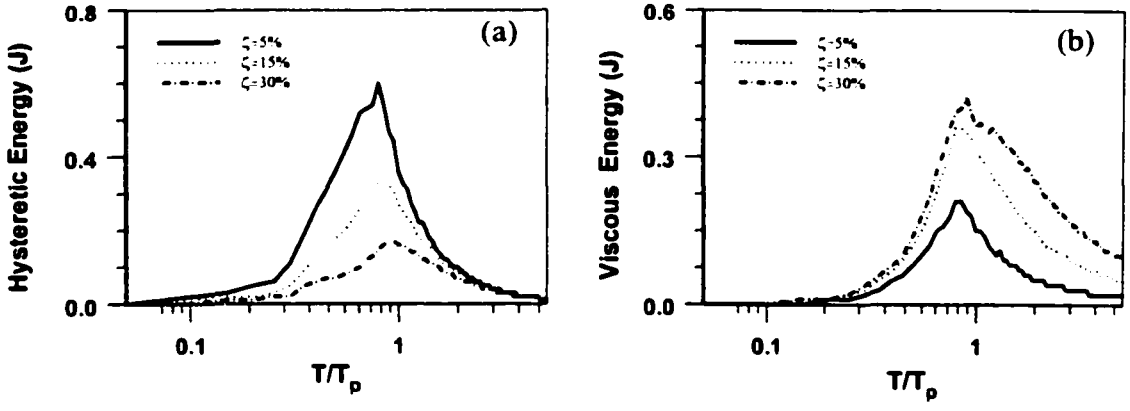

Figure 4-18: Hysteretic and viscous energy spectra for the inelastic structure with original displacement ductility μ=4.

by supplemental dampers increases for structures with $T/T_p > 0.3$ and the increase is quite significant for structures with $T/T_p > 1.0$. For long period structures with $T/T_p > 2.0$, although the supplemental dampers are effective in the energy dissipation, they are ineffective in preventing the hysteretic damage to the structure. For short period

structures with period $T/T_p < 1.0$, supplemental dampers are effective in reducing the hysteretic damage to the structures as shown in Figure 4-18(a).

Figure 4-19 shows the displacement ductility spectra of the elastic (μ=1) structure and the inelastic (μ=4) structure equipped with supplemental viscous dampers. It is observed from Figure 4-19(a) that the supplemental viscous dampers can more effectively reduce the displacement of elastic structures in the period range $0.3 < T/T_p < 2$, although the displacement decreases in the entire period range of $0 \leq T/T_p \leq 5$. For inelastic structures with $\mu = 4$, supplemental viscous dampers are more effective for short period structures ($T/T_p<1$), as shown in Figure 4-19(b). It is further observed from Figure 4-19(b) that supplemental dampers with a total structural damping ratio (inherent

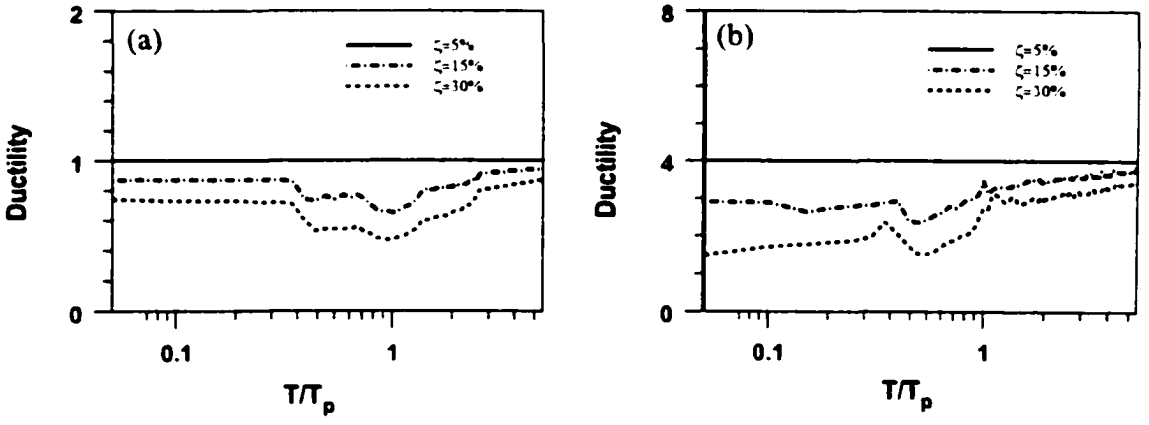

Figure 4-19: Displacement ductility spectra of the structure with viscous dampers: (a) elastic structure (μ=1); (b) inelastic structure (μ=4).

+ supplemental) of 30% are capable of reducing the displacement ductility of the structure with $T/T_p = 0.6$ and μ=4 to μ=2.5. For the long period structure, the displacement ductility decreases only slightly. Hence, these structures will undergo

slightly lesser damage than the design damage for μ=4, even by increasing damping ratio to 30% by supplemental dampers.

4.4.4 Yielding Damping System

Next, a yielding damping system is used as a supplemental damping device in a SDOF structure with displacement ductilities μ=1 and μ=4. The yielding damping system can be implemented with a friction damper. The sliding force, ε, of the friction damper is assumed as to be 10% and 20% of the maximum seismic inertial force. Figure 4-20 shows the input energy spectra for the elastic and inelastic structures equipped with supplemental friction dampers. It is observed from Figure 4-20(a) that the friction damper is effective in reducing the input seismic energy significantly for $T/T_p < 2$ for the elastic structure. However, the seismic energy increases slightly for $T/T_p > 2$. For the inelastic

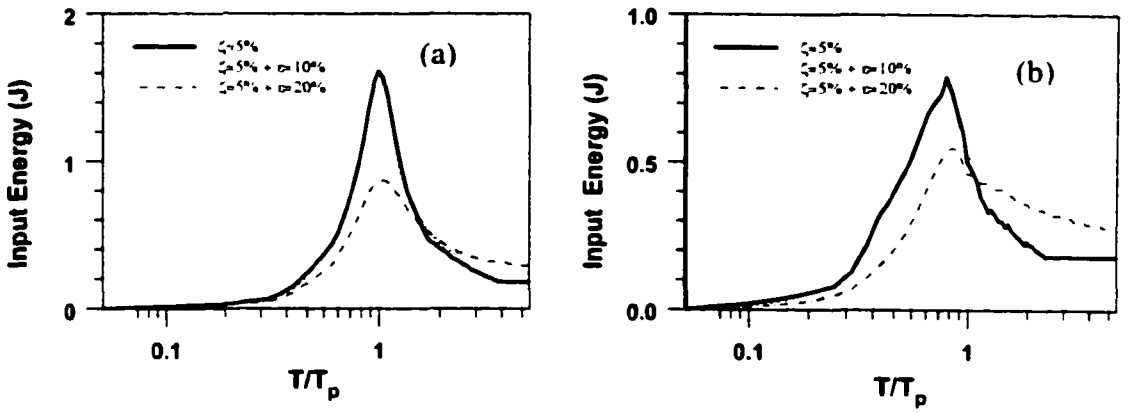

Figure 4-20: Input Energy spectra of structure with friction damper: (a) elastic structures (μ=1); (b) Inelastic structures (μ=4).

structure, as shown in Figure 4-20(b), the friction damper reduces the input seismic energy for $T/T_p<1$ (more predominantly around $T/T_p \approx 1$) and it increases the input energy for $T/Tp < 1$. Since the energy is dissipated by both the friction damper and the

hysteretic behavior of the structure, a comparative study is conducted for these two types of hysteretic energy dissipation mechanisms.

Figure 4-21(a) shows the hysteretic energy from the friction damper for both elastic and inelastic structures. For the elastic structure, significant amount of the hysteretic energy is dissipated by the friction damper. However, the dissipated hysteretic energy doesn't increase significantly by increasing the friction force from 10% to 20% of the maximum seismic inertial force. This may happen because of the locking in the friction damper at a higher friction force. Figure 4-21(b) shows the hysteretic energy dissipated due to the inelastic behavior of the structure. It is observed that the hysteretic energy due to inelastic behavior decreases drastically as the friction force increases, clearly indicating a lesser degree of damage in the structure using a larger friction force. The friction damper is more effective in reducing the hysteretic damage to the structure for $0.3 < T/T_p < 2$.

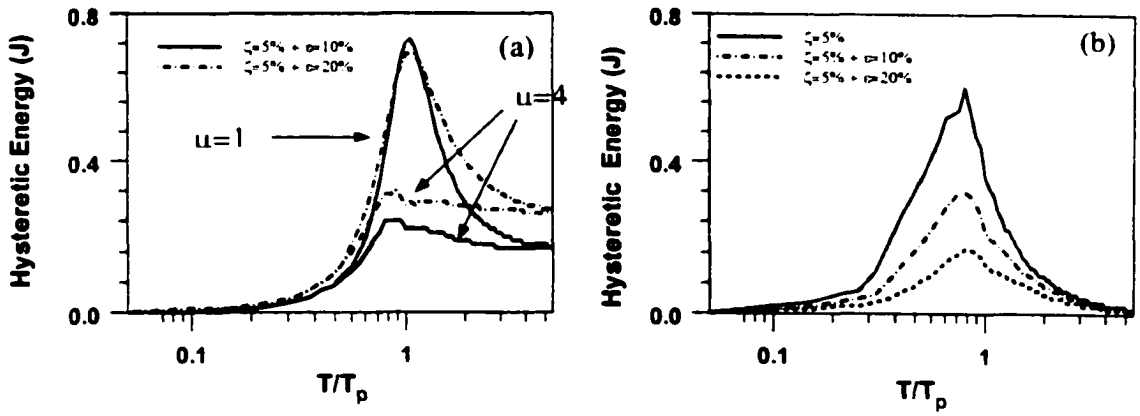

Figure 4-21: Hysteretic energy dissipated by: (a) Friction damper; (b) Structural damage (μ=4).

Figure 4-22(a) and (b) show the displacement ductility spectra for elastic (μ=1) and inelastic (μ=4) structures. For a comparative study, the ductility spectra for viscous dampers with a total structural damping of 15% and 30% are also shown in these figures. It is observed from Figure 4-22(a) that friction dampers are more effective than viscous dampers for long period elastic structures. For inelastic structures (μ=4), while friction dampers are effective over the period range of $0.2 < T/T_p < 5$, viscous dampers are more effective for short period structures. From the acceleration spectra of elastic and inelastic structures for both friction and viscous dampers, it has been observed that the acceleration of the structure with friction dampers is generally higher than that of the structure with viscous dampers.

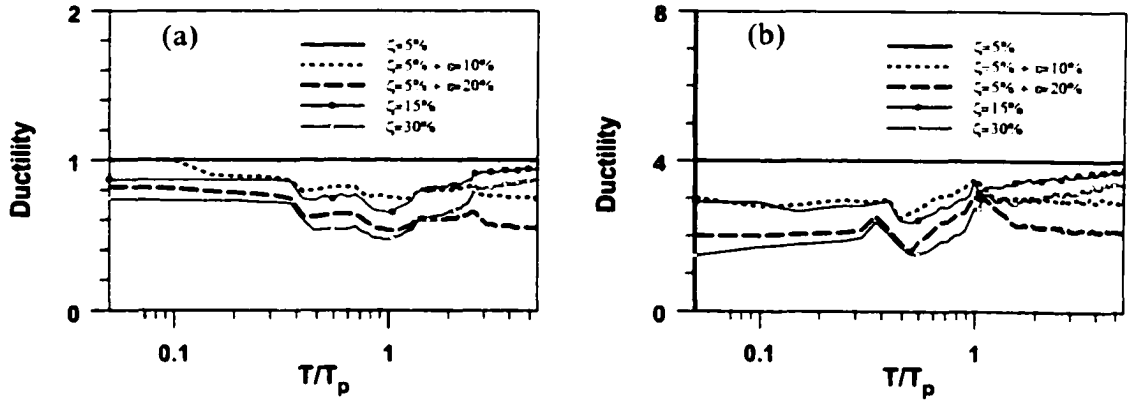

Figure 4-22: Displacement ductility spectra of the structure with friction dampers: (a) Elastic structure (μ=1); (b) Inelastic structure (μ=4).

4.5 Summary

In this study, the performance of the supplemental energy dissipation devices for elastic structures is investigated. Both numerical simulations and analysis results indicate that the displacement reduction factor of the supplemental viscous damping for elastic structures depends on the predominant period of the ground motion and the natural period of the structure. Structures benefit more from supplemental viscous damping if subject to the ground motion with a predominated period in the vicinity of the natural period of the structure. This is because the response of a long period structure depends mainly on the long period components in the near-field ground motion, and these long period components can be represented by the pulse model proposed in Chapter 3. This conclusion has been verified by a SDOF base-isolated building and a MDOF benchmark cable-stayed bridge subject to 40 recorded and simulated near-field ground motion records developed for the SAC project.

The performance of supplemental viscous damping and friction damping systems for elastic and inelastic structures has also been investigated when subject to pulse excitations. By adding the supplement energy dissipation devices, the energy input to the structure and the hysteretic energy dissipated by the structure, which is directly related to the damage of the structure, as well as the displacement ductility are investigated in detail. For elastic structure with μ=1, viscous dampers are effective in reducing the dynamic response as well as the energy input to the structure in the median period ranges. For structures with μ=4, viscous dampers have good performance for structures with short and median periods. For long period structures with μ=4, although viscous dampers dissipate more energies, more energies also get into the structure. Passive friction

dampers have good performance for elastic structures in median or long period ranges. For inelastic structures with μ=4, friction dampers have a good performance for the structure with any natural period.

CHAPTER 5

PROTECTING STRUCTURES FORM NEAR-FIELD GROUND MOTIONS USING ACTIVE CONTROLLERS

5.1 Introduction

Active control systems have been widely investigated in the last thirty years because of their wide ranges of adaptability to ground motions (e.g. Housner et al. 1997). In contrast to passive control systems, a number of advantages associated with active control systems can be cited as: (a) Active controller can be designed with quick response to external excitations, which is of critical importance for structures subjected to near-field ground motions; (b) The performance of active control systems is relatively insensitive to the site conditions and ground motions; (c) The effectiveness of active control systems depends on their capacity, and they can be designed easily to achieve specified control objectives.

For a typical active control system, control forces are developed based on the feedback information from the measured response of the structure and/or feedforward information from the external excitation as shown in Figure 2-2. To see the effects of control forces applied to a linear structure, consider a structure modeled by an n-degree-of freedom system. The equation of motion of the structural system can be written as

$$M\ddot{x}(t) + C\dot{x}(t) + Kx(t) = Du(t) + Hf(t) \qquad (5\text{-}1)$$

where M,C and K are the nxn mass, damping and stiffness matrices, respectively, x(t) is the n-dimensional displacement vector, f(t) is a m-dimensional external excitation vector,

and u(t) is a r-dimensional control force vector. The *nxr* matrix *D* and the *nxm* matrix *H* define the locations of the control force vector and the excitations, respectively.

5.1.1 Linear Control

Suppose that the feedback-feedforward configuration is used in which the control force u(t) is designed to be a linear function of the measured displacement x(t), velocity $\dot{x}(t)$ and excitation f(t). The control force vector takes the form of

$$u(t) = G_x x(t) + G_{\dot{x}} \dot{x}(t) + G_f f(t) \tag{5-2}$$

in which G_x, $G_{\dot{x}}$ and G_f are control gains. The substitution of Equation (5-2) into Equation (5-1) yields

$$M\ddot{x}(t) + (C - DG_{\dot{x}})\dot{x}(t) + (K - DG_x)x(t) = (E + DG_f)f(t) \tag{5-3}$$

It can be seen from Equation (5-3) that the effect of feedback control is to modify the structural parameters (stiffness and damping) so that the structure can respond to reduce the vibration caused by the excitation. The effect of the feedforward component is the modification of the excitation input to the structure.

The control gain in Equation (5-3) can be obtained from linear control algorithms such as LQR/LQG control, pole assignment / mode space control, and H_2/H_∞ control, etc. The advantages of linear control law are well understand, i.e., easy to design and easy to implement in practical applications. Furthermore, the stability of the controlled system can be guaranteed by using linear control laws. However, a major disadvantage of linear controllers is their slow response to external excitations. Since the peak response of the structure to seismic ground excitations usually occurs during the first few cycles of the control time history, the performance of the controller degrades as the control force is

developed by linear control algorithms with large rise time (Yang & Soong, 1988; Soong, 1990; Soong and Reinhorn, 1993). The performance is even worse for near-field ground motions, where the peak response of structures usually occurs due to the forced excitation of impulsive pulses.

5.1.2 Nonlinear Control

To decrease the rise time of the control force, nonlinear controllers are widely used to protect structures from environmental disturbances. The response overshot, rise time and settling time are important evaluation criteria for the performance of active controllers. Hatcher and Shinners (1982) investigated the control effect of a linear controller, nonlinear controller and adaptive controller for a SDOF dynamic system subject to a unit step force excitation. Their results indicate that the step response overshot, rise time and settling time obtained from nonlinear or adaptive controller are significantly smaller than that from the optimal linear controller in Equation (5-2). They emphasized that a linear controller may not be the best choice for minimizing the transient response. A nonlinear controller can be designed to give a better transient response than a linear controller.

In contrast to linear controllers that add linear term to the dynamic system, e.g., Equation (5-3), nonlinear controllers induce nonlinearities in the system. In general, nonlinearities can be classified as inherent (natural) and intentional (artificial) (Slotine and Li, 1991). Inherent nonlinearities are those which naturally come with the structural system itself. Examples of inherent nonlinearities include yielding structures, friction damped structures, etc. Intentional nonlinearities, on the other hand, are artificially introduced to structural systems by designing a suitable control algorithm. Nonlinear

control laws, such as optimal bang-bang control, sliding mode control and adaptive control, are typical examples of intentional nonlinearities.

Generally, nonlinear control can be classified as high-order nonlinear control (including hardening, Duffing and cross-term nonlinearities) and bang-bang nonlinear control. Typical formulas for such controllers are listed in Table 5-1 below.

Table 5-1 Typical Formulas for Nonlinear Control Forces

Force	u(t)
Hardening-Type	$g_x x(t)\|x(t)\| + g_{\dot{x}}\dot{x}(t)\|\dot{x}(t)\|$
Duffing-Type	$g_x \sum_{n=2,5,..} x^n(t) + g_{\dot{x}} \sum_{n=3,5,..} \dot{x}^n(t)$
Cross-Term-Type	$g_{\dot{x}}\dot{x}^2(t)x(t) + g_x x^2(t)\dot{x}(t)$
Bang-Bang-Type	u_{max} if $\dot{x}(t) > 0$; and u_{min} if $\dot{x}(t) < 0$;

5.1.3 Higher-Order Optimal Nonlinear Feedback Control

Research on high-order nonlinear feedback control can be found as early as 1950s. Lewis (1953) showed that the response of a linear second-order system could be improved using variable damping. He used a cross-term feedback control to eliminate the overshot and to improve the setting time of a positional servomechanism. Rekasius (1964) proposed an intentionally nonlinear controller to produce soft-saturation-type constraints on certain states, such as the velocity or acceleration. Instead of optimizing a non-quadratic performance index, a sequence of suboptimal controllers were obtained by Rekasius (1964). Bass and Webber (1966) established a higher-order performance criterion and derived a general nonlinear feedback control law. Moylan and Anderson (1973) presented nonlinear optimal regulators and isolated some useful properties of

those nonlinear regulators. Speyer (1976) discussed a nonlinear control law for a stochastic infinite time problem. Jacobson (1977) extended the linear quadratic control theory and founded a non-quadratic nonlinear feedback controller. Suhardjo et al. (1992) studied a class of high-order optimal controller to control the duffing nonlinear system. Wu et al. (1994) proposed a special cubic order control obtained by minimizing a non-quadratic performance index. The controller is similar to the cubic control derived by Speyer (1976). Tomasula et al. (1994) proposed a polynomial controller using tensor expansion method for a SDOF structure for a performance index that is quadratic in control and quadric in the states. More recently, Agrawal and Yang (1995, 1996a,b) proposed an optimal controller that is polynomial of any orders of the states of the structure system.

As mentioned earlier, the important properties of near-field ground motions are their high velocity and impulsive pulse excitations. The key evaluation criteria of nonlinear control to mitigate the peak response of structures subject to near-field ground motions are the response overshot and rise time. Therefore, it is reasonable to apply the nonlinear optimal controller proposed by Agrawal and Yang (1995, 1996a, b) to protect structures from near-field ground motions. A brief introduction of the optimal polynomial control (OPC) developed by Agrawal and Yang (1995, 1996a, b) will be presented in Section 5.2. The derivation and application of OPC control with acceleration penalty will be presented in Section 5.3. The numerical results of a SDOF structure with an active polynomial controller will be presented in Section 5.4. A hybrid control system for protecting structures from near-field ground motions using the combinations of active/active or passive/active controller will be proposed in Section 5.5.

5.2 Optimal Polynomial Controller

A brief description of the optimal polynomial control is presented in the following. A Detailed derivation is presented in Agrawal and Yang (1995, 1996a, b). Rewriting the Equation (5-1) in the state space, one obtains

$$\dot{Z}(t) = AZ(t) + BU(t) + E(t) \tag{5-4}$$

where Z(t) is a 2n state vector, A is a $2n \times 2n$ system matrix, B is $2n \times r$ controller location matrix, and E(t) is 2n excitation vector, respectively, given by

$$Z(t) = \begin{Bmatrix} X(t) \\ \dot{X}(t) \end{Bmatrix};\ A = \begin{bmatrix} 0 & I \\ -M^{-1}K & -M^{-1}C \end{bmatrix};\ B = \begin{bmatrix} 0 \\ M^{-1}D \end{bmatrix};\ E(t) = \begin{bmatrix} 0 \\ M\eta\ddot{x}_0(t) \end{bmatrix} \tag{5-5}$$

A general performance index J can be expressed as follows

$$J = J(Z_0, U(t), t_0) = S(Z_T, T) + \int_{t_0}^{T} L[Z(t), U(t), t]dt \tag{5-6}$$

where Z_T=Z(T) is the terminal state, $S(Z_T,T)$ is the terminal cost and L[Z(t),U(t),t] is a non-quadratic non-negative cost function. For the infinite time regulator problem, the performance index is minimized in the interval t_0=0 to $T = \infty$. The minimization of the general performance index in Equation (5-6) is not amenable to analytical solutions. However, a sub-class of the general performance index of Equation (5-6) can be assumed to be a polynomial performance index as follows

$$J = \int_0^{\infty} \left[Z^T QZ + U^T RU + \sum_{i=2}^{k} (Z^T M_i Z)^{i-1} (Z^T Q_i Z) + \bar{h}(Z) \right] dt \tag{5-7}$$

where the superscript T denotes transpose of a vector or a matrix and h(Z) is positive semi-definite

$$\bar{h}(Z) = \bar{h}_1(Z) = \left[\sum_{i=2}^{k}(Z^T M_i Z)^{i-1} Z^T M_i\right] B R^{-1} B^T \left[\sum_{i=2}^{k}(Z^T M_i Z)^{i-1} M_i Z\right] \qquad (5\text{-}8)$$

in which the argument t for Z(t) and U(t) has been dropped for simplicity of presentation. In equation (5-7), Q and Qi, i=2,3...,k, are appropriate positive semi-definite state weighting matrices; R is a positive definite control weighting matrix, and Mi, i=2,3...,k are positive definite matrices. The first two terms in Equation (5-7) are the classical quadratic terms, whereas the third term in summation is polynomial in Z of different orders higher than the quadratic term. The last term $\bar{h}(Z)$, Equation (5-8), is added such that simple analytical solutions can be obtained. Weighting matrices Q, R and Qi (i=2,3,...k) can be chosen arbitrary. However, the matrices Mi (i=2,3,....,k) are implicit functions of weighting matrices Qi (i=2,3,...,k). The relation between Mi and Qi will be defined later.

The minimization of the performance index in Equation (5-7) using classical conditions of optimality is very difficult, However, it can be derived based on the solution of the Hamilton-Jacobi-Bellman (H-J-B) equation [e.g. Anderson and Moore (1990), Lewis (1986)] using a function that is polynomial in terms of the states of the system. This polynomial function is required to satisfy all the properties of a Lyapunov function. Detailed derivations are presented in Agrawal and Yang (1995, 1996a, b). The optimal polynomial controller that minimizes the performance index in Equation (5-7) is obtained as follows

$$U(t) = -R^{-1} B^T P Z(t) - R^{-1} B^T \sum_{i=2}^{k}(Z^T M_i Z)^{i-1} M_i Z(t) \qquad (5\text{-}9)$$

where positive definite matrices P and Mi's are obtained by solving algebraic Riccati and Lyapunov equations, respectively,

$$PA + A^T P - PBR^{-1}B^T P + Q = 0 \tag{5-10}$$

$$M_i(A - BR^{-1}B^T P) + (A - BR^{-1}B^T P)^T M_i + Q_i = 0,\ i=2,3,\ldots,k \tag{5-11}$$

As can be seen from Equation (5-9), the nonlinear part of the controller is the sum of the polynomial of various orders in terms of the states of the system. Matrices P and Mi's in Equations (5-10) and (5-11) can be solved using any well-known numerical algorithms or using functions available in MATLAB.

Another possible optimal polynomial controller has the form of Equation (5-9), except that Mi (i=2,3,...,k) are determined from the matrix Riccati Equation, i.e.,

$$M_i(A - BR^{-1}B^T P) + (A - BR^{-1}B^T P)^T M_i - M_i BR^{-1}B^T M_i + Q_i = 0 \quad i=2,3,\ldots,k \tag{5-12}$$

In this case, the performance index J used is given by Equation (5-7) with

$$\bar{h}(Z) = \bar{h}_2(Z) = \bar{h}_1(Z) - \sum_{i=2}^{k}(Z^T M_i Z)^{i-1} Z^T M_i BR^{-1}B^T M_i Z \tag{5-13}$$

where $\bar{h}_1(Z)$ is given by Equation (5-8)

The performance of polynomial controller will be demonstrated in the following using the example presented in Agrawal and Yang (1995, 1996a). A SDOF structure is equipped with an active tendon control system. The structural parameters are: mass m = 2942 kg; natural frequency f = 4.1 Hz; and damping ratio ζ = 2.62%. Active tendons with a stiffness =385.3 KN and an angle of inclination =36° are used. The ground motion is the N-S component of the 1940 El Centro ground motion with a peak ground acceleration PGA=1.1668 m/sec^2, and the time axis has been scaled down by ½.

A linear controller based on LQR is also used to illustrate the performance of optimal polynomial control. The parameters of the linear controller are: $Q = \begin{bmatrix} K & 0 \\ 0 & M \end{bmatrix}$ and $R=2.5\times10^{-6}$. To achieve the same level of the peak displacement reduction, the optimal cubic controller is obtained by letting $R=2.5\times10^{-5}$, and $Q(1,1)=5K$, $Q_2(1,1)=4.8K$, respectively. The other elements of Q and Q_2 are zero. The peak displacements, accelerations and control forces of the linear and nonlinear controller, as well as that of the uncontrolled structure for the SDOF structure are presented in Table 5-2 below.

Table 5-2 Responses of linear and Nonlinear Controlled Structure

Quantity	Uncontrolled	Linear Controller	Nonlinear Controller
Peak displacement (cm)	0.478	0.192	0.192
Peak Acceleration (m/sec^2)	3.18	1.50	1.45
Peak Control force (KN)	___	2.14	2.24 (L: 1.06 +NL: 1.18)

It is observed that, to achieve the same level of displacement reduction, the peak control force and the peak acceleration of the optimal polynomial controller might be larger than that of the linear controller. However, the advantages of nonlinear controller are the low controller energy and quick response to the excitations. The first characteristic can be used to design hybrid control system to achieve multilevel control performance, and the latter is especially critical to design the control system for protecting structures from near-field ground motions because of the impulsive attributes of near-field ground motions.

Based on the controller design described above, the control force developed by the polynomial controller $u_P(t)$ and by the linear controller $u_L(t)$ are obtained as

$$u_P(t) = 9.76\times10^4 x + 2.03\times10^4 \dot{x} + 5.69\times10^{10} x^3 + 8.24\times10^9 \dot{x}x^2 + 2.23\times10^8 x\dot{x}^2 + 9\times10^6 \dot{x}^3 \quad (5\text{-}14)$$

$$u_L(t) = 1.91\times10^5 x + 4.41\times10^4 \dot{x} \quad (5\text{-}15)$$

To demonstrate the performance of these two controllers, the structure at the peak displacement is considered. Assuming the displacement of the structure is x=0.002 m, and velocity $\dot{x}$ =0, the control force developed by the linear and nonlinear controllers are 0.38 KN and 0.65 KN, respectively. However, if the peak displacement is doubled, the control force developed by the linear controller is doubled, and that by the nonlinear controller increases by 6 times (4.0 KN). Similarly, assuming the structure at equilibrium state with velocity $\dot{x}$ =0.05 m/sec and x=0, the control force developed by the linear and nonlinear controller are 2.2 KN and 2.14 KN, respectively. However, if the velocity increases to 0.1 m/sec, the control force developed by the linear controller is doubled, and that by the nonlinear controller increases by 5 times (11.03 KN). Hence, the nonlinear controller responds much faster than the linear controller.

For the SDOF structure with linear and nonlinear controllers designed above, the displacement responses of the uncontrolled and controlled structures are plotted in Figure 5-1(a) by varying the magnitude of the ground acceleration from 0.5 m/sec^2 to 6 m/sec^2. The corresponding controller forces for linear and nonlinear controller are plotted in Figure 5-1(b). It is observed that both the peak displacement and the peak control force for the LQR controller are linear functions of the magnitude of the seismic ground motion. However, for the nonlinear controller, if the peak control force of the nonlinear part is unlimited, both the peak displacement and the peak control force of the linear part of the nonlinear controller are limited to a certain upper threshold limit value. This

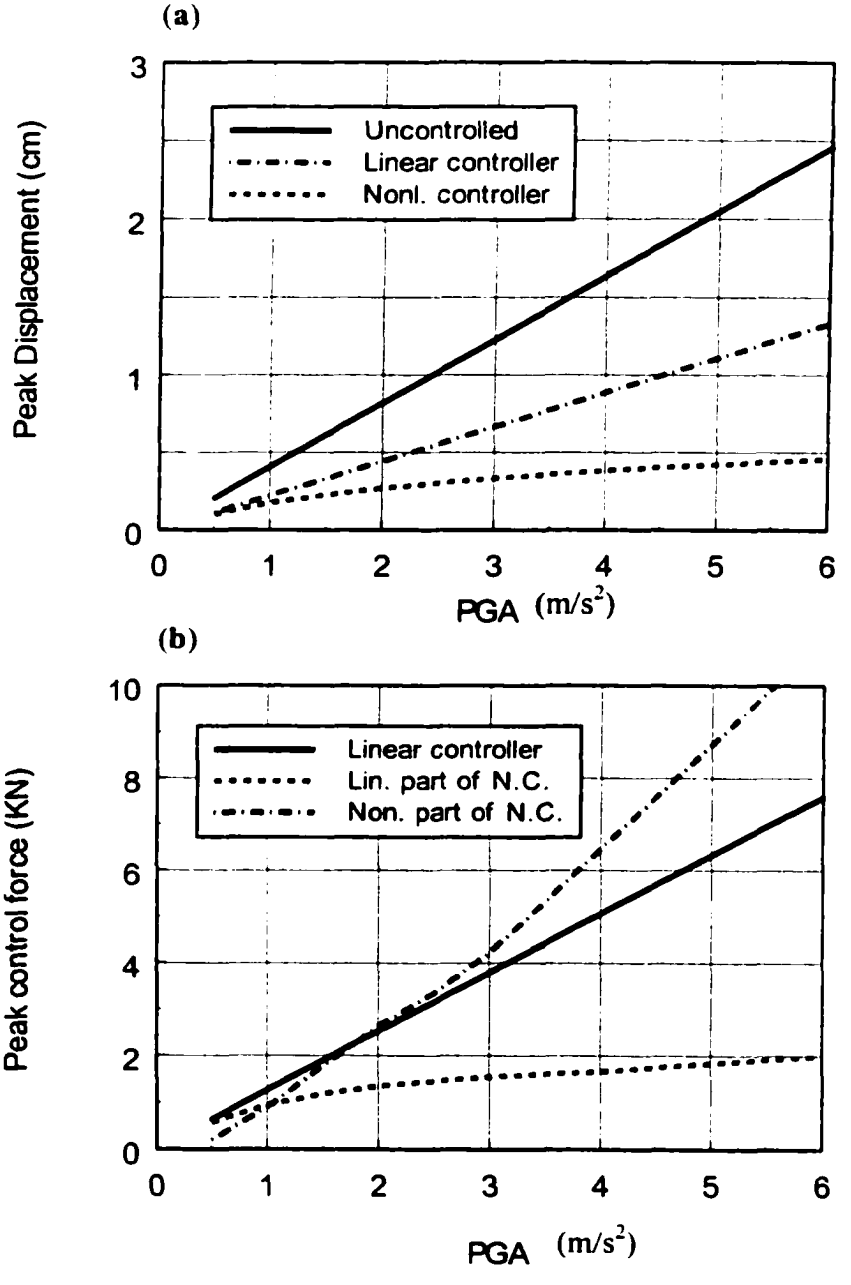

Figure 5-1: Peak displacement and control force for a SDOF system with linear LQR controller and optimal polynomial controller.

adaptive property of the nonlinear controller is very attractive for the design of hybrid control systems consisting of passive and active or passive and semi-active control systems for multilevel control objectives. In such hybrid control systems, a smaller damper/actuator can be used for weak earthquake episodes, and another damper/actuator with a larger capacity can be used to limit the response to certain threshold values during a strong near-field earthquake. The development of these hybrid controllers will be presented later in this chapter.

5.3 OPC with Acceleration Penalty

It has been shown in the previous section that the optimal polynomial controller can respond quickly to external excitations. This property is of great importance for designing control systems to protect structures from near-field ground motions. Further, both the peak displacement of the controlled structure and the linear control force asymptotically approach to certain limiting values. This property is very useful in the design of hybrid control systems or control systems for multilevel control objectives. In this section, the optimal polynomial controller with acceleration penalty will be derived and the application of this controller will be illustrated.

5.3.1. Controller Design

A polynomial performance index for the infinite time regulator problem is defined as:

$$J = \int_0^\infty \left[\mathbf{Z}_0^T \mathbf{Q}_0 Z_0 + U^T R_0 U + \sum_{i=2}^{k} (Z^T M_i Z)^{i-1} Z^T Q_i Z + \bar{h}(Z) \right] dt \qquad (5\text{-}16)$$

where

$$Z_0 = \begin{pmatrix} x \\ \ddot{x}_a \end{pmatrix} = \begin{bmatrix} I & 0 \\ -M^{-1}K & -M^{-1}C \end{bmatrix} \begin{Bmatrix} x \\ \dot{x} \end{Bmatrix} + BU = C_0 Z + BU \tag{5-17}$$

The weighting matrices Q_i and M_i and the function $\bar{h}(Z)$ are the same as that in Equation (5-8). The reason for the selection of Equation (5-16) as the performance index is based on the following reason. The total control force of the polynomial controller is composed the linear term and high order terms. The controller can be designed in such a manner that, for a given level of control objective, such as the peak displacement, the linear part of the control force is dominant while the nonlinear part is very small. If the displacement is beyond this level, the nonlinear control force increases rapidly to limit the displacement of the structure. It is desirable that the displacement of the structure is very small for small ground motions, and the dominant part of the control force is the linear part. In this case, the reduction of both the peak acceleration and peak displacement of the structure is the main control objective. However, for very strong ground motions, the high order part of Equation (5-16) is dominant, and the major objective is to control the peak displacement.

Substituting Equation (5-17) into Equation (5-16), one obtains

$$J = \int_0^\infty \left[Z^T Q_1 Z + Z^T S U + U^T S^T Z + U^T R U + \sum_{i=2}^{k} (Z^T M_i Z)^{i-1} Z^T Q_i Z + \bar{h}(Z) \right] dt \tag{5-18}$$

where

$$Q_1 = C_0^T Q_0 C_0 \; ; \; S = C_0^T Q_0 B ; \; R = R_0 + B^T Q_0 B \tag{5-19}$$

In order to eliminate the cross product term of U and Z in Equation (5-18), we assume that

$$U = \bar{U} - R^{-1}S^{T}Z \tag{5-20}$$

Equation (5-18) can be rewritten as

$$J = \int_0^{\infty}\left[\mathbf{Z}^{T}QZ + \bar{U}^{T}R\bar{U} + \sum_{i=2}^{k}(Z^{T}M_{i}Z)^{i-1}Z^{T}Q_{i}Z + \bar{h}(Z)\right]dt \tag{5-21}$$

where

$$Q = Q_{1} - SR^{-1}S^{T} \tag{5-22}$$

Substituting Equation (5-20) into Equation (5-4), one obtains the system in the state-space as

$$\dot{Z} = \bar{A}Z + B\bar{U} + E(t) \tag{5-23}$$

where

$$\bar{A} = A - BR^{-1}S^{T} \tag{5-24}$$

Then, the performance index in Equation (5-21) can be minimized subject to the constraint in Equation (5-23). The minimization of the performance index in Equation (5-24) results in the following controller $\bar{U}$

$$\bar{U} = -R^{-1}B^{T}PZ(t) - R^{-1}B^{T}\sum_{i=2}^{k}(Z^{T}M_{i}Z)^{i-1}M_{i}Z \tag{5-25}$$

where P and M are obtained by solving Lyapunov and Riccati equations in Equations (5-10) and (5-11).

5.3.2. Numerical Example of Acceleration Penalty

The performance of the optimal polynomial controller with acceleration penalty is demonstrated through an example of a bridge modeled as a SDOF structure with a mass $M=1.02\times10^{6}$ kg, stiffness $K=3.3\times10^{6}$ N/m and damping ratio $\zeta=2\%$ [Feng and Shinozuka (1993)]. The ground motions used in this study are typical ground motions, including the

NS component of the 1940 El Centro earthquake, 1985 Mexico earthquake and 1999 Gebze earthquake, 28 near-field ground motions measured from rock and soil site condition, and 22 typical long duration ground motions. Detailed information on these ground motions are listed in Appendix II.

The controllers are designed using the following parameters. For the cubic nonlinear controller without acceleration penalty we have: $R=2.5\times10^{-5}$, $Q(1,1)=100K$, $Q_2(1,1)=0.1K$, and the other elements of Q and Q_2 are zero. For the controller with acceleration penalty we have: $Q_0=\begin{bmatrix} 100K & 0 \\ 0 & 200M \end{bmatrix}$, $R_0=2\times10^{-5}$, $Q_2=\begin{bmatrix} 0.1K & 0 \\ 0 & 0 \end{bmatrix}$. Since the peak control force has a limitation in reality, a saturation of 4000 KN is imposed on the nonlinear part of both controllers. The response quantities of (i) the uncontrolled structure, (ii) the structure with two types of nonlinear controllers, and (ii) the peak control forces required by these controllers are presented in Table 5-3.

5.3.3. Effect of Acceleration Penalty

It is observed from Table 5-3 that the peak displacement of the uncontrolled structure is 141.8 cm. For both the nonlinear controllers with or without acceleration penalty, the peak displacement of controlled structure for all the ground motions is reduced below 20cm. With the acceleration penalty, the peak absolute acceleration of the structure is smaller than that of the controller without acceleration penalty for all the long duration ground motions and most of the other 31 ground motions, except for TAB-TR, TCU065NS, TCU065EW and TCU068EW ground motions, which are very strong ground motions. The peak displacements of the uncontrolled structure for these ground

Table 5-3 Response quantities of controlled and uncontrolled structure.

	Uncontrolled		Control Without Acceleration Penalty					Control with Acceleration Penalty				
Ground Motions	x (cm)	$\ddot{x}$ (g)	x (cm)	$\ddot{x}$ (g)	Total Force (KN)	Linear Force (KN)	Nonlinear Force (KN)	x (cm)	$\ddot{x}$ (g)	Total Force (KN)	Linear Force (KN)	Nonlinear Force (KN)
El Centro	25.0	0.08	7.1	0.13	1151	525	626	6.2	0.11	1048	488	640
Mexico	14.1	0.05	3.6	0.03	311	258	53	4.1	0.03	246	191	52
Gebze	56.9	0.19	8.8	0.15	1328	582	747	11.3	0.13	1260	543	707
Kobe JMA00	31.9	0.11	10.1	0.54	5336	1336	4000	11.5	0.52	5191	1179	4000
Kobe JMA90	48.6	0.16	9.9	0.52	5152	1152	4000	10.3	0.50	5005	1008	4000
Lands LCN000	42.5	0.14	7.0	0.10	849	517	374	8.9	0.09	817	429	487
Lands LCN275	116.8	0.39	13.1	0.41	3914	949	2966	13.9	0.39	3994	871	3160
Cape CMP00	67.6	0.22	13.1	0.52	4806	1075	3919	12.8	0.48	4434	961	4000
Cape CMP90	27.5	0.09	9.1	0.40	3582	966	2615	9.4	0.35	3215	817	2374
Loma LGP00	135.8	0.45	14.5	0.45	4476	1043	3433	15.4	0.44	4454	907	3590
Loma LGP90	34.0	0.11	8.6	0.18	1585	696	919	8.1	0.18	1670	572	1273
Sup. Hill 135	8.5	0.03	5.1	0.22	2171	785	1386	5.4	0.22	2137	679	1479
TCU084EW	89.1	0.29	15.3	0.55	5332	1332	4000	16.6	0.51	5220	1152	4000
CHY080NS	42.0	0.14	13.5	0.55	5324	1324	4000	14.4	0.51	5204	1140	4000
CHY080EW	29.3	0.10	13.7	0.55	5402	1402	4000	13.9	0.52	5170	1202	4000
Tabas LN	70.4	0.23	14.4	0.36	3433	932	2649	14.1	0.36	3408	762	2998
Tabas TR	104.1	0.34	15.2	0.37	3520	946	2738	16.9	0.38	3666	849	3247
Kobe TAK00	88.3	0.29	17.5	0.57	5344	1344	4000	17.2	0.52	5129	1177	4000
Kobe TAK90	81.6	0.27	14.9	0.53	5040	1107	4000	14.0	0.49	4832	956	4000
Cape Pet 00	27.1	0.09	7.8	0.22	2053	797	1337	7.4	0.21	2040	667	1438
Cape Pet90	52.0	0.17	11.6	0.53	5066	1066	4000	9.7	0.50	4852	959	4000
Duzce 270	75.5	0.25	14.1	0.25	2402	835	1567	16.6	0.23	2265	709	1524
Erzincan NS	59.8	0.20	14.0	0.38	3553	977	2660	14.3	0.35	3397	836	2730
Newhall 360	58.3	0.19	11.3	0.53	5118	1118	4000	10.2	0.50	4857	966	4000
Rinaldi 228	56.4	0.19	17.2	0.61	5856	1856	4000	15.6	0.56	5461	1599	4000

Table 5-3 Response quantities of controlled and uncontrolled structure (Continued)

Sylmar 052	131.9	0.44	15.4	0.51	5034	1162	3872	13.7	0.47	4623	962	3929
Sylmar 142	41.5	0.14	14.1	0.54	5426	1426	4000	13.3	0.52	5230	1214	4000
TCU065NS	101.4	0.33	12.6	0.40	3816	947	2869	12.8	0.40	3771	814	3145
TCU065EW	131.9	0.44	17.1	0.41	3805	1039	2837	17.7	0.42	3691	888	3490
TCU068NS	72.5	0.24	17.2	0.36	3556	958	2599	19.9	0.34	3485	857	2554
TCU068EW	141.8	0.47	17.9	0.32	3044	868	2205	19.9	0.35	3204	745	2820
Chile LL010	32.6	0.11	6.3	0.16	1555	677	878	7.2	0.13	1343	560	766
Chile LL100	11.1	0.04	4.2	0.08	655	423	239	3.4	0.06	573	361	239
Chil Vina200	14.8	0.05	5.4	0.13	1247	626	625	4.8	0.12	1195	528	666
Chil Vina290	12.9	0.04	4.0	0.08	766	462	304	3.4	0.07	664	392	319
Mex. Cal00	21.5	0.07	6.2	0.06	442	322	150	5.4	0.04	326	270	140
Mex. Cal90	14.4	0.05	3.7	0.04	306	255	51	3.3	0.03	224	195	56
Imperial NS	25.1	0.08	7.1	0.13	1157	527	630	6.2	0.11	1051	489	639
Imperial EW	38.9	0.13	9.1	0.10	899	493	425	9.1	0.09	768	416	494
Hach. EW	28.1	0.09	8.1	0.14	1381	636	745	8.5	0.12	1163	519	659
Hach. NS	30.1	0.10	6.5	0.11	1072	563	509	7.3	0.09	905	463	522
Mex. Occt1	2.6	0.01	1.2	0.01	73	72	1	1.5	0.01	66	63	2
Mex. Occt2	2.3	0.01	1.1	0.01	72	71	2	1.5	0.01	65	70	3
Miya. E41S	7.4	0.02	3.3	0.04	321	251	69	3.4	0.04	310	261	110
Miya. E41E	4.8	0.02	2.0	0.03	244	212	32	2.3	0.03	207	199	46
Olympia 182	4.4	0.01	1.6	0.02	166	154	12	1.3	0.02	143	137	14
Olympia 282	3.1	0.01	1.4	0.02	159	148	11	1.3	0.01	120	125	11
Mex. TacyE	12.7	0.04	3.2	0.02	170	159	14	4.0	0.02	141	122	23
Mex. TacyN	10.8	0.04	3.8	0.03	166	146	23	4.4	0.02	149	155	30
Taft N21E	11.5	0.04	3.4	0.03	316	268	51	4.6	0.03	284	195	69
Taft S69E	15.4	0.05	4.7	0.05	380	297	97	4.3	0.04	352	262	118
Chile Vlp070	14.7	0.05	3.5	0.05	437	322	114	2.8	0.04	364	273	92
Chile Vlp160	4.8	0.02	1.3	0.02	129	123	6	1.1	0.01	107	107	6

motions are greater than 100 cm. Hence, the controller with acceleration penalty reduces the acceleration at the expense of the displacement for these earthquakes.

5.4 Active Control System

Further numerical simulations are carried out to show the effects of near-field ground motions on the performance of active controllers. Since, the optimal polynomial controller with acceleration penalty introduces an additional weighting coefficient for accelerations, the optimal polynomial controller without acceleration penalty is used in the following to simplify the numerical simulation. It is observed from Table 5-3 that the nonlinear part of the control force is small for small excitations, while it is large for strong ground motions. Figure 5-2 shows the control force applied to the structure subject to the three typical ground motions. It should be pointed out that the controller is designed based on the widely used NS component of the 1940 El Centro ground motion. The controller is designed in such a manner that the peak control force of the linear part is at the same level as that of the nonlinear part. For the Mexico earthquake, since the ground motion is a typical long duration ground motion, the displacement time history of the uncontrolled structure increases gradually and reaches its peak value after several cycles. In this case, the nonlinear part of the control force is very small as shown Figure 5-2, since the linear part of the control force can reduce the oscillation of the structure very effectively. However, the Gebze motion during the 1999 Turkey earthquake is a typical near-field ground motion. The peak displacement of the uncontrolled structure is developed in an abrupt manner during this earthquake. Consequently, the nonlinear part of the control force for these ground motion is developed abruptly and it vanishes quickly, as shown in Figure 5-2.

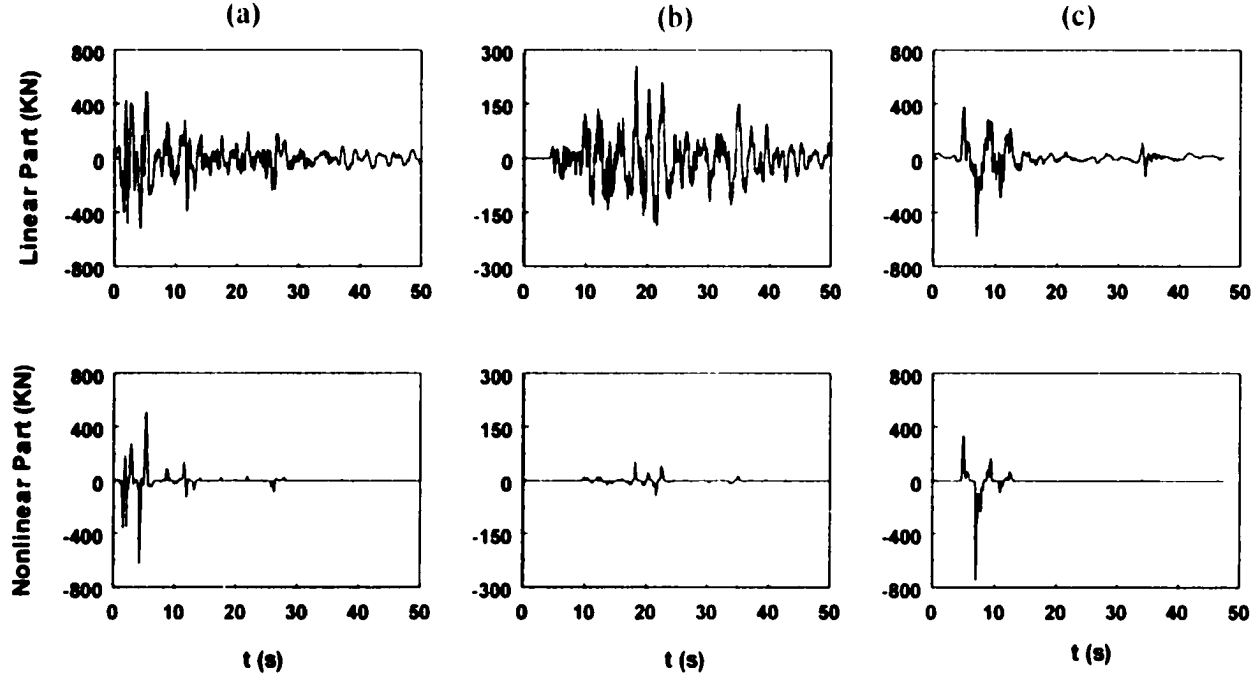

Figure 5-2: Control force time history of optimal polynomial controller of SDOF structure subject to three typical ground motions. Column: (a) El Centro earthquake; (b) Mexico Earthquake; (c) Gebze earthquake

Using optimal polynomial controller described previously without acceleration weightings, the peak displacements of the structure subject to 53 ground motions are plotted in Figure 5-3 for the controlled and uncontrolled structure. Near-field ground motions used in this study are the strongest ground motions recorded during recent earthquakes. However, if the peak control force capacity of the control device is unlimited, then the peak displacement can be limited to a certain value, i.e. 20 cm. In such a situation, the peak control force of the linear part is also limited to a certain value, i.e. 2000 KN, as shown in Figure 5-4. Additional control force during the strong earthquake is supplied by the nonlinear part of the controller. This additional part is very small for small earthquakes.

However, since the capacity of control devices is always limited in practical situations, a device saturation limit is imposed on the nonlinear part of the control force. Figure 5-5 and Figure 5-6 show plots of the peak displacement and peak control force, respectively, with and without nonlinear force saturation. It is observed from these figures that if the peak control force of the nonlinear part is saturated at 4000 KN, the peak displacement is still within the limitation of 20 cm. In this case, the total peak control force for linear and nonlinear parts is limited to 6000 KN. If the peak control force of the nonlinear part is saturated at 3000 KN, the TAK00 component of the Kobe earthquake is the only ground motion that results in a peak displacement greater than 20 cm, which is approximately 24 cm.

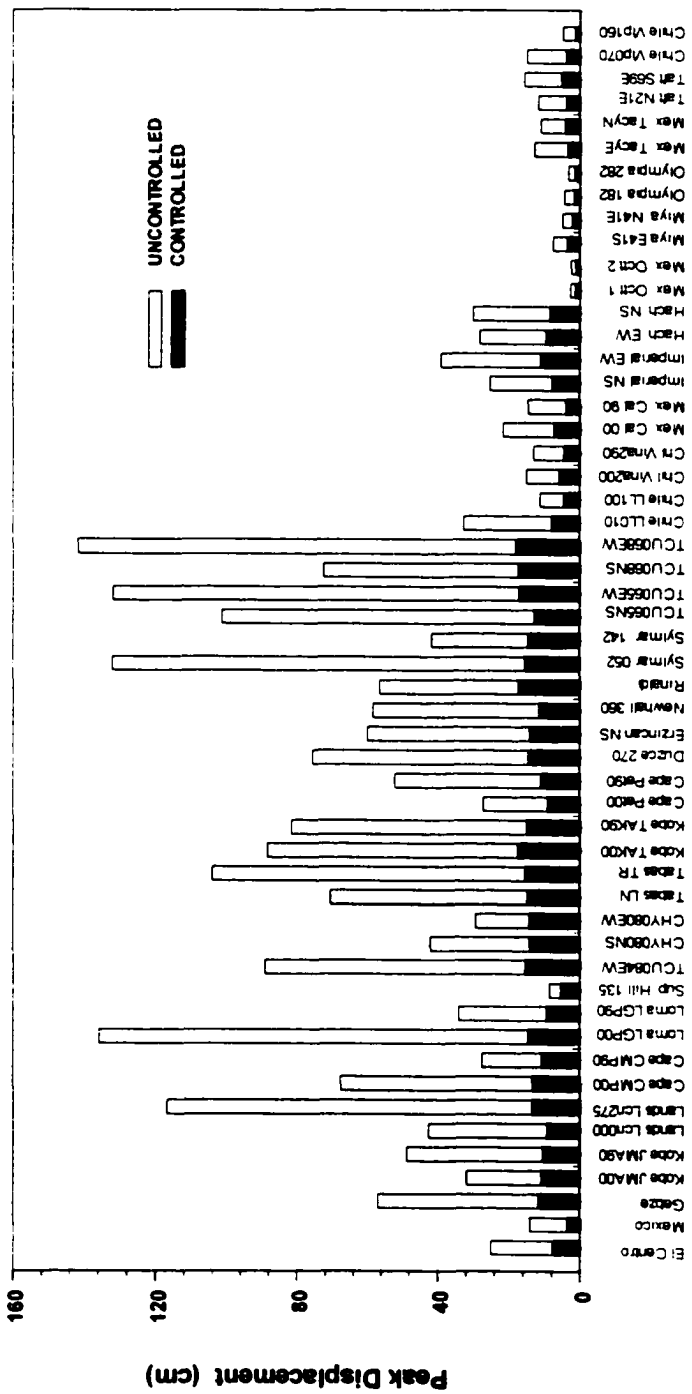

Figure 5-3: Peak displacement of the uncontrolled and controlled SDOF structure subject to 53 ground motions.

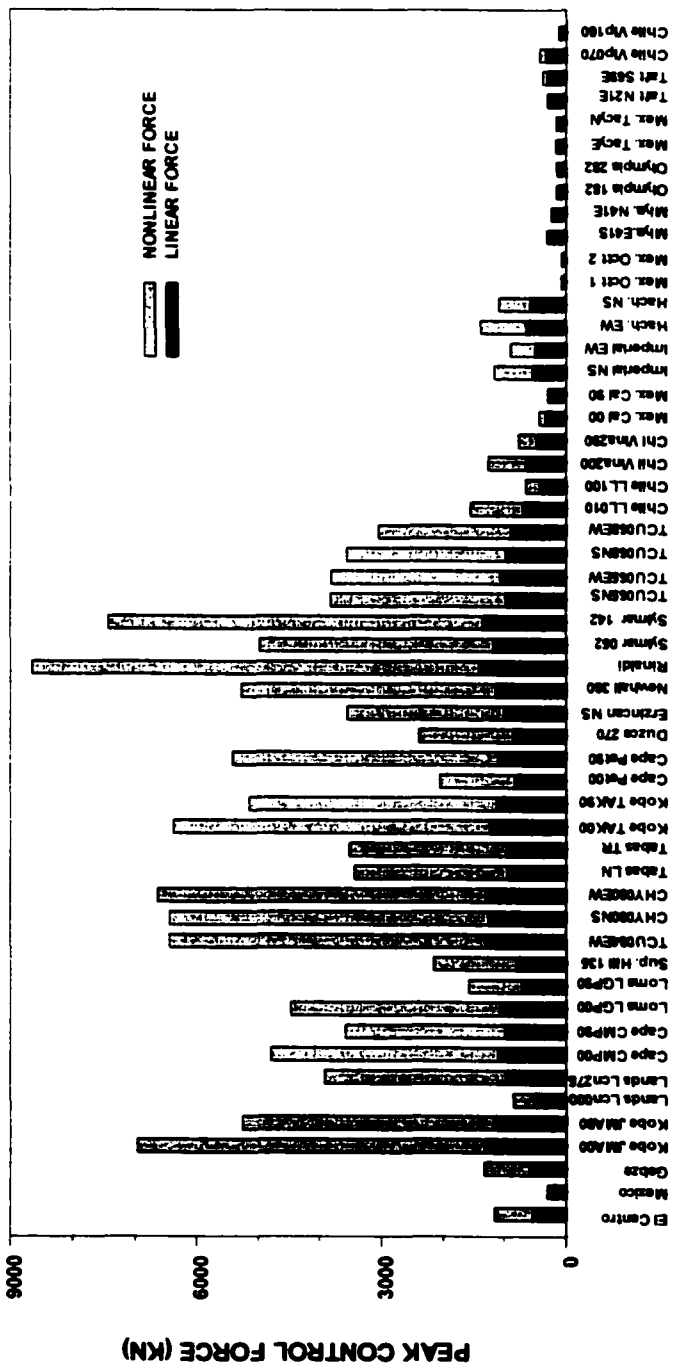

Figure 5-4: Peak control force of optimal polynomial controller subject to 53 ground motions.

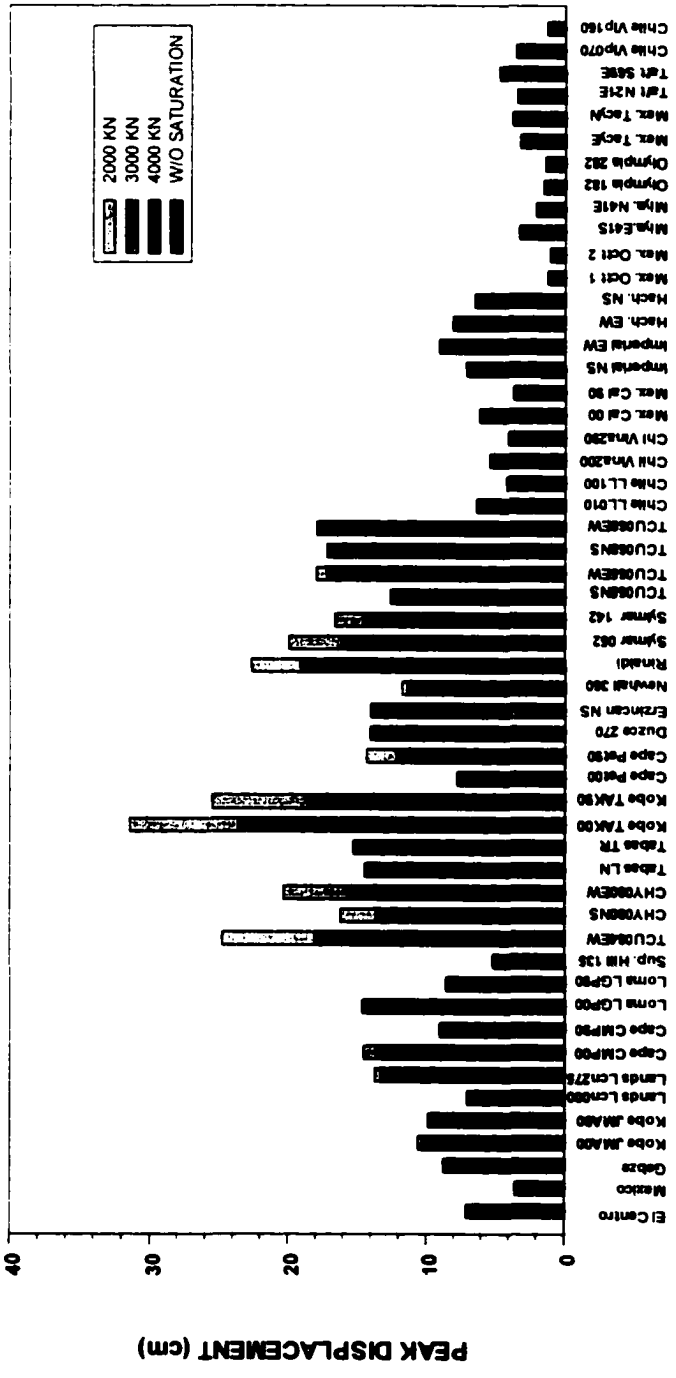

Figure 5-5: Peak displacement of optimal polynomial controller with and without nonlinear control force saturation.

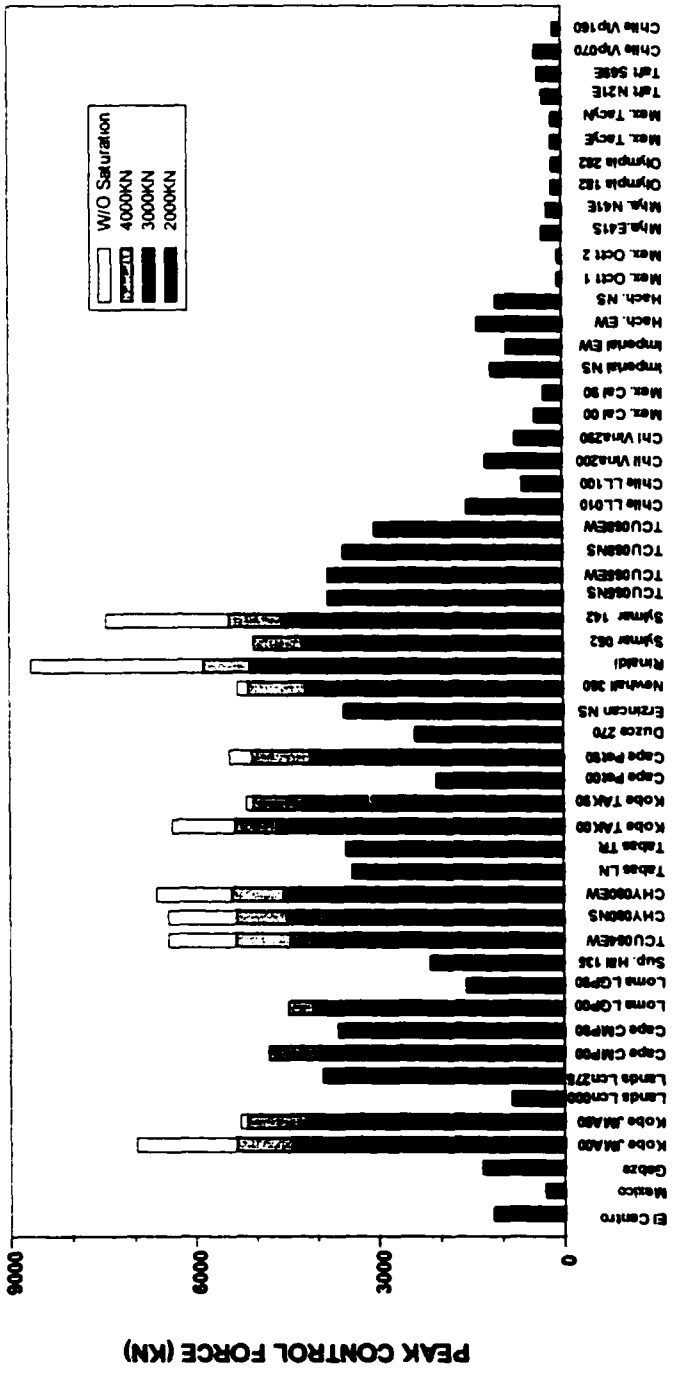

Figure 5-6: Peak control force of optimal polynomial control with nonlinear control force saturation.

5.5 Hybrid Control System

The optimal polynomial controller presented above, consists of linear and nonlinear parts. For small excitations, the control force from the nonlinear part is very small, whereas the nonlinear part control force is large to reduce the displacement effectively during strong excitations. Based on this control characteristic, two hybrid control systems will be proposed and investigated in detail in the following. The first hybrid control system consists of two active controllers with multilevel control objectives and the second hybrid control system is a combination of passive viscous dampers and a active control system.

5.5.1. Hybrid Active Control System

The first hybrid control system proposed consists of two actuators in parallel, referred to as the active/active hybrid control system. A smaller capacity linear actuator, whose control force is developed based on the linear part of the polynomial controller, is installed in parallel with a nonlinear actuator, whose control force is developed according to the high-order part of the polynomial controller. The active/active control system is designed such that (i) Only the linear actuator is activated during the small seismic events in order to mitigate the displacement and acceleration of the structure, and (ii) both linear and nonlinear actuators are activated during the strong earthquakes in order to reduce the peak displacement of the structure. Using the hybrid active/active control system described above, we assume that the nonlinear actuator is activated whenever the required nonlinear control force is greater than 500 KN, and this force is saturated at 4000 KN. The performance of this hybrid active control system is presented in Table 5-

4. It is observed from Table 5-4 that the performance of this system is similar to that of the fully active system. For very strong ground motions, both linear and nonlinear actuators work simultaneously, while only the linear actuator is activated during small ground motions.

5.5.2. Passive/Active Hybrid Control System

Alternatively, the aforementioned hybrid control system with multilevel control objectives can also be implemented by a combination of passive and active control systems, referred to the passive/active hybrid control system. In this system, the passive damper is used to reduce the responses of the structure during small excitations, and the nonlinear actuator is activated only if the required force is greater than a threshold level. The linear part of the polynomial controller is approximated by a linear fluid viscous damper. A passive damper with a 30% damping ratio is selected for the linear part of the polynomial controller with the corresponding damping coefficient c= 1.1×10^6 $N.(m/s)^{-1}$. Dampers with such a capacity are commercially available. By using this passive damper, the peak displacements of the structure subject to 53 ground motions are plotted in Figure 5-7 for the uncontrolled structure and the structure with a passive/active hybrid control system. The active actuator is activated whenever the required control force is greater than 500 KN, and it is saturated at 4000 KN. It is observed that the passive damper alone can't reduce the peak displacement of the structure within the limit of 20 cm. However, with the proposed hybrid control system, the peak displacement of the structure is reduced below 20 cm. The active actuator is only activated during the near-field ground motion. For smaller ground motions, the control force of the actuator is zero, indicating that the passive damper works alone for such earthquakes.

Table 5-4 Response quantities of structures with hybrid control systems.

	Uncontrolled		Active/active system					Active/passive system				
Ground Motions	**x (cm)**	**ẍ (g)**	**x (cm)**	**ẍ (g)**	**Total Force (KN)**	**Linear Force (KN)**	**Nonlinear Force (KN)**	**x (cm)**	**ẍ (g)**	**Total Force (KN)**	**Linear Force (KN)**	**Nonlinear Force (KN)**
El Centro	25.0	0.08	7.6	0.15	1415	589	825	7.1	0.15	1407	349	1059
Mexico	14.1	0.05	3.7	0.03	264	264	0	4.3	0.02	174	174	0
Gebze	56.9	0.19	11.4	0.17	1509	613	896	10.6	0.17	1603	393	1211
Kobe JMA00	31.9	0.11	10.6	0.54	5329	1329	4000	10.6	0.50	4867	867	4000
Kobe JMA90	48.6	0.16	10.3	0.52	5153	1153	4000	11.1	0.48	4739	739	4000
Lands LCN000	42.5	0.14	9.1	0.14	1192	544	652	10.0	0.13	1158	386	849
Lands LCN275	116.8	0.39	13.3	0.42	3987	970	3017	13.0	0.42	4027	588	3439
Cape CMP00	67.6	0.22	13.2	0.52	4804	1076	3919	13.4	0.49	4441	792	4000
Cape CMP90	27.5	0.09	10.5	0.40	3637	991	2646	9.9	0.40	3660	621	3039
Loma LGP00	135.8	0.45	14.5	0.45	4484	1046	3438	14.3	0.45	4470	642	3827
Loma LGP90	34.0	0.11	9.2	0.19	1733	714	1018	9.1	0.18	1590	448	1224
Sup. Hill 135	8.5	0.03	5.3	0.22	2157	788	1370	6.3	0.22	2147	502	1645
TCU084EW	89.1	0.29	15.3	0.55	5332	1332	4000	15.3	0.50	4898	898	4000
CHY080NS	42.0	0.14	13.9	0.55	5329	1329	4000	13.8	0.50	4875	875	4000
CHY080EW	29.3	0.10	14.1	0.55	5399	1399	4000	13.7	0.50	4931	931	4000
Tabas LN	70.4	0.23	14.6	0.36	3430	932	2649	14.6	0.36	3456	663	3056
Tabas TR	104.1	0.34	15.3	0.38	3563	953	2780	15.3	0.38	3568	616	3185
Kobe TAK00	88.3	0.29	17.4	0.57	5335	1335	4000	20.1	0.52	4853	853	4000
Kobe TAK90	81.6	0.27	14.8	0.53	5044	1112	4000	15.6	0.49	4653	727	4000
Cape Pet 00	27.1	0.09	8.9	0.22	2078	788	1356	8.9	0.22	2055	510	1620
Cape Pet90	52.0	0.17	10.9	0.53	5091	1091	4000	10.5	0.48	4668	680	4000
Duzce 270	75.5	0.25	14.4	0.23	2255	830	1426	14.6	0.21	2006	531	1553
Erzincan NS	59.8	0.20	14.0	0.38	3570	976	2671	14.0	0.38	3568	651	3061
Newhall 360	58.3	0.19	11.3	0.53	5119	1119	4000	11.4	0.49	4714	740	4000

Table 5-4 Response quantities of structures with hybrid control systems (Continued)

Rinaldi 228	56.4	0.19	17.2	0.61	5857	1857	4000	17.6	0.54	5201	1201	4000
Sylmar 052	131.9	0.44	15.3	0.51	5005	1162	3843	14.2	0.48	4766	766	4000
Sylmar 142	41.5	0.14	14.4	0.54	5413	1413	4000	14.3	0.50	4936	936	4000
TCU065NS	101.4	0.33	12.6	0.38	3628	946	2682	12.5	0.38	3611	576	3043
TCU065EW	131.9	0.44	17.0	0.41	3684	1031	2884	17.0	0.42	3574	674	3295
TCU068NS	72.5	0.24	17.2	0.37	3600	973	2628	17.1	0.37	3593	631	2990
TCU068EW	141.8	0.47	17.9	0.32	3021	875	2190	17.9	0.32	3039	599	2577
Chile LL010	32.6	0.11	7.8	0.16	1511	681	831	8.3	0.15	1362	430	990
Chile LL100	11.1	0.04	4.4	0.05	443	443	0	4.5	0.03	280	280	0
Chil Vina200	14.8	0.05	5.7	0.13	1184	616	615	6.3	0.11	1074	374	725
Chil Vina290	12.9	0.04	4.5	0.05	489	489	0	4.6	0.03	297	297	0
Mex. Cal00	21.5	0.07	7.2	0.05	349	349	0	7.6	0.04	681	227	500
Mex. Cal90	14.4	0.05	3.9	0.03	262	262	0	4.6	0.02	173	173	0
Imperial NS	25.1	0.08	7.6	0.15	1422	592	831	7.1	0.15	1408	351	1056
Imperial EW	38.9	0.13	10.9	0.12	1052	543	533	9.5	0.12	964	337	747
Hach. EW	28.1	0.09	9.4	0.14	1413	654	760	9.5	0.14	1359	408	950
Hach. NS	30.1	0.10	8.4	0.12	1144	593	551	9.3	0.12	1187	427	778
Mex. Occt1	2.6	0.01	1.2	0.01	72	72	0	1.5	0.01	49	49	0
Mex. Occt2	2.3	0.01	1.1	0.01	71	71	0	1.3	0.01	45	45	0
Miya. E41S	7.4	0.02	3.4	0.03	258	258	0	4.4	0.03	164	164	0
Miya. E41E	4.8	0.02	2.1	0.03	214	214	0	2.6	0.02	131	131	0
Olympia 182	4.4	0.01	1.6	0.02	155	155	0	1.6	0.01	97	97	0
Olympia 282	3.1	0.01	1.4	0.02	149	149	0	1.6	0.01	91	91	0
Mex. TacyE	12.7	0.04	3.4	0.02	161	161	0	4.8	0.02	111	111	0
Mex. TacyN	10.8	0.04	4.0	0.03	153	153	0	5.7	0.02	103	103	0
Taft N21E	11.5	0.04	3.6	0.03	269	269	0	4.8	0.02	176	176	0
Taft S69E	15.4	0.05	5.1	0.04	308	308	0	5.8	0.03	209	209	0
Chile Vlp070	14.7	0.05	3.8	0.04	334	334	0	4.5	0.03	221	221	0
Chile Vlp160	4.8	0.02	1.3	0.01	123	123	0	1.4	0.01	78	78	0

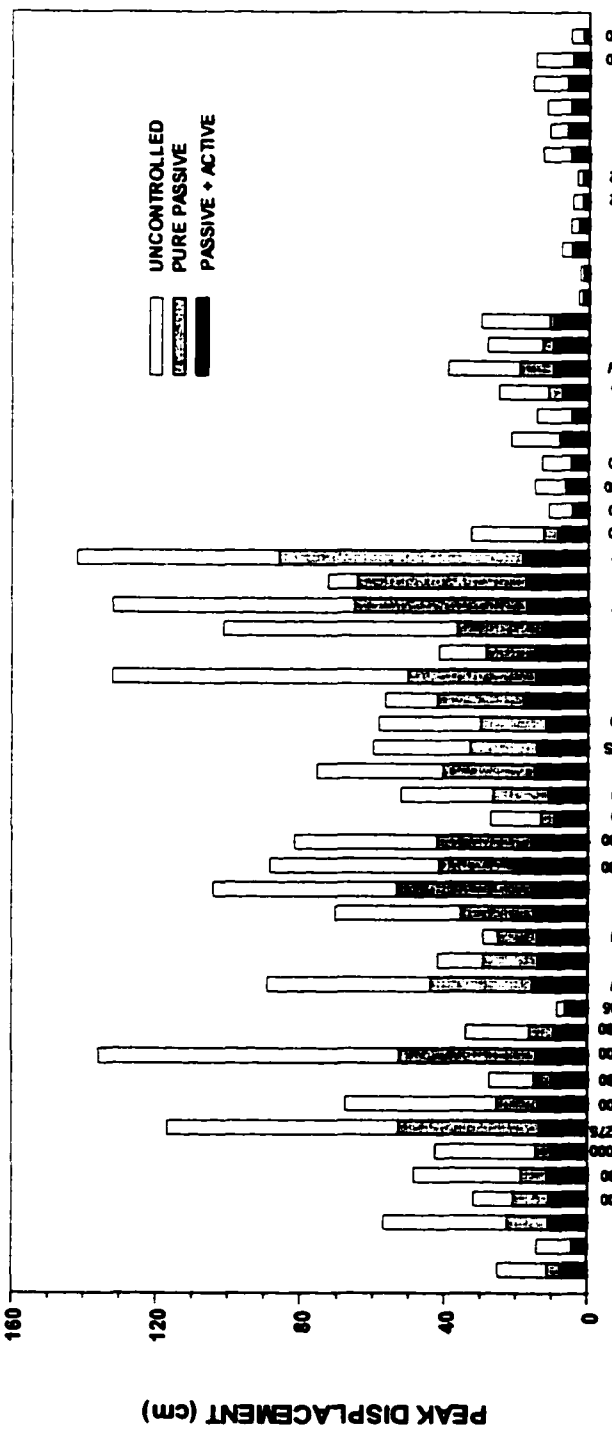

Figure 5-7: Peak displacement of structure with passive dampers and Hybrid (passive/active) controllers.

The performance of the passive/active hybrid control system proposed above is investigated further by using the analytical pulse model proposed in Chapter 3. The velocity pulses are used to represent the long period pulses in near-field ground motions, since the response quantities of long period structures are affected strongly by the long period components in near-field ground motions. A group of velocity pulses are generated using (i) the shape factors n=1, ζ_p=0.5, (ii) the peak ground acceleration =0.3g, and (iii) the pulse period T_p varying from 0.4 s to 8 s with an increment of 0.2 s. In this case, the corresponding peak ground velocity varies from 0.131 m/s to 3.28 m/s.

Figure 5-8(a) plots the peak displacement response for (i) the uncontrolled structure, (ii) the structure with passive dampers, and (iii) the structure with the proposed hybrid control system. Since the excitation is impulsive in nature, the active controller is triggered for all pulses with different pulse periods. The maximum peak displacement of the uncontrolled structure is 212.0 cm, and that of the structure with a passive damper is 112.6 cm. The corresponding quantity for the structure with passive/active hybrid control system is about to 20 cm, if the capacity of the nonlinear actuator is saturated at 4000 KN. In such a case, the peak control force of the passive damper is limited to 500 KN, as shown in Figure 5-8 (b). The peak control force required for the passive damper is 1700 KN if passive viscous dampers are used alone. Thus, the proposed passive/active hybrid control system not only limits the peak dynamic response to 20 cm during a wide-range of ground motions, but also protects the passive dampers during strong earthquakes.

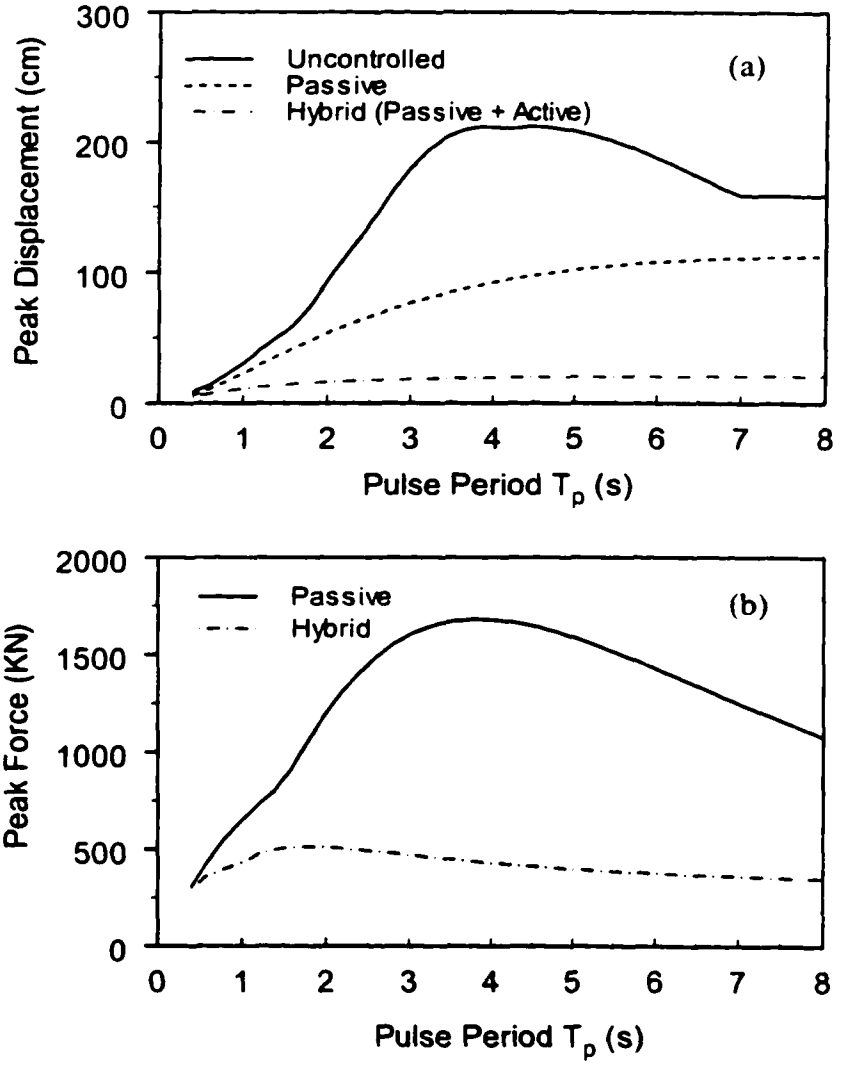

Figure 5-8: Peak response quantities of the SDOF structure subject to analytical velocity pulses: (a) Peak displacement of the uncontrolled structure, with passive dampers, and the proposed hybrid control system; (b) Peak forces of passive damper, and passive damper of passive/active hybrid control system.

5.6 Summary

In this chapter, the effectiveness of hybrid control systems in protecting structures against near-field earthquakes has been investigated. Because of the impulsive characteristics of near-field ground motions, polynomial controllers are more desirable than linear controller such as LQR/LQG. The most outstanding property of the polynomial controller is its ability to respond quickly to abrupt excitations and the control forces are developed as a function of the high order polynomial of the displacement. In this study, the high-order controller developed by Agrawal and Yang (1995, 1996a, b) is modified to account for the acceleration penalty. It has been demonstrated that this controller is very effective in mitigating the response of structures from near-field ground motions. By using 28 strong near-field ground motions and 22 long duration ground motions, it is also demonstrated that a hybrid active control system with multilevel control objectives can be implemented based on the polynomial control algorithm. Alternatively, a hybrid control system consisting of passive damper and active actuator is also effective in achieving the same control objectives.

CHAPTER 6

PROTECTING STRUCTURES FROM NEAR-FIELD GROUND MOTIONS USING SEMI-ACTIVE CONTROLLERS

6.1 Introduction

Because of the impulsive characteristics of near-field ground motions, high order optimal polynomial controllers have been demonstrated to be more effective than linear controllers in protecting structures from near-field ground motions. The most desirable property of the nonlinear controllers is their ability to quickly response to external excitations. In this chapter, the optimal polynomial controller investigated in Chapter 5 will be implemented by a hybrid control system consisting of a combination of passive dampers and semi-active control devices, such as semi-active friction dampers, ER dampers or MR dampers.

A brief state of art review of some semi-active controllers is presented at the beginning of this chapter. Several semi-active controllers using local measurements are introduced and their equivalent damping ratios are derived in Section 6.2. Section 6.3 introduces some semi-active controllers based on active control algorithms. A passive/semi-active hybrid control system, consisting of a passive linear viscous damper and a semi-active friction damper, will be proposed in Section 6.4. The application of the proposed passive/semi-active hybrid control system to a SDOF structure and a benchmark cable-stayed bridge will be presented in Sections 6.5 and 6.6, respectively.

6.2 Semi-Active Controllers Using Local Measurements

Because of the intrinsically nonlinear nature of semi-active control devices, the development of device-specific control strategies is an important and challenging task. Several control algorithms, which utilize only local information, are advantageous in terms of the cost, ease of implementation, robustness and tolerance to failures of individual dampers in the case of structures with multiple dampers. On the other hand, semi-active controllers that utilize states (displacement and velocities) of the structure, either fully measured or partially measured and estimated by observers, may be more adaptive to ground motion characteristics and less robust to the variation of structural parameters. A brief description of various semi-active devices has been presented Chapter 2. In the following, five semi-active friction control algorithms are investigated for their energy dissipative properties, such as the equivalent damping ratio, and their capability to limit the peak dynamic response during near-field earthquakes. The strategies presented in the following are called "damper" or "controller". These two terminologies imply semi-active control approaches.

6.2.1 Various Semi-active Controllers

(a) Reid Controller

The control force of the Reid damper (Reid 1956) is proportional to the current displacement across the damper device. The memory-less Reid controller is defined as

$$f(t) = \mu g \mid x \mid \mathrm{sgn}(\dot{x}) = \mu g x \cdot \mathrm{sgn}(x\dot{x}) \tag{6-1}$$

where g is the constant feedback gain with units of stiffness, μ is the coefficient of friction, and x is the displacement across the damper.

(b) Sequential Controller

In the sequential controller, the control force opposes the elastic force of the structure to reduce the acceleration of the system (Stammers and Sireteanu, 1998). The control force for a sequential controller is zero during loading ($x\dot{x} > 0$), and it is the same as that of Reid damper during unloading ($x\dot{x} < 0$). Hence, the control law for a sequential controller is obtained as

$$f(t) = \begin{Bmatrix} 0 & \text{for } x\dot{x} \geq 0 \\ -\mu g x & \text{for } x\dot{x} \leq 0 \end{Bmatrix} \tag{6-2}$$

It is observed from Equations (6-1) and (6-2) that the area of the hysteresis loop of the sequential controller is half of that of the Reid controller. Hence, the sequential controller is less efficient than the Reid controller. However, a semi-active sequential controller can be designed either for a suspension system to achieve zero acceleration in a moving vehicle or to generate a zero transmitted force to the foundation for a spring-mass machinery system subjected to an imbalance force. The concept can be applied to control base-isolated buildings using semi-active devices in order to reduce both the base acceleration and the drift simultaneously.

(c) Modulated Homogenous Friction (MHF) Controller

The Modulated Homogenous controller was first proposed by Inaudi (1997), and later modified by He and Agrawal (2001) to make it sliding continuously. For this controller, the control force is proportional to the previous peak displacement across the damper. Mathematically, the controller is expressed as,

$$f(t) = \mu g \, | \, P[x(t)] \, | \, \mathrm{sgn}(\dot{x}) \tag{6-3}$$

where g is the positive gain coefficient with units of stiffness and $P[x(t)]$ is the operator defined as follows:

$$P[x(t)] = x(s) \tag{6-4}$$

where s is the previous time instant when the velocity is zero ($\dot{x}(s) = 0$), and x(s) is the local peak of the deformation across the damper. Because the output of P[x(t)] is equal to the value of the input signal at the prior local peak, P[x(t)] is referred to as prior-local-peak operator.

(d) Visco-elastic Friction Controller

Chen and Chen (2000) proposed a semi-active control algorithm based on the non-linear Reid damping and viscous damping mechanisms for the control of a piezoelectric friction damper. The control force of the friction controller is given by

$$f(t) = \begin{cases} \mu[e\dot{x}(t) + gx(t)] & x\dot{x} > 0 \quad \text{(loading)} \\ \mu[e\dot{x}(t) - gx(t)] & x\dot{x} < 0 \quad \text{(unloading)} \end{cases} \tag{6-5}$$

where g and e are positive gain coefficients of the slip (displacement) and slip rate (velocity), and x(t) and $\dot{x}(t)$ are the displacement and velocity across the damper, respectively. In Equation (6-5), $f(t) = \mu e\dot{x}(t)$ when g=0, which represents a viscous damper; and $f(t) = \mu g\,|\,x(t)\,|\,\mathrm{sgn}(\dot{x})$ when e=0, which represents a non-linear Reid controller. Hence, the semi-active friction algorithm in Equation (6-5) essentially combines both the viscous and the non-linear Reid controller mechanisms.

(e) Resetting Semi-Active Stiffness Damper (RSASD)

According the mechanism of Resetting semi-active stiffness damper (RSASD), Yang et al (2000) proposed the control logic of RSASD, which uses the deformation of

the damper and the prior-local-peak deformation as the only feedback signal to determine the control force, expressed mathematically as

$$f(t) = k(|\, x - P[x(t)]\,|) \tag{6-6}$$

where k is the stiffness of the RSASD and P[x(t)] is the same operator defined in Equation (6-4). Obviously, the controller has memory because the past of the deformation signal is required to determine the current control force.

6.2.2 Equivalent Damping Ratios of Semi-active Controllers

If the parameters of the controller described above are held constant (i.e., no real-time control), the performance of all these controllers will be the same as the underlying passive damping hardware that is used to implement these controllers. The energy dissipative capability of control algorithms depends on the hysteretic loop of the algorithm. Unlike passive damping systems, hysteretic loops for semi-active damping systems can be generated artificially using a control algorithm. For a semi-active controller, the hysteretic loop is simply a plot of the control force versus the deformation across the damper. The area enclosed under the loop is the amount of energy dissipated. The equivalent damping ratio of the control algorithm is defined as the damping ratio of the linear viscous damper that will dissipate the same amount of energy as the semi-active controller. The energy dissipated by a viscously damped linear SDOF system under harmonic excitation during one complete cycle is defined by

$$\int_0^{T_n} f_d\, dx = \int_0^{T_n} c\dot{x}dx = 2\pi\zeta\omega\omega_n mA^2 \tag{6-7}$$

where $f_d = c\dot{x}$ is the damping force, $c=2\zeta m\omega_n$ is the viscous damping coefficient, x is the displacement response expressed by $x = A\sin(\omega t)$, A is amplitude, and ω_n and ω are the

natural and excitation frequencies, respectively. To study the energy dissipation of these controllers during a sinusoidal excitation, their equivalent damping ratios can be derived in the following.

(a) Reid Controller

With the assumption that the maximum damper force of the Reid controller is $f_{max}=\mu gA$, where A is the peak displacement of the structure, the energy dissipated by the Reid controller per cycle is

$$2\int_{-A}^{A} \mu g x dx = 2\mu g A^2 \tag{6-8}$$

By equating Equation (6-7) and Equation (6-8), one obtains the equivalent damping ratio of the Reid controller as

$$\xi_{eq} = \frac{2\mu g A^2}{2\pi m w^2 A^2} = \frac{\alpha}{\pi} \tag{6-9}$$

where α is the normalized force ratio defined by

$$\alpha = \frac{\mu g}{m\omega\omega_n} \tag{6-10}$$

(b) Sequential Controller

With the assumption that the maximum control force of a sequential controller is $f_{max}=\mu gA$, the energy dissipated by the Sequential controller per cycle is obtained as

$$2\int_{0}^{A} \mu g x dx = \mu g A^2 \tag{6-11}$$

By equating Equation (6-7) and Equation (6-11), one obtains the equivalent damping ratio of the sequential controller as

$$\xi_{eq} = \frac{\mu g A^2}{2\pi m \omega \omega_n A^2} = \frac{0.5\alpha}{\pi} \tag{6-12}$$

(c) Modulated Homogenous Friction (MHF) Controller

Assuming the maximum control force of the MHF controller is $f_{max}=\mu gA$, one obtains the energy dissipated by the MHF controller per cycle

$$2\int_{-A}^{A} \mu g A dx = 4\mu g A^2 \tag{6-13}$$

By equating Equation (6-7) and Equation (6-13), one obtains the equivalent damping ratio of the MHF controller as

$$\xi_{eq} = \frac{4\mu g A^2}{2\pi m \omega \omega_n A^2} = \frac{2\alpha}{\pi} \tag{6-14}$$

(d) Visco-elastic Friction (VEF) Controller

There are two coefficients, e and g in the viscous-elastic friction controller in Equation (6-5). For the sake of simplicity, we define $e=g/\omega$. In order to achieve the same maximum damper force, $f_{max}=\mu gA$, the controller (6-5) is adjusted by multiplying a coefficient $\sqrt{2}/2$. Then, the energy dissipated per cycle by the visco-elastic friction controller is obtained as

$$4\int_{0}^{A} (\frac{1}{\omega} \cdot \frac{\sqrt{2}}{2} \mu g \dot{x} + \frac{\sqrt{2}}{2} \mu g x) dx = \sqrt{2} \cdot (\pi/2 + 1) \mu g A^2 \tag{6-15}$$

By equating Equation (6-7) and Equation (6-15), one obtains the equivalent damping ratio of the visco-elastic friction controller as

$$\xi_{eq} = \frac{\sqrt{2}(\pi/2+1)\mu g A^2}{2\pi m \omega \omega_n A^2} = \frac{\sqrt{2}(\pi/2+1)\alpha}{2\pi} \approx \frac{1.82\alpha}{\pi} \tag{6-16}$$

(e) Resetting Semi-Active Stiffness Damper (RSASD)

In order to obtain the same maximum control force, $f_{max}=\mu gA$, the controller in Equation (6-6) is adjusted by multiplying a coefficient 1/2. Then, the energy dissipated per cycle by the RSASD is

$$2\int_0^A \frac{1}{2}\mu g(x - A)dx = 2\mu gA^2 \tag{6-17}$$

By equating Equation (6-7) and Equation (6-17), one obtains the equivalent damping ratio of RSASD as

$$\xi_{eq} = \frac{2\mu gA^2}{2\pi m\omega\omega_n A^2} = \frac{\alpha}{\pi} \tag{6-18}$$

The control rules, hysteretic loops and equivalent damping ratios of the semi-active controllers presented above are summarized in Table 6-1.

Table 6-1 Equivalent damping ratios of some semi-active controllers

Controllers	Control Law	Hysteretic Loop	Equivalent Damping Ratio
Reid Controller	$f(t) = \mu g \mid x \mid \mathrm{sgn}(\dot{x})$ $= \mu g\, x\,\mathrm{sgn}(x\dot{x})$	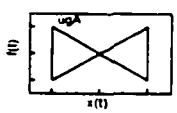	$\frac{\alpha}{\pi}$
Sequential Controller	$f(t) = \begin{cases} 0 & \text{for } x\dot{x} \geq 0 \\ -\mu gx & \text{for } x\dot{x} \leq 0 \end{cases}$	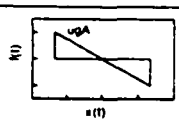	$\frac{0.5\alpha}{\pi}$
Modulated Homogenous Friction Controller	$f(t) = \mu g \mid P[x(t)] \mid \mathrm{sgn}(\dot{x})$	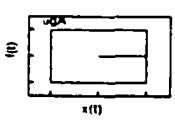	$\frac{2\alpha}{\pi}$
Visco-elastic Friction Controller	$f(t) = \begin{cases} \mu[e\dot{x}(t) + gx(t)] & x\dot{x} > 0 \\ \mu[e\dot{x}(t) - gx(t)] & x\dot{x} < 0 \end{cases}$	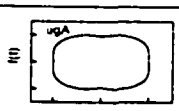	$\frac{1.82\alpha}{\pi}$
Resetting Semi-active Stiffness Damper	$f(t) = g(x - P[x(t)])$	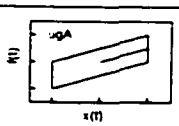	$\frac{\alpha}{\pi}$

6.2.3 Performance of Semi-active Controllers

The derivation of the equivalent damping ratio for various semi-active controllers above is based on the assumption that the structure is subject to a harmonic excitation. When a linear SDOF structure is subject to an earthquake ground motion, frequency components in the ground motion close to the natural frequency of the structure primarily contribute to the response of the structure. Hence, the response quantities in the frequency domain usually exhibit a significant amplification around the natural frequency of the structure. To illustrate the effect of ground motions on the efficiency of semi-active controllers, Figure 6-1 shows the response of a SDOF structure with a natural period of 2.5 seconds subject to the El Centro NS (1944, Imperial Valley) and Gebze NS (1999, Kocaeli earthquake) ground motions. The El Centro ground motion has a longer duration and a predominant period around 0.95 s. The Gebze ground motion, recorded 17 km away from the fault rupture, has a very short duration and a predominant period around 4.2 s. It is observed from Figure 6-1 that the response of the structure subject to the El Centro ground motion increases to its peak value gradually. On the other hand, the displacement response of the structure subject to the Gebze ground motion exhibits an abrupt peak during the first few seconds of the seismic episode. The response after the abrupt peak decreases gradually.

The performance of various semi-active controllers and the passive viscous damper is shown in Figure 6-2 where the structure is subject to these two earthquakes. Figure 6-2 presents the peak displacement of the structure versus the peak control force from the semi-active damper. The maximum control force of a damper is assumed to be 20 KN, which is approximately 5.6% of the weight of the structure. It is observed from

Figure 6-2(a) that the performance of the MHF controller is better than other controllers using the same peak control force for the El Centro earthquake. Since the MHF controller has the highest equivalent viscous damping ratio, it dissipates more energy than other controllers for long duration earthquakes, such as the El Centro NS (1944, Imperial Valley).

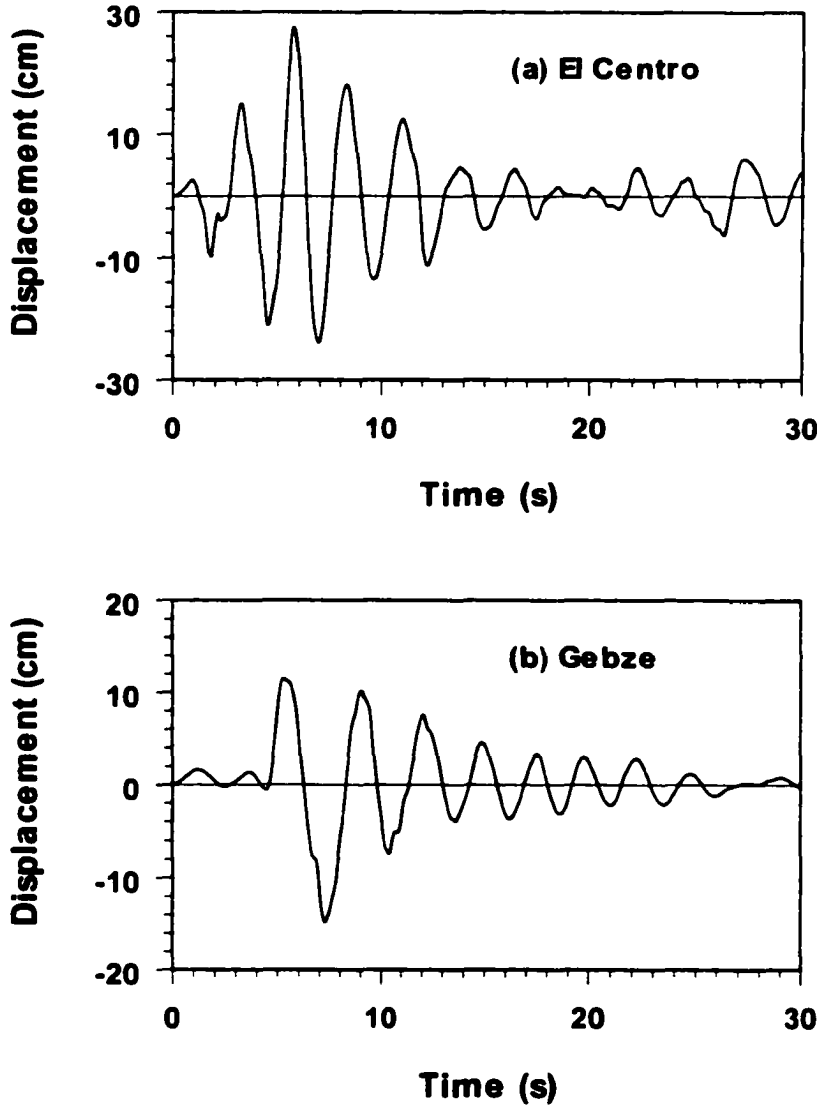

Figure 6-1: Displacement response of SDOF system with mass 36285 kg, T_n=2.5s and inherent damping 5% of critical.

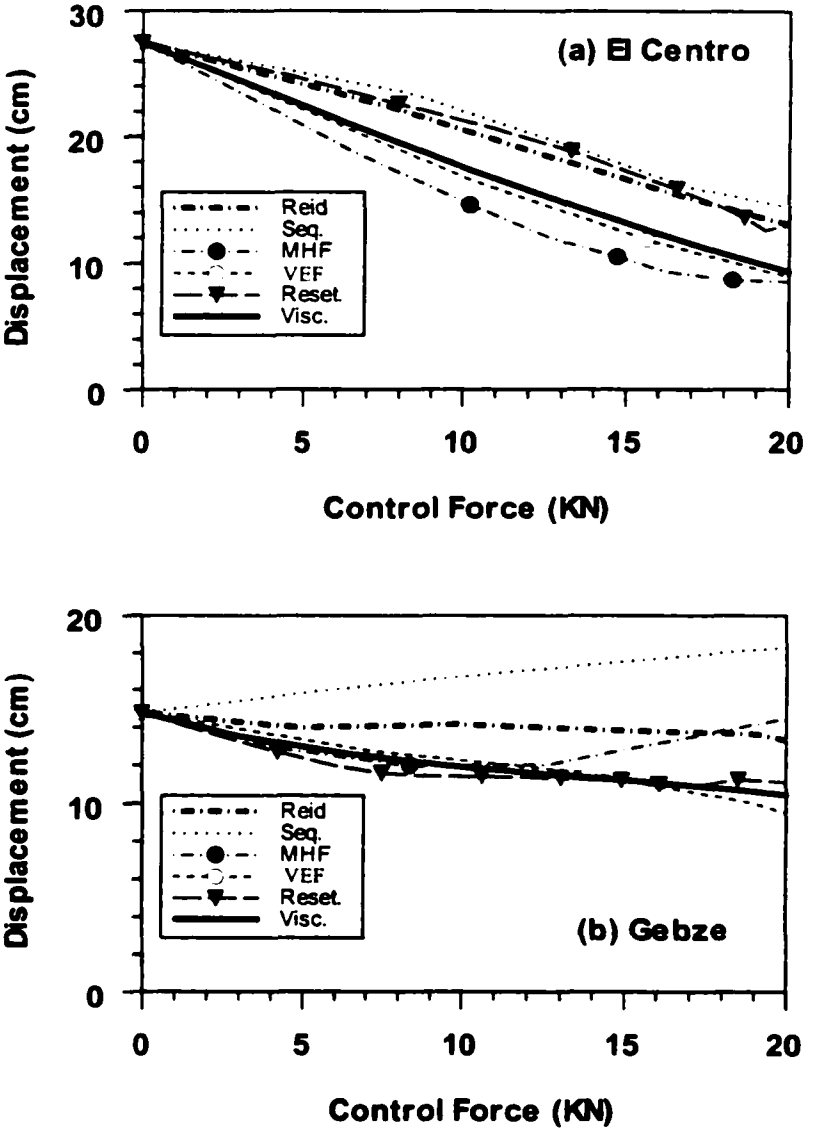

Figure 6-2: Displacement response of SDOF structure with various damping system subjected to El Centro and Gebze ground motions.

For the Gebze earthquake, where the peak displacement of the uncontrolled structure occurs in the first cycle of its oscillation, the controller with a maximum equivalent damping ratio (i.e., MHF controller) doesn't necessary perform best in reducing the response of the structure. It is observed from Figure 6-2 that the Resetting Semi-active stiffness damper is better than others, because its quick response to the abrupt displacement of the structure due to impulsive ground motions, such as the Gebze earthquake. Another reason for a better performance of the RSASD controller is that it adds stiffness to the structure and dissipates energy through the resetting mechanism.

6.3 Controllers Based on Active Control Algorithms

Semi-active controllers using a full-state feedback or dynamic output feedback are more adaptive in protecting structures by developing the required amount of control force according to the characteristic of the ground motion. These semi-active controllers are usually based on active control algorithms, such as, bang-bang control (McClamroch and Gavin 1995; Mukai et al. 1994), clipped optimal control (Patten et al. 1994a,b; Dyke et al. 1996b), bi-state control (Patten et al. 1994), fuzzy control method (Sun and Goto 1994; Symans and Kelly 1999), adaptive nonlinear control (Kamagata and Kobori 1994), sliding mode control (Yang et al. 1995c, 1996d), etc.

From the results presented in Chapters 3 and 4, it is obvious that the main characteristic of near-field ground motions is their high-magnitude and long-period velocity pluses. The peak response of uncontrolled structures subject to these ground motion pulses is usually developed in the first few cycles of the oscillation. Hence, an effective control strategy to limit the peak dynamic response of the structure should have

the ability to respond quickly to the effects of external excitations. Such properties are inherent to nonlinear controllers, e.g., optimal polynomial controllers proposed by Agrawal and Yang (1995, 1996) and investigated in Chapter 5. In this chapter, the optimal polynomial controller will be implemented by various combinations of passive and semi-active control devices.

Based on the conditions of optimality for linear systems, Agrawal and Yang (1995, 1996) derived an optimal polynomial controller as follows,

$$U(t) = -R^{-1}B^{T}PZ(t) - R^{-1}B^{T}\sum_{i=2}^{k}(Z^{T}M_{i}Z)^{i-1}M_{i}Z(t) \qquad (6\text{-}19)$$

where positive definite matrices P and M_i's are obtained by solving algebraic Riccati and Lyapunov equations, respectively,

$$PA + A^{T}P - PBR^{-1}B^{T}P + Q = 0 \qquad (6\text{-}20)$$

$$M_{i}(A - BR^{-1}B^{T}P) + (A - BR^{-1}B^{T}P)^{T}M_{i} + Q_{i} = 0,\ i=2,3,\ldots,k \qquad (6\text{-}21)$$

It can be seen from Equation (6-19) that the nonlinear part of the controller is the sum of the polynomial of various orders in terms of the states of the system. Matrices P and M_i's in Equations (6-20) and (6-21) can be solved using any well-know numerical algorithms or using functions available in MATLAB. The main advantage of the optimal polynomial is that it separates the required control into a linear part, which is effective for smaller and harmonic type of excitations, e.g., Mexico earthquake, and a nonlinear part which is effective in responding to the abrupt change of the structural response. The optimal polynomial controller can be designed to obtain a trade-off between linear and nonlinear parts by choosing weighting matrices Q and Q_i (i=2,3,...,k) appropriately.

Further, if the nonlinear control force is large enough, the polynomial controller can be designed to reduce the structural response to certain a threshold value irrespective

to the external excitation. This feature is of critical importance to achieve the control objective of civil engineering structures. For instance, the drift of an isolator for a base isolated building should be less than 40 cm or the interstory drift ratio of a high-rise building should be less than 0.5%.

6.4 Passive/Semi-Active Hybrid System

It is well-known that passive fluid viscous dampers are very effective and have been widely used to protect structures from strong ground motions. However, since the control force applied by a typical passive damper is a function of the response of structures, the efficiency of passive damping system depends both on the properties of ground motions and that of the structures. For example, passive fluid damper is very effective in reducing the response of short or medium period structures subject to ground motions. However, highly damped long period structures, such as base isolated buildings, may undergo large displacements when subject to strong ground motions with long period pulses are observed during recent major earthquakes, such as Kobe, Northridge, and Chi-Chi earthquakes. Increasing the viscous damping ratio through a higher level of supplemental damping may be a possible solution to reduce the displacement. However, increasing the viscous damping ratio beyond certain value may result in an increase of the acceleration response.

In this study, an innovative hybrid control system consisting of passive dampers installed in parallel to semi-active friction dampers is proposed for applications to structures subject to near-field earthquakes. The control force of the semi-active friction damper is regulated according to the nonlinear terms of the optimal polynomial controller

in Equation (6-19) whenever the required control force exceeds a certain threshold. The control force generated by linear term of the optimal polynomial controller is approximated using passive viscous dampers, i.e., $U_L = c\dot{x}$. Then, the nonlinear controller for the semi-active friction damper, U_{fn}, can be designed as

$$U_{fn} = \begin{cases} 0 & \text{if } U_{fn} < U_1 \\ U - U_L & \text{if } U_1 \le U_{fn} \le U_2 \text{ and } U_{fn}.\text{sgn}(\dot{x}) < 0 \\ U_2 & \text{if } U_{fn} > U_2 \text{ and } U_{fn}.\text{sgn}(\dot{x}) < 0 \\ 0 & \text{if } U_{fn}.\text{sgn}(\dot{x}) > 0 \end{cases} \tag{6-22}$$

where U_1 is the lower threshold value at which the semi-active friction controller is activated, U_2 is the upper threshold of the device capacity, U_L is the force applied by passive viscous dampers (the linear part of the polynomial controller), and $\dot{x}$ is the velocity across the friction damper. In Equation (6-22), lower and upper thresholds U_1 and U_2 are designed by numerical simulations considering the whole spectrum of ground motions for a site. It is observed from Equation (6-22) that the nonlinear control force U_{fn} is zero for $U_{fn} < U_1$ in which only the passive viscous damper is utilized to reduce the vibration of the structure. When U_{fn} exceeds the device capacity U_2, the nonlinear control force is saturated at the U_2 level. Unlike the active controller that always applies the force on the structure, the proposed semi-active controller applies force only when $U_{fn}.\text{sgn}(\dot{x}) < 0$.

The proposed hybrid control system has several advantages over passive or active systems. For structures subject to ground motions, such as 1985 Mexico City earthquake, the passive viscous term is effective in dissipating the input seismic energy because of a gradual buildup of the response. However, during strong seismic events such as near-field ground motions, the structure undergoes a large displacement response due to

impulsive long period pulses. In such situations, the nonlinear part will be activated to reduce the response of the structures aggressively. Hence, the adaptability of the proposed hybrid control system is similar to that of active control system. It has been observed through numerical simulations that the performance of the active control systems is relatively insensitive to the site conditions and ground motions. However, the energy required for the semi-active friction damper is much smaller than that for an equivalent active system. Two examples will be used to illustrate the performance of the proposed hybrid control system. Although the semi-active friction damper is used to illustrate the performance of the proposed hybrid control system, other dampers, such as MR/ER dampers can also be used to obtain a similar level of performance.

6.5 Example 1: SDOF System

The first example used herein is the same example illustrated in Chapter 5. A bridge is modeled as a SDOF structure with a mass $M=1.02\times10^{6}$ kg, stiffness $K=3.3\times10^{6}$ N/m and damping ratio $\zeta=2\%$. The polynomial controller is designed by selecting $R=2.5\times10^{-5}$, $Q(1,1)=100K$, $Q(1,2)=Q(2,1)=Q(2,2)=0$, $Q_2(1,1)=0.1K$, $Q_2(1,2)=Q_2(2,1)=Q_2(2,2)=0$, and K is the stiffness of the structure. In this chapter, the optimal polynomial controller in Equation (6-19) will be implemented by a pure semi-active controller and a (passive/semi-active) hybrid controller proposed. To illustrate the adaptability of the proposed hybrid control system to various ground motions, 53 typical recorded near-field and long duration ground motions as well as the analytical velocity pulse model proposed in Chapter 3 are used in the following study.

6.5.1 Recorded Ground Motions

It has been observed that the coefficient of the displacement feedback in the linear controller is quite small as compared to the velocity feedback coefficient. Hence, the linear part of the controller is approximated by $U_L = g_2\dot{x}$, where g_2 is the velocity feedback coefficient. The peak control force of the semi-active friction control system is saturated to 6000 KN. The performance of the semi-active friction controller for 53 ground motions is shown in Table 6-2.

The performance of the proposed hybrid control system is investigated by combining a passive viscous damper with 30% damping ratio and a semi-active friction controller based on the nonlinear part of the polynomial controller designed above. Extensive numerical simulations using 53 earthquake ground motions are conducted to obtain the control force thresholds U_1 and U_2 as 500 KN and 4000 KN, respectively. The semi-active controller of the hybrid control system is only triggered when the ground motion is strong enough such that the passive damper alone cannot fulfill the specified control objectives.

Figure 6-3 shows the peak displacement of: (i) the uncontrolled structure, (ii) the structure with only passive dampers (linear term), and (ii) the structure with the proposed hybrid control system. It is observed from Figure 6-3 that passive dampers are very effective in reducing the peak displacement of the structure subject to long duration ground motions during the Mexico City earthquake. The displacement reduction for this earthquake is 70%. However, the displacement reduction using the same design of passive viscous dampers during the TCU068EW (Chi-Chi earthquake) is 40% and that for TCU068NS is only 25%. This is because the peak displacement of the uncontrolled

structure subject to long duration ground motions during the Mexico City earthquake is usually developed after several cycles of oscillations. Linear viscous dampers are quite effective in reducing the peak response for such earthquakes. However, for near-field ground motions, which contain impulsive components, the peak displacement usually occurs in the first few cycles of oscillation. Since the peak displacement is developed in a abrupt manner during these earthquakes, linear passive viscous dampers, whose control force is a proportional to the velocity of the structure, cannot provide enough control force to reduce the responses of the structures to a satisfactory range. Increasing passive viscous damping not only may further reduce the peak displacement response but also may increase the acceleration of the structure.

For the proposed hybrid control system, the semi-active friction damper (nonlinear part) can be designed appropriately not to be activated for long duration earthquakes such as the 1985 Mexico City ground motion or the 1985 Chile ground motion, since the passive damper alone is capable of achieving the control objective. Thus, it is observed from Figure 6-3 that the peak displacement for both passive and passive/semi-active hybrid cases is the same for these ground motions, since the semi-active friction damper is not activated. However, the semi-active friction controller is designed to be triggered to provide impulsive type control force when the structure is subject to near-field ground motions, such as the Gebze and TCU068NS ground motions. Hence, the peak displacement of the structure using the proposed hybrid control system is limited to 30 cm during all the 53 ground motions. Figure 6-3 clearly shows the additional reduction of the peak response obtained by the proposed hybrid control system over the passive damper only. It should be pointed out that the capability of a protective

system to limit the displacement of a structure to a certain value for a broad spectrum of earthquake ground motions is of critical importance for the isolator of base isolated buildings and high-rise buildings.

Figure 6-4 shows the bar chart of the peak displacement using passive/active hybrid controller and passive/semi-active controller. In the passive/active hybrid controller case, while the linear part in Equation (6-19) is used, the nonlinear part in Equation (6-19) is saturated at 4000 KN to keep the maximum applied force at a similar level for these two controllers. It is observed from Figure 6-4 that the performance of the passive/semi-active hybrid control system is similar to that of the passive/active hybrid control system. This is because the linear parts of both controllers are implemented by a passive viscous damper with almost the same force characteristics, and numerical simulations show that the nonlinear part of the control force due to the abrupt change of the state of the structure is mostly opposite to the velocity of the structure, i.e., the 4^{th} condition in the hybrid controller, Equation (6-22). Hence, $U_{fn}.\mathrm{sgn}(\dot{x}) > 0$ occurs infrequently during the peak dynamic response duration.

The peak control force of the hybrid control system (i.e., passive and semi-active friction forces) is shown in Figure 6-5. For long duration ground motions, such as Mexico City earthquakes, the semi-active friction damper doesn't apply any force. For all near-field ground motions, the semi-active friction controller responds quickly by applying a high level of control force to limit the peak dynamic response of the structure. The peak control force is required only a few times during the entire seismic episode. For a structure with passive viscous dampers only, the force applied by viscous dampers will increase in proportional to the velocity response of the structure. Hence, the passive

control force during the extreme event, such as Chi-Chi earthquake, may be much higher than the design capacity of the damper and the damper may undergo stroke saturation in such a situation. For the structure with the proposed hybrid control system, the peak passive control force required during all earthquakes is less than 1000 KN. Hence, the semi-active friction component of the proposed hybrid system reduces both the displacement response of the structure and the control force demand for passive viscous dampers.

Since the performance of the proposed hybrid control system depends on the device threshold limit U_2 of the damper, numerical simulations are conducted by varying the value of U_2 from 2000 KN to 4000 KN. For U_2= 4000 kN, the maximum of the peak displacements of the structure subject to 53 ground motions is within 30 cm. However, reducing U_2 to 3000 KN, the maximum of the peak displacements for 53 ground motions is still within the limitation of 30 cm, and the peak displacement for all the ground motions doesn't change significantly except Kobe TAK00, Kobe TAK90, and Northridge Rinaldi ground motions. For U_2= 2000 KN, the peak displacement for only one ground motion (Kobe TAK00) exceeds 30 cm. This maximum of the peak displacements during the Kobe TAK00 earthquake is approximately 34.5 cm. Hence, the upper threshold U_2 can be designed appropriately to satisfy device limitations and the response control objectives.

The peak accelerations of (i) the structure with a hybrid control system, (ii) the structure with passive dampers, and (iii) the uncontrolled structure are plotted in Figure 6-7. It is observed that, although the peak accelerations of the structure with the proposed

hybrid control system is higher than that of the structure with passive dampers, it is much smaller than the uncontrolled building.

Table 6-2 Response quantities and control force of the uncontrolled and controlled structure

Ground Motions	Uncontrolled		SAFD			Hybrid passive/semi-active system				
	x (cm)	$\ddot{x}$ (g)	x (cm)	$\ddot{x}$ (g)	Total Force (KN)	x (cm)	$\ddot{x}$ (g)	Total Force (KN)	Linear Force (KN)	Non-linear Force (KN)
El Centro	25.02	0.08	7.06	0.13	1152	9.30	0.18	1777	436	1341
Mexico	14.07	0.05	3.50	0.03	309	4.27	0.02	174	174	0
Gebze	56.89	0.19	8.83	0.15	1368	18.79	0.22	1976	440	1558
Kobe JMA00	31.86	0.11	10.16	0.61	6000	16.45	0.49	4846	846	4000
Kobe JMA90	48.63	0.16	9.89	0.51	5252	14.29	0.48	4740	740	4000
Lands LCN000	42.45	0.14	7.19	0.10	814	14.46	0.06	425	425	0
Lands LCN275	116.82	0.39	13.26	0.41	3947	18.37	0.43	4186	697	3489
Cape CMP00	67.61	0.22	13.14	0.52	4805	19.77	0.49	4439	779	4000
Cape CMP90	27.54	0.09	9.05	0.39	3564	14.50	0.30	2954	684	2270
Loma LGP00	135.79	0.45	14.78	0.45	4469	17.39	0.44	4449	677	3776
Loma LGP90	33.96	0.11	8.57	0.18	1562	11.29	0.25	2342	504	1988
Sup. Hill 135	8.50	0.03	5.13	0.22	2146	5.93	0.18	1865	498	1367
TCU084EW	89.09	0.29	15.27	0.62	6000	19.22	0.50	4868	868	4000
CHY080NS	41.95	0.14	13.53	0.61	6000	14.88	0.49	4874	874	4000
CHY080EW	29.25	0.10	13.71	0.61	6000	14.56	0.50	4882	882	4000
Tabas LN	70.40	0.23	14.39	0.36	3433	20.06	0.37	3568	601	3169
Tabas TR	104.12	0.34	15.27	0.37	3526	20.46	0.43	3773	675	3457
Kobe TAK00	88.34	0.29	15.18	0.63	6000	20.11	0.51	4850	850	4000
Kobe TAK90	81.56	0.27	14.75	0.54	5153	17.81	0.49	4692	797	4000
Cape Pet 00	27.06	0.09	7.75	0.22	2056	12.66	0.23	2219	520	1757
Cape Pet90	52.05	0.17	11.49	0.54	5419	11.99	0.48	4719	719	4000
Duzce 270	75.52	0.25	14.05	0.24	2379	21.27	0.36	3671	578	3511
Erzincan NS	59.84	0.20	13.99	0.38	3539	17.82	0.37	3636	686	3015
Newhall 360	58.29	0.19	11.24	0.52	5278	12.74	0.49	4689	712	4000
Rinaldi 228	56.42	0.19	16.43	0.64	6000	17.22	0.54	4993	993	4000
Sylmar 052	131.94	0.44	15.19	0.50	4881	20.02	0.48	4561	777	4000
Sylmar 142	41.49	0.14	14.04	0.61	6000	14.53	0.48	4905	905	4000
TCU065NS	101.44	0.33	12.54	0.40	3811	18.56	0.38	3565	652	3053
TCU065EW	131.87	0.44	16.99	0.41	3730	19.32	0.43	3816	729	3519
TCU068NS	72.49	0.24	17.22	0.36	3562	27.91	0.49	4132	770	3994
TCU068EW	141.83	0.47	17.93	0.32	3025	23.08	0.49	3897	628	3741
Chile LL010	32.63	0.11	6.39	0.15	1533	12.44	0.06	1738	451	1309
Chile LL100	11.07	0.04	4.13	0.07	649	4.50	0.03	280	280	0

Table 6-2 Response quantities and control force of the uncontrolled and controlled structure (Continued)

Chil Vina200	14.83	0.05	5.36	0.13	1235	6.30	0.05	385	385	0
Chil Vina290	12.87	0.04	4.04	0.08	763	4.58	0.03	297	297	0
Mex. Cal00	21.48	0.07	6.03	0.06	440	7.99	0.04	227	227	0
Mex. Cal90	14.37	0.05	3 63	0.04	303	4.56	0.02	173	173	0
Imperial NS	25.12	0.08	7.04	0.13	1158	9.35	0.18	1780	438	1341
Imperial EW	38.94	0.13	9.02	0.10	896	15.64	0.18	2555	416	2313
Hach. EW	28.12	0.09	8.04	0.14	1371	12.76	0.17	443	443	0
Hach. NS	30.05	0.10	6.42	0.11	1071	10.87	0.05	424	424	0
Mex. Occt1	2.64	0.01	1.22	0.01	73	1.51	0.01	49	49	0
Mex. Occt2	2.31	0.01	1.10	0.01	71	1.33	0.01	45	45	0
Miya. E41S	7.43	0.02	3.31	0.04	322	4.43	0.03	164	164	0
Miya. E41E	4.82	0.02	2.05	0.03	244	2.63	0.02	131	131	0
Olympia 182	4.37	0.01	1.54	0.02	166	1.57	0.01	97	97	0
Olympia 282	3.12	0.01	1.41	0.02	158	1.60	0.01	91	91	0
Mex. TacyE	12.65	0.04	3.20	0.02	165	4.79	0.02	111	111	0
Mex. TacyN	10.76	0.04	3.77	0.03	168	5.69	0.02	103	103	0
Taft N21E	11.54	0.04	3.44	0.03	313	4.83	0.02	176	176	0
Taft S69E	15.43	0.05	4.70	0.05	379	5.80	0.03	209	209	0
Chile Vlp070	14.72	0.05	3.46	0.05	436	4.50	0.03	221	221	0
Chile Vlp160	4.76	0.02	1.26	0.02	129	1.42	0.01	78	78	0

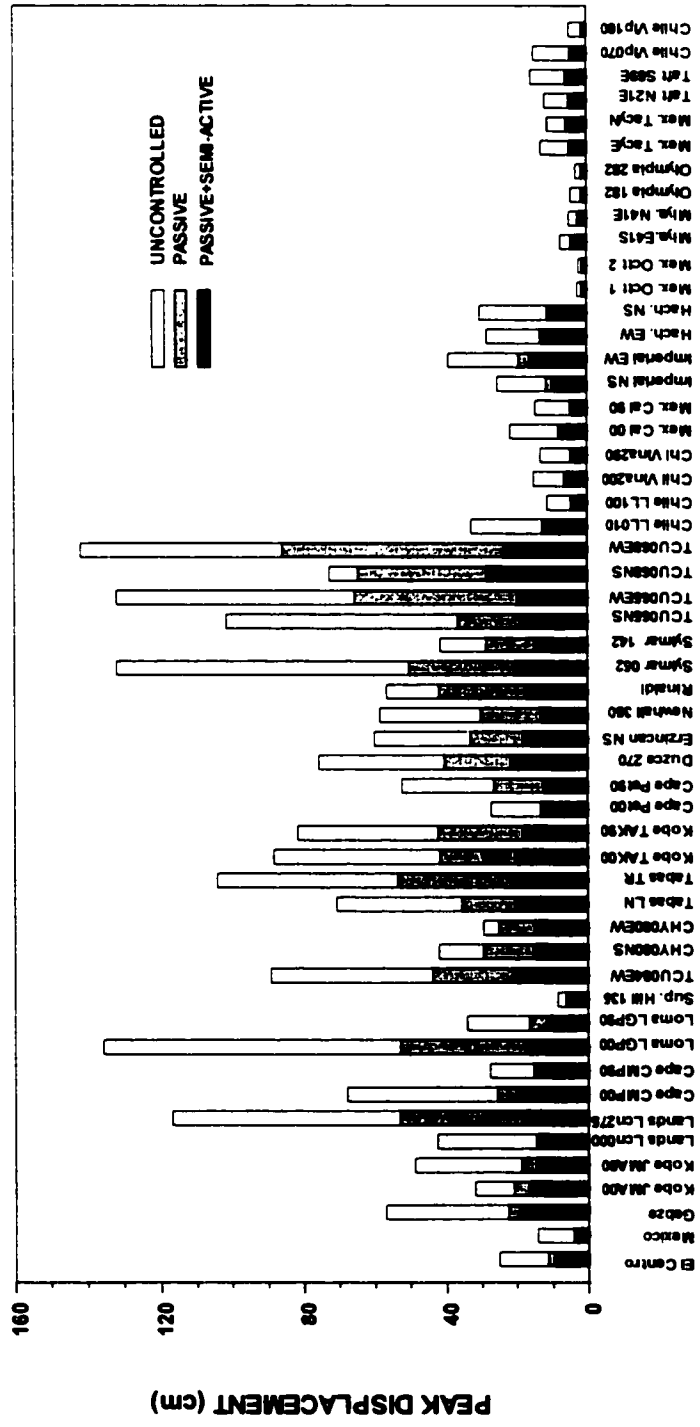

Figure 6-3: Peak Displacement of SDOF structure with passive/semi-active hybrid control system subject to 53 ground motions.

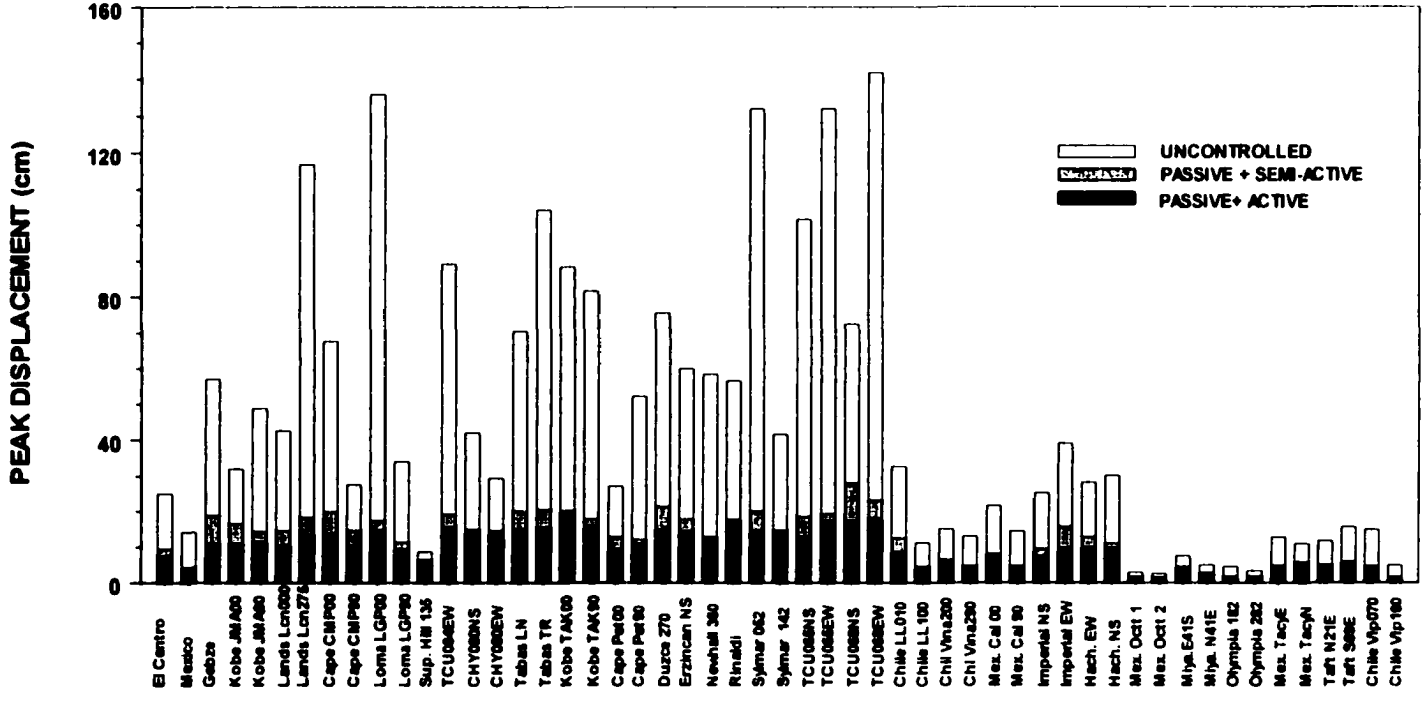

Figure 6-4: Comparison of passive/active and passive/semi-active hybrid control system in a SDOF structure subject to 53 ground motions.

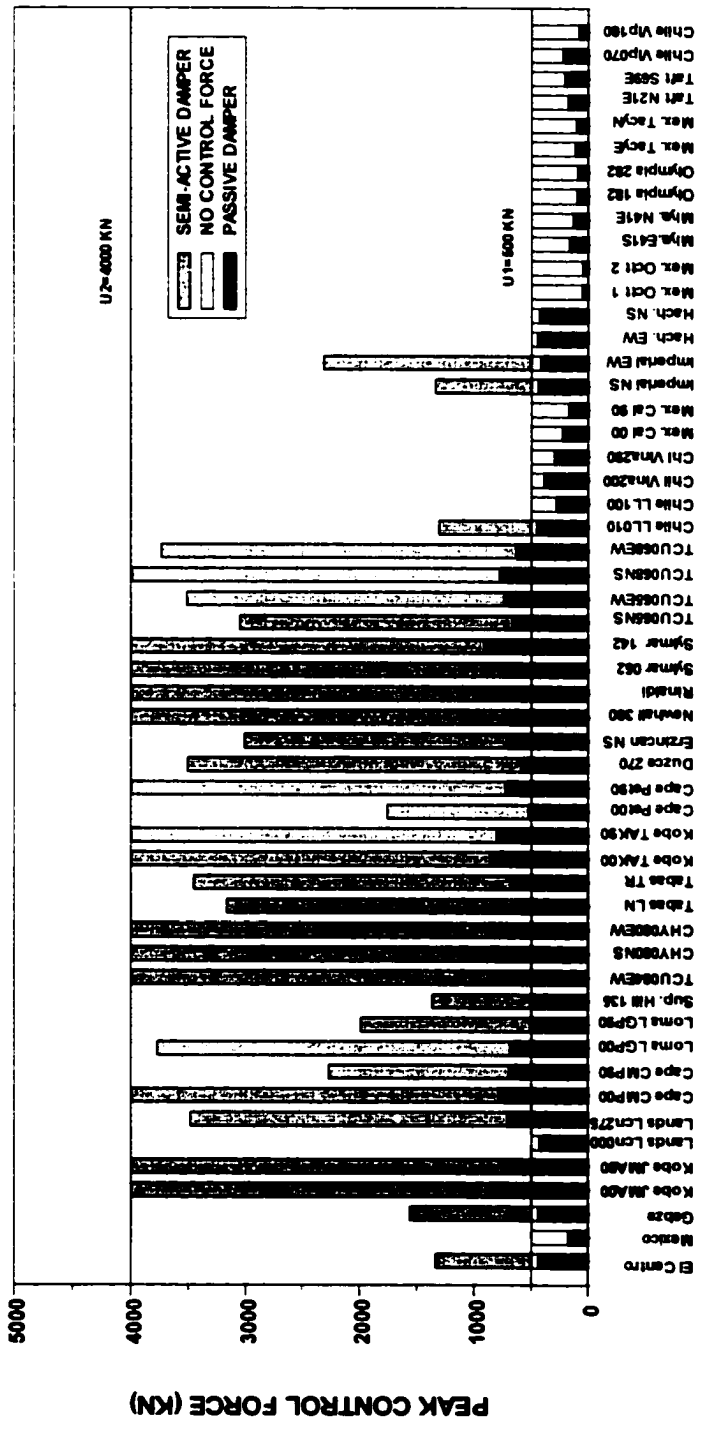

Figure 6- 5: Peak control force of hybrid control system.

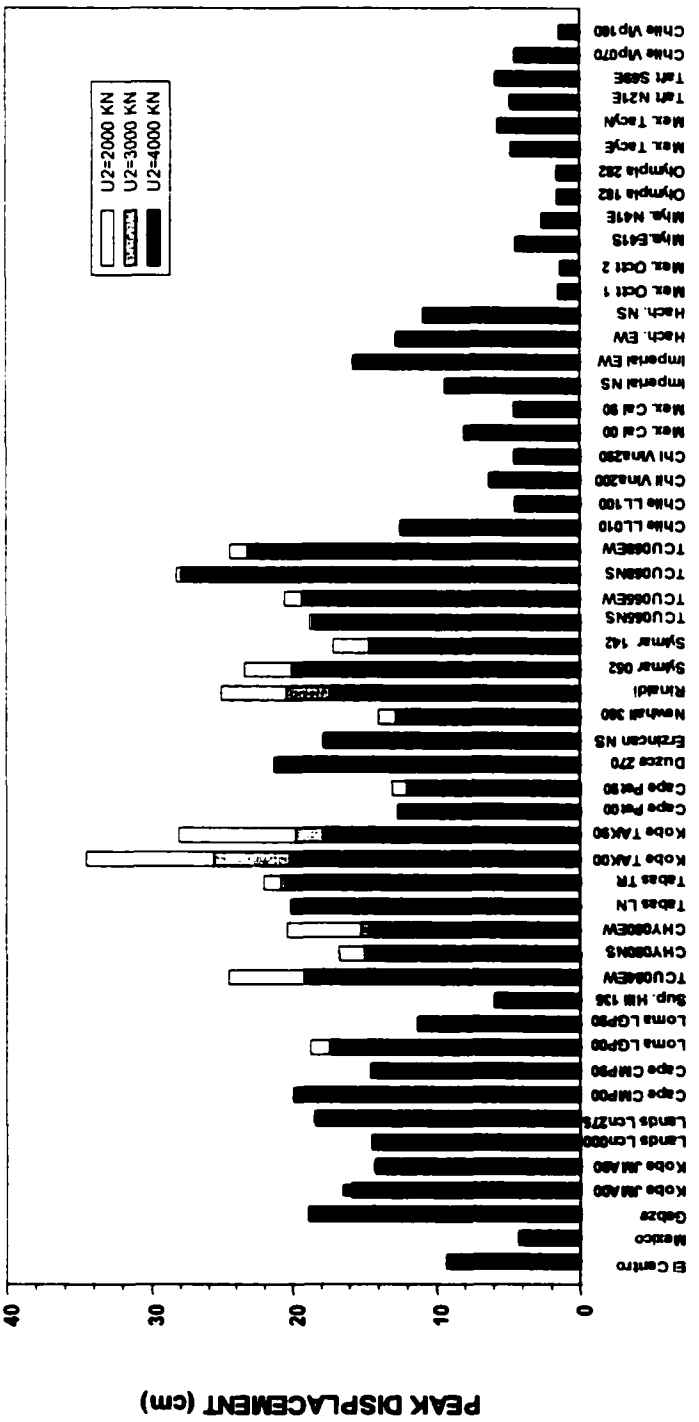

Figure 6-6: The effect of device capacity threshold, U_2, of the semi-active friction damper.

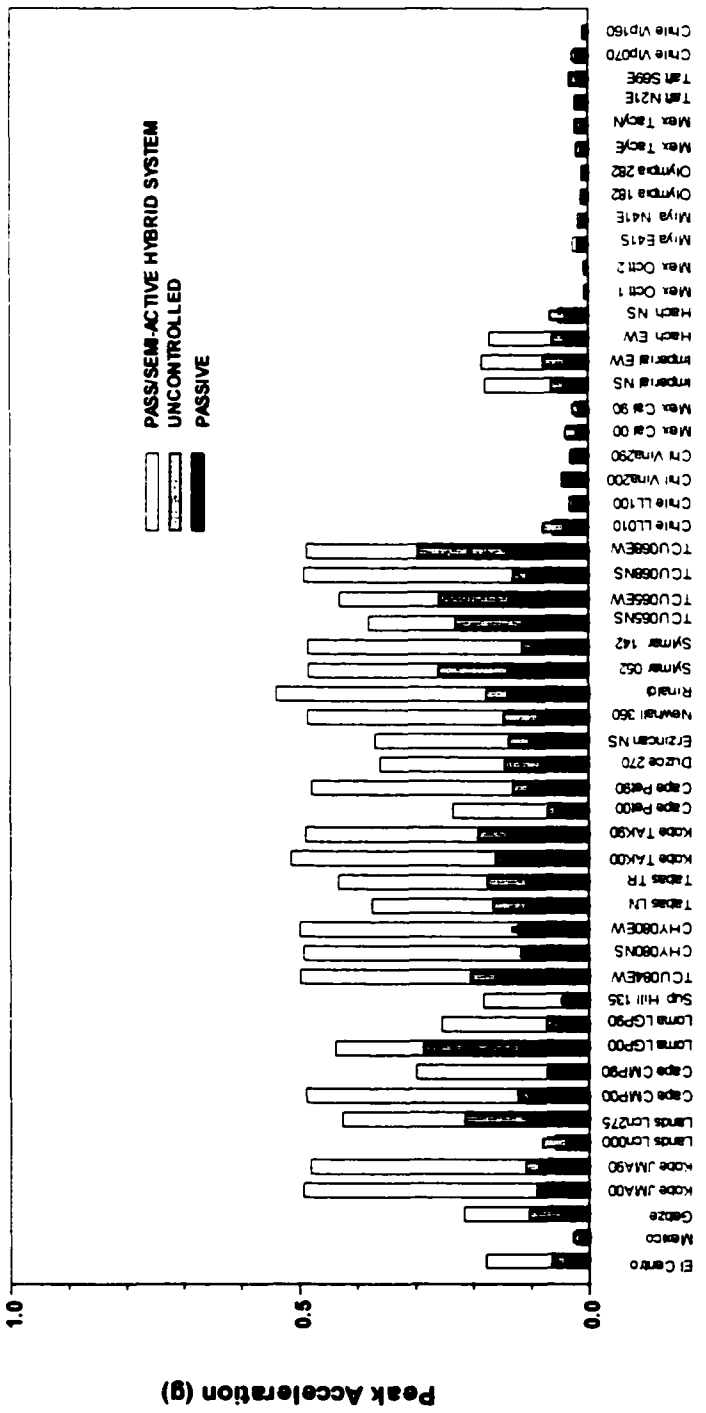

Figure 6-7: Peak acceleration of the structure with passive and hybrid control systems.

6.5.2 Analytical Velocity Pulses

The performance of the hybrid control system subject to the proposed velocity pulses is investigated in the following. The velocity pulses are used to represent the long period pulses in near-field ground motions, since response quantities of long period structures are mainly affected by the long period components in the near-field ground motion. It is shown in Chapter 3 that these long period velocity pulses can be reasonably modeled by the analytical model utilizing the pulse period T_p, and the shape factor n and ζ_p. For a given structural site, the predominant period T_p is a relative stable quantity, which can be obtained by some attenuation model. For example, Somerville (1998) developed a preliminary model that relates the time domain parameters of the near-field ground motion pulses to the earthquake magnitude and distance. In the following, a group of velocity pulses are generated by using the shape factors n=1, ζ_p=0.5, and varying the pulse period T_p from 0.4 s to 8 s with an increment of 0.2 s. Further, the peak ground acceleration PGA=0.3g is used, and the corresponding peak ground velocity PGV is varied from 0.131 m/s to 3.28 m/s. This range of PGV is realistic since the largest PGV of recorded ground motions is 2.63m/s for the TCU068NS component of the 1999 Chi-Chi earthquake. The predominant period of this ground motions is approximately T_g=8 s.

Figure 6-8(a) presents the peak displacement response of (i) the. Since the excitation is impulsive in nature, the semi-active controller is triggered by all decaying pulses with different pulse periods. The maximum peak displacements are 212.0 cm, 112.6 cm and 35 cm, respectively, for the uncontrolled structure, the structure with passive dampers, and the structure with the proposed hybrid control system.

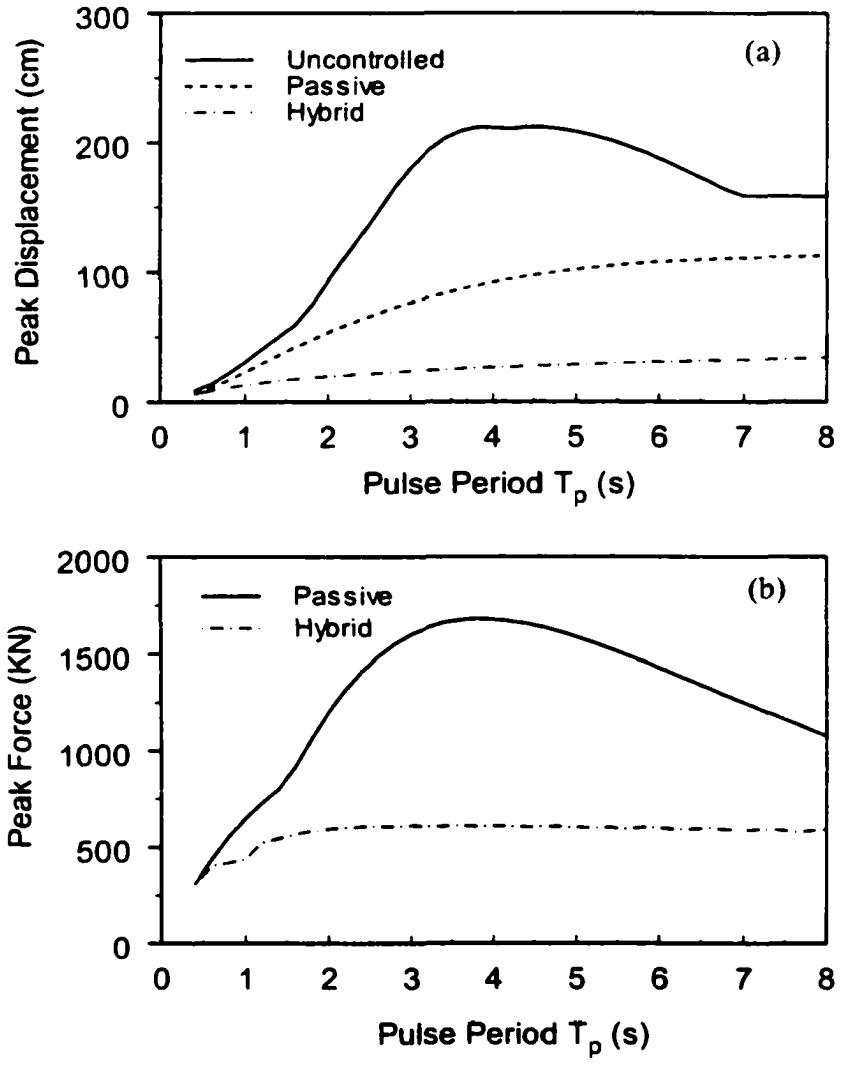

Figure 6-8: SDOF structure subject to decaying velocity pulses: (a) Peak displacement of uncontrolled, passive damped and hybrid controlled structure; (b) Peak force of passive damper of passive only and the hybrid control system.

Figure 6-8(b) presents the peak force of the passive damper for the structure with passive damper alone and for the structure with the proposed hybrid control system. It is observed from Figure 6-8 that the peak force required for the pure passive damper case is 1700 KN, whereas the passive force is limited to 600 KN for the proposed hybrid control system. This clearly demonstrated that the proposed hybrid control system not only reduces the peak response, but also protects passive dampers during the strong earthquake.

As a result, the proposed hybrid control system is effective in reducing the displacement of structure to a certain value for a broad spectrum of ground motions. The performance of the proposed hybrid control system is similar to that of the pure active polynomial control system. The peak control force of the semi-active friction damper is impulsive in nature and it is only required during a few instances in the entire seismic episode. The peak control force can be designed to satisfy the device limitations and the response reduction objectives.

6.6 Benchmark Cable-Stayed Bridge

The proposed hybrid control system consisting of passive viscous dampers and semi-active friction dampers is applied to the benchmark cable-stayed bridge developed by Dyke et al. (2000). A brief description of the benchmark bridge model is already presented in Chapter 4.

6.6.1 Controller

The controller is designed based on the following reduced order model of the benchmark cable-stayed bridge presented in Dyke et al. (2000):

$$\dot{x}_r = A_r x_r + B_r u + E_r \ddot{x}_g \tag{6-23}$$

$$y = C_y x_r + D_y u + F_y \ddot{x}_g + v \tag{6-24}$$

$$z = C_z x_r + D_z u + F_z \ddot{x}_g \tag{6-25}$$

where x_r is the reduced-order state vector with a dimension of 30; $\ddot{x}_g$ is the ground acceleration; u is 8x1 control input; y and z are the measured output vector and the controlled output vector, respectively; v is a measurement noise vector; and A_r, B_r, E_r, C_y, D_y, F_y, C_z, D_z, F_z are appropriate matrices.

The optimal polynomial controller for the linear system can be obtained by minimizing a polynomial performance index:

$$J = \int_0^\infty \left[x_r^T Q x_r + u^T R u + \sum_{i=2}^{K} (x_r^T M_i x_r)^{i-1} (x_r^T Q_i x_r) + \bar{h}(x_r) \right] dt \tag{6-26}$$

in which

$$\bar{h}(x_r) = \left[\sum_{i=2}^{K} (x_r^T M_i x_r)^{i-1} x_r^T M_i \right] B R^{-1} B^T \left[\sum_{i=2}^{K} (x_r^T M_i x_r)^{i-1} M_i x_r \right] \tag{6-27}$$

where Q and Q_i, i=2, 3,...,k, are positive semi-definite state weighting matrices, R is a (8x8) positive definite weighting matrix, and M_i, i=2,3,...k are positive-definite matrices. The first two terms in Equation (6-26) are the classical quadratic terms, whereas the third term in the summation is polynomial in x_r of different orders higher than the quadratic term. The last term is added such that a simple analytical solution can be obtained. Due to the nonlinear nature of the controller, it is difficult to construct appropriate weighting matrices Q and Q_i for z. Hence Q and Q_i are chosen by neglecting the contributions of u and $\ddot{x}_g$ in z as follows:

$$Q = C_z^T Q_d C_z \; ; \; Q_i = C_z^T Q_{di} C_z \; ; \; i=2,3...,k \tag{6-28}$$

where Q_d and Q_{di} are (9x9) diagonal weighting matrices. Elements of the matrices Q_d and Q_{di} should be chosen by considering the relative importance of the elements in z_r.

An optimal polynomial control law is obtained analytically by minimizing the performance index as [Agrawal and Yang (1995, 1996)]:

$$u(t) = -R^{-1}B^T P x_r(t) - R^{-1}B^T \sum_{i=2}^{K} (x_r^T M_i x_r)^{i-1} M_i x_r \tag{6-29}$$

where P and M_i are the solutions of algebraic Riccati matrix and Lyapunov equations in Equations (6-20) and (6-21).

6.6.2 Kalman-Bucy estimator for x_r

The implementation of the optimal polynomial controller in Equation (6-29) requires the knowledge of the reduced order vectors x_r. The Kalman-Bucy filter will be used in approximation to estimate the reduced-order states from the measured output vector y as follows:

$$\dot{\hat{x}}_r = A_r \hat{x}_r + Bu + L_0(y_r - C_y \hat{x}_r - D_y u) \tag{6-30}$$

where $\hat{x}_r$ is the estimated state and L_0 is the observer gain matrix. For on-line integration, the observer in equation (6-30) can be written as:

$$\dot{\hat{x}}_r = (A_r - L_0 Cy)\hat{x}_r + (B - D_y)u + L_0 y \tag{6-31}$$

Since the polynomial controller is non-linear, the on-line implementation of the observer in Equation (6-31) requires not only the measurement vector y but also the control force u. It should be mentioned that the Kalman-Bucy filter is applicable only to the LQG controller in which the separation principle holds. For the polynomial controller considered herein, the Kalman-Bucy filter is used for approximation only.

In order to design the hybrid control system for the benchmark cable-stayed bridge, eight equal capacity control devices are used between the deck and tower and bent 1 and bent 4, respectively. The required control force is calculated from the polynomial controller in Equation (6-29). The hybrid control system consists of passive linear viscous dampers and semi-active friction dampers. Since the linear viscous damper is very effective in reducing the peak responses of structures subject to long duration ground motions, i.e., Mexico City ground motion, passive viscous dampers can be designed to achieve the control objectives for such earthquakes. However, for near-field ground motions or some very strong ground motions, which induce an abrupt development of the peak response, nonlinear control forces, which are capable of mitigating the peak response.

The control force of the polynomial controller, Equation (6-29), is implemented by the hybrid control system consisting of passive viscous dampers and the semi-active controller, Equation (6-22). Limits U_1 and U_2 for the semi-active controller are determined by numerical simulations as 1000 KN and 5000 KN, respectively. The simulink block for the passive/semi-active hybrid control system is shown in Figure 6-9.

6.6.3 Numerical Simulation

A total of 8 equal capacity passive linear fluid dampers are placed between the deck and bent 1, pier 2, 3 and 4, of the bridge. The coefficient of the linear viscous damper is c=3500 KN.$(m/s)^{-1}$. The corresponding damping ratio of the first mode of the bridge is approximately 30%, i.e., 27% supplemental [3500x8/(2x5.1x10^6x1.1)] damping plus 3% inherent damping. To construct the proposed hybrid control system, 8 semi-active friction dampers are placed in parallel with the passive fluid dampers. It is

assumed that the passive dampers alone could not reduce the responses of the bridge to a satisfactory range during strong earthquakes, and the semi-active friction dampers are triggered to achieve the desired control objectives. The control forces generated by the semi-active dampers vary between the limits U_1=1000KN and U_2=5000 KN.

The set of 53 ground motions used in the previous example are used herein to investigate the performance of the proposed hybrid control system. To illustrate the performance of the proposed hybrid control system, the results of the uncontrolled bridge subject to 53 ground motions are also investigated. The uncontrolled bridge employs sixteen 6.67MN shock transmission devices as the connection between the tower and the deck. Shock transmission devices are installed in the longitudinal direction to allow for the expansion of the deck due to temperature changes. Under dynamical loads, these devices are extremely stiff and are assumed to behave as rigid links. Figures 6-10 and 6-11 show the bar plots of the shear force and the overturning bending moment at the base of the towers for the bridge with shock transmission devices (uncontrolled) and passive viscous dampers. These figures show that fully restraining the deck in the longitudinal direction results in unacceptably large shear forces and overturning bending moments at the base of towers. However, replacing the shock transmission devices with passive viscous dampers results in a significant reduction of the peak shear force and the overturning bending moment of towers for each ground motion.

It is observed from Figure 6-11 that the peak overturning moment at the tower base is reduced only slightly by the use of passive viscous dampers for the TCU068NS earthquake. Figure 6-12 shows the bar chart of the peak deck displacement for 53 ground motions. It is observed that the peak deck displacement of the bridge with passive viscous

dampers is excessive for the earthquakes such as TCU068NS and TCU068EW. In fact, the peak deck displacement is almost 1.4 m for the bridge with passive viscous dampers for the TCU068NS earthquake.

To reduce the response of the bridge further, semi-active friction dampers are installed in parallel with passive viscous dampers to form the proposed hybrid control system. A cubic order polynomial controller, Equation (6-29), is designed for the semi-active friction dampers by considering: $R=\mathbf{I}_{8x8}$, $Q=5000\mathbf{I}_{4x4}$, and $Q_2=C_z^T Q C_z/15$. The semi-active friction dampers are triggered whenever the force of the nonlinear part of the polynomial controller exceeds 1000 KN and the peak force is saturated at 5000 KN. The measurement noise from sensors is assumed to be the same as that used in Dyke et al. (2000).

It is observed from Figure 6-12 that the semi-active friction damper is activated only for 38 strong ground motions. For the remaining 15 long duration and small ground motions, only the passive viscous dampers are utilized to reduce the responses of the bridge. It indicates that the proposed hybrid control system is capable of reducing the response of the structures according to the magnitude of excitations.

Figure 6-12 presents the peak deck displacement of the cable-stayed bridge with passive viscous dampers and with the proposed hybrid control system. When the cable-stayed bridge is equipped with passive viscous damper above, the peak deck displacement exceeds 1 m for both TCU068NS and TCU068EW earthquakes. However, with the proposed hybrid control system, i.e., semi-active friction dampers are installed in parallel with the passive viscous dampers at each location, the peak deck displacement is reduced effectively below 65 cm for all ground motions. It is also observed that the

hybrid control system is more attractive for ground motions with long predominant periods, such as TCU065NS, TCU065EW, TCU068NS, TCU068EW, LCU275 and TABAS-TR earthquakes. By using the hybrid control system, the overall maximum peak bending moment of towers at deck level reduces from $7.9x10^5$ KN.m (for TCU068NS earthquake) to $4.2x10^5$ KN.m (for TCU068EW earthquake) as shown in Figure 6-16.

Figure 6-13 shows the bar chart of the peak base shear of the bridge with passive viscous dampers and with the proposed hybrid control system. It is observed that the peak base shear of the bridge with the proposed hybrid control system is higher than that with passive viscous dampers for some earthquakes. This happens because the nonlinear semi-active friction controller induces high frequency dynamics, resulting in an increase of the absolute acceleration of the bridge.

Figure 6-14 shows the bar chart of the peak shear of towers at deck level for the bridge with passive viscous dampers and with the proposed hybrid control system. It is observed that the hybrid control system is capable of reducing the peak shear of the towers at the deck level significantly for several earthquakes, although this quantity increase slightly for few other earthquakes.

Figure 6-15 shows the peak overturning moment at the tower base of the bridge with passive dampers and with the hybrid control systems. It is observed that the proposed hybrid control system is capable of reducing the peak overturning moment at the tower base drastically for some earthquakes, such as TABAS-TR, TCU068NS.

Figure 6-16 shows the peak bending moment of the tower at deck level for the bridge with passive viscous dampers and with the proposed hybrid control system. It is observed that the hybrid control system is effective in reducing the peak bending moment

of the towers at deck level for most of the near-field earthquakes. However, the performance of the hybrid control system is remarkable for TCU068NS and TCU068EW earthquakes.

Figure 6-17 presents the bar chart of the peak cable deviation for the bridge with passive dampers and with the proposed hybrid control system. The peak cable deviation is defined as

$$J_{dev} = \max_{i,t} \left| \frac{T_{ai}(t) - T_{0i}}{T_{0i}} \right| \tag{6-32}$$

where T_{0i} is the nominal pretension in the ith cable and $T_{ai}(t)$ is the actual tension in the cable as a function of time. It is observed from Figure 6-17 that the peak cable deviation for the bridge with the proposed hybrid control system decreases whenever the semi-active friction damper is triggered. Figure 6-18 presents the maximum and minimum cable tensions in terms of the ultimate cable tension of the i th cable, T_{fi}. The acceptable range of the cable tension is specified as $0.2T_{fi}$ to $0.7T_{fi}$. It is observed from Figure 6-18 that the peak cable tension falls below the minimum cable tension of $0.2\ T_{fi}$ for 15 ground motions when passive dampers are used in the bridge. On the other hand, the maximum cable tension falls below $0.2\ T_{fi}$ for only 5 ground motions when the hybrid control system is used in the bridge.

Results described above demonstrate that the proposed hybrid control system is effective in reducing the responses quantities of the cable-stayed bridge for all external excitations. The semi-active friction dampers are activated only during strong ground motions, while only passive dampers are utilized during small or long-duration ground motions. Semi-active friction dampers of the hybrid control system are particularly effective in reducing the response quantities of the cable-stayed bridge subject to ground

motions with large predominant periods. The peak deck displacement and the peak bending moment of tower at deck level for the bridge with the proposed hybrid control system decrease significantly as compared to that of the bridge with the passive damping system alone. Finally, The overall performance of the cable-stayed bridge with the hybrid control system is improved significantly over that of the bridge with the passive damping system alone.

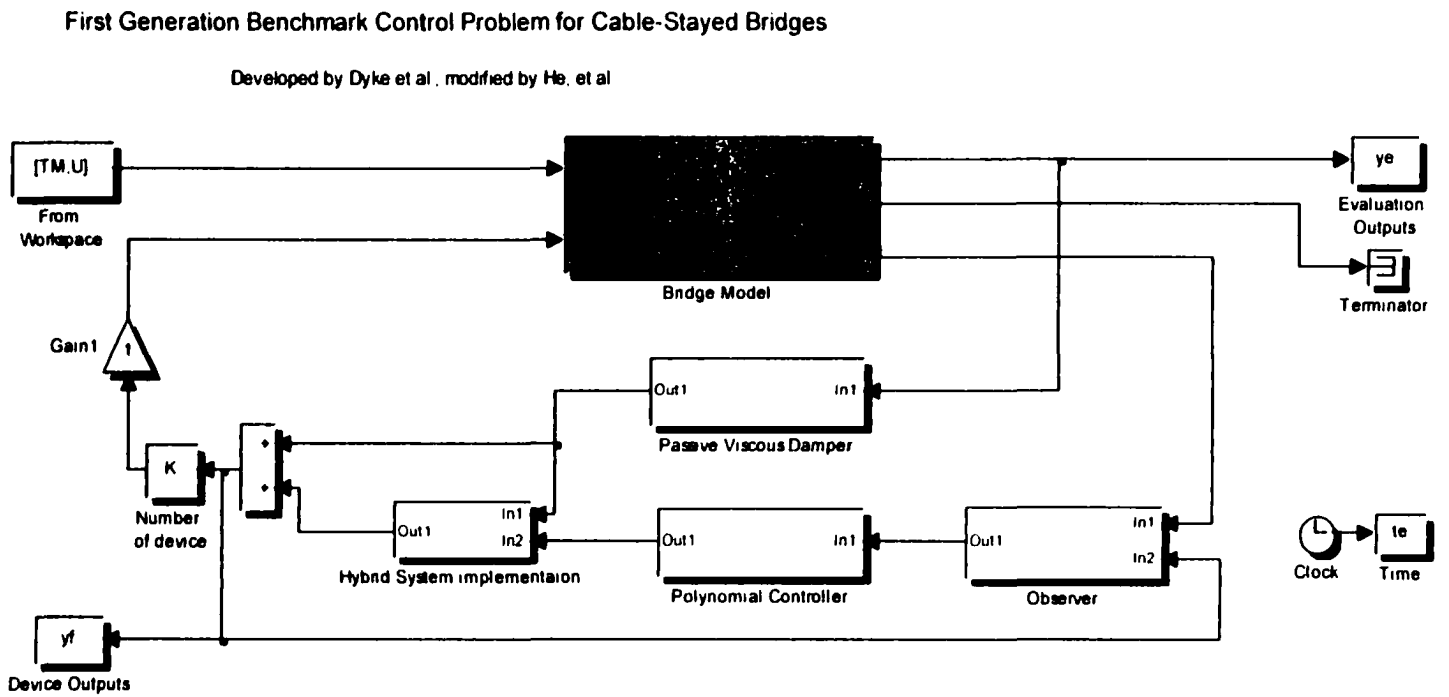

Figure 6-9: Simulink model of hybrid control system for benchmark cable-stayed bridge problem

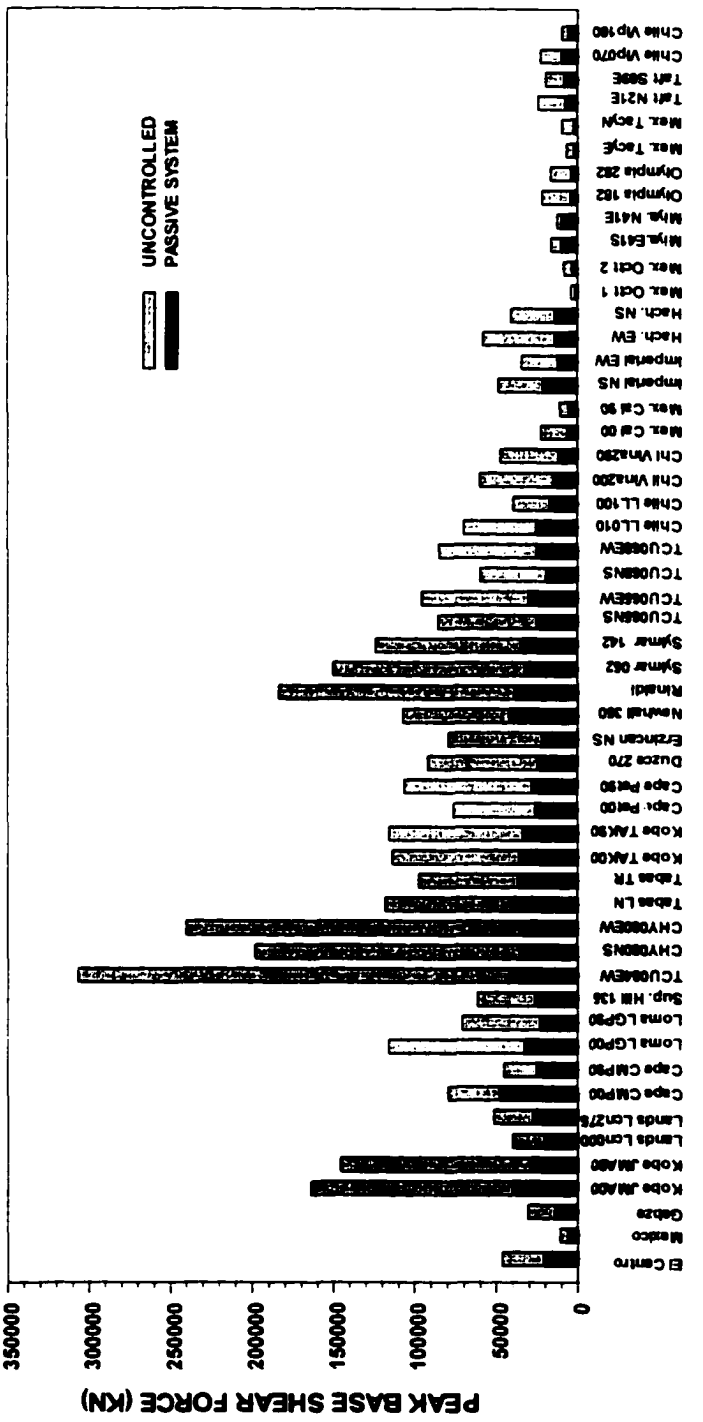

Figure 6-10: Peak base shear at the base of towers of the bridge with rigid links (uncontrolled) and with passive viscous dampers.

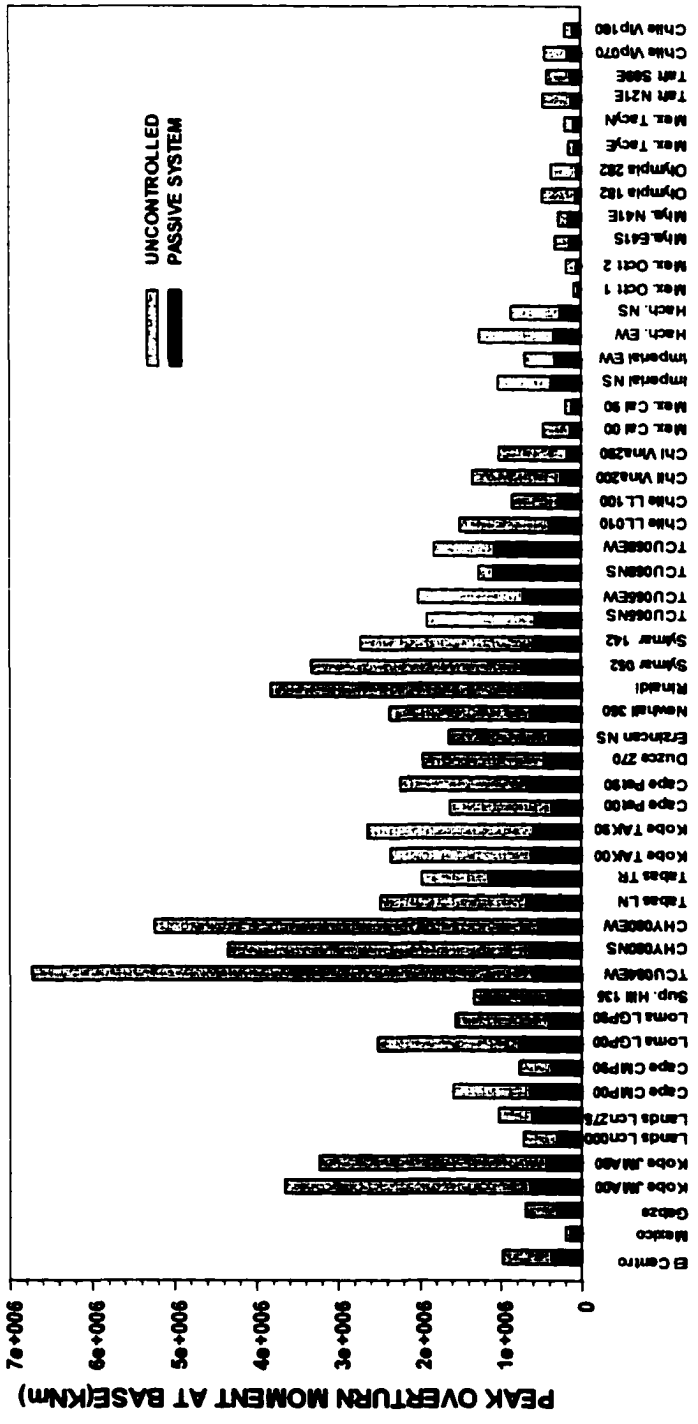

Figure 6-11: Peak overturning moment at the base of towers of the bridge with rigid links (uncontrolled) and with passive dampers.

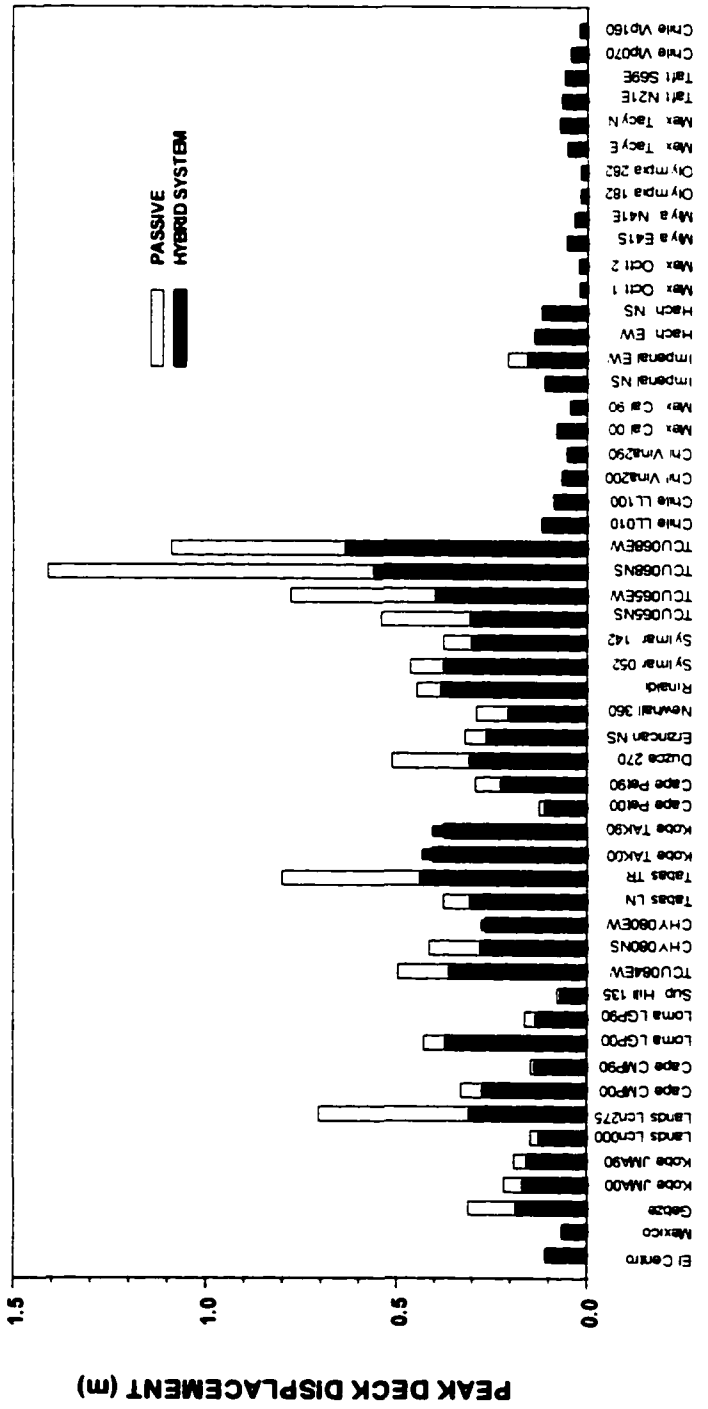

Figure 6-12: Peak deck displacement of the bridge with passive dampers and hybrid control system.

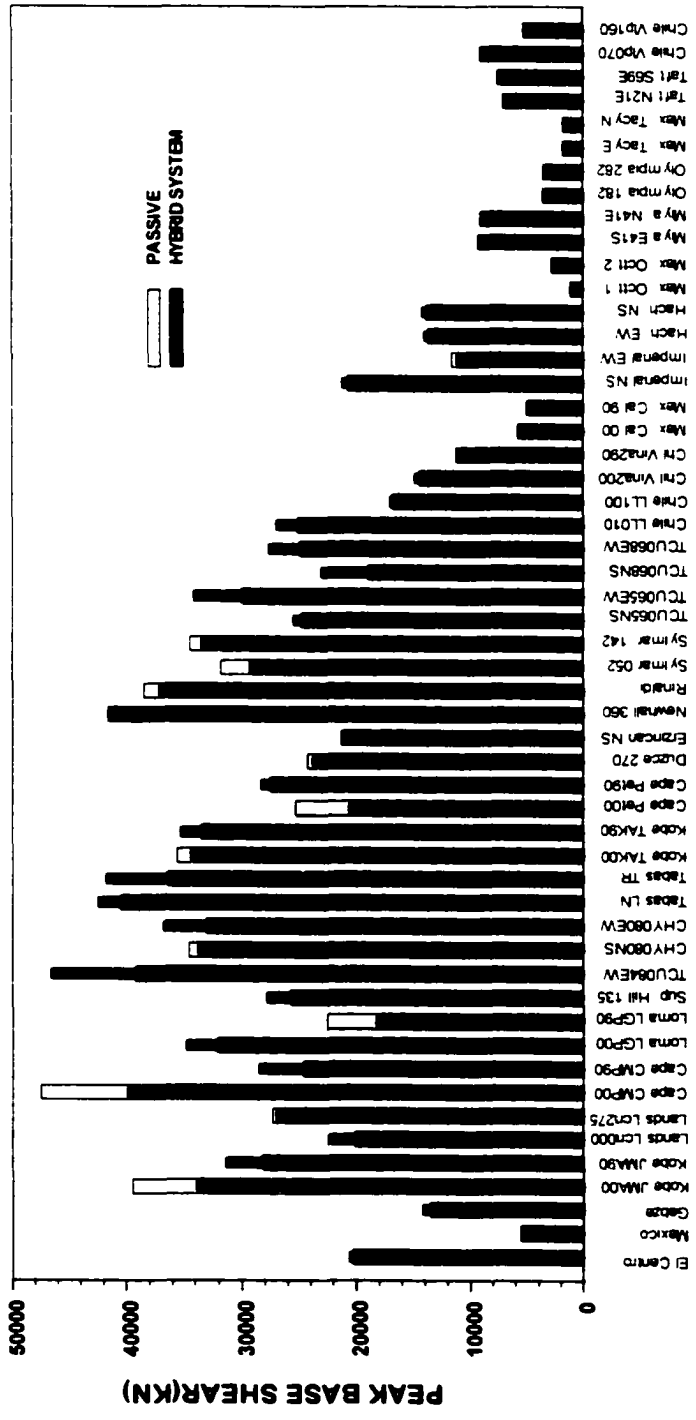

Figure 6-13: Peak base shear of the bridge with passive dampers and hybrid control system.

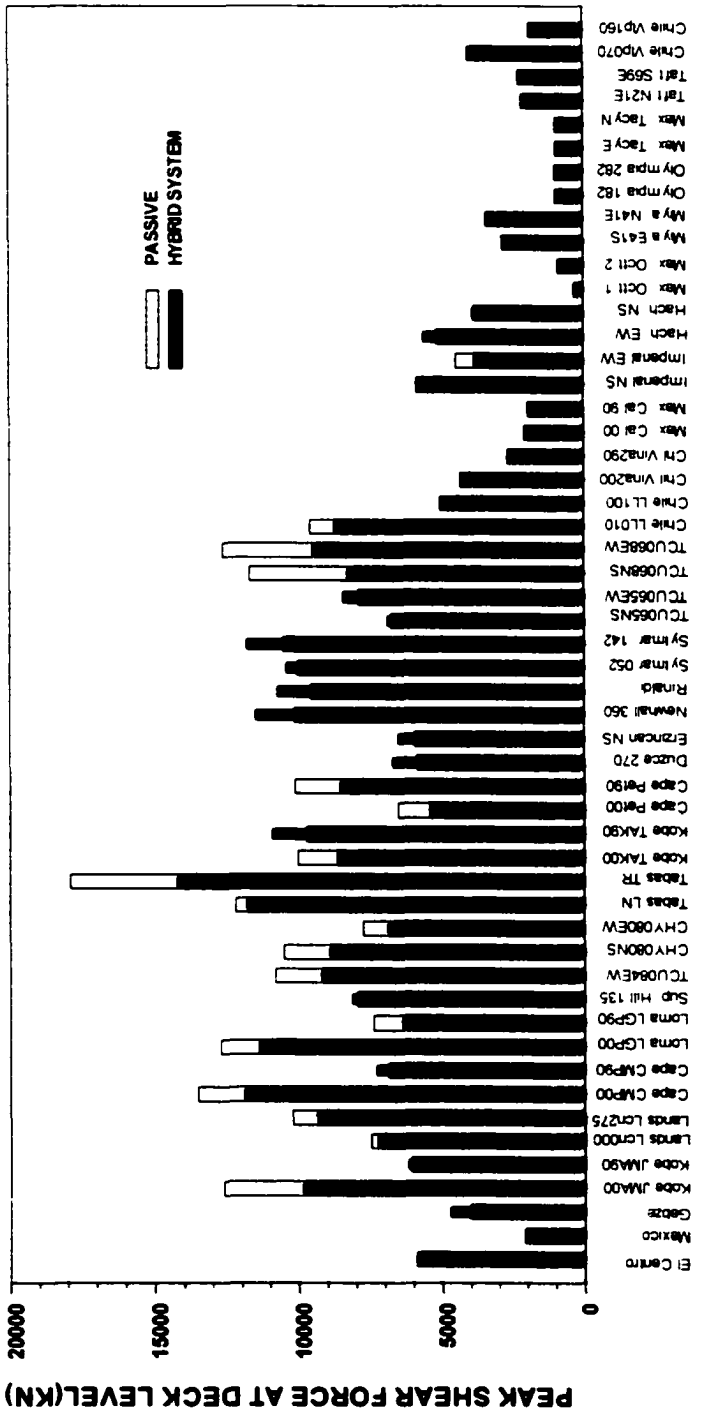

Figure 6-14: Peak shear force of the towers at deck level for the bridge with passive dampers and hybrid control system.

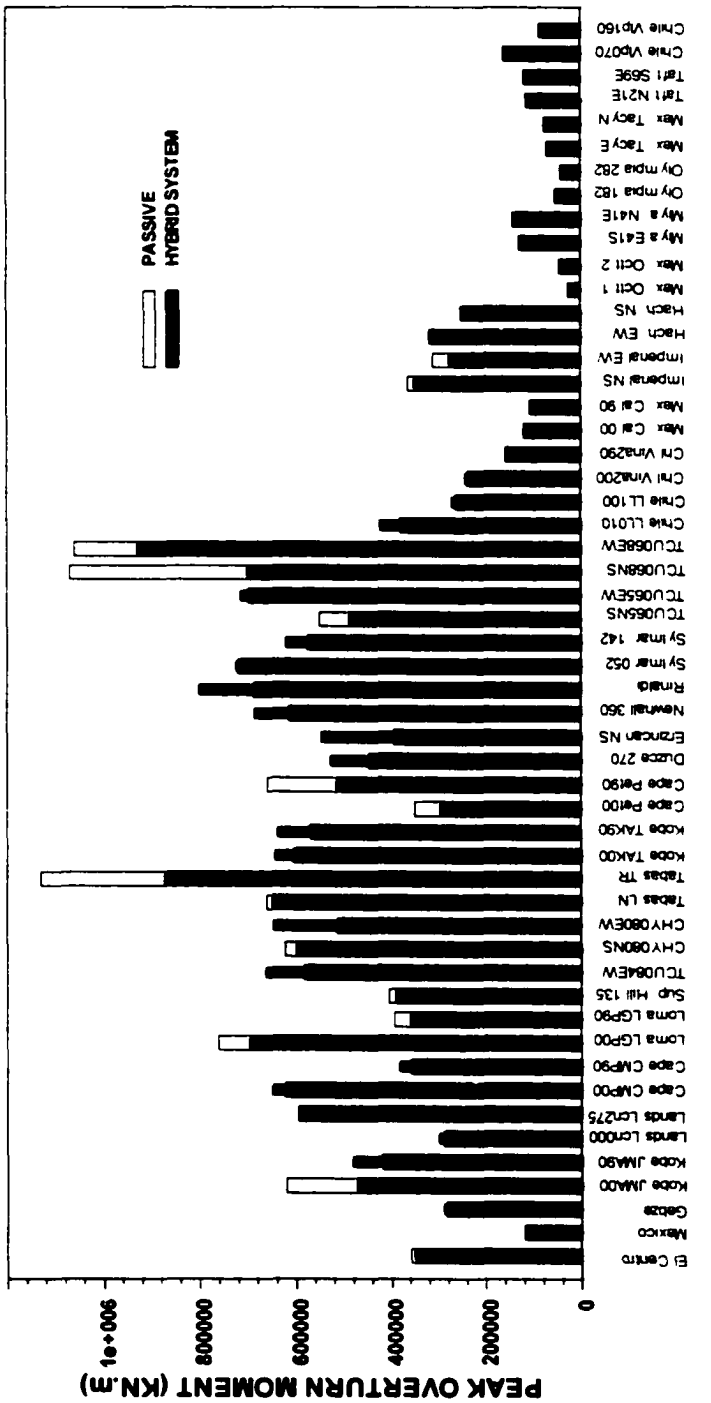

Figure 6-15: Peak overturning moment at the tower bases for the bridge with passive dampers and hybrid control system.

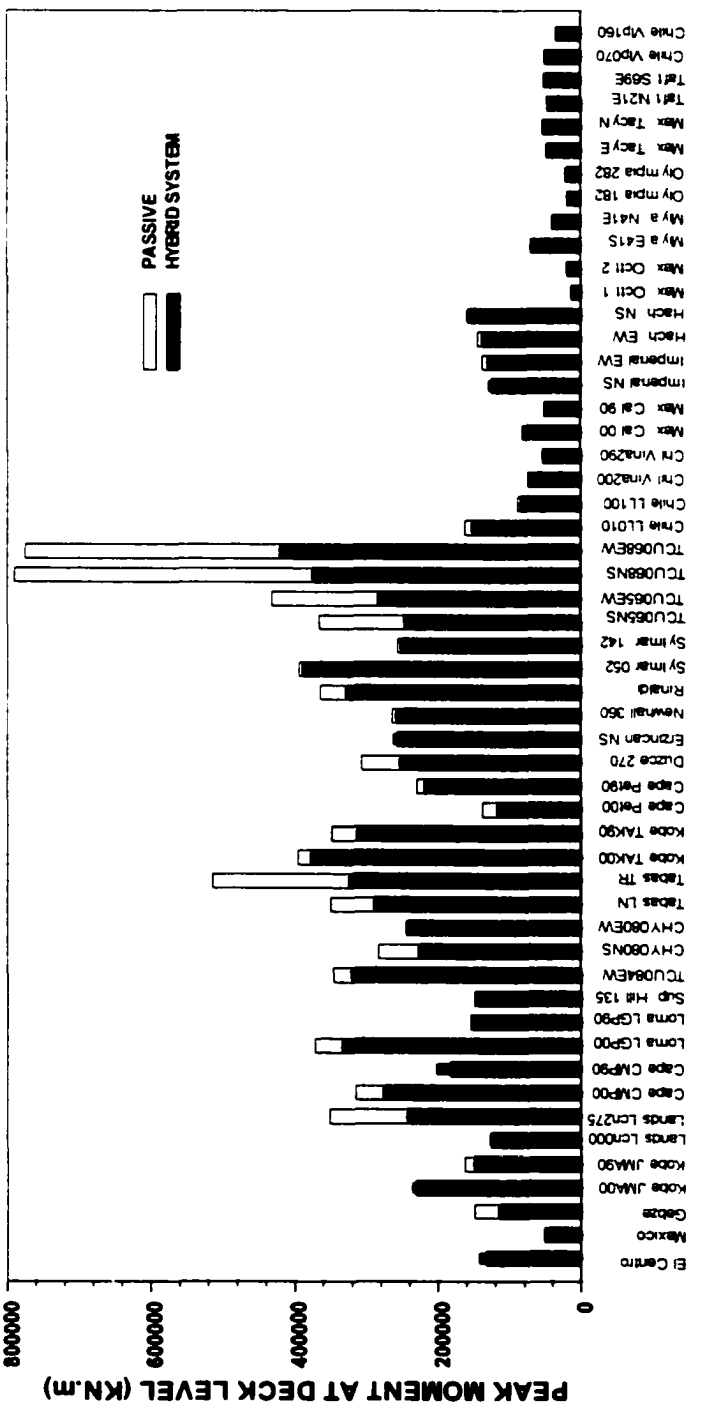

Figure 6-16: Peak bending moment of the towers at deck level for the bridge with passive dampers and hybrid control system.

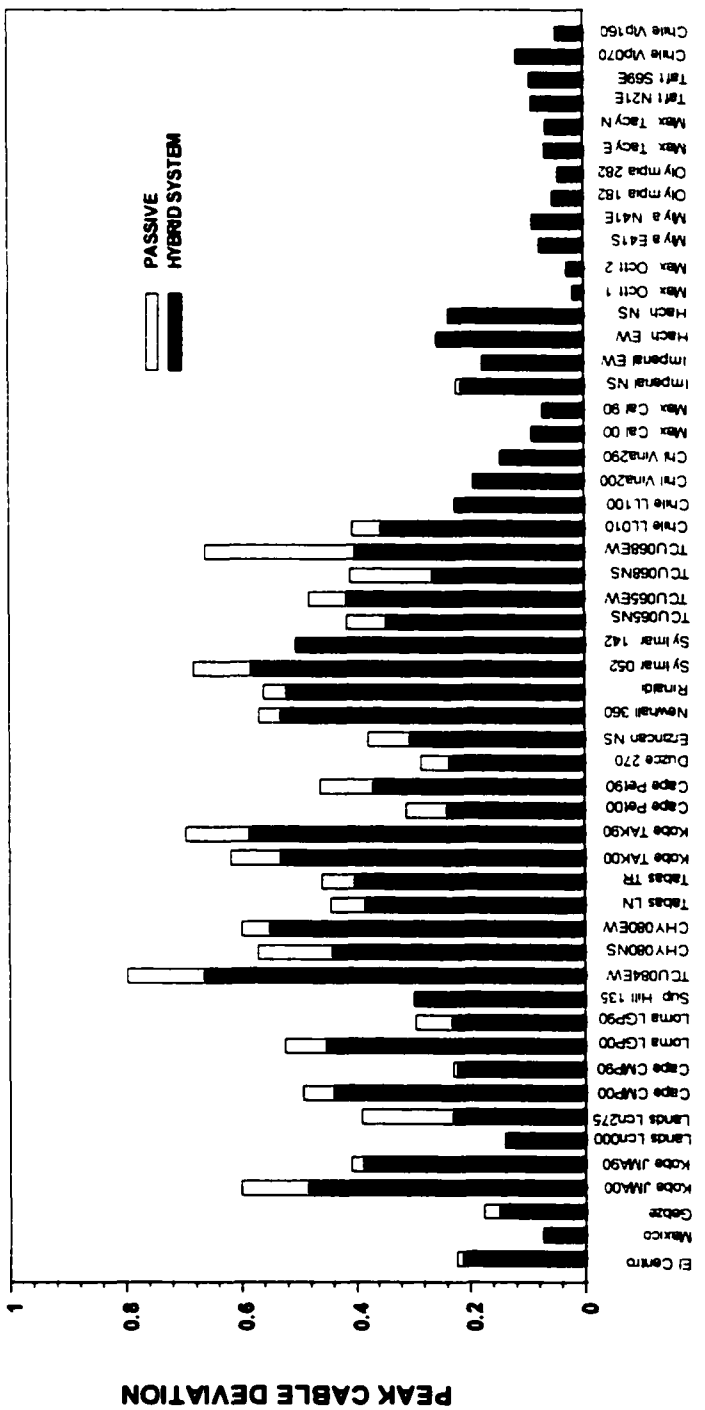

Figure 6-17: Peak cable deviation of the bridge with passive dampers and hybrid control system.

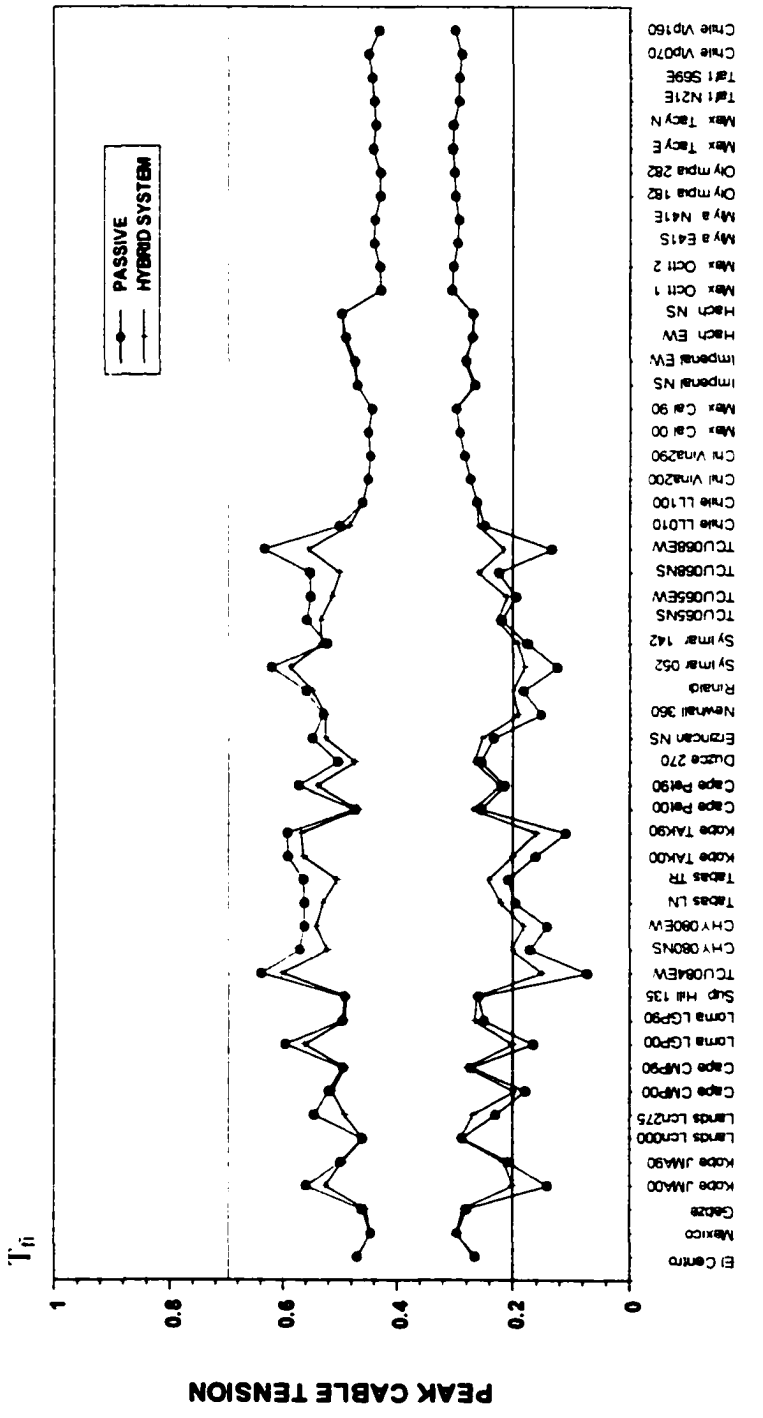

Figure 6-18: Peak cable tension of the bridge with passive dampers and the hybrid control system.

6.7 Summary

In this chapter, a hybrid control system is proposed and investigated for structures subject to near-field earthquakes. The proposed hybrid control system consists of linear viscous dampers installed in parallel with semi-active friction dampers. A nonlinear control method based on an optimal polynomial controller is proposed for the semi-active friction damper. The semi-active friction damper is triggered when the required control force exceeds a certain lower threshold value and the control force is saturated at an upper threshold value representing the device capacity. The applications of the proposed hybrid control system are demonstrated for a SDOF structure and the benchmark cable-stayed bridge. Numerical simulation results indicate that the hybrid control system is very effective in reducing the displacement of the structure to a certain value for a broad spectrum of ground motions. The performance of the proposed hybrid control system is similar to that of the pure active polynomial control system. The peak control force of the semi-active friction damper is impulsive in nature and is required during a few instances of the entire seismic episode. The semi-active friction damper can be designed to satisfy device limitations and the response reduction objectives.

CHAPTER 7

PERFORMANCE OF ACTIVE AND SEMI-ACTIVE CONTROLLERS USING GROUND MOTION FILTERS

7.1 Introduction

LQR, and H_2/LQG control algorithms are commonly used to design active control systems for civil infrastructures subject to seismic excitations, assuming that seismic excitations are either white noises or neglected. As a result, the optimality of these "optimal" control algorithms can't be guaranteed in the presence of seismic excitations. Hence, Panariello et al. (1997) proposed the "optimal" structural control via the training of an ensemble of earthquakes. It was suggested by Yang (1975) that the earthquake excitation could be modeled as a filtered white noise process, i.e., the output of a white noise process (a shot noise process) through a shape filter. Then the LQR controller can be designed based on the augmented system consisting of the structures and the filter [Yang (1975)]. This approach was also carried out for nonlinear hysteretica civil engineering structures [Yang et al (1994c)]. Following this method, Yoshioka et al. (2002) and Ramallo et al. (2002) used the Kanai-Tajimi filter, which assumes that the ground motion is the acceleration response of white noise passing through a second order dynamic system with a damping ratio ζ_p and a stiffness coefficient per unit mass ω_p^2. It is noted that the Kanai-Tajimi filter has higher energies in the low frequency range, which will affect the response of long period structures. It has been shown in Chapter 3 that fault normal component of the ground motion in forward direction of faults contain

narrow-band pulses. Periods of these pulses increase with the surface magnitude of seismic events (Somerville 1998). In this chapter, the optimal controllers for active and semi-active control systems will be designed by including a filter model of the seismic excitation in the controller design. The design of the controller is based on an augmented system consisting of the structural system and an excitation shaping filter. The shape filter is obtained from the transfer function of Equation (3-2) if the velocity pulses in near-field ground motions are modeled by the analytical model in Chapter 3. In this chapter, the transfer function of the near-field ground motion will be derived in Section 7.2. The power spectral density of the proposed analytical model and the Kanai-Tajimi filter will be compared using recorded ground motions in Section 7.3. The design of the optimal controller will be obtained based on the augmented system in Section 7.4. An example illustrating the performance of active and semi-active optimal controllers will be presented in Section 7.5.

7.2 Laplace Transform of Near-field Ground Motions

An analytical model, $\dot{u}_p$, for the ground velocity $\dot{x}_g$ has been proposed in Chapter 3 as

$$\dot{x}_g \approx \dot{u}_p = C \cdot t^n e^{-at} \cdot \sin bt \; ; \; a = \zeta_p \omega_p \; ; \; b = \sqrt{1-\zeta_p^2} \cdot \omega_p \tag{7-1}$$

where ζ_p is the decay factor of the sinusoidal pulse, ω_p is the frequency, and C is the initial amplitude of the pulse. Hence, the ground acceleration $\ddot{x}_g$ can be approximated by $\ddot{u}_p$, and obtained by differentiating Equation (7-1) as

$$\ddot{x}_g \approx \ddot{u}_p = C \cdot t^n e^{-at} \cdot \left[\left(\frac{n}{t} - a \right) \sin bt + b \cos bt \right] \tag{7-2}$$

The transfer function of Equation (7-2) can be obtained from the Laplace Transform of Equation (7-1). Equation (7-1) can be rewritten as

$$\dot{u}_p = C \cdot t^n \cdot e^{-at} \cdot \sin bt = t^n \cdot h(t);\ h(t) = C \cdot e^{-at} \cdot \sin(bt) \tag{7-3}$$

The Laplace Transform of h(t) in Equation (7-3) is obtained as

$$\mathscr{L}[h(t)] = H(s) = \frac{C \cdot b}{(s+a)^2 + b^2} \tag{7-4}$$

Hence, the Laplace Transform of $\dot{u}_p$ in Equation (7-3) is given by

$$\mathscr{L}[\dot{u}_p(t)] = \mathscr{L}[t^n \cdot h(t)] = (-1)^n H^{(n)}(s) = (-1)^n \cdot Cb \cdot \left[\frac{1}{(s+a)^2 + b^2}\right]^{(n)} \tag{7-5}$$

Since $u_p(0) = \dot{u}_p(0) = 0$, $\mathscr{L}[u_p(0)] = \mathscr{L}[\dot{u}_p(0)] = 0$, the Lapalce Transform of $\ddot{u}_p(t)$ can be expressed as

$$\mathscr{L}[\ddot{u}_p(t)] = s \cdot \mathscr{L}[\dot{u}_p(t)] - \mathscr{L}[\dot{u}_p(0)] - \mathscr{L}[x_p(0)] = (-1)^n \cdot Cb \cdot s \cdot \left[\frac{1}{(s+a)^2 + b^2}\right]^{(n)} \tag{7-6}$$

The explicit form of Equation (7-6) is difficult to obtain for an arbitrary value of n. Equation (7-6) is written in the following for special cases when n is a positive integer:

$$\mathscr{L}[\ddot{u}_p(t)] = \frac{Cb \cdot s}{[(s+a)^2 + b^2]}, \qquad \text{for n=0} \tag{7-7}$$

$$\mathscr{L}[\ddot{u}_p(t)] = \frac{2Cb \cdot (s+a)s}{[(s+a)^2 + b^2]^2}, \qquad \text{for n=1} \tag{7-8}$$

$$\mathscr{L}[\ddot{u}_p(t)] = \frac{2Cb \cdot [3(s+a)^2 - b^2]s}{[(s+a)^2 + b^2]^3}, \quad \text{for n=2} \tag{7-9}$$

$$\mathscr{L}[\ddot{u}_p(t)] = \frac{24Cb \cdot (a+s) \cdot (a^2 - b^2 + 2as + s^2]s}{[(s+a)^2 + b^2]^4}, \qquad \text{for n=3} \tag{7-10}$$

Note that the order of the poles of the transfer function increases as n increases, while the positions of the poles remain unchanged.

7.3 Power Spectral Density

The Kanai-Tajimi shape filter is widely used to construct ground motion time histories from specified response spectra in earthquake engineering. It is also widely used to model earthquake excitation for the design for active, semi-active or passive controllers, either in the time domain or frequency domain. [i.e. Filiatrault and Cherry (1990); Spencer et al. 1994; Romallo et al. (2001)]. In Kanai-Tajimi filter, it is assumed that the ground motions is the absolute acceleration output of a non-stationary white noise process passing through a second order system with a stiffness per unit mass, ω_g^2, and a damping ratio, ζ_g. The transfer function of the Kanai-Tajimi filter is,

$$F(s) = \frac{2\zeta_g \omega_g s + \omega_g^2}{s^2 + 2\zeta_g \omega_g s + \omega_g^2} \tag{7-11}$$

Assuming that the parameters ω_p and ζ_p used in the analytical model, Equation (7-1), are the same as ω_g and ζ_g in the Kanai-Tajimi Filter, and letting $\omega_g=2\pi$ and $\zeta_g=0.3$ in Equations (7-7) and (7-11), we plot the normalized magnitude of Equations (7-7) and (7-11) in Figure 7-1. It is observed from Figure 7-1 that the kani-Tajimi filter has a higher magnitude in the low frequency range. On the other hand, the analytical model has a higher magnitude in the frequency range higher than $\omega_g=2\pi$.

Figure 7-2 shows plots of (i) power spectral densities of two typical recorded ground motions; namely, Rinaldi Receiving Station (RRS228) and Sylmar County Converter (SCS142) components of the Northridge earthquake, and (ii) the corresponding

power spectral densities of both the Kanai-Tajimi filter and the proposed pulse model. It is observed that the energy of the proposed model is concentrated in vicinity of the predominant frequency of the ground motion. The Kanai-Tajimi filter overestimates the energy in the low frequency range, while the pulse model underestimates energy in the high frequency range, since it excludes high frequency components in the ground motion. The low-pass property of the pulse model is more suitable for the controller design, since the response of long period structures is less affected by the high frequency components.

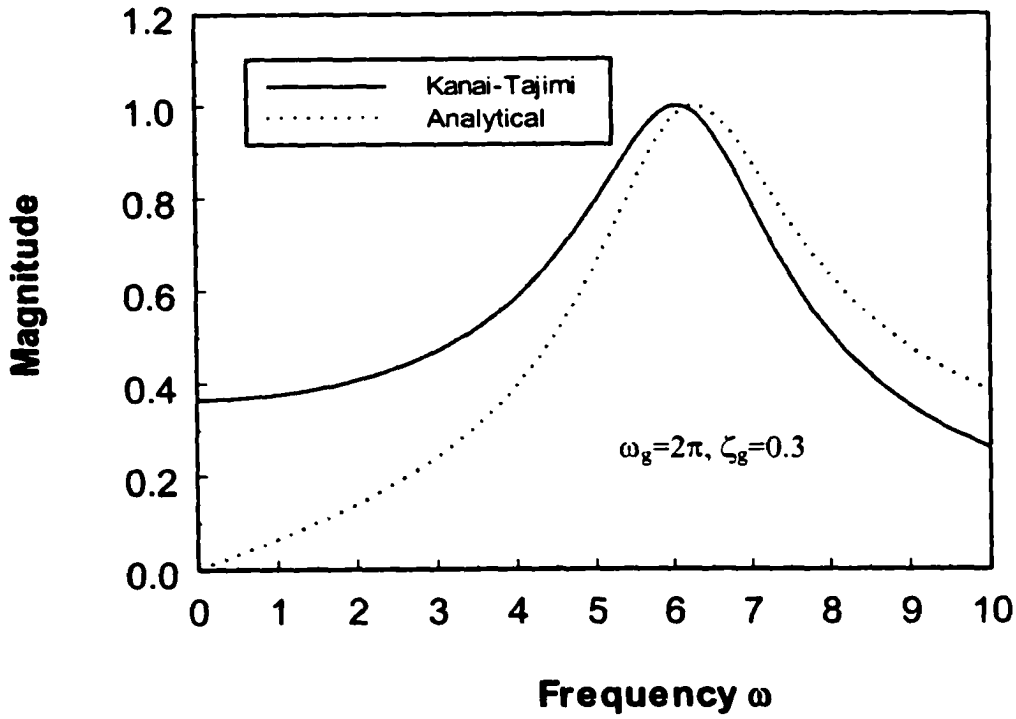

Figure 7-1: Frequency contents of the Kanai-Tajimi filter and the analytical pulse model.

(a)

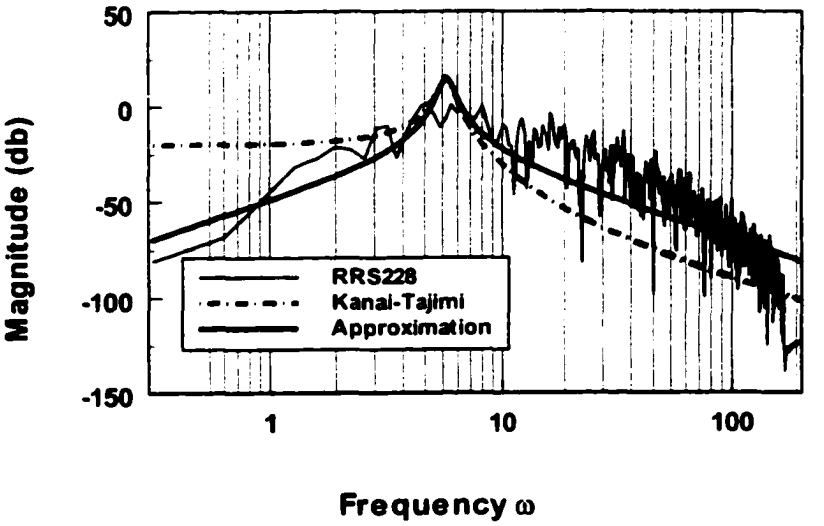

(b)

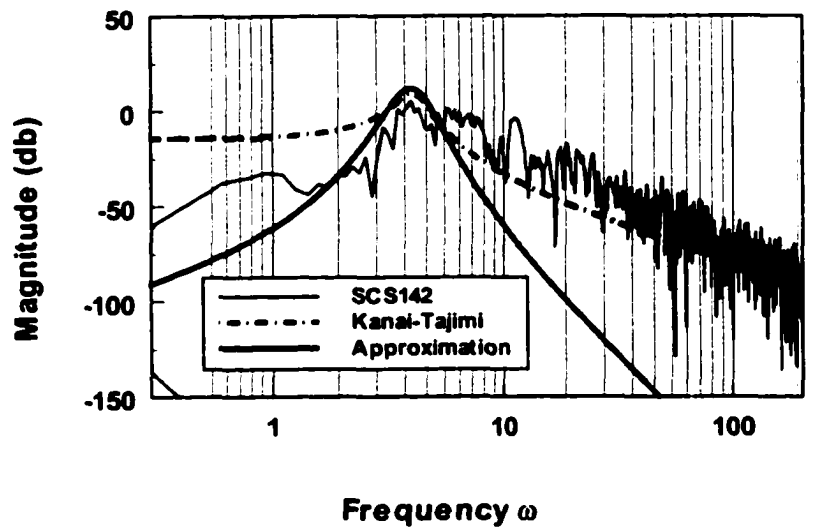

Figure 7-2: Power spectral density of recorded ground motions, Kanai-Tajimi filter and analytical pulse model: (a) RRS228, Rinaldi receiving station, 1994 Northridge earthquake; (b) SCS142, 1994 Northridge Earthquake.

7.4 Optimal Control Design

Consider an n-DOF structure with the following state space equation of motion:

$$\dot{X} = AX + Bu + E\ddot{x}_g \tag{7-12}$$

where X, u and $\ddot{x}_g$ are the state vector, control force and ground motion, respectively. Matrices A, B and E are matrices as follows:

$$A = \begin{bmatrix} 0 & I \\ -M^{-1}K & -M^{-1}C \end{bmatrix}; \; B = \begin{bmatrix} 0 \\ M^{-1}H \end{bmatrix}; \; E = \begin{bmatrix} 0 \\ M^{-1}\eta \end{bmatrix} \tag{7-13}$$

In Equation (7-13), M, C and K are the mass, damping and stiffness matrices of the structure, respectively, H is the controller location matrix, and η is the excitation influence vector.

For the purpose of controller design, the input excitation can be modeled as filtered white noise. The shape filter which can be obtained from transfer function in Equation (7-6), is written in state space as

$$\begin{cases} \dot{\xi} = A_w\xi + B_w w \\ \ddot{x}_g = C_w\xi \end{cases} \tag{7-14}$$

where w is the scalar white noise excitation. For n=1, the denominator of Equation (7-6) is the 4^{th} order of s, and the dimensions of A_w, B_w and C_w in Equation (7-14) are 4x4, 4x1 and 1x4 respectively.

Combining Equation (7-13) and Equation (7-14), one obtains the augmented system as

$$\begin{bmatrix} \dot{X} \\ \dot{\xi} \end{bmatrix} = \begin{bmatrix} A & EC_w \\ 0 & A_w \end{bmatrix} \begin{bmatrix} X \\ \xi \end{bmatrix} + \begin{bmatrix} B \\ 0 \end{bmatrix} u + \begin{bmatrix} 0 \\ B_w \end{bmatrix} w \tag{7-15}$$

Let $X_a=[X^T \xi^T]^T$ be the augmented state vector. Then, Equation (7-15) can be written as

$$\dot{X}_a = A_a X_a + B_a u + E_a w \tag{7-16}$$

The measured outputs of the control system include selected response quantities of the structure and the ground acceleration $\ddot{x}_g$,

$$Y = C_y X_a + D_y u + v \tag{7-17}$$

where v is measurement noise. The controlled output vector is expressed as

$$Z = C_z X_a + D_z u \tag{7-18}$$

The optimal controller for the augmented system in Equation (7-16) can be obtained by minimizing the following performance index using the H_2/LQG strategy

$$J = \lim_{\tau \to \infty} \frac{1}{\tau} E\left[\int_0 \{Z^T Q Z + u^T R u\} dt \right] \tag{7-19}$$

where Q and R are weighting matrices for regulated outputs and control forces, respectively. The minimization of J in Equation (7-19) subject to the constraint in Equation (7-16) results in an optimal controller

$$u = -K X_a \tag{7-20}$$

where K is the control gain matrix. Since it is not possible to measure the state X_a, the estimated state $\hat{X}_a$ can be obtained using the Kalman-Bucy filter,

$$\dot{\hat{X}}_a = (A_a - L C_y)\hat{X}_a + (B_a - L D_y)u + LY \tag{7-21}$$

where L is the observer gain matrix.

The control force in Equation (7-20) can be implemented by active control devices such as hydraulic actuators. It can also be implemented by a semi-active friction damper using the following algorithm,

$$U_{semi-active} = \begin{cases} -K\hat{X}_s & \text{when } u \cdot \text{sgn}(\dot{x}) < 0 \\ 0 & \text{otherwise} \end{cases} \quad (7\text{-}22)$$

7.5 Numerical Example

In order to illustrate the performance of the proposed controller, the two-DOF base-isolated building investigated by Ramallo et al. (2002) is used. The mass, damping coefficient and stiffness of the base-isolator are 6800 kg, 3.74 KN.(m/s)$^{-1}$, and 232KN/m, respectively, and the corresponding quantities for the superstructure are 29485 kg, 23.71 KN(m/s)$^{-1}$ and 11912 KN/m, respectively. The natural period of the base-isolated building is 2.5 s, and corresponding damping ratio of the first mode is 2%. Four typical near-field ground motions used to investigate the performance of the proposed controller are: the NS component of the ground motion recorded at Takatori Station during the 1995 Kobe Earthquake (TAK000); the fault-normal component of the ground motion recorded at Rinaldi Receive Station during the 1994 Northridge Earthquake (RRS228); the fault-normal component of recorded at Sylmar Converter Station during the 1994 Northridge Earthquake (SCS142); and the NS component recorded at JMA Station during the 1995 Kobe Earthquake (KJM000). The acceleration and velocity time histories of these ground motions and their corresponding analytical models are plotted in Figure 7-3. It is observed from Figure 7-3 that, although there are discrepancies between the recorded time histories and the corresponding pulses models, the pulse model captures the low frequency components of the recorded ground motions well.

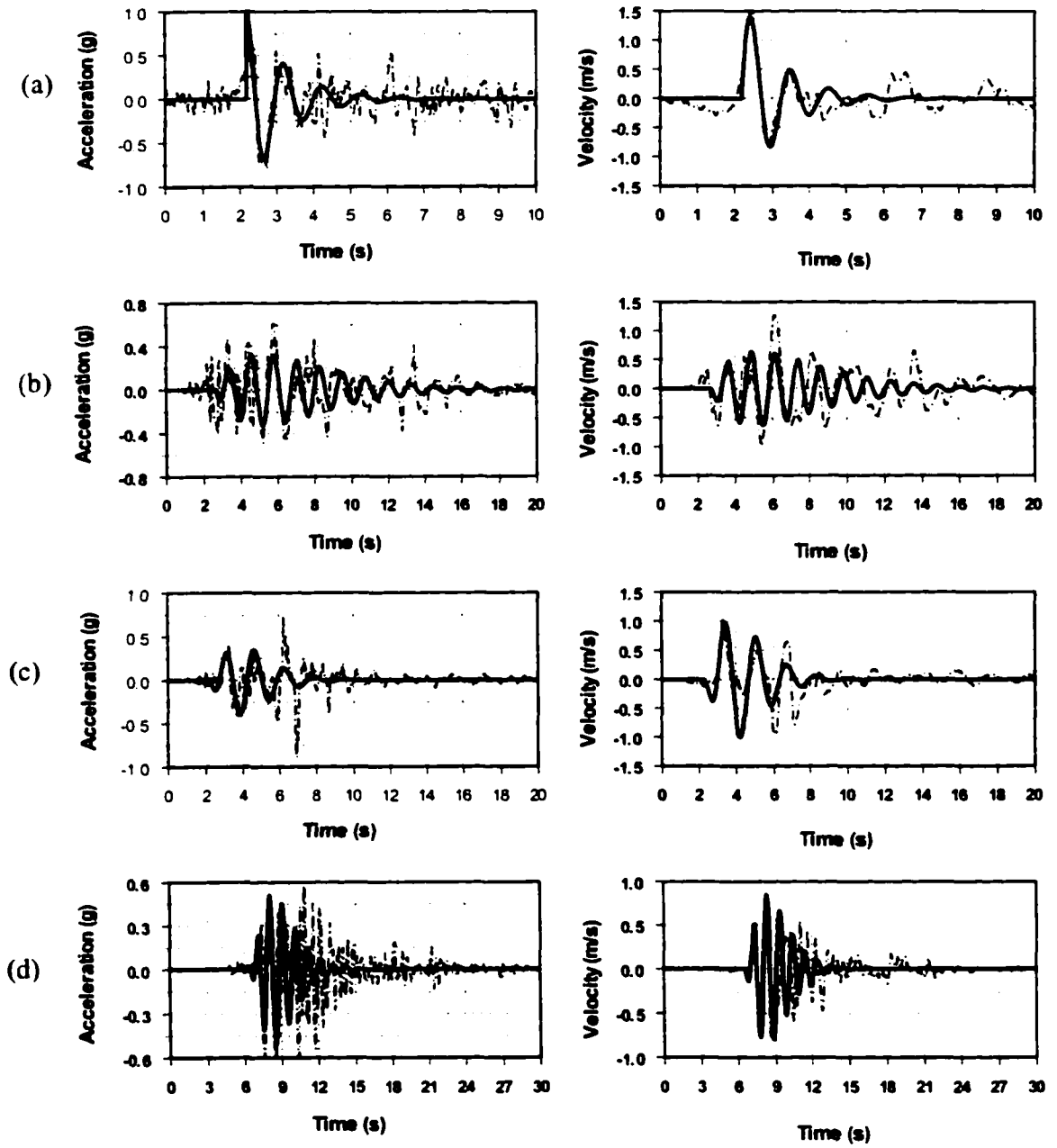

Figure 7-3: Acceleration and velocity time history of recorded ground motions and corresponding analytical model: (a) Rinaldi Receiving Station during 1994 Northridge Earthquake (RRS228); (b) Takatori Station during 1995 Kobe Earthquake (TAK000); (c) Sylmar Converter Station during 1994 Northridge Earthquake (SCS142); (d) JMA Station during 1995 Kobe Earthquake (KJM000).

Figure 7-4 shows the Simulink block diagram for the structure-control system. The measured outputs for the estimation of $\hat{X}_a$ are the displacement of the base isolator, the absolute accelerations of the base and the superstructure, and the acceleration of the ground motion. In the design of the controller, the analytical model of the ground motion is used to incorporate the effect of the frequency content of the ground motion on the gain matrix K. The responses to be regulated are the displacements and accelerations of the base and the superstructure. The nonzero elements of the weighting matrices are selected as $Q(1,1)=2x10^5$, $Q(2,2)=2x10^6$. By varying the weighting matrix R, the response quantities of the base-isolated building equipped with the proposed controller are plotted in Figures 7-5 to 7-8 for four earthquake ground motions.

To evaluate the performance of the proposed control approach, the performances of passive linear viscous dampers, standard LQR controller with a full state feedback and, the LQG controller with an observer are also investigated. For the passive damper case, the response quantities of the base and superstructure are calculated for the damping ratio of the first mode from 2% (inherent damping) to 82% by varying the damping coefficient from 0 to 150 $KN.(m/s)^{-1}$. The standard LQG controller is designed by using the measurements of (i) the displacement of the base, and (ii) absolute accelerations of the base and the superstructure.

It is observed from Figure 7-5 to 7-8 that the peak displacement of the base isolator decreases with the increase of the control force for all control strategies. Also, the reduction in the drift of isolators using the proposed approach is more than other strategies, except for Takatori NS record (TAK000). On the other hand, the reduction for (i) the peak drift of the superstructure, and (ii) the peak absolute accelerations of the base

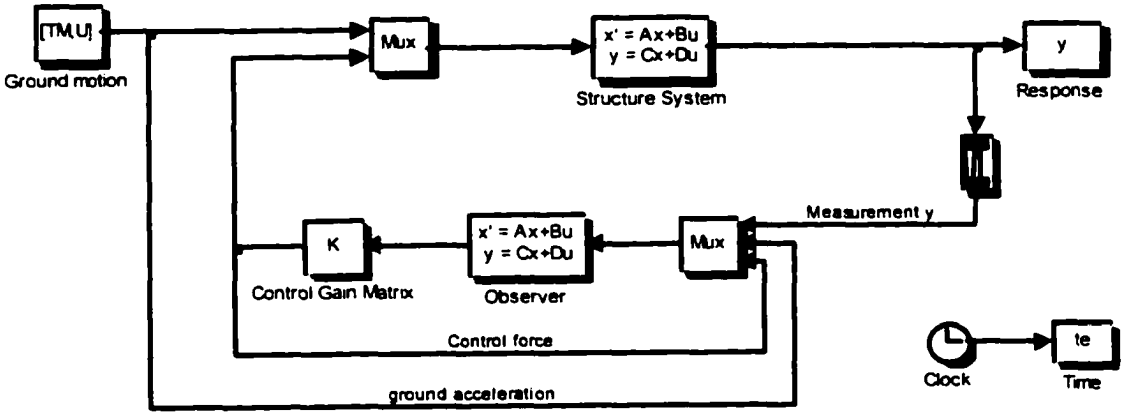

Figure 7-4: Simulink block diagram of controllers.

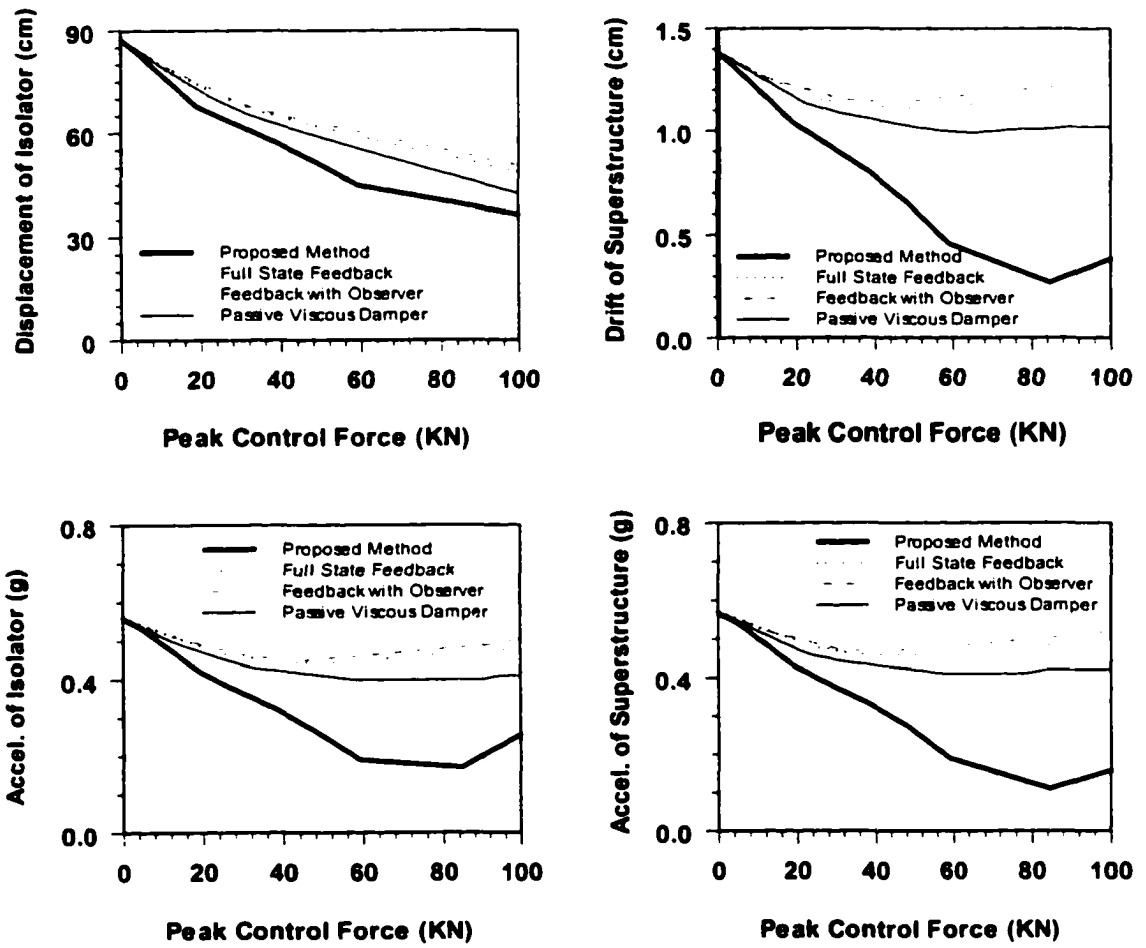

Figure 7-5: Performance comparison of base-isolated building with various control system subject to TAK000 record measured at Takatori Station during 1995 Kobe Earthquake.

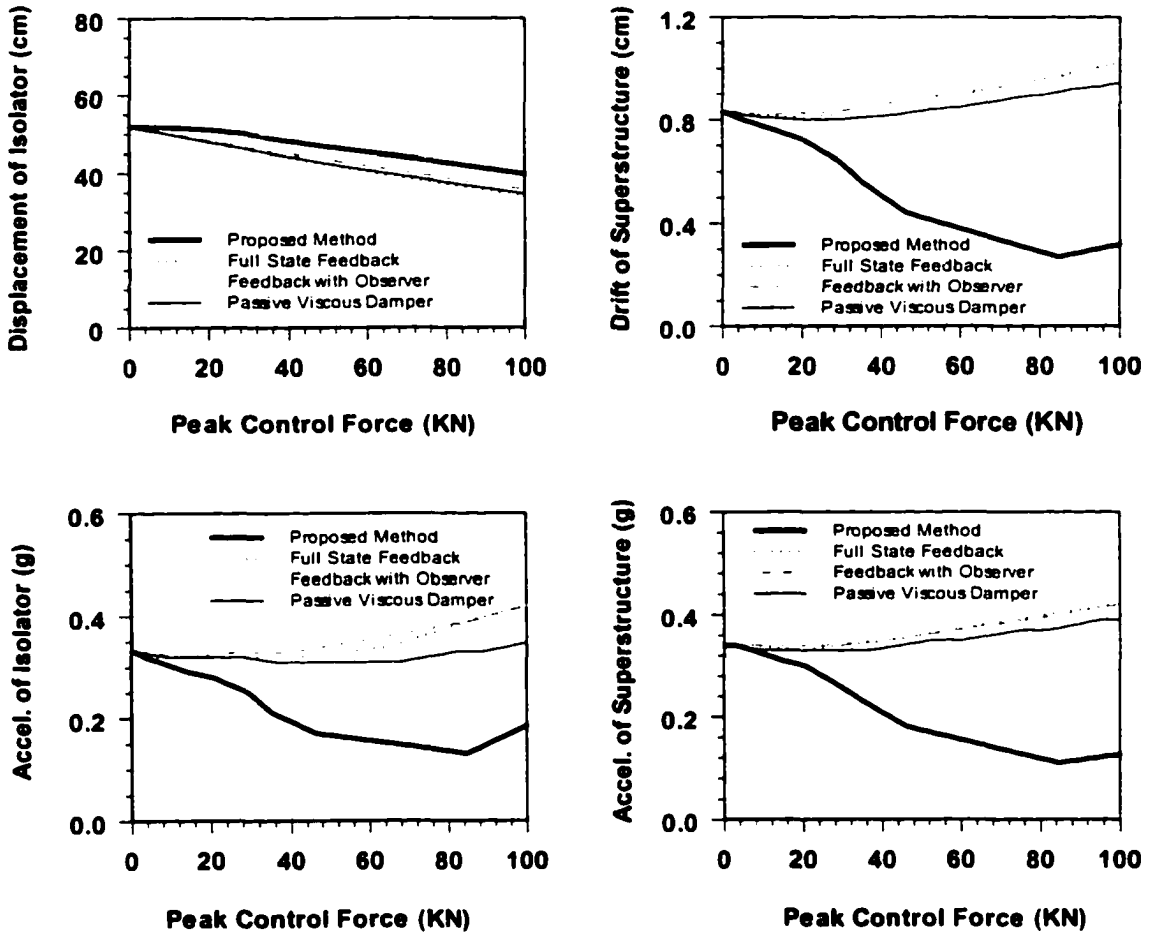

Figure 7-6: Performance comparison of base-isolated building with various control system subject to RRS228 record measured at Rinaldi Receiving Station during 1994 Northridge Earthquake.

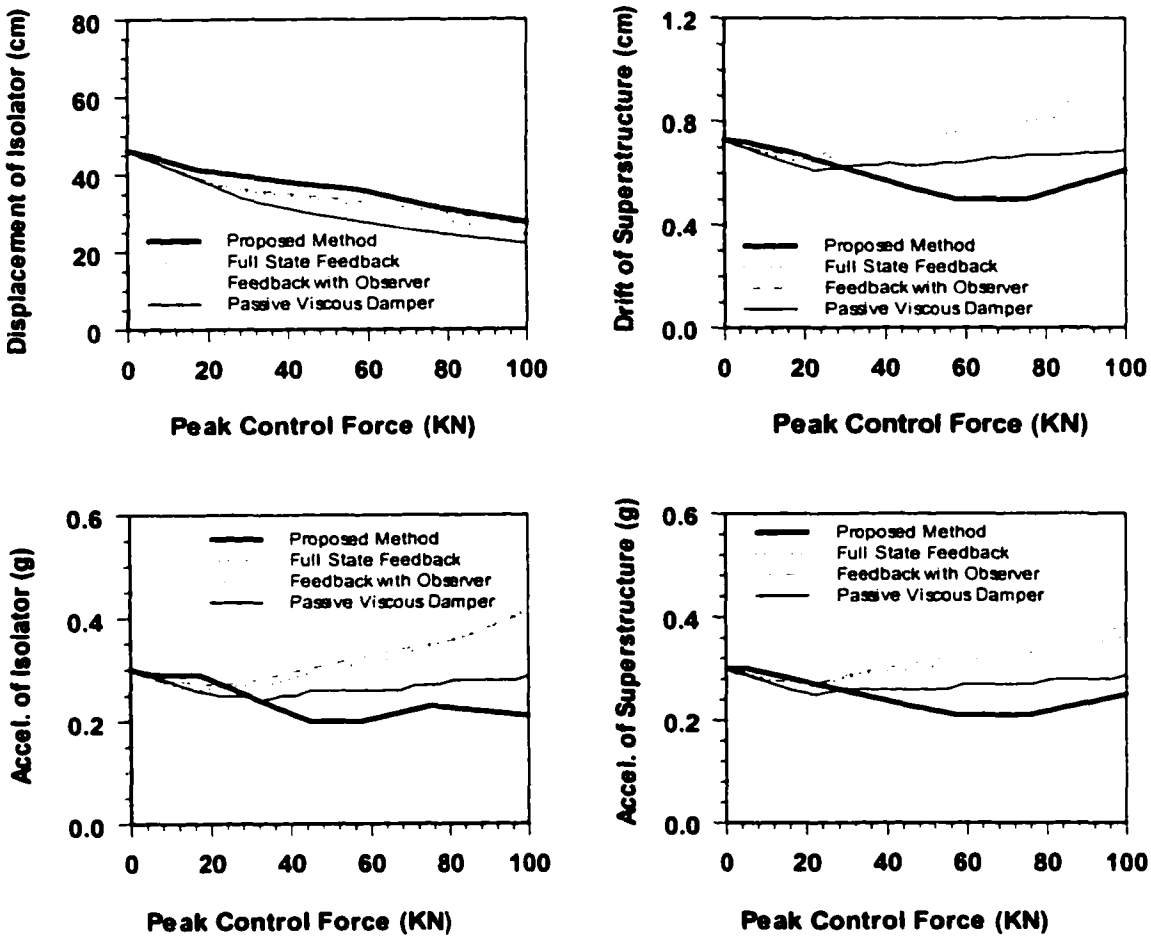

Figure 7-7: Performance comparison of base-isolated building with various control system subject to SCS142 record measured at Sylmar Converter Station during 1994 Northridge Earthquake.

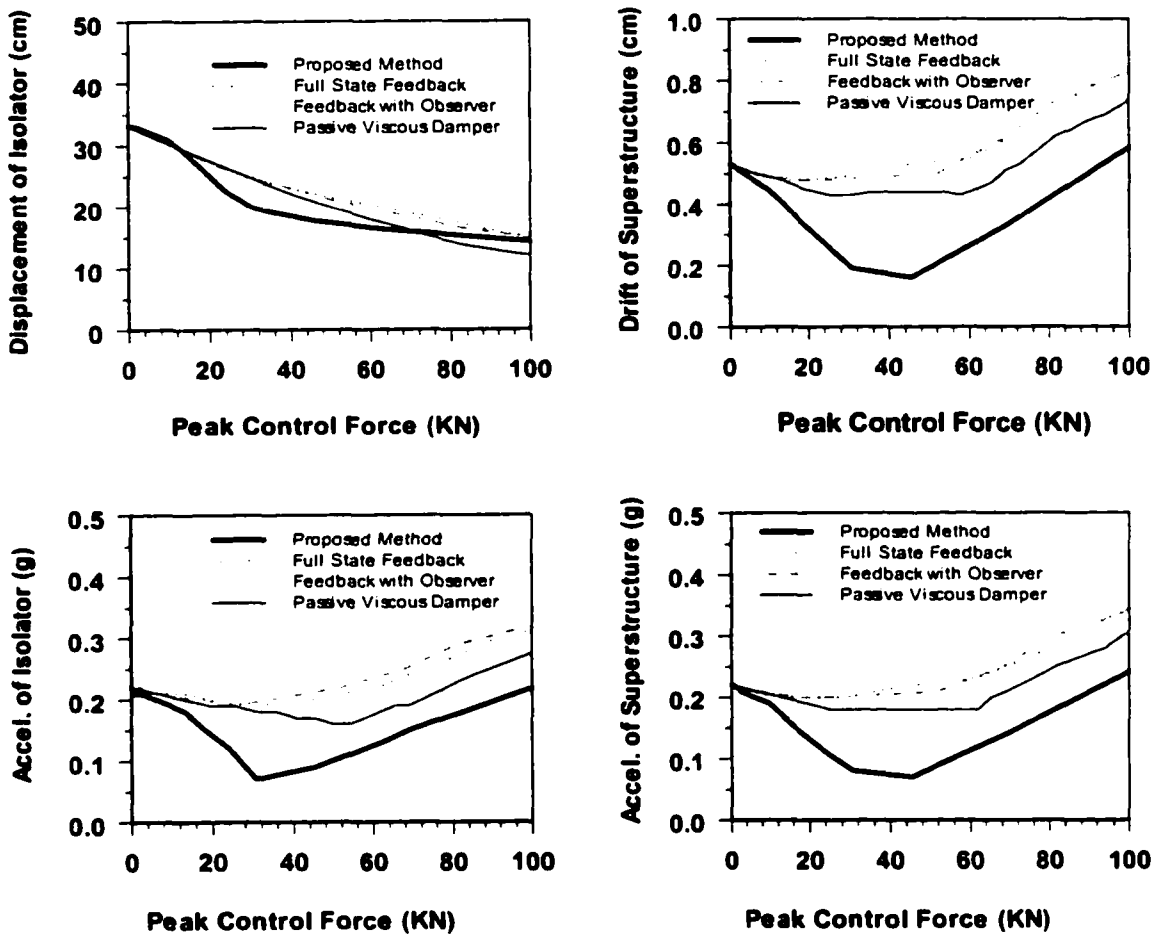

Figure 7-8: Performance comparison of base-isolated building with various control system subject to KJM000 recorded at JMA Station during 1995 Kobe Earthquake.

isolator and the superstructure using the proposed approach are significantly more than that based on other approaches and the passive damper case for all earthquakes considered. The most remarkable characteristic of the proposed approach is that it is capable of reducing the peak response quantities of both the isolator and the superstructure simultaneously. In general, the response quantities of the superstructure and the acceleration of the base increase as the peak drift of the isolator decreases for passive, and semi-active control approaches.

Table 7-1 shows comparisons between the performance of the proposed approach with that of passive viscous dampers and active control using full-scale measurements for four earthquakes considered. In Table 7-1, x_b, x_s, $\ddot{x}_b$ and $\ddot{x}_s$ are the peak drift of the isolator, the peak drift of the superstructure, the peak absolute acceleration of the base, and the peak absolute acceleration of the superstructure, respectively, and $|F|_{max}$ is the peak control force. Column (3) of Table 7-1 shows the peak response quantities of the uncontrolled building. It is observed that the peak drifts of the isolator for RRS228, TAK000, SCS142 and KJM000 earthquakes are 55.28 cm, 89. 53 cm, 46.23 cm and 33.23 cm, respectively. These peak drifts are excessive and much larger than 40 cm limited by the design code. To reduce the drift of the isolator, we first design a passive viscous damper with a damping coefficient of 6.5×10^3 KN.$(m/s)^{-1}$, referred to as "high viscous damping" case. The response quantities for this case are shown in Column (4) of Table 7-1. It is observed that passive viscous dampers are capable of reducing the drift of base isolator to a value less than 40 cm, although there is a slight increase in other response quantities for RRS228 earthquake, and slight decrease in other response quantities for TAK000, SCS142 and KJM000 earthquakes. Next, we design an active

Table 7-1 Comparison of Various Control Systems

Earthquake	Response	Un-controlled	Linear Viscous Damper (ζ=37%)	Active Control I	Active Control II	Semi-active Control	Linear Viscous Damper (ζ=15%)
(1)	(2)	(3)	(4)	(5)	(6)	(7)	(8)
RRS228	x_b (cm)	55.28	36.47	32.58	31.24	30.78	46.09
	x_s (cm)	0.88	1.00	1.12	0.41	0.83	0.87
	$\ddot{x}_b$ (g)	0.35	0.37	0.48	0.15	0.15	0.33
	$\ddot{x}_s$ (g)	0.36	0.41	0.46	0.15	0.14	0.36
	$\|F\|_{max}$		106.11	123.55	50	50	46.65
TAK000	x_b (cm)	89.53	39.42	39.01	33.77	39.47	55.46
	x_s (cm)	1.43	0.94	1.20	0.59	0.92	0.97
	$\ddot{x}_b$ (g)	0.57	0.38	0.48	0.12	0.15	0.38
	$\ddot{x}_s$ (g)	0.59	0.39	0.49	0.13	0.15	0.40
	$\|F\|_{max}$		92.87	115.83	50	50	49.41
SCS142	x_b (cm)	46.23	26.28	26.94	27.86	23.08	32.77
	x_s (cm)	0.73	0.66	0.82	0.31	0.65	0.63
	$\ddot{x}_b$ (g)	0.30	0.26	0.37	0.09	0.11	0.24
	$\ddot{x}_s$ (g)	0.30	0.27	0.34	0.09	0.10	0.26
	$\|F\|_{max}$		67.52	85.94	50	50	32.21
KJM000	x_b (cm)	33.23	16.89	11.68	17.22	13.24	17.71
	x_s (cm)	0.53	0.47	0.52	0.62	0.64	0.32
	$\ddot{x}_b$ (g)	0.22	0.19	0.20	0.08	0.10	0.13
	$\ddot{x}_s$ (g)	0.22	0.20	0.22	0.08	0.09	0.13
	$\|F\|_{max}$		65.62	60.12	50	50	18.54

controller using a full-state feedback, referred to as the "Active Control I" in Table 7-1. The case of Active Control I designed as the standard LQR technique to achieve a similar level of performance as that of the passive damper case. As observed from Table 7-1, the peak control forces for the case of Active Control I are higher. Next, an active controller is designed by using the approach proposed in this research by considering $Q=2.x10^5$, $R=10^{-6}$. The ground motion filter is designed for each ground motion base on the analytical pulse model presented in Chapter 3. The controller in this case is referred to as

"Active Control II". Since devices have a force limitation, the peak control force for Active Control II is saturated at 50 KN. It is observed from Column (6) of Table 7-1 that the peak drift of the isolator has been reduced to a level similar to that of the "High Viscous Damping" and "Active Control I" cases. However, unlike other cases, the drift of the superstructure and the absolute accelerations of the base and the superstructure have been reduced drastically, while the peak control force is limited to 50 KN. This is because the inclusion of the ground motion filter in the controller design makes the controlled structure orthogonal to the ground motion input. In practical applications, it may not be possible to use Active Control II because of the dependence of the control system on the external power supply. Hence, the proposed control approach is implemented by the semi-active control approach in Equation (7-22). Results for this case are shown in Column (7) of Table 7-1. The peak control force in the case of semi-active control is limited to 50 KN. It is observed that the performance of the semi-active control case is quite similar to that of the Active Control II case, although the peak drift of the superstructure increases slightly for some earthquakes. To show the performance of a passive viscous damper with a force capacity close to 50 KN during RRS228, an additional case of passive viscous damping with $c=2.5x10^3$ KN$(m/s)^{-1}$ is also designed to increase the natural damping of the structure to 15%. It is observed from Table 7-1 that the performance of this case is much inferior to that of the case for Active Control II and semi-active control.

Hence, the performance of a controller can be improved drastically if the information about the external excitation is known in advance. Such information includes the predominant period T_p and the shape parameters ζ_p and n. Indeed, for a given site, an

approximate estimate of these parameters can be obtained from the attenuation relationship. Numerical simulations also indicate that the performance of the strategy depends on the model of the external excitation. The better the state of the shape filter can be estimated, the better the performance of the proposed control approach will be.

7.6 Summary

In this chapter, a novel optimal controller is designed based on the augmented system including the structure system and the excitation shape filter. The shape filter can be obtained from the transfer function of the proposed velocity pulses of near-field ground motions. The performance of the proposed control strategy is demonstrated through a base-isolated building subject to four typical near-field ground motions. Simulation results demonstrate that the proposed controller is very effective in reducing both the peak displacement of the base isolator and the peak inter-story drift of the superstructure, as well as that of the absolute acceleration of the superstructure. This control algorithm can be implemented with semi-active dampers. The performance of the semi-active damper is superior to (i) the passive linear viscous damper, and (ii) active control in which the seismic excitations are treated as white noises. However, the proposed controller should be designed with a predominant period of the ground motion known prior, and the performance of the proposed controller also depends on the estimation of the ground motion. Further research is needed to resolve these problems.

CHAPTER 8

CONCLUSIONS AND RECOMMENDATIONS FOR FUTURE RESEARCH

8.1 Conclusions

In this research, the effectiveness of smart energy dissipation systems, e.g., passive dampers, semi-active dampers and active control systems, in protecting structures subject to near-field ground motions has been investigated. Through the analysis of a large number of historical time-history records of near-field ground motions, it has been observed that the destructiveness of near-field ground motions is due to their long period and large amplitude impulsive velocity pulses, which may impart a large input energy to the structure at the beginning of the earthquake. These long period pulses impose a large displacement ductility demand on short period structures, and cause large displacements of long period structures, such as base isolated buildings or high-rise buildings. The traditional approach of the seismic-resistant design is to design structures to sustain earthquakes with sufficient strength capacity and to deform in a ductile manner. Such a design philosophy is based on the assumption that the structure dissipates the input seismic energy in the form of the hysteretic energy through the damage in structural members. However, observations during recent destructive seismic events show that the values of ductility ratios high more than 4 cause an unacceptable level of damage in the absence of appropriate energy dissipation devices. Hence, recent recommendations, such as FEMA 356 (2000) and FEMA 368 (2000), allow for the rehabilitation of old buildings

and the design of new structures using energy dissipation devices to dissipate the input seismic energy.

Energy dissipation devices are commonly known as structural control systems, such as passive dampers, semi-active dampers, active control systems, etc. Significant progress has been made in the development of various types structural control devices and control algorithms. However, a systematic study of the effect of near-field ground motions on the efficacy of these structural control devices is still to be conducted. The performance of a structural control system depends on the device characteristics, control algorithm, controlled structure, and properties of excitations. To develop an effective and efficient control system, it is necessary to investigate every aspect of a control system and the relationship among these aspects, such as the relationship between the parameters of the control algorithm and excitation, device specific control algorithms, etc. In this study, a systematic investigation of the near-field ground motion pulses and their effect on the performance of passive, semi-active and active control systems has been conducted. After the properties of near-field ground motions are investigated quantitatively through an analytical pulse model, an innovative hybrid control system is proposed for the protection of structures from strong near-field ground motions. The major conclusions of the research presented in this thesis are summarized in the following.

An analytical model for velocity pulses in near-field ground motions is presented based on a systematic investigation of the performance of structural control systems. It has been demonstrated that the decaying sinusoidal function is capable of capturing the kinematic characteristics of long period velocity pulses observed in most of the near-field

ground motions. This analytical model can be used for long period structures, such as base isolated building, high-rise buildings, cable-stayed bridges, etc., since the response of these structures is dominated mostly by the long period components in near-field ground motions. The properties of the analytical pulse model have been investigated in detail. A closed-form solution of a linear SDOF structure with supplemental linear viscous dampers and subject to the analytical pulse model has been derived.

The behavior of structures with or without supplemental energy dissipation devices is investigated using a SDOF elastic or elastic-perfectly-plastic structure subject to the proposed analytical pulse model. By adding supplement energy dissipation devices, the energy input to the structure, the hysteretic energy dissipated by the structure, and the displacement ductility of the SDOF structure is investigated in detail. For an elastic structure with μ=1, viscous dampers are effective in reducing the dynamic response as well as the energy input to the structure with a medium period. For structures with a displacement ductility of μ=4, viscous dampers have good performance for structures with short and middle periods. For long period structures with μ=4, although viscous dampers dissipate more energy, they also input more energy to the structures. As a result, viscous dampers are not effective in reducing the displacement ductility much below μ=4 to prevent a substantial damage. Passive friction dampers have a good performance for elastic structures with a medium to long period. For inelastic structures with a displacement ductility of μ=4, passive friction dampers have good performance for structures with all natural periods. Similar conclusion is also obtained by investigating the behavior of a SDOF structure and the benchmark cable-stayed bridge, subject to 40 recorded and simulated near-field ground motions developed for the SAC project.

Due to the impulsive nature of near-field ground motions, high-order polynomial controllers are more capable of protecting structures from near-field ground motions. The most remarkable and important property of polynomial controllers is that they can respond quickly to pulse-type excitations, since the control force is a high order polynomial of the state of the structure. It has been demonstrated that the optimal polynomial controller is very effective in mitigating the response of structures subject to near-field ground motions. However, the practical implementation of optimal polynomial controllers through pure active control may not be possible, because a large amount of external power supply is required during earthquakes. Hence, an innovative hybrid control system is proposed in this study. The hybrid control system can be implemented by the active/ active control system with multilevel control objectives, or the passive/ active system, or the passive/semi-active system to minimize the dependence on external power supply and to increase the reliability of the control system.

In the active/active hybrid control system, a smaller actuator applies the control force corresponding to the linear part of the controller, whereas a second actuator applies the force required by the nonlinear part of the controller. The nonlinear controller is activated only when the force required by the linear part exceeds a certain threshold level. The performance of the hybrid control system is investigated for a SDOF structure subject to a set of recorded ground motions and the analytical pulse model. The set of recorded ground motions consists of 3 typical ground motions, 28 strong near-field ground motions, and 22 long duration far-field ground motions. Numerical simulations show that the nonlinear part of the controller can be designed to be activated only for large near-field ground motions.

In the proposed passive/semi-active hybrid control system, linear viscous dampers are installed in parallel with semi-active friction dampers. The linear viscous dampers are designed to approximate the forces required by the linear part of the polynomial controller and the semi-active friction dampers supply the force required by the nonlinear part of the polynomial controller. The semi-active friction dampers are triggered only when the required force by the nonlinear part exceeds a certain lower threshold value. Further, the force supplied by the semi-active friction dampers is saturated at an upper threshold value corresponding to the device capacity. The application of the proposed hybrid control system is investigated for a SDOF structure and the benchmark cable-stayed bridge subject to the set of ground motions and the analytical pulse model. Numerical simulations demonstrate that the proposed hybrid control system is very effective in reducing the displacement of a structure to a certain limiting value for a broad spectrum of ground motions. The performance of the proposed hybrid control system is similar to that of the pure active polynomial control system. The peak control force of the semi-active friction damper is impulsive in nature and it is required only in a few instances of the entire seismic episode. The peak control force can be designed to satisfy device limitations and the response reduction objectives. The proposed hybrid control system is promising for practical applications, since both components of the hybrid control system, i.e., passive viscous dampers and semi-active friction dampers, are inherently dissipative in nature.

A shaping filter for the earthquake excitation has been proposed using the analytical pulse model. A novel optimal controller is designed based on the augmented system consisting of the structural system and the excitation input shape filter. The

performance of this controller is investigated for a 2DOF base-isolated building subject to four near-field ground motions. Numerical results indicate that the proposed pure active controller is very effective in reducing the peak displacement of the base isolator, the peak interstory drift of the superstructure, and the absolute accelerations of the base and the superstructure. The optimal controller can be implemented by a semi-active damper. In this case, the performance of the semi-active damper is superior to that of (i) passive linear viscous dampers with a higher force capacity, and (ii) the active control system designed by conventional LQG method. Further, the performance of the semi-active damper is similar to the active controller designed by using a input shaping filter.

8.2 Future Research Directions

Although an analytical model of near-field ground motion pulses has been proposed, the characteristics of near-field ground motions need to be investigated in detail. The development (or improvement) of the design guidelines for structures close to the seismic source requires a thorough understanding of the near-field response phenomena. Recent seismic design codes, e.g. the 1997 UBC code, have incorporated the near-field effects by introducing the source type and distance dependent near-field factors to the conventional design spectrum. However, it is believed that these factors may not be able to address the severity of the near-field phenomena adequately. FEMA 356 (2000) and FEMA 368 (2000) present some guidelines for the rehabilitation of old buildings and the design of new buildings using passive energy dissipation devices without considering near-field effects. Hence, the following aspects of near-field effects on the current seismic design practice need to be investigated.

1). The elastic seismic design spectra developed for ordinary ground motions may not be suitable for near-field ground motions. Similarly, the strength reduction factor, R, versus the displacement ductility, μ, curve for inelastic seismic design spectra should be derived by considering near-field ground motions.

2). FEMA 356 (2000) and 368 (2000) allow the rehabilitation of old buildings and the design of new buildings using passive energy dissipation devices. The amount of supplemental damping is described by an equivalent damping ratio that is appropriate for ordinary ground motions. However, this ratio may not be suitable when the structure is subject to impulsive, pulse-type excitations. It is shown that the performance of passive energy dissipation systems depends significantly on the pulse period, T_p, and the decay factor, ζ_p. This aspect of FEMA 356 and FEMA 368 needs to be investigated in detail. Experimental verification of this aspect should also be carried out using shaking table tests.

4). Experimental verifications of the proposed hybrid control system should be conducted to determine its effectiveness and potential for practical applications.

5). More theoretical investigations on active or semi-active control algorithms taking into account the excitation input shape filter need to be conducted. The performance and applicability of the proposed hybrid controller should be verified through shaking table tests.

Appendix I Near-Field Ground Motions used in SAC Project

Near-Field Ground Motions Derived from Historical Acceleration Records						
EQ code	Description	Earthquake Magnitude	Distance (km)	Pred. Period T_p (s)	PGA (cm/sec^2)	PGA (g's)
nf01	fn Tabas, 1978	7.4	1.2	5.3	882.85	0.90
nf02	fp Tabas, 1978	7.4	1.2	4.7	958.67	0.98
nf03	fn Loma Prieta, 1989, Los Gatos	7.0	3.5	2.9	703.78	0.72
nf04	fp Loma Prieta, 1989, Los Gatos	7.0	3.5	2.9	449.36	0.46
nf05	fn Loma Prieta, 1989, Lex. Dam	7.0	6.3	1.1	672.86	0.69
nf06	fp Loma Prieta, 1989, Lex. Dam	7.0	6.3	4.2	362.95	0.37
nf07	fn C. Mendocino, 1992, Petrolia	7.1	8.5	0.8	625.60	0.64
nf08	fp C. Mendocino, 1992, Petrolia	7.1	8.5	0.8	642.24	0.65
nf09	fn Erzincan, 1992	6.7	2.0	2.1	423.90	0.43
nf10	fp Erzincan, 1992	6.7	2.0	1.9	448.29	0.46
nf11	fn Landers, 1992	7.3	1.1	4.6	699.62	0.71
nf12	fp Landers, 1992	7.3	1.1	6.2	783.89	0.80
nf13	fn Nothridge, 1994, Rinaldi	6.7	7.5	1.0	872.72	0.89
nf14	fp Nothridge, 1994, Rinaldi	6.7	7.5	2.7	381.03	0.39
nf15	fn Nothridge, 1994, Olive View	6.7	6.4	2.6	718.16	0.73
nf16	fp Nothridge, 1994, Olive View	6.7	6.4	0.5	583.79	0.60
nf17	fn Kobe, 1995	6.9	3.4	0.9	1067.20	1.09
nf18	fp Kobe, 1995	6.9	3.4	1.3	563.99	0.57
nf19	fn Kobe, 1995, Takatori	6.9	4.3	1.3	771.10	0.79
nf20	fp Kobe, 1995, Takatori	6.9	4.3	1.2	416.11	0.42
Near-Field Ground Motions Derived from Physical Simulations						
EQ code	Description	Earthquake Magnitude	Distance (km)	Pred. Period T_p (s)	PGA (cm/sec^2)	PGA (g's)
nf21	fn Elysian Park 1	7.1	17.5	3.6	842.50	0.86
nf22	fp Elysian Park 1	7.1	17.5	0.7	875.07	0.89
nf23	fn Elysian Park 2	7.1	10.7	1.3	1768.10	1.80
nf24	fp Elysian Park 2	7.1	10.7	0.8	885.75	0.90
nf25	fn Elysian Park 3	7.1	11.2	2.1	993.28	1.01

Appendix I Near-Field Ground Motions used in SAC Project (Continued)

nf26	fp Elysian Park 3	7.1	11.2	1.0	643.02	0.66
nf27	fn Elysian Park 4	7.1	13.2	2.4	904.44	0.92
nf28	fp Elysian Park 4	7.1	13.2	0.9	628.51	0.64
nf29	fn Elysian Park 5	7.1	13.7	2.4	1139.20	1.16
nf30	fp Elysian Park 5	7.1	13.7	0.7	499.29	0.51
nf31	fn Palos Verdes 1	7.1	1.5	2.4	954.88	0.97
nf32	fp Palos Verdes 1	7.1	1.5	1.1	456.81	0.47
nf33	fn Palos Verdes 2	7.1	1.5	2.7	949.26	0.97
nf34	fp Palos Verdes 2	7.1	1.5	1.1	454.53	0.46
nf35	fn Palos Verdes 3	7.1	1.5	1.5	856.58	0.87
nf36	fp Palos Verdes 3	7.1	1.5	1.6	408.23	0.42
nf37	fn Palos Verdes 4	7.1	1.5	1.9	777.92	0.79
nf38	fp Palos Verdes 4	7.1	1.5	2.1	557.58	0.57
nf39	fn Palos Verdes 5	7.1	1.5	2.9	898.08	0.92
nf40	fp Palos Verdes 5	7.1	1.5	2.9	589.15	0.60

Appendix II 53 Ground Motions Used In Active or Hybrid Control System

	Ground motion recordings	PGA (g)
1	1940, El Centro, Mw=7.0, El Centro Array #9, El Centro	0.348
2	1985 Mexico City , Mexico	0.143
3	1999 Turkey Earthquake, Gebze	0.265
4	1995 Kobe Earthquake, Mw=6.9, JMA Station, KJM000	0.817
5	1995 Kobe Earthquake, Mw=6.9, JMA Station, KJM090	0.618
6	1992 Landers Earthquake, Mw=7.2, Lucerne Station, LCN000	0.805
7	1992 Landers Earthquake, Mw=7.2, Lucerne Station, LCN275	0.727
8	1992 Cape Mendocino Earthquake, Mw=7.0, Cape Mendocino Station, CPM000	1.497
9	1992 Cape Mendocino Earthquake, Mw=7.0, Cape Mendocino Station, CPM090	1.039
10	1989 Loma Prieta Earthquake, Mw=6.9, LGPC station, LGP000	0.570
11	1989 Loma Prieta Earthquake, Mw=6.9, LGPC station, LGP090	0.607
12	1987 Superstition Hills Earthquake, Mw=6.6, Superstition Station, SUP-135	0.894
13	1999 Chi-Chi Earthquake, Mw=7.6, TCU084 Station, TCU084EW	1.009
14	1999 Chi-Chi Earthquake, Mw=7.6, CHY080 Station, CHY080NS	0.902
15	1999 Chi-Chi Earthquake, Mw=7.6, CHY080 Station, CHY080EW	0.968
16	1978 Tabas Earthquake, Mw=7.4, Tabas Station, TAB-LN	0.836
17	1978 Tabas Earthquake, Mw=7.4, Tabas Station, TAB-TR	0.852
18	1995 Kobe Earthquake, Mw=6.9, Takatori Station , TAK000	0.612
19	1995 Kobe Earthquake, Mw=6.9, Takatori Station , TAK090	0.649
20	1992 Cape Mendocino Earthquake, Mw=7.0, Petrolia Station, PET000	0.590
21	1992 Cape Mendocino Earthquake, Mw=7.0, Petrolia Station, PET090	0.662
22	1999 Duzce, Turkey Mw=7.1, Duzce Station, DZC270	0.535
23	1992 Erzincan, Turkey Mw=7.1, Duzce Station, ERZ-NS	0.515
24	1994 Northridge Earthquake, Mw=6.7, New Hall Fire Station, NWH360	0.590
25	1994 Northridge Earthquake, Mw=6.7, Rinaldi Receiving Station, RRS228	0.799
26	1994 Northridge Earthquake, Mw=6.7, Sylmar Converter Station, CSC052	0.613
27	1994 Northridge Earthquake, Mw=6.7, Sylmar Converter Station, CSC142	0.897
28	1999 Chi-Chi Earthquake, Mw=7.6, TCU065 Station, TCU065NS	0.603
29	1999 Chi-Chi Earthquake, Mw=7.6, TCU065 Station, TCU065EW	0.814
30	1999 Chi-Chi Earthquake, Mw=7.6, TCU068 Station, TCU068NS	0.462
31	1999 Chi-Chi Earthquake, Mw=7.6, TCU068 Station, TCU068EW	0.566
32	1985 Chile Earthquake, Llollelo Station, Llolleio010	0.712
33	1985 Chile Earthquake, Llollelo Station, Llolleio100	0.445
34	1985 Chile Earthquake Vina Del Mar 200	0.363

Appendix II 53 Ground Motions Used In Active or Hybrid Control System (Continued)

35	1985 Chile Earthquake, Vina Del Mar 290	0.237
36	1985 Michoacan Earthquake, Calteta De Campos 00	0.141
37	1985 Michoacan Earthquake, Calteta De Campos 90	0.141
38	1940 Imperial valley, NS	0.349
39	1940 Imperial valley, EW	0.214
40	1968 Hachinohe Earthquake, EW	0.210
41	1968 Hachinohe Earthquake, NS	0.318
42	1985 Michoacan Earthquake, Occt 1	0.021
43	1985 Michoacan Earthquake, Occt 2	0.055
44	1978 Miyagi-oki Earthquake, E41S	0.226
45	1978 Miyagi-oki Earthquake, N41E	0.211
46	1949 Olympia Earthquake, 182	0.068
47	1949 Olympia Earthquake, 282	0.067
48	1985 Michoacan Earthquake, Tacy EW	0.034
49	1985 Michoacan Earthquake, Tacy NS	0.035
50	1952 Taft Lincoln Tunnel N21E	0.156
51	1952 Taft Lincoln Tunnel S69E	0.179
52	1985 Chile Earthquake, Valparaiso 070	0.176
53	1985 Chile Earthquake, Valparaiso 160	0.165

REFERENCES

1. Abrahamson, N. (2001), Incorporating Effects of Near Fault Tectonic Deformation Into Design Ground Motions, University at Buffalo seminar, URL: http://civil.eng.buffalo.edu/webcast/

2. Akbay, Z. and Aktan, H.M., (1991). Actively Regulated Friction Slip Braces, *Proc. 6th Canadian Conf. Earthq. Engrg.*, Univ. of Toronto Press, Toronto.

3. Akbay, Z. and Aktan, H.M., (1995). Abating Earthquake Effects on Buildings by Active Slip Brace Devices, *Shock Vibration*, **2**: 133-142.

4. Agrawal, A.K. and Yang, J.N. (1995), "Nonlinear Optimal Polynomial Control for Linear and Nonlinear Structures", Technical Report NCEER-95-0019. National Center for Earthquake Engineering Research, December 11, 1995.

5. Agrawal, A.K. and Yang, J.N. (1996a), "Optimal Polynomial Control of Seismic-Excited Linear Structures", Journal of Engineering Mechanics, ASCE, Vol. 122, No. 8, pp. 753-761.

6. Agrawal, A.K., and Yang, J.N. (1996b), "Optimal Polynomial Control for Civil Engineering Structures Using Static Output Feedback", The Chinese Journal of Mechanics, Vol. 12, No. 1, pp. 91-102.

7. Agrawal, A.K., and Yang, J.N. (1997), "Static Output Polynomial Control for Linear Structures", Journal of Engineering Mechanics, ASCE, Vol. 123, No. 9.

8. Agrawal, A.K., Yang, J.N., and Wu, J.C. (1998a), "Applications of Optimal Polynomial Controller to a Benchmark Problem", J. Earthquake Engineering and Structural Dynamics, Vol. 27, No., 11.

9. Agrawal, A.K. and Yang, J.N., (2000a). Semi-Active Control Strategies For Buildings Subject To Near-Field Earthquakes, *Proc. SPIE. in Smart Structures and Materials 2000: Smart Systems for Bridges, Structures, and Highways*, 3988: 359-370, March 6-8, Newport Beach, CA.

10. Agrawal, A.K. and Yang, J.N., (2000b). Hybrid Isolation Systems For Buildings Subject to Near-Field Earthquakes, *Proc. of 2000 Structures Congress and Exposition*: Advanced Technology in Structural Engineering, ASCE, 2000 CD-ROM, 8 Pages, May 8-10, Philadelphia, PA.

11. Agrawal, A.K. and He, W.L., (2000). Semi-Active Control of Seismically Excited Benchmark Building Using A Resetting Semi-Active Stiffness Damper, *Proc. 2nd European Conference on Structural Control*, European Association for the Control of Structures, Champs-sur-Marne, France, July 3-6.

12. Agrawal, A.K., He, W.L., and Yang, J.N. (2002a), Performance Evaluation of some semi-active control systems for benchmark cable-stayed bridge, The 7th US National Conf. of Earthquake Engineering, July 22-24, Boston.

13. Agrawal, A.K., Yang, J.N. and He, W.L. (2002b), Performance Evaluation of some semi-active control systems for benchmark cable-stayed bridge, The 3rd world conference on structural control, April 7-12. Italy.

14. Agrawal, A.K. and He, W.-L. (2002c), A analytical approximation of near-fault ground motions pulses for flexible structures, 15th ASCE Engineering Mechanics Conference, June 2-5, Columbia University, New York, NY.

15. Agrawal, A.K., Yang, J.N. and He, W.-L. (2003), "Performance evaluation of some passive and semi-active control for a Benchmark Cable-stayed bridge", *Journal of Structural Engineering*, ASCE, Vol.129 (7), pp 884-894.

16. Alavi, B. and krawinkler, H., (2001). Effects of near-fault ground motions on frames structures, The John A. Blume Earthquake Engineering Center Research Report No. 138, Feb.

17. Alt, T. R., Jabbari, F. and Yang, J. N. (2000), "Reliable Control Design For Building Under Seismic Excitation," J. Earthq. Engrg. and Struct. Dyn., Vol. 29, pp. 241-257.

18. Anderson, B.D.O and Moore, J. (1990), Optimal control: linear quartic methods, Prentice Hall International Editions, Englewood Cliffs, NJ.

19. Anderson, J.C., and Bertero, V.V. (1987). Uncertainties in establishing design earthquake. *Journal of Structural Engineering, ASCE* **113**(8): 1709–1724.

20. Bass, R.W. and Weber, R.F. (1966), Optimal nonlinear feedback control derived from quartic and high-order performance criteria, IEEE Trans. On automatic control, Vol. AC-11, No. 3, pp.448-454.

21. Benioff, H., (1955). Mechanism and strain characteristics of the white wolf fault as indicated by aftershock sequence, Earthquakes in Kern County, California, During 1955, *California Division of Mines Bulletin*, No. 171, 199-202.

22. Bertero, V., Mahin, S., and Herrera, R., (1978). Asismic Design Implications of near-fault San Fernando earthquake records, *Earthquake Engng Struct. Dyn.*, **6**: 31-42.

23. Brodsky, E. E. and H. Kanamori (2001). The elastohydrodynamic lubrication of faults, *J. Geophy. Res.*, 106, 16357-16374.

24. Burton SA, Makris N, Konstantopoulos I, Antsaklis PJ. (1996). Modeling the response of ER damper: phenomenology and emulation. *Journal of Engineering Mechanics* , 122(9): 897–906.

25. Cai G.-P., Huang, J.Zh., Sun, F. and Wang, Ch. (2000). Modified sliding-mode bang-bang control for seismically. *Earthquake Engng Struct. Dyn.*, 29: 1647-1657.

26. Chang, K.C., Soong, T.T., Oh, S.T., and Lai, M.L. (1992). Effect of ambient temperature on viscoelastically damped structure. *J. of Struct. Engrg.*; 118(7): 1955-1973.

27. Chang, K. C., Soong, T.T., Oh, S.T., and Lai, M.L. (1995). Seismic behavior of steel frame with added viscoelastic dampers. *J. of Struct. Engrg.*., 121(10): 1418-1426.

28. Chen, G.D. and Chen, C.C. (2000), "Behavior of Piezoelectric friction dampers under dynamic loading", Proc. SPIE Symp. on Smart Structures and Materials:

Smart Systems for Bridges, Structures, and Highways, Newport Beach, CA, Vol. 3988, pp.54-63.

29. Chen, C.C. and Chen, G.D. (2001), "A High Efficiency Control Logic for Semi-Active Friction Dampers", Proc. 2001 Structures Congress, May 21-23, Washington, D.C., CD-ROM, 11 Pages.

30. Chopra, A.K., Chintanapakdee, C. (2001). Comparing response of SDF systems to near-fault and far-fault earthquake motions in the context of spectral regions. *Earthquake Engng Struct. Dyn.*, **30**:1769–1789.

31. Dowdell, D.J. and Cherry, S., (1994). Semi-Active Friction Dampers for Seismic Response Control of Structures, *Proc. 5th U.S. National Conf. on Earthq. Engrg.*, 1994(**I**): 819-828, CA.

32. Dupont P., Kasturi P. and Stokes A.(1997), Semi-active control of friction damper. *Journal of Sound and Vibration*, **202**(2): 203-218.

33. Dyke, S.J., Spencer, B.F. Jr., Sain, M.K. and Carlson, J.D., (1996a). Modeling and Control of Magnet-orheological Dampers for Seismic Response Reduction, *Smart Materials and Structures*, **5**: 565-575.

34. Dyke, S.J., Spencer, B.F. Jr., Sain, M.K. and Carlson, J.D., (1996b). Seismic response reduction using magnetorheological dampers, Proc., IFAC World Cong., Vol. L, Int. Fed. Of Automatic Control, 145-150.

35. Dyke, S.J., Yi, F., Frech, S. and Carlson, J.D., (1999), Application of Magnet-orheological Dampers to Seismically Excited Structures, *Proceedings of the 17th International Modal Analysis Conference (IMAC)*, Society for Experimental Mechanics, Kissimmee, Florida, Feb. 8 -11.

36. Dyke S. J., Bergman L. A., Turan G. and Caicedo J. M. (2000). Benchmark Control Problem for Seismic Response of Cable-Stayed Bridges, *Proceedings of the 3rd international Workshop on Structural Control, IASC*, Champs-sur-Marne, France, July 7–10; Benchmark Paper and data available at http://wusceel.cive.wustl.edu /quake/.

37. Ehrgott RC, and Masri SF. (1992). Modeling the oscillatory dynamic behavior of electrorheological materials in shear. *Smart Materials and Structures*, 1(4): 275–85.

38. Fajfar P, Vidic T and Fischinger M. (1990). A measure of earthquake motion capacity to damage medium period structures. *Soil Dynamics and Earthquake Engineering*; **9**(5): 236–242.

39. Fajfar P, Vidic T. (1994). Consistent inelastic design spectra: hysteretic and input energy. *Earthquake Engineering and Structural Dynamics*; **23**: 523-532.

40. FEMA 273 (1997): NEHRP Guidelines for the Seismic Rehabilitation of Buildings, Federal Emergency Management Agency 273, Washington, DC.

41. FEMA 302 (1997): NEHRP Recommended Provisions for Seismic Regulations for New Buildings and Other Structures, Federal Emergency Management Agency 302, Washington, DC.

42. FEMA 356 (2000): Pre-standard and Commentary for the Seismic Rehabilitation of Buildings, Federal Emergency Management Agency 356, Washington, DC.

43. FEMA 368 (2000): NEHRP Recommended Provisions for Seismic Regulations for New Buildings and Other Structures, Federal Emergency Management Agency 368, Washington, DC.

44. Feng Q. and Shinozuka M. (1990). Use of a variable damper for hybrid control of bridge response under earthquake. Proceedings of U.S. National Workshop on Structural Control Research, Los Angeles, CA, 1990: 107–12.

45. Feng MQ, Shinozuka M, Fujii S.(1992), Experimental and analytical study of a hybrid isolation system using friction controllable sliding bearings. Report No. NCEER 92-0009, National Center for Earthquake Engineering Research, Buffalo, NY.

46. Feng MQ., (1993), Application of hybrid sliding isolation system to buildings. Journal of Engineering Mechanics. 119(10): 90–108.

47. Feng MQ, Shinozuka M, Fujii S. (1993). Friction controllable sliding isolation system. Journal of Engineering Mechanics;119(9):1845-64.

48. Feng. Q. and Shinozuka, M (1993). Control of seismic response of bridge structures using variable dampers. *Journal of Intelligent Mat. Sys. and Struct.* 4, 117-122.

49. Filiatrault, *A.*, and Cherry, S. (1990). Seismic design spectra for friction- damped structures, *J. of Struct. Engrg.* ASCE, **116**(5): 1334-1355.

50. Fu, Y. and Kasai, K. (1998), "Comparative study of frames using viscoelastic and viscous dampers", *J. Struct. Eng.*, **124:5**, 513–552.

51. Fujita, T., et al., (1994), Semiactive Seismic Isolation Using Controllable Friction Damper, *Bull. Earthq. Resistant Structure Res. Center*, **27(2)**: 21-31.

52. Gavin, H.P., Hanson, R.D. and Filisko, F.E. (1996a). Electrorheological Dampers, Part I: Analysis and Design, *J. Appl. Mech.*, ASME, **63**(3): 669-675.

53. Gavin, H.P., Hanson, R.D. and Filisko, F.E. (1996b). Electrorheological Dampers, Part I: Testing and Modeling, *J. Appl. Mech.*, ASME, **63**(3): 676-682.

54. Goel, R. K. (1997), "Seismic response of asymmetric systems: Energy based approach", *J. Struct.Eng.*, **123:11**, 1444–1453.

55. Hall J.F. (1998), Seismic response of steel frame buildings to near-source ground motions. *Earthquake Engng. Struct. Dyn.*, **27**: 1445-1464.

56. Hall, J., Heaton, T., Halling, M. and Wald, D., (1995). Near-source ground motion and its effect on flexible buildings, Earthquake Spectra, Vol. 11, No. 4, 569-605.

57. Hatcher, R.P., and Shinners, S.M. (1982). Adaptive control techniques for reducing settling time, Proc. 1982 American Control Conference, Vol. 2, 658-659.

58. He, W.L., Agrawal, A.K. and Mahmoud, K. (2001), Control of Seismically Excited Cable-stayed Bridge Using Resetting Semi-Active Stiffness Dampers. Journal of bridge engineering ASCE., **6**(6): 502-511.

60. He, W.-L. and Agrawal, A. K., (2002a), Performance of structures with passive dampers subject to near-fault ground motions. International Conference on Advances in Building Technology (ABT 2002), Dec. Hong Kong.

61. He, W.-L. and Agrawal, A.K. (2002b), A hybrid control system for protection of structures from near-fault earthquakes, *International Conference on Advances and New Challenges in Earthquake Engineering Res.*, August 15-17, Harbin, China.

62. He, W.-L. and Agrawal, A. K., (2002c), Energy Transfer Approach for the Design of Passive Energy Dissipation Systems, 15th ASCE Engineering Mechanics Conference, June 2-5, Columbia University, New York, NY.

63. He, W.-L. and Agrawal, A. K., (2002d), A hybrid control system for base-isolated buildings, *Proc. of U.S.-Japan Cooperative Research Program on Smart Structural Systems and Urban Seismic Disaster Mitigation*, October 18-19, Tsukuba, Japan.

64. He W.L., Agrawal, A. K., and Yang, J.N. (2003), A Novel Semi-Active Friction Controller for Linear Structures Against Earthquakes. *Journal of Structural Engineering*, ASCE, Vol. 129(7), pp 941-950.

65. Heaton T.H., Hall J.F. et al. (1995). Response of High-Rise and Base-Isolated Buildings to a Hypothetical Mw 7.0 blind thrust earthquake. *Science*; Vol. **267**; Issue 5195: 206-211.

66. Housner GW. (1959), Behaviour of structures during earthquake. *Journal of the Engineering Mechanics Division*, ASCE: **85**(4): 109–129.

67. Housner GW, Bergman LA, Caughey TK, Chassiakos AG, Claus RO, Masri SF, Skelton RE, Soong TT, Spencer BF and Yao, JTP. (1997). Structural control: past, present and future. *Journal of Engineering Mechanics*, ASCE; **123**(9): 897-971.

68. Hrovat D, Barak P, Rabins M. (1983). Semi-active versus passive or active tuned mass dampers for structural control. *Journal of Engineering Mechanics*, ASCE; **109**(3): 691–705.

69. Hsu, C.C., Calise, A.J., Goodno, B.J. and Craig, J.I. (1995), Performance Evaluation of Robust Controllers in Earthquake Structural Dynamics Problems with Large Hysteretic Nonlinearities, Proceedings of American Control Conference, Seattle, WA, June.

70. Inaudi, J.A. (1997), Modulated Homogeneous Friction: A Semi-Active Damping Strategy, *J. Earthq. Engrg. and Structural Dyn.*, **26**: 361-376.

71. Iwan, W. D. (1980), "Estimating inelastic response spectra from elastic spectra", *Earthquake Eng. Struct. Dyn.* **8**: 375–388.

72. Iwan, W.D., and Chen X. (1994). Important near-field ground motion data from the Landers earthquake. *Proceedings of the 10th European Conference on Earthquake Engineering*, A.A. Balkema, Rotterdam, The Netherlands, 1:229-234.

73. Jabbari, F., Schmitendorf, W.E. and Yang, J.N. (1995), "H_∞ Control for Seismic-Excited Buildings with Accelerations Feedback", Journal of Engineering Mechanics, ASCE, Vol. 21, No. 9, pp. 994-1002.

74. Jacobson, D.H. (1977). Extensions of linear-quadratic control, optimization and matrix Theory, Academic Press, New York.

75. Jangid R.S. and Kelly J.M. (2001), Base isolation for near-fault motions. *Earthquake Engng Struct. Dyn.*, **30**: 691-707.

76. Jansen L.M. and Dyke S.J. (2000), Semiactive control strategies for MR dampers: comparative study. *Journal of the Engineering Mechanics*, ASCE, 126(8): 795-803.

77. Johnson, E.A., Ramallo, J.C., Spencer, B.F. and Sain, M.K. (1998). Intelligent Base Isolation Systems, *Proc. Second World Conference on Structural Control*, 367-376, Kyoto, Japan.

78. Kappos AJ. (1997), Seismic damage index for RC buildings: evaluation of concepts and procedures. *Progress in Structural Engineering and Materials*, **1**(1): 78-87.

79. Kamagata, S., and Kobori, T. (1994). Autonomous adaptive control of active variable stiffness system for seismic ground motion, Proc., Frist world Conf. On Struct. Control, TA4:33-42.

80. Kelly J.M. (1999), The role of damping in seismic isolation. *Earthquake Engng. Struct. Dyn.*, **28:** 3-20.

81. Kobori T et al. (1991). Dynamic loading test of real scale steel frame with active variable stiffness device. *Journal of Structural Engineering*, 37B: 317-328.

82. Kobori T et al. (1993). seismic response controlled structure with active variable stiffness system. *Earthquake Engineering and Structural Dynamics*, **22**: 925-941.

83. Kose, I.E., Schmitendorf, W.E., Jabbari, F. and Yang, J.N. (1996), "H_∞ Active Seismic Response Control Using Static Output Feedback", Journal of Engineering Mechanics, ASCE, Vol. 122, No. 7, pp. 651-659.

84. Kose, I.E., Jabbari, F., Schmitendorf, W.E., and Yang, J.N. (1998), "Controllers for Quadratic Stability and Performance of a Benchmark Problem", Journal of Earthquake Engineering and Structural Dynamics, Vol. 27, No.11, pp. 1385-1397.

85. Kuehn J.L. and Stalford H.L. (2000), Stability of a Lyapunov Controller for a Semi-active Structural Control System with Nonlinear Actuator Dynamics. *Journal of Mathematical Analysis and Applications*: **251:** 940-957.

86. Kurata N., Kobori T. Takahash, M., Niwa, N. and Midorikawa, H. (1999). Actual seismic response controlled building with semi-active damper system. *Earthquake Engineering and Structural Dynamics*, **28:** 1427-1447.

87. Kuwamura H & Galambos TV. (1989), Earthquake load for structural reliability. *Journal of Structural Engineering* ASCE, **115**(6): 1446–1462.

88. Lee-Glauser, G. I., Ahmadi, G., and Horta, L. G. (1999), Integrated passive/active vibration absorber for multistory buildings. *J. Struct. Engrg.*, ASCE.; **123** (5).

89. Lewis, J.B. (1953). The use of nonlinear feedback to improve the transient response of a servomechanism, AIEE Trans. On Automatic Control, AC-16, 785-793.

90. Lewis, F.L. (1986), Optimal control, John-Wiley & Sons.

91. Liao, W.-I, Loh, Ch.-H. and Wan, Sh. (2001). Earthquake responses of RC moment frames subjected to near-fault ground motion. *Struct. Design Tall Build.*; **10**: 219-229.

92. Loh Ch.H. et al. (2000), Ground motion characteristics of the Chi-Chi earthquake of 21 September 1999. *Earthquake Engng Struct. Dyn.*, **29**: 867-897.

93. Lu, J.B. and Skelton, R.R, (1998). Covariance control using closed-loop modelling for structures, *Earthquake Engineering & Structural Dynamics*, 27(11): 1367-1383.

94. MacRae, G. A., Morrow, D. V. and Roeder C. W., (2001). Near-fault ground motion effects on simple structures. *Journal of Structural Engineering* ASCE, **127**(9): 996-1004.

95. Mahin, S., Bertero, V., Chopra, A., and Collins, R., (1976). Response of the olive view Hospital main building during the San Fernando Earthquake, Earthquake Engineering Center, UC, Berkeley, Report No. UCB/EERC-76/22, Oct.

96. Makris, N. and Constantinou, M. C. (1991). Fractional-derivative Maxwell model for viscous dampers. *J. Struct. Engrg.*, ASCE, **117**(9): 2708-2724.

97. Makris, N., Constantinou, M. C., and Dargush, G. F. (1993a). Analytical model of viscoelastic liquid dampers. *J. Struct. Engrg.*, ASCE, **119**: 3310-3325.

98. Makris, N., Dargush, G. F., and Constantinou, M. C. (1993b). Dynamic analysis of generalized viscoelastic fluids. *J. Engrg. Mech.*, ASCE, **119**: 1663-1679.

99. Makris N, Burton SA, Hill D, Jordan M. (1996). Analysis and design of ER damper for seismic protection of structures. *Journal of Engineering Mechanics*, 122(10): 1003–1011.

100. Makris N. (1997). Rigidity-plasticity-viscosity: can electrorheological dampers protect base-isolated structures from near-source ground motions? *Earthquake Engineering and Structural Dynamics*, **26**: 571-591.

101. Makris N. and Shih-Po Ch. (1998). Effect of Damping Mechanisms on the Response of Seismically Isolated Structures. *PEER Report 1998/06*, Pacific Earthquake Engineering Research Center, University of California, Berkeley, November.

102. Makris N. and Shih-Po Ch., (2000a). Effect of viscous, viscoplastic and friction damping on the response of seismic isolated structures. *Earthquake Engineering and Structural Dynamics*; **29**: 85-107.

103. Makris N. and Shih-Po Ch., (2000b). Response of damped oscillators to cycloidal pulses. *Journal of Engineering Mechanics* ASCE; **2**: 123-131

104. Malhotra P.K., (1999). Response of building to near-field pulse-like ground motions. *Earthquake Engng. Struct. Dyn.*; **28**: 1309-1326.

105. Manfredi G. (2001), Evaluation of seismic energy demand. *Earthquake Engineering and Structural Dynamics*; **30**: 485-499.

106. Matheu E.E, Singh M.P. and Beattie C. (1998), Output feedback Sliding-mode control with generalized sliding surface for civil structures under earthquake excitation. *Earthquake Engng Struct. Dyn.*; **27**: 259-282.

107. McCabe SL & Hall WJ. (1989). Assessment of seismic structural damage. *Journal of Structural Engineering* ASCE, **115**(9): 2166–2183.

108. MaClamroch, N.H., and Gavin, H.P. (1995), Closed loop structural control using electrorheological dampers, Proc. Am. Control conf. 4173-4177.

109. Molyan, P.J. and Anderson, B.D.O. (1973), Nonlinear regulator theory and an inverse optimal control problem, IEEE Trans. On automatic control, Vol. AC-18, No. 5, pp.460-465.

110. Mukai, Y. Tachibana, E. and Inoue, Y. (1994). Experimental study of active fin system for wind-induced structural vibrations, Proc., Frist World Conf. On Structural Control, WP2-52-WP2-61.

111. Nagarajaiah, S.M., Riley, M.A. and Reinhorn, A.M. (1993), Hybrid Control of Sliding Isolated Bridges, J. of Engineering Mechanics, ASCE, 119, pp. 2317-2332.

112. Nagarajaiah, S., (1994), Fuzzy controller for structures with hybrid isolation system, Proceedings First World Conference on Structural Control, Univ. of Southern California, California, TA2-67-76.

113. Nagarajaiah, S., and Mate, D. (1998a), "Semi-active control of continuously variable stiffness system", Proc. 2nd world Conf. On Structural Control, Vol.1, Wiley, New York, pp. 397-406.

114. Nagarajaiah, S., and Mate, D. (1998b), "Development of a semi-active continuously variable stiffness device", Proc. ASCE, 12th Engrg. Mech. Conf., ASCE, Reston, VA, pp. 257-260.

115. Nagarajaiah, S., Sahasrabudhe, S., and Iyer, R. (2000a), "Seismic Response of Sliding Isolated Bridges with Smart Dampers Subjected to Near Source Ground Motions," Proc. Structures Congress, ASCE, Philadelphia, CD ROM.

116. Nagarajaiah, S., Sahasrabudhe, S., and Iyer, R. (2000b), "Earthquake Protection of Bridges using Sliding Isolation System and MR Dampers," Proc. Third International Workshop on Structural Control, ENPC, Paris, pp. 375-383.

117. Nagarajaiah, S. and Varadarajan, N. (2000), "Novel Semi-active Variable Stiffness Tuned Mass Damper With Real Time Retuning Capability", Proc. 14th ASCE Engrg. Mech. Conf., Austin, TX, May 21-24, 6 pages (CD-ROM).

118. Nasu T. et al. (2001). Active variable stiffness system with non-resonant control. *Earthquake Engineering and Structural Dynamics*; **30**: 1597–1614.

119. Nemir DC, Lin Y, Osegueda RA. (1994). Semi-active motion control using variable stiffness. *Journal of Structural Engineering*; 120(4):1291–306.

120. Nishitani A. and Inoue Y. (2001). Overview of the application of active/semi-active control to building structures in Japan. *Earthquake Engineering and Structural Dynamics*; **30**: 1565–1574

121. Niwa N., Kobori T., Takahashi, M., Midorikawa, H. and Mizuno, T. (2000). Dynamic loading test and simulation analysis of full-scale semi-active hydraulic damper for structural control. *Earthquake Engng Struct. Dyn.*; **29**: 789-812

122. Pall, A. S., and Marsh, C. (1982). Response of friction damped braced frames. *J. of struct. Div.*, ASCE; **108**(6): 1313-1323.

123. Panariello, G. F.; Betti, R. and Longman, R. W. (1997). Optimal structural control via training on ensemble of earthquakes. *Journal of Engineering Mechanics*, ASCE 123 (11), pp. 1170-1179

124. Patten W.N, He, Q., Kuo, C.C., Liu L and Sack R.L. (1994a). Suppression of vehicle induced bridge vibration via hydraulic semi-active vibration dampers, Proc., Frist World Conf. On structure control, FA1, 3-38.

125. Patten W.N, He, Q., Kuo, C.C., Liu L and Sack R.L. (1994b). Seismic structural control via hydraulic semi-active vibration dampers. Proc., Frist World Conf. On structure control, FA2, 83-89.

126. Patten WN, Kuo CC, He Q, Liu L and Sack RL. (1994c). A controlled semi-active hydraulic vibration absorbers for bridges. *Journal of structure Engineering*, ASCE: **122**(2): 187-192.

127. Patten WN, Kuo CC, He Q, Liu L and Sack RL. (1998). A primer on design of semi-active vibration absorber (SAVA). *Journal of the Engineering Mechanics*, ASCE, **124**(1): 61-68

128. Powell GH & Allahabadi R. (1988), Seismic damage prediction by deterministic methods: concepts and procedures. *Earthquake Engineering and Structural Dynamics* 1988: **16**: 719-734.

129. Ramallo, J.C., Johnson, E.A. and Spencer Jr., B.F. (2000a). "'Smart' Base Isolation Systems." 14th Analysis & Computational Specialty Conference, Proceedings of the 2000 Structures Congress & Exposition, May 8-10, Philadelphia, Pennsylvania.

130. Ramallo, J. C.; Johnson, E. A. and Spencer, B. F., Jr (2002). "Smart" base isolation systems. Journal of Engineering Mechanics, ASCE 128(10), pp 1088-1099.

131. Rao P. B. and Jangid R.S. (2001), Performance of sliding systems under near-fault motions. *Nuclear Engineering and Design*; **203**: 259–272.

132. Reinhorn, A.M., Soong T.T. and Yen, C.Y. (1987), "Base-Isolated Structures With Active Control", Recent Advances in Design, Analysis, Testing and Qualification Methods, PVP-Vol.127, ASME, pp.413-419.

133. Rekasius, Z.V. (1964), Suboptimal design of intentionally nonlinear controller, IEEE Trans. Automatic control, Vol. AC-9, No.4, pp.380-386.

134. Robinson W.H., (2000).Seismic isolation of civil buildings in New Zealand. *Progress of Structures & Engineering Materials*; **2**: 328-334.

135. Ruzzene M., Fasana A et al. (1997), Natural frequency and dampings identification using wavelet transform: application to real data. *Mechanical Systems and Signal Processing*. **11** (2): 207-218.

136. Sadek, F., Mohraz, B., and Riley, M. A. (1999). "Linear procedures for structures with velocity-dependent dampers", *Journal of Structural Engineering*, Vol. 126, No. 8, 887-895.

137. Sahasrabudhe, S., and Nagarajaiah, S. (2000a), "Sliding Isolated Structures with Smart Dampers," Proc. Int. Conf. On Advances in Structural Dynamics, Hong Kong, CD ROM.

138. Sahasrabudhe, S., Nagarajaiah, S. and Hard, C. (2000b) "Experimental Study of Sliding Isolated Buildings with Smart Dampers Subjected to Near Source Ground Motions," Proc. Eng. Mech. Conf. EM 2000, ASCE, UT Austin, CD ROM.

139. Sahasrabudhe, S. and Nagarajaiah, S. (2001), "Sliding Isolated Buildings with Smart Dampers : Shaking Table Studies", Proc. 2001 Structures Congress, May 21-23, Washington, D.C., CD-ROM, 8 Pages.

140. Sarbjeet S. and Datta T.K. (2000), Nonlinear sliding mode control of seismic response of building frames. *Journal of Engineering Mechanics*, No.4: 340-347.

141. Schmitendorf, W.E., Jabbari, F. and Yang, J.N. (1994), "Robust Control Techniques for Buildings Under Earthquake Excitation", Earthquake Engineering and Structural Dynamics, Vol. 23, No. 5, pp. 539-552.

142. SEAOC blue book (1996). Recommended lateral force requirmrnts and commentary, Structural Engineers Association of California, sixth edtion, Sacramentto, California.

143. Seber, G. A. F. and Wild C.J., (1989), Nonlinear Regression, New York: Wiley.

144. Setareh M. (2001), Application of semi-active tuned mass dampers to base-excited systems. *Earthquake Engng. Struct. Dyn.*, **30**: 449-462

145. Shames IH and Cozzarelli FA. (1992). *Elastic and Inelastic Stress Analysis.* Prentice-Hall, Englewood Cliffs, NJ.

146. Singh, J., (1985). Earthquake ground motions: implication for designing structures and reconciling structural damage, Earthquake Spectra, Feb. 1985, 239-270.

147. Singh M.P., Matheu E.E et al. (1997), Active and Semi-active control of structures under seismic excitation. *Earthquake Engineering and Structural Dynamics*; **26**: 193-213.

148. Skinner, R. I., Kelly, J. M., and Heine, A. J.(1975), Hysteresis dampers for earthquake-resistant structures. *Earthquake Engineering and Structural Dynamics*, **3**: 287-296.

149. Slotine, J-J. E., and Li, W. (1991). Applied nonlinear control. Prentice Hall, Englewood Cliffs, NJ.

150. Sommerfeld, A.(1950). *Mechanics of Deformable Bodies*, Academic, San Diego, Calif.

151. Somerville, P. G. and Graves, R. W. (1993), Conditions that give rise to unusually large long period ground motions, *The Structural Design of Tall Buildings*, **2**: 211-232.

152. Somerville, P., (1998), Development of an improved representation of near-fault ground motions SMIP98 Seminar on Utilization of Strong-Motion Data: Oakland, California, September 15, 1998: Proceedings, California Division of Mines and Geology, Sacramento, pages 1-20

153. Soong TT. (1990). *Active structural control: Theory and Practice*, Longman, England and Wiley, New York.

154. Soong, TT. and Reinhorn, A. M. (1993). An overview of active and hybrid structural control research in the U.S. *The structural design of tall buildings*, **2**: 192-209.

155. Soong TT. And Constantinou MC. (1994). Passive and active structural vibration control in civil engineering. New York: Springer.

156. Soong TT. And Dargush GF. (1997). Passive energy dissipation systems in structural engineering. New York: Wiley.

157. Soong, TT. and Spencer, B.F. (2002). Supplemental energy dissipation: state-of-the-art and state-of-the practice, *Engineering Structures*, 24: 243–259.

158. Spencer BF, Dyke SJ, Sain MK, Carlson JD. (1997), Phenomenological model for magnetorheological dampers. *Journal of Engineering Mechanics*, **123**(3): 230–8.

159. Spencer, B.F., Jr., Suhardjo, J. and Sain, M.K. (1994), "Frequency Domain Optimal Control strategies for Aseismic Protection", Journal of Engineering Mechanics, ASCE, Vol. 120, Jan. pp. 135-158.

160. Spencer Jr., B.F., Timlin, T.L. and Sain, M.K. (1995), " On the Solution of the Nonlinear Optimal Control Problem", Journal of Optimization Theory and Applications, submitted in January.

161. Spencer, B.F., Jr., Dyke, S.J., Sain, M.K. and Carlson, J.D. (1997a), "Phenomenological Model of a Magnetorheological Damper", J. Engrg. Mech., ASCE, 123(3), pp. 230-238.

162. Spencer, B.F., Jr., Carlson, J.D., Sain, M.K. and Yang, G. (1997b), "On the Current Status of Magnetorheological Dampers: Seismic Protection of Full-Scale Structures", Proc. American Control Conference, Albuquerque, NM, pp. 458-462.

163. Spencer, B.F., Jr. and Sain, M.K. (1997c), "Controlling Buildings: A New Frontier in Feedback", IEEE Control Systems, 17(6), pp. 19-35.

164. Spencer, Jr., B.F., Dyke, S.J., and Deoskar, H.S. (1998a), " Benchmark Problems in Structural Control-Part 1: Active Mass Driver System, and Part 2: Active Tendon System." J. Earthquake Engineering and Structural Dynamics.

165. Spencer, B.F., Jr., Christenson, R.E. and Dyke, S.J. (1998b), "Next Generation Benchmark Control Problem for Seismically Excited Buildings", Proc. Second World Conference on Structural Control, Kyoto, Japan, June 29-July 1.

166. Spencer, B.F., Johnson, E.A. and Ramallo, J.C. (2000), "Smart isolation for seismic control", JSME International Journal Series C-Mechanical Systems Machine Elements And Manufacturing, 2000 SEP, Vol. 43, No. 3, pp. 704-711.

167. Speyer, J.L. (1976), A nonlinear control law for a stochastic infinite time-problem, IEEE Trans. On automatic control, Vol. AC-21, No. 4, pp.560-564.

168. Stammers, C.W. and Sireteanu (1998), Vibration control of machines by use of semi-active dry friction damper. *Journal of Sound and Vibration*, **209**(4): 671-684.

169. Suhardjo, J., Spencer Jr., B.F. and Kareem, A. (1992), "Active Control of Wind Excited Buildings: A Frequency Domain Based Design Approach." Journal of Wind Engineering and Industrial Aerodynamics, Vol. 41-44, pp. 1985-1996.

170. Suhardjo, J., Spencer, B.F. and Sain, M.K. (1992). Nonlinear optimal control of a Duffing system, Int. J. Nonlinear Mechanics, 27-157-172.

171. Symans M.D. and Constantinou M.C. (1997). Seismic testing of a building structure with a semi-active fluid damper control system. *Earthquake Engineering and Structural Dynamics*; **26**: 759-777.

172. Symans M.D. and Kelly S.W. (1999). Fuzzy logic control of bridge structures using intelligent semi-active seismic isolation systems. *Earthquake Engineering and Structural Dynamics*; **28**: 37-60.

173. Symans, M.D. and Constantinou, M.C. (1999). Semi-active control systems for seismic protection of structures: a state-of-the-art review, *Engineering Structures*, **21**(6): 469-487.

174. Sun, L., and Goto, Y. (1994). Application of fuzzy theory to variable dampers fro bridge vibration control. Proc., First World Conf. Struct. Control, WP1.31-40.

175. Tomasula, D.P., Spencer Jr., B.F. and Sain, M.K. (1994), Limiting extreme structural response using an efficient nonlinear control law, Proc. first world conference on structural control, pp. FP4-22 to FP4-31, USC publication, L.A., CA.

176. Tomasula, D.P., Spencer Jr., B.F. and Sain, M.K. (1996), "Nonlinear Structural Control for Limiting Extreme Dynamic Responses," Journal of Engineering Mechanics, ASCE, Vol. 122, No. 3, pp. 218-229.

177. Tsai, C. *S.*, and Lee, H. H. (1993). Application of viscoelastic dampers to high-rise buildings. *J. Struct. Engrg.*, ASCE, **119**(4): 1222-1233.

178. Tsai, C. *S.*, and Tsai, K. C. (1995). TPEA device as seismic damper for high-rise buildings. *J. Engrg. Mech.*, ASCE, **121**(10): 1075-1081.

179. Tso WK, Zhu TJ & Heidebrecht AC. (1993), Seismic energy demands on reinforced concrete moment-resistant frames. *Earthquake Engineering and Structural Dynamics*, **22**: 533–545.

180. Uang C. M., and Bertero V. V., (1988), Use of energy as a design criterion in earthquake resistant design, *Report No. UCB/EERC*-88/18, Earthquake Engineering Research Center, University of California at Berkeley.

181. Uang CM, Bertero VV. (1990), Evaluation of seismic energy in structures. *Earthquake Engineering and Structural Dynamics*; **19**: 77-90.

182. Uniform Building Code (1997). International Conference of Building Officials, Whittier, California.

183. Vidic T, Fajfar P & Fischinger M. (1994), Consistent inelastic design spectra: strength and displacement. *Earthquake Engineering and Structural Dynamics*; **23**: 523–532.

184. Wada A, Huang YH & Iwata M. (2000). Passive damping technology for building in Japan. *Progress of Structures & Engineering Materials*; **2**: 335-350.

185. Wan, Y.K., Ghaboussi, J., Venini, P. and Nikzad, K. (1995), Control of structures using neural networks, Smart Materials and Structures, Vol. 4, pp. 49-57.

186. Whittaker, A. *S.*, Bertero, V. V., Thompson, C. L-o and Alonso, L. I. (1991). Seismic testing of steel plate energy dissipation devices. *Earthquake Spectra*; **7**(4): 563-604.

187. Wong Kevin K. F. and Wang YM. (2001), Energy-based damaged assessment on structures during earthquakes. *The Structural Design of Tall Buildings*; **10**: 135–154.

188. Wong Kevin K. F. and Yang R. (2001), Evaluation of response and energy in actively controlled structures. *Earthquake Engineering and Structural Dynamics*, **30**: 1495–1510.

189. Wu, J., and Hanson, R. D. (1989). "Study of inelastic spectra with high damping." *J. Struct. Engrg.*, ASCE, 115(6), 1412–1431.

190. Wu J.C., Yang J.N. and Agrawal A.K. (1998), Application of sliding mode control to Benchmark Problems. *Earthquake Engng. Struct. Dyn.*, **27**: 1247-1265.

191. Wu, Z.G., Gattulli, V., Lin, R.C. and Soong, T.T. (1994), Implementable control law for peak response reduction, Proc. first world conference on structural control, pp. TP2-50 to TP2-59, USC publication, L.A., CA.

192. Xia, C., and Hanson, R. D. (1992). Influence of ADAS element parameters on building seismic response. *J. Struct. Engrg.*, ASCE, **118**(7): 1903-1918.

193. Yamada K. and Kobori T. (1995). Control algorithm for estimating future responses of active variable stiffness structure. *Earthquake Engineering and Structural Dynamics*; 24:1085–99.

194. Yang, J.N., (1975), "Application of optimal control theory to civil engineering structures", *Journal of Engineering Mechanics*, ASCE, Vol. 101, No.EM6, 1975, pp.819-838.

195. Yang, J.N., and Soong, T.T.(1988), "Recent advancement in active control of civil engineering structures", *Journal of Probabilistic Engineering Mechanics*, Vol.3, No.4, 1988, pp.179-188.

196. Yang, J.N. and Danielians, A. (1991), "Aseismic Hybrid Control Systems for Building Structures", *Journal of Engineering Mechanics*, ASCE, 117 (4), pp. 836-853.

197. Yang, J.N. and Li, Z. and Liu, S.C. (1992a), "Control of Hysteretic System Using Velocity and Acceleration Feedbacks", J. of Engr.. Mech., ASCE, 118 (11), pp. 2227-2245.

198. Yang, J.N., Li, Z. and Danielians, A. (1992b), "Hybrid Control of Nonlinear and Hysteretic Systems II", Journal of Engineering Mechanics, ASCE, Vol. 118, No. 7, pp. 1441-1456.

199. Yang, J.N. and Li, Z. (1993), "Hybrid Control of Seismic-Excited Bridge Structures Using Variable Dampers", in Structural Engineering in Natural Hazards Mitigation, Vol. 1, pp. 778-783, ASCE Structures Congress, April, Irvine, CA.

200. Yang, J.N., Li, Z., Wu, J.C. and Kawashima, K. (1994a), "A seismic Hybrid Control of Bridge Structures", Proc. 5th Nat'l. Conf. on Earthquake Engineering, Vol. 1, pp. 861-870, Chicago, IL.

201. Yang, J.N., Li, Z. and Vongchavalitkul, S. (1994b), "A Generalization of Optimal Control Theory: Linear and Nonlinear Control", J. of Engineering Mechanics, ASCE, Vol. 120, No. 2, pp. 266-283.

202. Yang, J.N., Li, Z. and Vongchavalitkul, S. (1994c), "Stochastic Hybrid Control of Hysteretic Structures", Journal of Probabilistic Engineering Mechanics, Vol. 9, pp. 125-133.

203. Yang, J.N., Li, Z., Wu, J.C. and Hsu, I.R. (1994d), "Control of Sliding-Isolated Buildings Using Dynamic Linearization", Journal of Engineering Structures, Vol. 16, No. 6, pp. 437-444.

204. Yang, J.N., Wu, J.C., Agrawal, A.K. and Li, Z. (1994e), "Sliding Mode Control for Seismic-Excited Linear and Nonlinear Civil Engineering Structures", National Center For Earthquake Engineering Research, Technical Report NCEER-94-0017.

205. Yang, J. N., Li, Z., Wu, J. C., Kawashima, K. and Unjoh, S. (1994f) "Hybrid Control Systems for Seismic-Excited Bridges, "Proc. 3rd U.S.- Japan Workshop on Protective Systems for Bridges, pp. 3-65 to 3-79, Feb., Berkeley, CA.

206. Yang, J.N., Wu, J.C. and Agrawal, A.K. (1995a), "Sliding Mode Control of Seismic-Excited Linear Structures", Journal of Engineering Mechanics, ASCE, Vol. 121, No. 12, pp. 1330-1339, Dec. 1995.

207. Yang, J.N., Wu, J.C. and Agrawal, A.K. (1995b), "Sliding Mode Control of Nonlinear and Hysteretic Structures", Journal of Engineering Mechanics, ASCE, Vol. 121, No. 12, pp. 1386-1390, Dec. 1995.

208. Yang, J.N., Wu, J.C., Kawashima, K. and Unjoh, S. (1995c), "Hybrid Control of Seismic-Excited Bridge Structures", Journal of Earthquake Engineering and Structural Dynamics, Vol. 24, No. 11, pp. 1437-1451.

209. Yang, J.N., Wu, J.C., Reinhorn, A.M., Riley, M., Schmitendorf, W.E. and Jabbari, F. (1996a), "Experimental Verifications of H-infinity and Sliding Mode Control for Seismic-Excited Buildings", Journal of Structural Engineering, ASCE, Vol. 122, No. 1, pp. 69-75.

210. Yang, J.N., Wu, J.C., Reinhorn, A.M. and Riley, M. (1996b), "Control of Sliding-Isolated Buildings Using Sliding Mode Control", Journal of Structural Engineering, ASCE, Vol. 122, No. 2, pp. 83-91.

211. Yang, J.N., Agrawal, A.K., and Chen, S. (1996c), "Optimal Polynomial Control of Seismically Excited Non-Linear and Hysteric Structures", Journal of Earthquake Engineering and Structural Dynamics, Vol. 25, No. 11, pp. 1211-1230.

212. Yang, J. N., Wu, J. C. and Li, Z. (1996d), "Control of Seismic-Excited Buildings using Active Variable Stiffness Systems", J. Engineering Structures, 18(8), pp. 589-596.

213. Yang, J.N., Wu, J.C., Agrawal, A.K., and Hsu, S.Y. (1997), "Sliding Mode Control With Compensators for Wind and Seismic Response Control", Journal of Earthquake Engineering and Structural Dynamics, Vol. 26, pp. 1137-1156.

214. Yang, J.N., Wu, J.C., Samali, B. and Agrawal, A.K. (1998), "A Benchmark Problem for Response Control of Wind-Excited Tall Buildings", Proc. of 2nd World Conference on Structural Control, Kyoto, Japan, pp. 1407-1416.

215. Yang, J. N, Kim, J. H. and Agrawal, A. K. (1999), "Seismic Response Control Using Semi- Active Stiffness Dampers", Proc. Int. Workshop on Seismic Isolation, Energy Dissipation and Control of Structures, 312-319, Seismological press, Guangzhou, China.

216. Yang, J. N., Kim, J.H., and Agrawal, A.K. (2000a), "A Resetting Semi-Active Stiffness Damper for Seismic Response Control", J. Struct. Engrg., ASCE, Vol. 126(12), pp. 1427-1433.

217. Yang, J. N., and Agrawal, A. K. (2000b), "Protective Systems For High-Technology Facilities Against Microvibration and Earthquake", International Journal of Structural Engineering and Mechanics, Vol. 10, No.6, pp. 561-575.

218. Yang, J. N., and Agrawal, A. K. (2000c), "Protective System Technology For Building Structures Against Near-Field Earthquakes ", Proc. International Workshop on Annual Commemoration of Chi-Chi Earthquake, Vol. II-Technology Aspect, pp. 76-87, National Center for Research on Earthquake Engrg., Taipei, Taiwan.

219. Yang, J.N., Lin, S., Kim, J.H., and Agrawal (2000d), A.K., "Optimal Design of Passive Supplemental Dampers Based on H_∞ and H_2 Performances", in Advanced Technology in Structural Engineering, CD RAM, 8 Pages, ASCE, Proc. ASCE 2000 Structures Congress & Exposition, Philadelphia, PA.

220. Yang, J. N., Agrawal, A. K., and He., W. (2000e)," Response Control of Nonlinear Structures Using a Semi-Active Stiffness Damper", in Advances in Structural Dynamics, Vol.I, pp. 349-356, Elsevier Science Ltd., Proceedings of International Conference on Advances in Structural Dynamics, Dec. 13-15, Hong Kong.

221. Yang, J.N., Agrawal, A.K., Samali, B. and Wu, J.C. (2000f), "A Benchmark Problem For Response Control of Wind-Excited Tall Buildings", Proceedings of Fourteenth Engineering Mechanics Conference, ASCE, May 21-24, 2000, Texas, Austin.

222. Yang, J.N., Agrawal, A.K., Samali, B. and Wu, J.C. (2000g), "A Benchmark Problem For Response Control of Wind-Excited Tall Buildings Using Wind Tunnel

Data", Proc. of Second European Conference on Structural Control, July 3-6, 2000, Paris, France.

223. Yang, J. N., Lin, S., and Jabbari, F. (2001), " Performance-Based Controller For Civil Engineering Structures ", Proc. of 2001 American Control Conference, Arlington, VA.

224. Yang, J.N., Lin, S., Kim, J.H., and Agrawal, A.K. (2002a), "Optimal Design of Passive Supplemental Dampers Based on H_∞ and H_2 Performances"; to appear in Journal of Earthquake Engineering and Structural Dynamics.

225. Yang, J.N., and Agrawal, A.K. (2002b), " Semi-Active Hybrid Control systems For Nonlinear Buildings Against near-Field Earthquakes", paper accepted for publication in J. of Engineering Structures.

226. Yang, J.N., Agrawal, A.K. and He, W.L. (2000), Response Control of Nonlinear Structures Using A Semi-Active Stiffness Damper, *Proc. International Conf. on Advances in Structural Dynamics*, Hong Kong, 13-15 December.

227. Yoshioka, H.; Ramallo, J. C. and Spencer, B. F. (2002). "Smart" base isolation strategies employing magnetorheological dampers Journal of Engineering Mechanics, ASCE 128(5), pp. 540-551

228. Zahrah T, Hall J. (1984), Earthquake energy absorption in SDOF structures. *Journal of Structural Engineering*; **110**(8): 1757-1772.

229. Zhao B., Lu X.L., Wu, M.Zh. and Mei, Zh.X. (2000). Sliding mode control of buildings with base-isolation hybrid protective system. *Earthquake Engng Struct. Dyn.*; **29**: 315-326.

230. Zhu T.J., Tso W.K. & Heidebrecht AC. (1988), Effect of peak ground a/v ratio on structural damage. *Journal of Structural Engineering* ASCE; **114**: 1019–1037.

231. Zhu, G. and Skelton, R.E. (1994), "Output Covariance Constraint Problem with Disturbance Feedback", Proceedings of the First World Conference on Structural Control, Pasadena, CA, August, FP4 32-41.